EVALUATION OF A ROTARY REGENERATIVE BURNER FOR LEAN MIXTURES OF GASEOUS FUELS

by

CONSTANTINE MOUTSOS, B.Sc., M.Sc., D.I.C.

A Thesis submitted for the degree of Doctor of Philosophy of the University of London

Imperial College of Science and Technology
Department of Chemical Engineering
and Chemical Technology

February 1987

To dearest Liza
for her encouragement, devotion and genuine understanding.

Στους αγαπημένους μου γονείς
Ανδρόνικο και Ανδρομάχη
σαν απειροελάχιστο δείγμα της
ευγνωμοσύνης μου για τη
στοργή τους και τον συνεχή
αγώνα τους.

Abstract

A novel heat recirculating burner, incorporating a rotary regenerator, has been developed and tested, and shown to provide for continuous, stable combustion of methane - air mixtures at concentrations substantially below the normal lower limit of flammability (2.6% methane in air by volume, compared to 5.3%) and at inlet mixture flowrates up to 800 cm^3/s.

Running times in excess of 9 hours have been achieved, and stable combustion near the normal lower flammability limit has been demonstrated even with heat abstraction equivalent to 39% of the calorific value of the fuel. A comprehensive description of the mechanical, thermal and combustion characteristics of the system has been obtained. Three combustion chamber geometries and two rotary regenerator matrices, one tubular ceramic and one flame trap metallic, have been tested.

The ceramic matrix has been found to be more effective than the metallic one, and leanest combustion has been achieved in the system with the hemispherical chamber of the largest volume. The efficiency of all systems has been shown to increase with increasing matrix rotational speed but only up to a maximum. The flame temperature has been determined to be close to the constant limiting flame temperature of 1400 K and to increase slowly with increasing inlet flowrate. Combustion with limit mixtures has not been found to be complete and small quantities of CO and CH_4 were always detected in the exhaust.

A mathematical model predicting the stability characteristics of the burner has been developed and shown to accurately predict the observed trends.

Acknowledgements

I would like to express my most sincere gratitude to Dr. D. Dugwell, my supervisor, for his continuous and invaluable encouragement, and his excellent councel and guidance throughout the course of this research programme.

Thanks are also due to those members of the Departmental Mechanical Workshop who, with useful advice contributed to the development of the experimental system. Likewise the expertise of the Analytical and Photographic services has been greatly beneficial and the efforts of Mr. I. Drummond and Mr. L. Moulder merit special thanks.

The financial support provided by the Science and Engineering Research Counsil is gratefully appreciated.

Last and most certainly not least, a big thank-you to three great friends of mine, D. Liatsis, L. Mantzos and P. Stavropoulos who shared my anxious and happy moments and whose companionship and friendship will always be fondly remembered.

Nomenclature

Latin characters

A:	Heat transfer area	(m^2)
A_f:	Frontal matrix area	(m^2)
a:	A power	-
C:	Heat capacity	(J/Kg)
C:	Heat capacity rate	(J/Kg s)
C:	A constant	-
C_D:	Discharge coefficient	-
c_p:	Specific heat	(J/Kg K)
De:	Dean number	-
d:	Diameter	(m)
E:	Activation energy	(J/mole)
F_N:	Force acting in the normal direction	(N)
f:	Percentage of fuel in mixture by volume	-
Gg:	Gas mass flux	(Kg/m^2 s)
Gr:	Grashof number	-
H:	Enthalpy	(J/Kg)
$\bar{h}$:	Mean heat transfer coefficient	(J/m^2 s K)
$\bar{h}$:	Hausen heat transfer coefficient	(J/m^2 s K)
h:	Convective heat transfer coefficient	(J/m^2 s K)
k:	Thermal conductivity	(J/m s K)
k':	Effective thermal conductivity	(J/m s K)

L:	Characteristic length	(m)
l:	Length of matrix passages	(m)
l:	Length of metallic strips used for the construction of the flame trap matrix	(m)
M:	Mass flowrate	(Kg/s)
M:	Torque	(Nm)
m:	Mass	(Kg)
n:	Number of turns of corrugated and plane strips of flame trap matrix	
n_c:	Number of subdivisions in the gas stream direction	
n_r:	Number of subdivisions in the "solid" stream direction	
P:	Power	(W)
P:	Pressure	(N/m^2)
Pr:	Prandtl number	-
Q:	Heat rate	(J/s)
Q_c:	Heat of combustion	(J)
q:	Heat of combustion per unit volume of fuel	(J/m^3)
R:	Ideal gas constant	(J/mole K)
Re:	Reynold's number	-
R:	Radius	(m)
r:	Radius	(m)
St:	Stanton number	-
T:	Temperature	(K)
t:	Time for which matrix is subjected to either gas stream	(s)
U:	Overall heat transfer coefficients	(J/m^2 s K)
u:	Velocity	(m/s)

V:	Volumetric flowrate	(m^3/s)
x:	Matrix wall thickness	(m)
x:	Thermal entry length	(m)
z:	Height of liquid column in manometer	(m)

Greek characters

α:	A constant	-
β:	Radius of curvature	(m)
Δ:	Difference in	-
ϵ:	Regenerator effectiveness	-
η:	Dimensionless time	-
θ:	Angle	(rad)
λ:	Thermal expansion coefficient	(m/m K)
μ:	Viscosity	(Kg/m s)
μ:	Coefficient of friction	-
ξ:	Dimensionless length	-
ρ:	Density	(Kg/m^3)
ϕ:	Angle	(rad)
ψ:	A constant	-

Subscripts

Avg:	Average
a:	Ambient
b:	Burnt for adiabatic case
br:	Bearing-rotor contact

by: Bypass leakage

c: Cold

cc: Combustion chamber

cr: Corrugated metal strip

e: Equivalent

f: Final

fr: Free

g: Gas

h: hot

i: initial

in: at the entry or on the inside

$L_{1,2,3}$: Lost from positions 1,2 and 3 respectively

l: Leakage to environment

lm: Log mean

m: Maximum

o: Volume fraction of fuel at normal lower flammability limit

o: orifice

oc: occupied

out: At the outlet, on the outside

p: Products

pl: Plane strip

r: Recirculated

S: Solid

Sr Seal-rotor contact

st st: 316 Stainless steel

T: Total

U: Unburnt

Contents

Title page 1

Abstract 2

Acknowledgements 3

Nomenclature 4

Contents 8

List of Figures and Tables 12

Introduction

Chapter 1 Combustion in heat recirculating burners

1.1. Introduction 23

1.2. Principles of combustion with heat recirculation 23

1.3. Thermodynamic models of combustion in heat recirculating burners 28

1.4. Stability characteristics of heat recirculating burners for combustion of lean fuel mixtures 34

1.5. Previous work on heat recirculating burners for combustion of lean fuels 39

1.6. Scope of this study on a rotary regenerator burner 43

Chapter 2 High temperature rotary regenerators

2.1. Introduction 54

2.2. General on rotary regenerators 55

2.3. Thermal design of rotary regenerators 60

2.4. Mechanical design of high temperature rotary regenerators 71

Chapter 3 Thermal design and commissioning of the rotary regenerative burner

3.1. Introduction 85

3.2 Overall design of the rotary regenerative burner 85

3.3 Thermal and mechanical design of the rotor and matrix assembly 88

3.4. Combustion chamber design 101

3.5 The sealing system 105

3.6 The rotor drive assembly 111

3.7. Hot commissioning of the rotary regenerative burner 112

3.8. Estimation of bypass and leakage flowrates during cold operation of the rotary regenerative burner 118

Chapter 4 Mathematical modelling of combustion within the rotary regenerative burner

4.1 Introduction 143

4.2 General philosophy of modelling of the rotary regenerative burner 143

4.3 Modelling of processes within the combustion chamber 145

4.4. Modelling of heat transfer within the rotating matrix 155

4.5. Computer program and predicted stability characteristics 161

Chapter 5 Experimental apparatus and techniques

5.1. Introduction 171

5.2. The experimental programme 171

5.3. The experimental apparatus 173

5.4. Experimental operating procedure 186

Chapter 6 Experimental results and discussion

6.1. Introduction 201

6.2. Experimental results for methane combustion in the metallic matrix burner 202

6.3. Discussion of results for combustion in the metallic matrix burner 206

6.4. Experimental results and discussion for methane combustion in the ceramic matrix burner 210

6.5. Experimental results and discussion for methane combustion in the ceramic matrix burner with combustion chamber of different size and configuration 218

6.6. Gas analysis and combustion chamber gas temperature measurement results and discussion 223

6.7. Experimental results and discussion for combustion with heat abstraction 228

6.8. Photographic evidence of combustion within the rotary regenerative burner 231

Chapter 7 Summary and conclusions 235

Appendix A 261

Appendix B 275

Appendix C 281

Appendix D 285

Appendix E 293

Appendix F 297

References 319

List of Figures and Tables

Figure (1.1): Enthalpy profiles in ordinary and heat recirculating burners 48

Figure (1.2): Variation of reaction rate with temperature, with (B) and without (A) depletion of reactants . 48

Figure (1.3): Flammability limits (percent fuel by volume) for hydrocarbon/air mixtures as a function of initial mixture temperature 49

Figure (1.4): Thermodynamic model for variable specific heat and no heat losses 50

Figure (1.5): Thermodynamic model for constant specific heat and heat losses from several points 50

Figure (1.6) Characteristic stability curves for burners with heat recirculation 51

Figure (1.7): "Swiss Roll" burner 52

Figure (1.8): Experimental stability characteristics of several "Swiss Roll" burners 53

Figure (2.1): Types of rotary regenerator (a) disk type (b) drum type 77

Figure (2.2): Nomenclature for the plane matrix regenerator . . 77

Figure (2.3): Progress of temperature with time in a thick stone 78

Figure (2.4): Circumferential and radial elements for modelling of the heat exchange process within the matrix 78

Figure (2.5): Effect of solid to air capacity rate ratio on cold side effectiveness for B.S.C. regenerator . 79

Figure (2.6): Effect of l/d on ϵ_c for G_{gh} = 1.0 and 0.5 for the B.S.C. regenerator 80

Figure (2.7): Effect of $\frac{A_{fc}}{A_{fh}}$ on ϵ_c for G_{gc} = 0.5, 1.0 and G_{gh} = 1.0 for the B.S.C. regenerator 81

Figure (2.8): Effect of hole size and wall thickness on ϵ_c for the B.S.C regenerator 82

Figure (2.9): Effect of hot gas inlet temperature on ϵ_c for B.S.C. regenerator 83

Figure (2.10): Effect of leakage on ϵ_c for B.S.C. regenerator . 84

Figure (3.1): The rotary regenerator burner (schematic representation) 125

Figure (3.2): The rotary regenerative burner 126

Figure (3.3): The parts of the rotary regenerative burner . . 126

Figure (3.4): The regenerator rotor 127

Figure (3.5): The metallic matrix rotor 128

Figure (3.6): Dimensions of the flame trap matrix 128

Figure (3.7): Matrix rotational speed against matrix size for 90% effectiveness

Matrix surface area against matrix diameter . . . 129

Figure (3.8): Regenerator effectiveness against matrix rotational speed

% CH_4 by volume required for limiting combustion against matrix rotational speed 130

Figure (3.9): The ceramic matrix 131

Figure (3.10): Schematic representation of equipment for measurement of pressure drop through half the matrix 131

Figure (3.11): Pressure drops for flow through
(a) the metallic matrix and
(b) the ceramic matrix 132
Figure (3.12): The 90 mm i.d. hemishperical chamber of concrete walls 133
Figure (3.13): The "Top hat" structure and the wooden mandril for construction of the 90 mm i.d. chamber . . . 133
Figure (3.14): The transparent quartz 90 mm i.d. dome 134
Figure (3.15): The quartz dome attached on the upper sealing ring (bolts not shown) 134
Figure (3.16): The upper sealing and compacting rings of the prototype unit 135
Figure (3.17): The lower section of the prototype unit 135
Figure (3.18): The upper compacting ring of the modified unit . 135
Figure (3.19): The upper sealing ring of the modified unit . . 136
Figure (3.20): The upper sealing and compacting ring of the modified unit 136
Figure (3.21): Lower section of the modified unit 137
Figure (3.22): The lighter combustion chamber structure 137
Figure (3.23): The rotor of the modified unit 138
Figure (3.24): Paths for leakages to the environment, V_l, and bypass leakages, V_{by} 138
Figure (3.25): Schematic representation of equipment for obtaining relationship between $P_{in} - P_{out}$ and V_{by} (bypass leakage rate) 139
Figure (3.26): Variation of the bypass leakage rate with the pressure difference across the radial seal . . . 140
Figure (3.27): Variation of bypass flowrate with inlet flowrate 141

Figure (3.28): Variation of the leakage rate to the environment with the inlet flowrate 142

Figure (4.1): The matrix interfaces for the case of clockwise rotation 166

Figure (4.2): Matrix element for modelling of heat transfer within the regenerator 166

Figure (4.3): Solid and gas temperatures within a 2x2 grid of elements for modelling of heat transfer in the matrix 167

Figure (4.4): Burner predicted stability characteristics . . . 168

Figure (4.5): Effectiveness vs inlet flowrate (1.2 revs/min) and Effectiveness vs rotational speed (800 cm^3/s) 169

Figure (4.6): Burner predicted stability charcteristics for 1.2 revs/min 170

Figure (5.1): The flow measuring equipment 194

Figure (5.2): The thermocouple and support quartz rod 195

Figure (5.3)a: Thermocouple positions in relation to the two sections (entry and exit) of the matrix 195

Figure (5.3)b: Distance of the thermocouples (A,B) from the matrix upper surface (90 mm diameter combustion chamber) 196

Figure (5.3)c: Distance of thermocouples (A,B) from the matrix upper surface (60 mm diameter combustion chamber) 196

Figure (5.4): The suction pyrometer and the flow measuring equipment for temperature measurement 197

Figure (5.5): The flow measuring equipment for gas sampling . 197

Figure (5.6): The 8 turn coil within the 60 mm diameter combustion chamber 198

Figure (5.7): Variation of "Top hat" container upper surface temperature with time during three experimental runs 199

Figure (5.8): Variation of exhaust gas temperature with time during three experimental runs 200

Figure (6.1): Flame stability characteristics for metallic matrix system and 60 mm diameter hemispherical combustion chamber
0 revs/min matrix rotational speed 234

Figure (6.2): Flame stability characteristics for metallic matrix system and 60 mm diameter hemispherical combustion chamber
0.6 revs/min matrix rotational speed 235

Figure (6.3): Flame stability characteristics for metallic matrix system and 60 mm diameter hemispherical combustion chamber
1.2 revs/min rotational speed 236

Figure (6.4): Flame stability characteristics for the metallic matrix system and 60 mm diameter hemispherical combustion chamber
2.4 revs/min matrix rotational speed 237

Figure (6.5): Flame stability characteristics for the metallic matrix system and 60 mm diameter hemispherical combustion chamber
4 revs/min matrix rotational speed 238

Figure (6.6): Effect of matrix rotational speed on the metallic matrix system stability characteristics (60 mm i.d. hemispherical combustion chamber) . . 239

Figure (6.7): Leakage rates to the surrounds during hot operation of the metallic matrix system 240

Figure (6.8): Flame stability characteristics for the ceramic matrix system and 60 mm i.d. hemispherical combustion chamber
0 revs/min matrix rotational speed 241

Figure (6.9): Flame stability characteristics for the ceramic matrix system and 60 mm i.d. hemispherical combustion chamber
0.6 revs/min matrix rotational speed 242

Figure (6.10): Flame stability characteristics for the ceramic matrix system and 60 mm i.d. hemispherical combustion chamber
1.2 revs/min matrix rotational speed 243

Figure (6.11): Flame stability characteristics for the ceramic matrix system and 60 mm i.d. hemispherical combustion chamber
2.4 revs/min matrix rotational speed 244

Figure (6.12): Effect of matrix material and geometric configuration on the stability characteristics . 245

Figure (6.13): Predicted and experimental stability characteristics for the ceramic matrix system with the 60 mm hemispherical combustion chamber . 246

Figure (6.14): Effect of combustion chamber size and geometric configuration on the ceramic matrix system stability characteristics (1.2 revs/min case) . . 247

Figure (6.15): Effect of heat abstraction on the stability characteristics of the ceramic matrix, 60 mm diameter hemispherical combustion chamber system (1.2 revs/min) 248

Figure (6.16): Flame for inlet flowrate of 168 cm^3/s and non-limiting mixture 249

Figure (6.17): Flame for inlet flowrate of 81 cm^3/s and limiting mixture 249

Figure (6.18): Flame for inlet flowrate of 384 cm^3/s and non-limiting mixture 250

Figure (6.19): Flame for inlet flowrate of 384 cm^3/s and mixture composition approaching the limiting . . 250

Figure (6.20): Flame for inlet flowrate of 384 cm^3/s and limiting mixture 251

Figure (6.21): Flame for inlet flowrate of 790 cm^3/s and non-limiting mixture 251

Figure (6.22): Flame for inlet flowrate of 790 cm^3/s and limiting mixture 252

Figure (B.1): Force acting on the rotor in the horizontal plane (forces in the vertical plane are not shown) . . 280

Figure (B.2): Frictional forces acting between the upper and lower circumferential seals and the rotor upper and lower surfaces respectively 281

Figure (D.1): Combustion chamber dimensions 292

Figure (D.2): Simplified burner geometry for calculation of heat losses from the system 292

Figure (F.1): Predicted stability characteristics corrected for leakages (i.e. in terms of actual flowrates through the matrix) 318

List of Tables

Table (6.1) 221

Table (6.2) 226

Table (6.3) 229

Table (A.1) 266

Table (A.2) 270

Table (A.3) 272

Table (C.1) 283

Table (C.2) 283

Table (C.3) 284

Table (C.4) 284

Table (F.1) 297

Table (F.2) 314

Table (F.3) 316

Table (F.4) 317

Introduction

In the course of this research programme the design and characterization of a novel burner were undertaken. This burner is capable of sustaining stable unaided combustion in premixed gaseous fuels of composition below that of their normal lower flammability limit.

Normally such potential fuels are non-combustible due to the deleterious effect of the diluent heat capacity on the reaction temperature. The resultant low temperatures adversely affect the reaction rate which is strongly dependent on temperature according to an Arrenius law. The range within which fuel-air mixtures are combustible have been shown to be dependent on factors such as prereaction mixture temperature, system pressure and diluent nature (I.1, I.2, I.3). Increase in prereaction temperature results in lowering of the lower flammability limit and elevation of the upper one. For a variety of gaseous hydrocarbon fuels the lower limit was observed to decrease linearly with increasing prereaction or unburnt temperature (I.2). Lean fuel-air mixtures can, therefore, be rendered flammable if they are supplied with the required amount of preheat.

For combustion to be self sustained, preheat must be obtained from within the burner system and the obvious source is the heat carried by the combustion products. Heat transfer from products to reactants, but without dilution of the reactants, necessitates the existence of a heat exchanger keeping the two streams separate.

In the heat exchanger-burner system developed here, a rotary regenerator was employed as the heat exchanger. In rotary regenerators, heat exchange is achieved by heat being continuously stored in, and removed from, a solid medium which is a matrix rotating across the two ducts carrying the cold and hot gases. The passages of rotary regenerator matrices can be of very small diameter and, therefore, large heat transfer area per unit volume of matrix can be provided. This results in units which are compact and of low capital cost.

The development of burners, such as the rotary regenerator burner, that are able to burn lean fuel mixtures, would greatly contribute to the reduction of fossil fuel consumption and also prevent some particularly undesirable pollutants from being released to the atmosphere. As an example of the potential for energy saving, we may consider that the methane content of the ventilation air from mines would alone be adequate to provide the entire power requirements of the colliery machinery in Britain (I.4).

More generally, lean hydrocarbon-air mixtures are produced from a wide variety of industrial processes and are either exhausted to the atmosphere or incinerated with the help of additional fuel. In large chemical and petrochemical plants, lean hydrocarbon air mixtures are produced both during normal operation at steady state, and also during start-up or shut-down. For example, the exhaust gases from an ammonia plant contain hydrogen, nitrogen, methane and argon. At present these gases are mixed with natural gas and incinerated. A heat recirculating burner has

the potential to burn them on their own and also provide heat for other uses. Heat would, therefore, be produced from a fuel of "negative cost".

Other examples of lean fuel mixtures, that can be rendered flammable by heat recirculation, are gases from driers and methane-air mixtures from fermanting wastes.

Finally, heat recirculating combustion systems, burning very lean mixtures, could be used for room heating. No pollutants are generated due to the low temperatures in these burners and the saturated vapour pressure of conventional liquid fuels would be quite sufficient to enable air saturated with fuel at room temperature to be burned without previous atomisation or pumping. The humidification, heating and sterilization, for example, at hospital atmospheres by injecting a small proportion of hydrogen-rich fuel into the air before its passage through the burner was considered (I.6).

Heat recirculating burners, from a fundamental point of view, elevate any substance capable of even the smallest exothermic reaction to the status of fuels. Clearly, however, the smaller the heat content of the mixture, the more effective the heat exchanger that has to be used for its combustion.

Chapter 1

Combustion in heat recirculating burners

1.1. Introduction

The general principles and benefits of combustion with heat recirculation from products to reactants are developed. Two different methods of imparting combustion energy to the reactants (i.e. with and without dilution of reactants by products) are contrasted.

The combustion of fuel mixtures below the lower flammabilty limit, which is the purpose in this project, is shown to be possible in heat exchanger burner systems. The thermodynamics of such systems are developed and a theory predicting their stability characteristics is described.

A survey of the literature on burners recirculating heat alone is presented and the reasons for selecting a rotary regenerator as the heat exchanger of the system under investigation are given.

1.2. Principles of combustion with heat recirulation

In ordinary premixed flames the flame temperature is absolutely associated with the heating value of the fuel and the initial mixture strength. Refering to figure (1.1a) the adiabatic

final flame temperature for unit mass of mixture can be obtained from the following:

$$Q_c = H_f - H_i = \int_{T_i}^{T_f} c_{pgp}\, dT \qquad (1.2\text{-}1)$$

where Q_c : heat of combustion (J)

c_{pgp}: specific heat capacity of products at constant pressure (J/Kg K)

H: enthalpy (J/Kg)

T: temperature (K).

Subscripts f and i refer to the final and initial states respectively, the latter being synonymous in this case with T_u (unburnt) and the former with T_m (maximum). It is important to work in terms of enthalpy so as to avoid taking into account dissociation which is important at high combustion temperatures. This absolute dependence of flame temperature on fuel-air ratio can, however, be eliminated if the further variable of energy addition to the reactants is introduced. Energy can be imparted by such methods as radiation, adiabatic compression and electrical heating but of greater economic viability is the recirculation of some of the combustion energy (1.1).

One of the most frequently used methods, based on the above principle, for increasing the flame temperature and, therefore, the reaction rate, is the recirculation of some of the hot reaction products. Vortexing and consequently mixing of products with reactants is induced at the appropriate region in the burner by means of a baffle or a change in the contour of the combustion

chamber. In this case, however, preheating is accompanied by dilution of the reactants by products. The two proceed simultaneously as during ordinary flame propagation. Since the reaction rate depends on temperature according to an Arrhenius type relationship, i.e. exp (-E/RT), for small admixtures of products, it is much more temperature than composition dependent. As more products are admixed, however, the increase in the reaction rate increasingly falls short of that which can be achieved by recirculating heat alone. This is quite apparent from the different shapes of the curves in figure (1.2)(1.2). Curves A and B give the variation of reaction rate with heat recirculation, alone and by recycling hot products respectively. While the difference between the two is not significant for small amounts of recycle, a point is reached in the case of recycling products when the rate does not increase any further. The rate is decreased by dilution more than it is increased by the small remaining temperature increment.

The concept of heat recirculation, as used in this project, involves transfer of heat from the burnt gases back to the new reactants without the limiting effect of physical mixing and dilution. The presence of a heat exchanger keeping products and reactants separate is thus basic to the subject of this thesis.

Introduction of a heat exchanger between products and reactants results in the enthalpy profile along the flow coordinate of the exchanger-burner system to be as shown in figure (1.1b). The maximum flame temperature is increased and its value depends on the amount of heat, Q_r, "borrowed" from the products

(1.5). A common feature of the burners in figure (1.1) is that $H_f = H_i + Q_c$ because, in the steady state, and in the absence of heat losses, the exit enthalpy must correspond to the total energy input.

Heat recirculating burners such as the one in figure (1.1b) have been described by the term "excess enthalpy burners" (1.5, 1.6), the reason for this being that the enthalpy of the flame is in excess of both reactants and products.

The heat recirculated to an excess enthalpy flame can theoretically be made arbritarily large simply by extension of the heat exchanger area. In practice, however, reaction in premixed reactants will proceed as soon as the temperature is sufficiently raised. This might occur before the whole area of the exchanger has been utilized. Such pre-ignition limits the maximum excess enthalpy attainable by effectively reducing the size of the heat exchanger. In addition the melting points of materials of construction and the formation of high temperature pollutants, such as nitric oxide, place an upper limit to the maximum amount of recycle. In this project limitations of this nature, i.e. associated with very high temperatures, do not apply. Heat recirulation will not be used to augment flame temperatures of flammable mixtures but instead to stablize flames within normally non-flammable lean fuel-air mixtures.

As mentioned in the introduction, mixtures of hydrocarbons and air are only flammable with certain ranges of composition which have been shown to depend on the initial temperature of the mixture.

An experimental study by Smith (I.2) resulted in the important finding that the lower limit is a linear function of the initial mixture temperature. The fuel concentration at the lean limit decreases with increasing initial temperature of the mixture.

All fuels examined were shown to exhibit a negative temperature ceofficient of the limit, varying from - 0.0013% fuel K^{-1} for n-hexane, to - 0.0048% fuel K^{-1} for methane. The data obtained by Smith are replotted in figure (1.3). The overall conclusion that can be drawn from the above information is that all mixtures of practical interest can be rendered flammable by preheating the reactants to temperatures in excess of 1250 K. In an "excess enthalpy" burner this preheat can be provided from within the system, which means that such systems are potentialy capable of sustaining combustion, without the addition of extraneous energy, in mixtures below the lower flammabiltiy limit. Clearly, however, the leaner the mixture the larger the heat that would have to be recycled and, therefore, the more efficient the heat exchanger that would have to be employed. An additional factor limiting the leaness of mixtures that could be burned in a practical "excess enthalpy burner" is the rate of heat loss from the system.

It must, finally, be mentioned here that some heat recirculation occurs in virtually every kind of practical burner. Radiant flux from product gases with sufficient emissivities and hot furnace walls, is intercepted by the burner. This will, in turn, preheat the reactants. Because heat recirculation is always

present in combustion systems involving conduction within and radiation between solid surfaces, this sometimes affects other mechanisms that are being used for a certain purpose. Cyclone furnaces, designed for combustion of low grade fuels (1.3), involve the recycling of hot products rather than of heat alone, and are, therefore, not revelant to the subject of this thesis, except in so far as heat recirculation plays a part. It has been proven (1.4) that their behaviour can only be fully explained if the inevitable and appreciable contribution from recycling heat is taken into account.

1.3. Thermodynamic models of combustion in heat recirculating burners

The thermodynamic model of combustion in heat recirculating burners, originally developed by Hardesty and Weinberg (1.5, 1.6) was further extended by Malik (1.7).

In all the cases developed it is assumed that the flame is confined to the combustion chamber, that the heat exchanger is of the counter-current mode and that there is no dissociation of the molecules in the flame. The latter is well justified since for lean mixtures the burnt temperature is considerably less than 2000 K and the extent of dissociation is, therefore, small.

The two most realistic cases developed are as follows:

(a) The specific heat of the gases is variable and there are no heat losses.

The specific heat of a gaseous mixture is dependent on the temperature and composition of the mixture. To account for this variation, average specific heats for products and reactants between some reference temperature and the temperature of interest are used here.

With reference to the burner-heat exchanger system shown in figure (1.4), the heat balances in terms of enthalpies are:

$$M_g(H_{gu} - H_{gi}) = M_g(H_{gm} - H_{gf}) = Q_r \qquad (1.3\ 1)$$

$$M_g(H_{gm} - H_{gu}) = M_g(H_{gb} - H_{gi}) = M_g(H_{gf} - H_{gi}) = Q_c \quad (1.3\text{-}2)$$

where M_g: gas mixture mass flowrate (kg/s)

$H_{g\ subscript}$: gas enthalpy at a certain point round the system (J/Kg)

Q_r: Heat recirculated (J/s)

Q_c: Heat of combustion (J/s)

subscript i: refers to incoming gas

u: refers to unburnt mixture

m: refers to burnt gas

f: refers to exhaust gas

b: refers to burnt mixture but for adiabatic burner.

From solving eqn. (1.3-1) for H_u and substituting in eqn. (1.3-2) the following is obtained.

$$H_{gm} = H_{gb} + \frac{Q_r}{M_g} \qquad (1.3\text{-}3)$$

Since the specific heats are not constant but vary throughout the system, the driving force for counter-current heat transfer must be represented by a log mean temperature difference given by:

$$\Delta T_{glm} = \frac{(T_{gf} - T_{gi}) - (T_{gm} - T_{gu})}{\ln \frac{(T_{go} - T_{gi})}{(T_{gm} - T_{gu})}} \qquad (1.3\text{-}4)$$

The heat recycled is, therefore, given by

$$Q_r = U\ A\ \Delta T_{glm} \qquad (1.3\text{-}5)$$

where U: overall heat transfer coefficient (J/s m^2 K)

A: heat transfer area available (m^2).

Writing eqn. (1.3-3) in terms of temperatures and specific heats and substituting for Q_r from eqn. (1.3-5), the following is obtained.

$$T_{gm} = \frac{c_{pgpd} T_b}{c_{pgpm}} + \left[\frac{UA}{M_g c_{ppm}}\right] \frac{(T_{gf} - T_{gi}) - (T_{gm} - T_{gu})}{\ln \frac{(T_{gf} - T_{gi})}{(T_{gm} - T_{gu})}}$$

$$= \alpha_1 T_{gb} + \alpha_2 \frac{(T_{gf} - T_{gi}) - (T_{gm} - T_{gu})}{\ln \frac{(T_{gf} - T_{gi})}{(T_{gm} - T_{gu})}} \qquad (1.3\text{-}6)$$

where c_{pgpm}: average products specific heat between T_{gm} and reference temperature (J/Kg K)

c_{pgpb}: average products specific heat between T_{gb} and reference temperature (J/Kg K).

Equation (1.3-6) gives the maximum temperature in terms of two dimensionless quantities α_1 and α_2, the adiabatic flame temperature and the driving force for heat transfer. The quantity α_2 compares the ability of the exchanger to transfer heat, to the heat capacity of the gas. Since the value of T_m increases with increasing α_2, systems must be designed to maximise α_2.

(b) Heat is lost from several points round the system and specific heat of gases is constant.

In this case the heat losses from the cold and hot sides of the heat exchanger and the combustion chamber are accounted for.

The theoretical model, with reference to which the following heat balances can be written, is shown in figure 1.5.

$$M_g c_{pg}(T_{gf} - T_{gi}) = Q_c - Q_L \qquad (1.3\text{-}7)$$

$$M_g c_{pg}(T_{gu} - T_{gi}) = Q_r - Q_{L_1} \qquad (1.3\text{-}8)$$

$$M_g c_{pg}(T_{gm} - T_{gf}) = Q_r + Q_{L_3} \qquad (1.3\text{-}9)$$

$$M_g c_{pg}(T'_{gm} - T_{gu}) = Q_c \qquad (1.3\text{-}10)$$

$$M_g c_{pg}(T'_{gm} - T_{gm}) = Q_{L_2} \qquad (1.3\text{-}11)$$

For the adiabatic case

$$M_g c_{pg}(T_{gb} - T_{gi}) = Q_c \qquad (1.3\text{-}12)$$

From eqn. (1.3-10) and (1.3-12)

$$(T'_{gm} - T_{gu}) = T_{gb} - T_{gi} \qquad (1.3\text{-}13)$$

Substituting in the above for T'_m from eqn. (1.3-11) the following is obtained

$$(T_{gb} - T_{gi}) = \frac{Q_{L_2}}{M_g c_{pg}} + (T_{gm} - T_{gu}) \qquad (1.3\text{-}14)$$

Substituting for T_{gu} from eqn. (1.3-8) and dividing both sides by $T_{gb} - T_{gi}$, eqn. (1.3-14) becomes

$$\frac{T_{gm} - T_{gi}}{T_{gb} - T_{gi}} = 1 + \frac{Q_r}{Q_c} - \frac{Q_{L_1}}{Q_c} - \frac{Q_{L_2}}{Q_c} \qquad (1.3\text{-}15)$$

This gives the relation between the actual maximum temperature in the system and the adiabatic flame temperature.

The driving force for heat transfer is not constant, due to the heat losses from the cold and hot sides of the exchanger not being identical. The log mean driving force, for the counter-current heat exchanger under consideration here, is

$$\Delta T_{glm} = \frac{(Q_c - Q_{L_2}) - (Q_c - Q_L)}{M_g c_{pg} \ln \frac{Q_c - Q_{L_2}}{Q_c - Q_L}} \qquad (1.3\text{-}16)$$

Since $Q_r = U\ A\ \Delta T_{lm}$, substituting in eqn. (1.3-15) for Q_r gives

$$\frac{T_{gm} - T_{gi}}{T_{gb} - T_{gi}} = 1 + \frac{UA}{M_g c_{pg}} \left[\frac{Q_{L_1} + Q_{L_3}}{Q_c \ln \frac{Q_c - Q_{L_2}}{Q_c - Q_L}} \right] - \frac{Q_{L_1} + Q_{L_2}}{Q_c}$$

$$= 1 + \alpha \left[\frac{Q_{L_1} + Q_{L_3}}{Q_c \ln \frac{Q_c - Q_{L_2}}{Q_c - Q_L}} \right] - \frac{Q_{L_1} + Q_{L_2}}{Q_c} \qquad (1.3\text{-}17)$$

It is evident from eqn. (1.3-17) that the larger the value of α the larger the maximum temperature that can be achieved and, therefore, the leaner the mixture that can be burned. In going to gases of lower heat content the system losses become more important even though they might become smaller. The ultimate limit of operation is of course set by the approach of Q_c/Q_{L_2} to unity.

Both theoretical models, developed above, are only approximate. Throughout a heat recirculating combustion system, the temperature of the gases varies continuously. This implies continuous variation of the heat losses and specific heats, however such an analysis would be mathematically complicated. The heat exchanger employed might not be countercurrent and its exact geometry must be known. The heat transfer coefficient is a function of the geometry of the exchanger and also the operating conditions.

Finally the flame might not be confined to the combustion chamber. Depending on the heat-up rate, flowrate and composition of the reactants, flashback or blow-off might occur.

1.4. Stability characteristics of heat recirculating burners for combustion of lean fuel mixtures

The range of flowrates over which stable combustion can be sustained is a very important parameter for any burner, a wide range always being desirable. This is even more so with lean fuel burners as there would be little point in being able to initiate combustion in very lean mixtures if the reaction rate was so slow that blow-off occured at even the lowest flow-rates.

A theory that qualitatively predicts the stability characteristics of a family of heat recirculatinng burners was developed by S.A. Lloyd *et al* (1.8).

In establishing the theory the thermodynamic model shown in figure (1.5) was assumed to apply. It accounts for heat losses occuring from the hot and cold sides at the exchanger and the combustion chamber and assumes a constant gas specific heat.

Limiting the theory to any particular heat transfer mode was avoided by using a mean heat transfer coefficient, $\bar{h}$, with an arithmetically averaged temperature difference.

The heat balances describing the system in figure (1.5) were given in the previous section. It can be shown that

$$T_{gm} - T_{gi} = \frac{Q_r}{M_g c_{pg}} + \frac{Q_c}{M_g c_{pg}} - \frac{1}{M_g c_{pg}} (Q_{L_2} + Q_{L_1}) \qquad (1.4\text{-}1)$$

In this case the heat recirculated from the products to the

reactants is given by

$$Q_r = \bar{h}\, A \left[\frac{T_{gm} + T_{gf}}{2} - \frac{T_{gu} + T_{gi}}{2}\right] \qquad (1.4\text{-}2)$$

Writing eqn. (1.4-1) in terms of heat losses, Q_{L_1}, Q_{L_2}, Q_{L_3} and heat of combustion, Q_c, leads to

$$Q_r = \frac{\bar{h}\, A}{M_g c_{pg}} \left[Q_c - Q_{L_2} - \frac{1}{2}\,(Q_{L_1} + Q_{L_3})\right] \qquad (1.4\text{-}3)$$

To simplify the discussion it is assumed here that the flame reaction zone is thin such that $Q_{L_1} \to 0$. Substituting for Q_r in eqn. (1.4-1), $T_{gm} - T_{gi}$ can be written as

$$T_{gm} - T_{gi} = \left[1 + \frac{\bar{h}\, A}{M_g c_{pg}}\right] \frac{Q_c}{M_g c_{pg}} - \left[\frac{\bar{h}\, A}{2M_g^2 c_{pg}^2}\,(Q_{L_1} + Q_{L_3}) + Q_{L_1}\right] \qquad (1.4\text{-}4)$$

The heat of combustion, Q_c, can be written in terms of the volume fraction of the fuel in the mixture, f, the heat of combustion per unit volume of fuel, q_r, and the gas density ρ_g.

$$Q_c = \frac{f M_g q_r}{\rho_g} \qquad (1.4\text{-}5)$$

Substituting for Q_c in eqn. (1.4-4) gives

$$T_{gm} - T_{gi} = \left[1 + \frac{\bar{h}\, A}{M_g c_{pg}}\right] \frac{f\, q_r}{\rho_g c_{pg}} - \left[\frac{\bar{h}\, A}{2M_g^2 c_{pg}^2}\,(Q_{L_1} + Q_{L_3}) + \frac{Q_{L_1}}{M_g c_p^2}\right] \qquad (1.4\text{-}6)$$

The keystone of this theory is the experimental observation (1.8, 1.11) that, at least for certain heat recirculating burner systems and some fuels, the stability limit behaves in the same way as the flammability limit in stationary gases. Several authors (I.1, I.2) have previously reported that the lean flammability limit varies with initial mixture temperature in such a way that the final flame temperature remains constant for each fuel. The decrease in fuel required to maintain the mixture at the limit when the initial temperature is raised is such that the decrease in heat of combustion exactly balances the increase in thermal enthalpy. The constant flame temperature is of the order of 1400 K for methane.

The experimental observation that for certain heat recirculating burners (double spiral (1.8), spouted bed (1.11)) the flame temperature at the limit, irrespective of flow velocity, heat losses, or fuel concentration, remains constant for one fuel is rather surprising and unexpected. It implies that the criteria governing flame stability in fast flowing gases are similar to those applying to flammability limits in large volumes of stationary mixtures.

This behaviour has, however, been explained in terms of the ratio of preheating to combustor residence time (1.12). In both the above mentioned systems the cross-sectional area increases from a very small value in the heat exchanger to a very large one in the combustion chamber. The preheating time is small and consequently there is very little chance of ignition and combustion taking place before the combustor. In addition the

linear flow velocity in the combustion chamber can be made very small and it is this feature that causes the stability criteria to be similar to those governing the flammability limits.

The constant flame temperature at the low flammability limit was claimed to be attributable (1.10) to the limiting reaction rate being constant and, because of the high hydrocarbon combustion activation energy, much more temperature than composition dependent.

Returing to eqn. (1.4-6) it is obvious that for very high mass flowrates, i.e. as $M_g \rightarrow \infty$, $fq_r/\rho_g c_{pg}$ becomes equal to the constant $T_{gm} - T_{gi}$. This is the temperature rise across the flame front at the limit of flammability without preheating. At very high flowrates both heat transfer and heat losses become unimportant and T_{gm} is the normal adiabatic flame temperature at the limit of flammability. The fuel content, at high mass flowrates, must, therefore, tend towards its limit value of f_o. Hence for $M_g \rightarrow \infty$,

$$\frac{fq_r}{\rho_g c_{pg}} = T_{gm} - T_{gi} = \frac{f_o q_r}{\rho_g c_{pg}} \qquad (1.4\text{-}7)$$

If there are no heat losses from the system, substituting for $T_{gm} - T_{gi}$ from eqn. (1.4-7) in eqn. (1.4-6) gives

$$\frac{f}{f_o} = \frac{M_g c_{pg}}{M_g c_{pg} + \bar{h}A} \qquad (1.4\text{-}8)$$

which indicates that for very small mass flowrates f/f_o tends to $M_g c_{pg}/\bar{h}A$.

In the presence of heat losses and for $M_g \rightarrow 0$, dividing both sides of eqn. (1.4-6) by $T_{gm} - T_{gi}$ gives

$$\frac{f}{f_o} = \frac{\bar{h}A(Q_{L_1} + Q_{L_3})}{2M_g c_{pg}(T_{gm} - T_{gi})} \qquad (1.4\text{-}9)$$

which tends to infinity. In this case the heat recirculated becomes small by comparison to the heat lost, which must be supplied at very low throughputs by burning mixtures of higher fuel content. The statement that f/f_o in eqn. (1.4.-9) tends to infinity is not accurate, not only because the heat losses were assumed to be constant but also because fq_r reaches a maximum at the stoichiometric composition. The total heat lost from any system cannot be bigger than the heat input. The rate of heat loss depends on the system goemetry and temperature and the rate of mass flow. As the mass flowrate is decreased both heat input and heat loss decrease simultaneously.

The general theory developed above leads to a stability curve of the general form of figure (1.6).

In conclusion it must be mentioned that the above theory can only be considered as a crude approximation, but it is quite reasonable that it should provide one limiting idealization as the ratio of preheating to combustor residence time tends to zero. It is only valid for fuel mixtures outside the normal flammability limits since, for mixtures richer than the lean limit of

flammability, it predicts flames that are always stable. This of course is not true.

1.5. Previous work on heat recirculating burners for combustion of lean fuels

In the last fifteen years a considerable amount of research has been carried out with the object of burning lean fuel air mixtures in heat exchanger-burner systems.

Professor Weinberg in his 1971 paper (1.1) examined the relative merits of burning at high and low temperatures and concluded that high combustion temperatures would lead to high combustion intensities, high thermodynamic efficiency (in the case of conversion to power), high heat tranfer rates to surfaces on which dissociated species can recombine, high ionization and the opportunity of producing endothermic products by sudden quenching.

After considering several means of augmenting flame temperatures, he proposed that recirculating some of the combustion energy would be the most economically viable. He then contrasted recirculating combustion energy (a) by mixing of products with reactants and (b) by recirculating heat alone via a heat exchanger between the products and reactants. It was concluded that the latter would be more desirable since in the former the rate of reaction is eventually limited by the dilution effect.

It was finally proposed that such heat-exchanger burner

systems could be used for maintaining combustion in lean fuel-air mixtures.

The feasibility of burning well below the flammability limit was first demonstrated experimentally by Hardesty and Weinberg (1.5), in a system constructed of coaxial fused silica tubing surrounded by a silvered vacuum jacket. The transparency of silica in the infra-red, together with the large external surface areas associated with straight tubing made it difficult, however, to minimise heat losses from this system.

Lloyd and Weinberg (1.8, 1.9, 1.10) in their work on the combustion of lean fuel mixtures, tested several heat recirculating burners, all incorporating heat exchangers of different goemetries. They concluded, however, that the most effective and simplest configuration, was that of the "Swiss roll" burner. This consists of a spiral plate heat exchanger surroungding the combustion chamber and is shown in figure (1.7).

The "Swiss roll" burner can be visualized as a long straight countercurrent heat exchanger that has been wound round the central conbustion chamber. Each channel containing hot products is in contact with two channels containing cold reactants at different temperatures and *visa versa*. Heat transfer is, therefore, taking place across both sides of every channel.

The device is protected against heat losses from the sides by a layer of cold reactants and many surfaces are provided between the combustion chamber and the surroundings.

The stability characteristics of several "Swiss roll" burners were obtained with methane as the fuel. These are plots of

mixture flowrate versus percentage at the point just before extinction. They are reproduced here in figure (1.8). It is apparent from these graphs that even small "Swiss roll" burners are capable of sustaining combustion in extremely lean methane-air mixtures. In addition the range of flowrates over which stable combustion is achieved is very large. The stability curves of figure (1.8) were compared with predictions based on the empirical limiting flame temperature using a numerical model of heat transfer within, and heat loss from, the spiral with excellent agreement.

Proffesor Takeno *et al* (1.13, 1.14, 1.15) developed a methematical model for combustion within porous plugs or other systems which increase heat recycle by increasing the thermal conductivity within the combustion zone itself. The flame structure is, therefore, modified. Stability is governed by the burning velocity. As soon as the flow velocity exceeds the burning velocity, blow-off occurs.

In the "Swiss roll" burner, described previously, the flame is not modified in any way, since it has no way of knowing where the recycled heat originates and the stability is enhanced due to the small linear velocities in the large combsustion chamber.

Kotani and Takeno (1.16) carried out experiments in an axisymmetric tubular burner incorporating a ceramic tube bundle with four perforated ceramic plates, two on either side of the tube bundle. The tube bundle was employed for improving heat conduction within the flame zone and the perforated plates for preventing heat losses. During experiments the flame, depending

on flowrate and mixture strength, stabilized before, inside, and after the tube bundle. Stable combustion with mixtures down to 3% of methane in air by volume was achieved.

Kawamura *et al* (1.17) used a coaxial cylindrical tube counter-current heat exchanger with the reactant flow surrounding the product stream. In the absence of a combustion chamber as such, an annular flame stabilised where the reactants entered the outer tube. Under such conditions the limit was a function of flame speed. Stable combustion at quite high flow rates and with mixtures down to 4% of methane in air by volume was obtained.

Echigo *et al* (1.18) preheated reactants by radiation from a porous permeable wall to the burner body. The permeable wall was heated by the outflowing products. Combination in exceedingly lean city gas-air mixtures (down to 1% fuel by volume) was reported.

The systems described so far are not suitable for combustion of gaseous, solid and viscous liquid fuels that pyrolyse to solid or liquid products, since these would block the channels of the particular heat exchanger. Beds of moving particulates are ideal for burning such fuels, provided they can be arranged so that the particulates cross a flame in which any pyrolysis products are burnt.

For this Arbib *et al* (1.11) used a particulate bed of the spouted type for combustion of lean fuel mixtures. Their spouted bed burner was a cylindrical vessel that was open at the top, with a small centrally located orifice at the bottom and filled with particles. The jet of gas through the orifice caused a central

column of particles to rise at high velocity and emerge in the form of a fountain from the top of the bed. The particles then fell back onto the annular region between the spout and the wall and traveled slowly downward in a dense phase. When the bed was provided with a fuel-air mixture a conical flame stabilized where the fountain of particles emerged from the top of the bed. The small proportion of reactants percolating the descending phase formed an annular flat flame which was continuous with the main conical flame. Heat was recirculated to the incoming gas by the hot particles that were being entrained.

It was shown that the deeper the bed the leaner the mixtures that could be burnt. The leanest mixture burnt was approximeately 65% of the normal limit of flammability. An approximate gas temperature calculation revealed that the assumption of a constant limiting flame temperature was well founded.

1.6. Scope of this study on a rotary regenerator burner

The experimental and theoretical work on a number of heat recirculating burners has conclusively shown that in such systems flames can be stablized in very lean fuel mixtures and over a wide range of flow rates.

The requirements that led to the considerable efforts in developing such burners are (a) the conservation and more efficient use of a wider range of fuels and (b) the reduction in pollutant emissions. These are still of vital importance since

both at the present, and in the near future, the overwhelming proportion of all our energy will be released by combustion; it was 96% in 1975 and it is expected to exceed 80% even in 2000 (1.19)

In this project, pursuing again the subject of improving combustion efficiency and minimizing pollution, an alternative heat-exchanger burner system for lean combustion will be designed and tested. A rotary regenerator has been selected as the heat recycling medium. In rotary regenerators, as mentioned previously, exchange of heat between the hot and cold gas streams is accomplished by the exposure of a third medium, the porous matrix, alternately to the two flows. The heat flows successively into, and out of, the third medium which thereby undergoes a cycle of temperature. The passages in rotary regenerator matrices can be of very small diameters, which means that the heat transfer area to matrix volume ratio can be large, resulting in highly efficient and compact units of low capital cost. For this reason metallic rotary regenerators have attracted considerable attention, and have been developed and employed in a wide variety of commercial installations for duties such as space heating, heat recovery from medium temperature gas turbine and boiler plant waste gases. In addition, considerable research has been recently carried out by the British Steel Corporation in developing a ceramic rotary regenerator for the purpose of providing high temperature (up to 1100^{o}C preheat) combustion air to oil or gas fired steel reheating furnaces.

The reasons for which a rotary regenerator was selected, for the system under investigation here, are as follows:

(A) Stable combustion of extremely lean fuel mixtures requires (a) massive heat recirculation from products to reactants and (b) the heat losses from both the heat exchanger and combustion chamber sides to be as small as possible. Alternatively the area provided for heat transfer must be large and that for heat loss small. This is very much the case with rotary regenerators.

(B) Stable combustion of lean fuels at large throughputs requires (a) the heat exchanger passages to be small (so that preignition does not occur) and (b) the combustion chamber volume to be large so that stabiltiy is governed by low flammablility limit criteria. In a rotary regenerator burner the passages in the heat exchanger can in theory be as small as necessary without the detrimental loss of heat transfer area. In practice, of course, the minimum size is limited by pressure drop and ease of construction considerations. The combustion chamber volume is not related to the size of the exchanger and only heat loss considerations impose an optimum maximum.

(C) All the heat exchanger burner systems described in the previous section were built for purposes of laboratory reseach. Further research would, however, be required for the construction of practical systems of the rigidity and durabiltiy necessary for industrial units. As an example, a pilot plant scale "Swiss role" burner constructed at the

Sunbury Research Centre of British Petroleum (1.7) was found to have a tendency to buckle. Such problems did not arise with the laboratory scale system, whose construction was not very rigid allowing, therefore, differential thermal expansion.

Very little additional research would, however, be required for the construction of a practical rotary regenerator burner. Rotary regenerators have already received considerable attention and high temperature systems have been constructed.

In the course of this project the feasibility of using a rotary regenerator as the heat exchanger in a heat-exchanger burner system for the combustion of lean fuel mixtures was investigated. A simple laboratory scale rotary regenerator burner was designed and constructed for this purpose. The stability characteristics of the burner, i.e. mixture flowrates versus percentage of fuel by volume at extinction, both with a metallic flame trap matrix and a tubular ceramic matrix, were determined for five matrix rotational speeds.

The effect of size and goemetry of the combustion chamber on the stability characteristics was investigated by carrying out experiments with two hemispherical chambers of different volumes and one cylindrical one. The validity of the theory of a constant limiting flame temperature was examined by accurately measuring gas temperatures in the combustion chamber with a suction pyrometer.

Analysis of the product and combustion chamber gases was

performed for determining the combustion efficiency of the system and for obtaining estimates of the rates at which leakages to the environment and interleakages occured.

The process of flame stability in the combustion chamber was further examined by using a transparent quartz combustion chamber that rendered the flame visible for photography.

Finally the possibility of burning lean fuel mixtures with simultaneous heat abstraction was investigated.

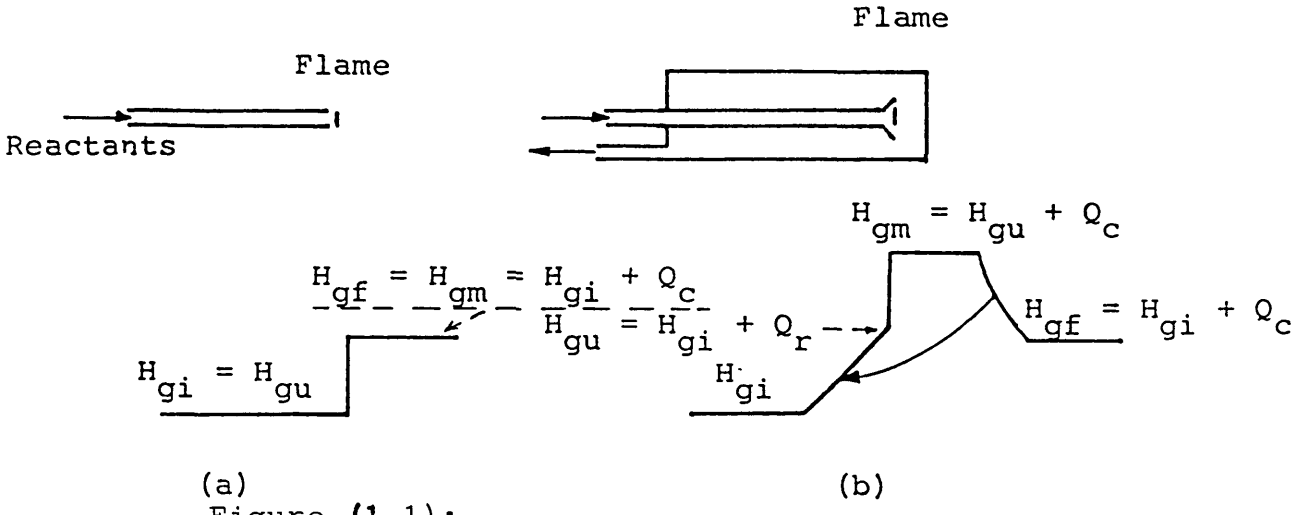


Figure (1.1):
Enthalpy profiles in ordinary and heat recirculating burners

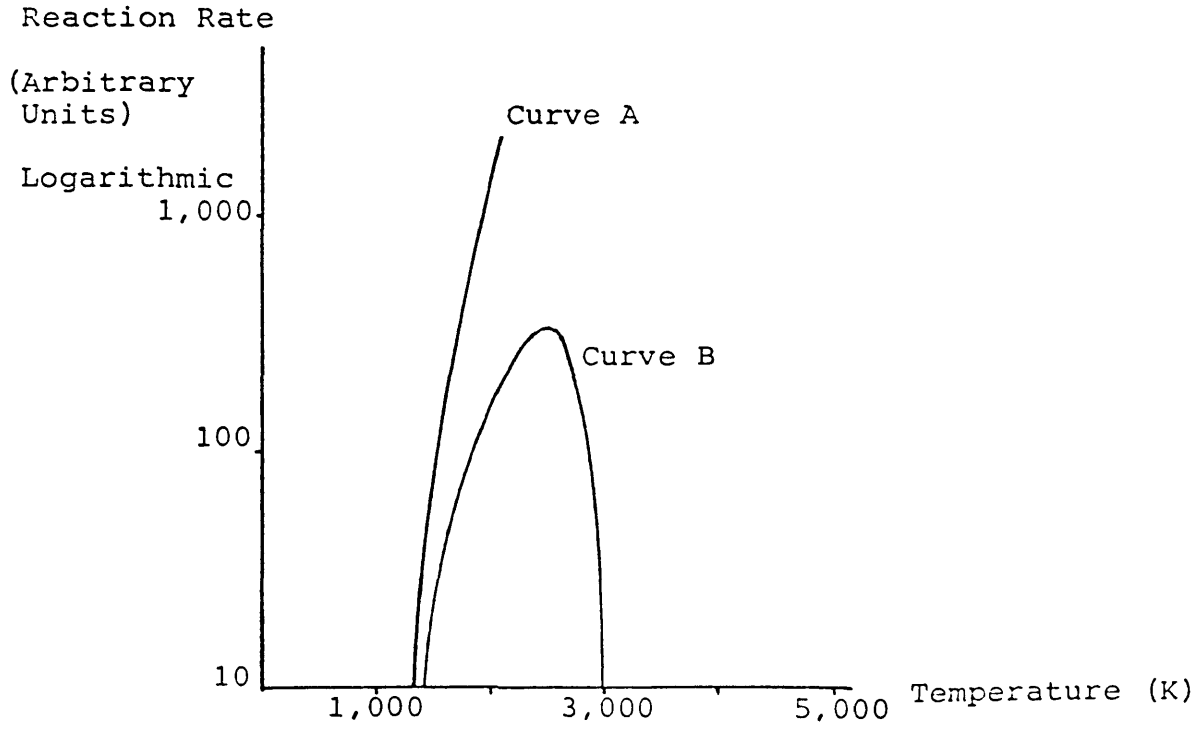


Figure (1.2):
Variation of reaction rate with temperature, with (B) and without (A) depletion of reactants

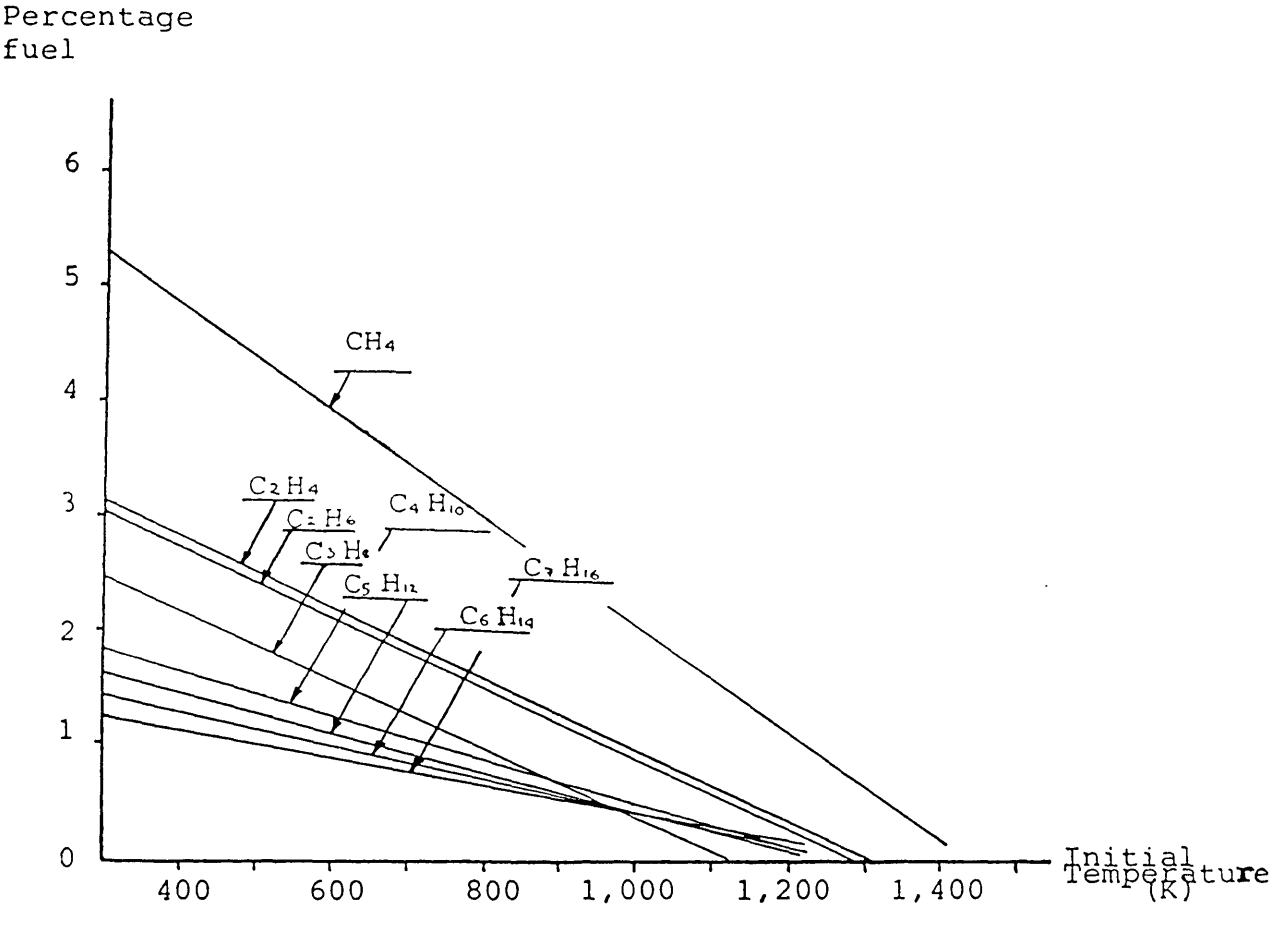


Figure (1.3):
Flammability limits (percent fuel by volume) for hydrocarbon/air mixtures as a function of initial mixture temperature

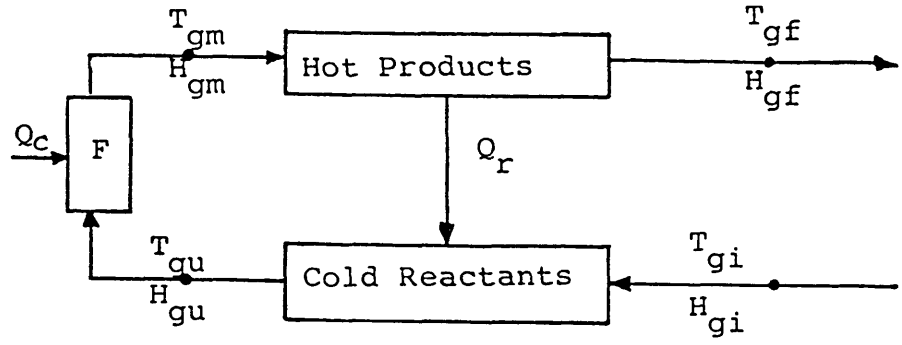


Figure (1.4):
Thermodynamic model for variable specific heat and no heat losses

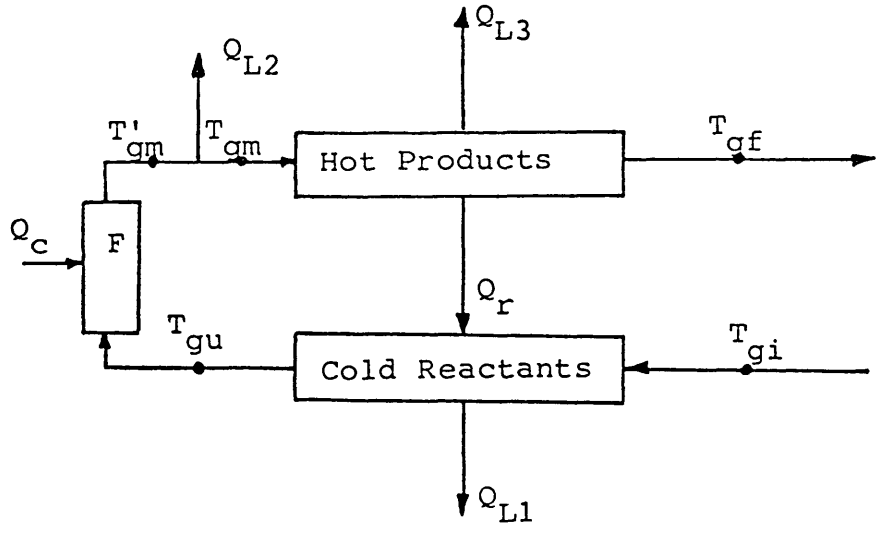


Figure (1.5):
Thermodynamic model for constant specific heat and heat losses from several points

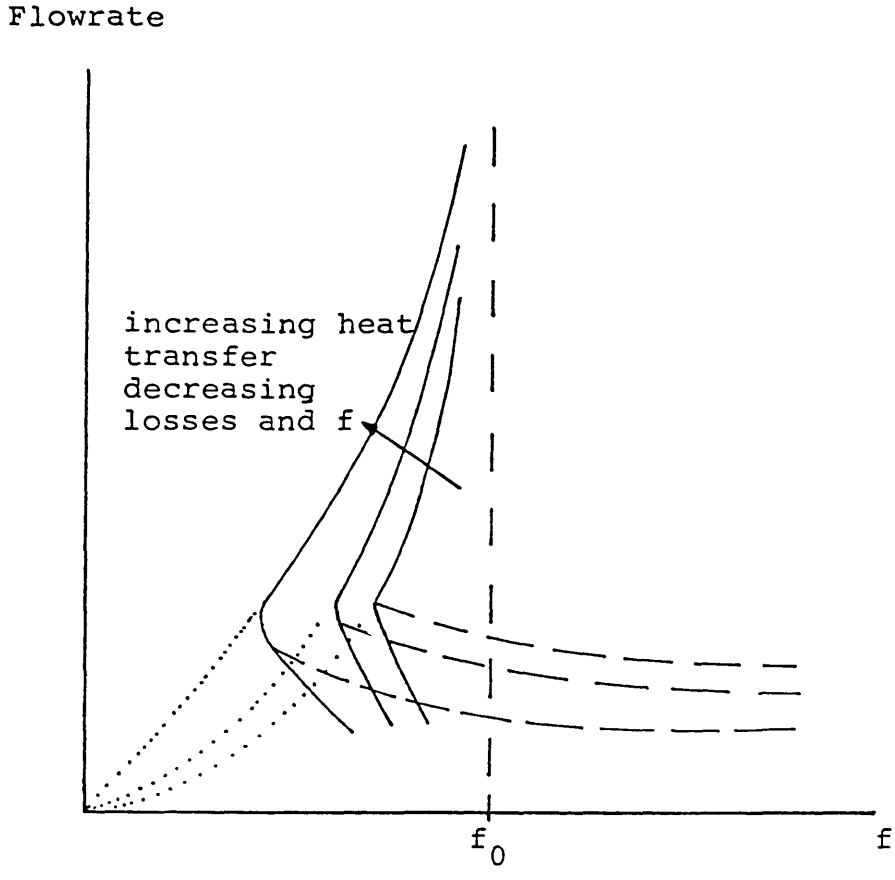


Figure (1.6):
Characteristic stability curves for burners with heat recirculation

—— —— —— flowrate tends to zero

..... heat losses tend to zero

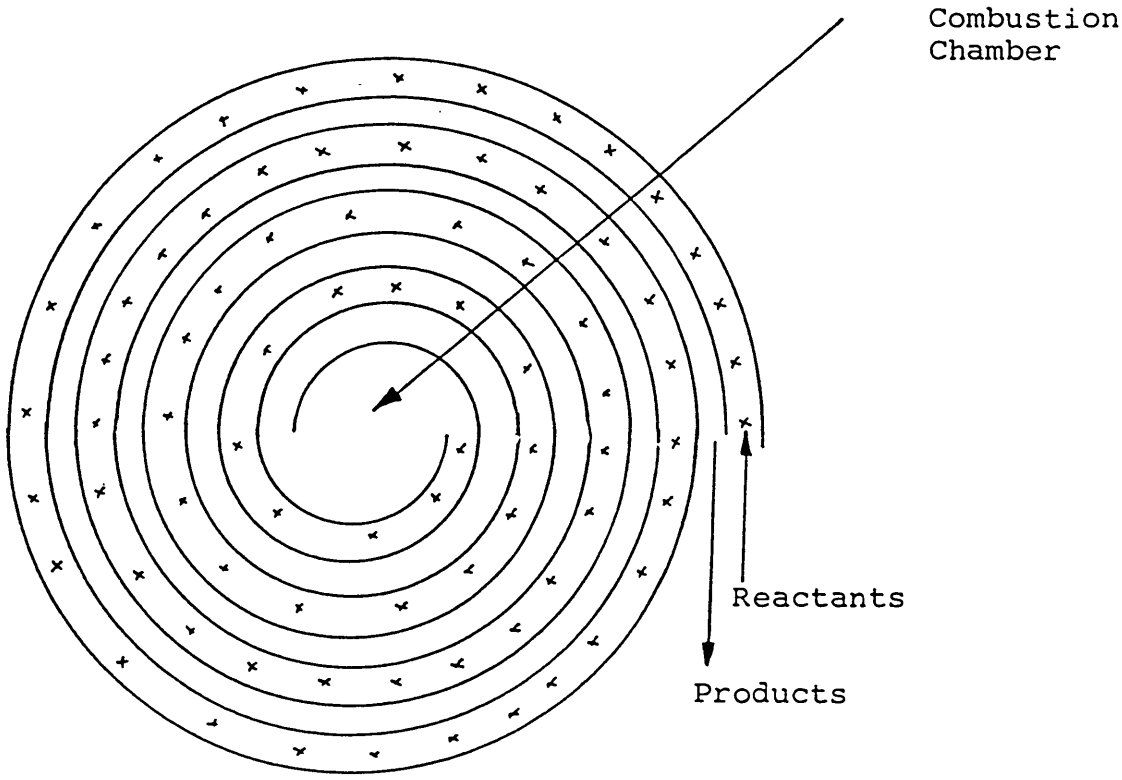


Figure (1.7):
"Swiss Roll" burner

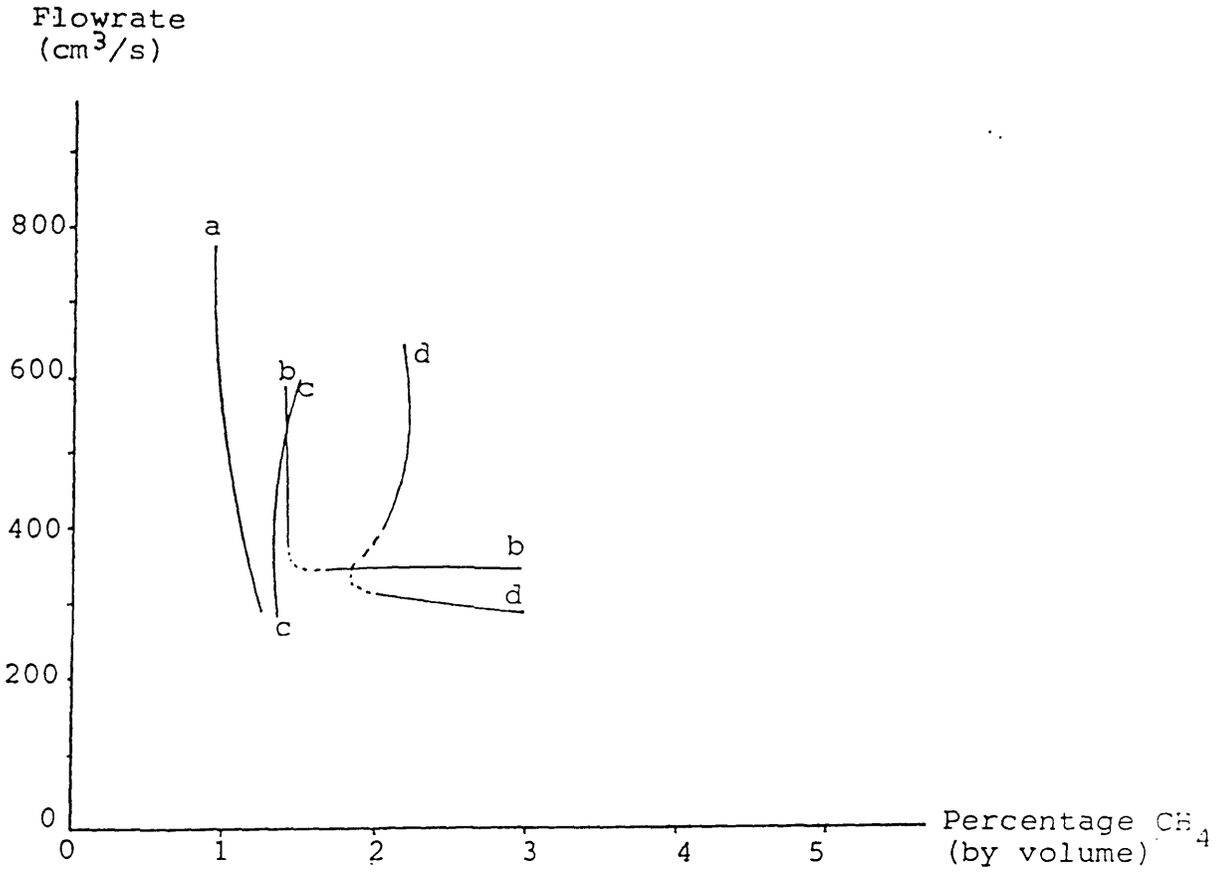


Figure (1.8):
Experimental stability characteristics of several "Swiss roll" burners

(a) Nine turn spiral in a dewar vessel
(b) Eight turn spiral in mineral wool insulation
(c) Thirteen turn spiral in mineral wool insulation
(d) Four and a half turn spiral in mineral wool insulation

CHAPTER 2

High Temperature Rotary Regenerators

2.1. Introduction

The principles of operation of the rotary regenerator are described and the partial differential equations governing heat transfer within the solid matrix are presented.

Rotary regernators are contrasted to ordinary recuperators and are found to offer, for the same heat transfer area, lower thermal efficiencies, but to be capable of providing much larger heat transfer areas per unit volume.

The methods that have been employed for the thermal design of rotary regenerators are mentioned, but special attention is given to a method applicable here and developed by the British Steel Corporation (B.S.C.), for high temperature ceramic rotary regenerators.

Finally the mechanical problems associated with high temperature regenerators and the mechanical design features employed to solve them by B.S.C. are described.

2.2. General on rotary regenerators

In ordinary heat exchangers, also called surface heat exchangers or recuperators, the two fluids exchanging heat energy are separated by a solid wall. In regenerators, however, the same space is alternately occupied by two gas streams. (Regenerators for liquids do not seem to be used.) During the so-called "heating-up" period the warmer gas delivers heat to the walls confining it or to solid matter distributed over the space. This heat is then removed by the colder gas during the cooling period.

This system has the advantage that the heat does not have to pass through a wall but is stored and released in the solid, penetrating it to a depth that will vary according to the operating conditions. Static regenerators have been used as air preheaters in open-hearth and blast furnaces providing air preheats of up to 1100^{o}C, as well as in plants for liquefaction and separation of gases at cryogenic temperatures (2.1).

With static regenerators, continuous operation can only be achieved if more than one (at least two) units are used. A number of switching values and connecting ducts are also required and these tend to complicate the system, introducing significant dead spaces. Cycling output temperature is a further drawback. Continuous operation with a single regenerator unit can, however, be achieved in rotary regenerators in which a solid matrix rotates through the hot and cold gas streams, continuously undergoing heating and cooling.

Rotary regenerators may be classified according to whether the fluids flow axially or radially (2.2). In the axial or disk regenerator shown in figure (2.1a) the matrix is built in the shape of a disk. The disk is mounted coaxially in a round cylinder divided into two ducts. The two gases flow countercurrently through the matrix which is rotated by means of an external drive. Any point in the matrix passes alternately through the two streams carrying heat from one side to the other. In the radial or drum regenerator, shown in figure (2.1b), the gases flow radially and countercurrently through the cylindrical matrix, which is coaxially mounted with two round ducts. The inner duct and the annular space are divided in the axial direction into two parts, one for the cold fluid and the other for the hot fluid.

Whilst the priciple of operation of the regenerator allows an unlimited choice of the materials and form of the heating surface, operating temperatures, nature of gases and the need for a uniform structure of predictable performance must be considered before the best matrix for the particular duty is selected.

Depending on the temperature range over which the regenerator is operated, plastic, metalic and ceramic matrices have been used. For low temperature applications, such as air conditioning, polyethylene terephthalate polyester film matrices have been used (2.3). In rotary regenerators, operated at hot gas temperatures of up to 500-600^{o}C, preheating air for gas turbines (2.4) and boilers (2.5), metallic and ceramic matrices have been employed. For even higher air preheat, temperatures, from furnace gases of a

corrosive and abrasive nature, ceramic matrices are absolutely necessary. A novel ceramic rotary regenerator developed by the British Steel Coorporation provides air preheats of up to 770°C from waste gases at 1200°C (2.6).

The selection of the best heating surface geometry, for any particular application, is governed by criteria such as:

(a) The structure must be uniform, easily fabricable and of predictable performance.

(b) Pressure drops must be acceptable.

(c) Regenerator must be cost effective.

(d) The ratio of heat transfer area to matrix volume must be high.

For metallic matrices, a wide range of surface geometries have been used. Units with metallic flat plate, flame trap, cylindrical tube and wire mesh matrices are only a small sample of the various types of rotary regenerators described in the literature.

Ceramic matrices of complicated internal structure may be impossible to construct. Only simple geometry matrices, such as the flame trap matrix and the continuous channel matrix are being commercially used (2.6).

The single most important characteristic of both ceramic and metallic matrix rotary regenerators is that, without introducing large pressure drops and without being excessively bulky, they must provide very large heat transfer surface areas. The equivalent diameter of the matrix passages can be made quite small and by increasing their number and reducing their length the

pressure drops can be kept quite low. Shortness of length is considered good design practice for most types of surfaces (2.7). Rotary regenerators compare favourably in that respect with, for example, shell and tube recuperators (2.1). In these the heat transfer surface area can only be increased by either increasing the length or the number of the tubes. Their diameter is fixed due to availability restrictions and the necessity of avoiding contact between them. Increasing the length of the tubes increases the pressure drop and using a larger number results in increased bulk and investment costs.

The short matrix passages and the periodic reversal of flow within the rotary regenerators prevents any permanent flow stagnation regions in the matrix. As a consequence, continuous and effective self-cleaning of the passages takes place. This behaviour has been demonstrated convincingly in long service experience with Ljunstrom air preheaters, employed extensively in boilers with the dirtiest of fuels (2.7).

Rotary regenerators, when compared to ordinary recuperators, have several disadvantages which are as follows:

(a) The effectiveness of rotary regenerators (ratio of heat actually exchanged to heat that would be exchanged if the cold gas temperature at the exit was equal to the hot gas temperature at the entry) is smaller than that of a countercurrent recuperator (2.8) of the same area.

(b) With disk rotary regenerators, leakages can occur and they are of three types:

(1) Leakages to atmosphere. To prevent these, circumferential seals on both sides of the matrix are required.

(2) Interleakages. Depending on the relative pressure of the two gas streams, either cold or hot gas can enter the other stream. These leakages can be minimised by two tangential seals across both flat faces of the matrix.

(3) Carry over loss. An amount of gas, trapped within the rotating matrix, is carried over to the other side. These cannot be prevented but only reduced by operating the system at low rotational speeds.

The overall amount of leakage must be kept as low as possible and this loss proved to be the major development problem, especially with systems operating at high absolute and relative pressures. (In turbine systems 4 to 7 atm pressure differentials exist between the compressed air and low pressure exhaust gas) (2.7).

Despite the above, rotary regenerators appear to be the most economically viable means of recovering heat from high temperature exhausts, where ceramics of good heat corrosion and oxidation resistance are essential. Success in building ceramic recuperators has been limited due to difficulties in manufacturing ceramic shapes of any but the minimum degree of complexity, and in sealing and jointing the relatively small sections used in actual systems.

2.3. Thermal design of rotary regenerators

The differential equations describing the heat transfer process within a regenerator were derived by Hausen (2.9). Similar equations, but developed from the standpoint of their application to the rotary regenerator, were presented by Sogin, H. and Hussan, K.E. (2.2).

The assumptions involved in the derivation of the equations are as follows:

(a) Both the solid and gas phase are continuous and homogeneous. In practice the matrix may be considered homogeneous if the material is so finely divided that the sizes of the voids and individual solid elements are very small compared to the overall volume of the matrix.

(b) Regular periodic conditions of temperatures within the matrix are established. This means that the temperature at any point in the matrix solid repeats itself periodically. At each point in space, through which the matrix passes the temperature is independent of time.

(c) The temperature of the fluids at the entrances to the matrix is assumed uniform. The temperatures at the exit do vary from point to point.

(d) Heat transfer within the matrix only takes place between solid and gas and it is by convection. An element of the solid does not exchange any heat energy with the surrounding elements. Within each element the conductivity is infinite in the direction normal to the fluid flow and zero in the

direction parallel to the gas flow. This assumption is satisfied by either steel or ceramic matrices of small wall thickness (2.7).

(e) The convective heat transfer coefficient is constant in both streams. This means that influences of transients in the boundary layers and of variations in the gas properties are neglected. This assumption may be justified by the facts that the transients are of relatively brief duration and that the thermal properties of the gases change relatively little with temperature.

(f) Thermal expansion or contraction of the gases, during heating or cooling, changes their velocity as they pass through the matrix. The influence of these variations are omitted from the theory in order to simplify the mathematics. Calculations of Saunders and Smoleniec (2.10) indicate that this assumption is justifiable.

(g) The matrix is stretched out so that its motion is rectilinear and its shape is planar. The equations are directly applicable to the disk type regenerator.

For the derivation of the differential equations, an element of volume, of dimensions δx by δy and $\delta z = 1$ m, is considered. As can be seen from figure (2.2) the matrix length in the direction of the gas flow is l, the matrix velocity, in a direction normal to that of the gas stream is u_s and the fluid velocity is u_g.

Under steady state conditions, thermal energy is carried in the x-direction by the gas and in the y-direction by the solid and also the gas trapped in the interstices of the matrix element.

Heat balances round the element of figure (2.2) lead to the following being obtained for the solid, T_s, and gas, T_g, temperatures

$$\frac{\partial T_s}{\partial y} = \frac{h\, A'''}{u_s C'''_s} (T_g - T_s) \qquad (2.3\text{-}1)$$

$$\frac{\partial T_g}{\partial x} + \frac{u_s}{u_y} \frac{\partial T_s}{\partial y} = \frac{h\, A'''}{M''_g c_{pg}} (T_s - T_g) \qquad (2.3\text{-}2)$$

where h: heat tranfer coefficient (J/s m^2 K)

A''': heat transfer area per unit volume of matrix (m^2/m^3)

C'''_s: heat capacity of solid per unit volume of matrix (J/s m^3 K)

M''_g: gas mass flowrate per unit frontal area of matrix (Kg/m^2)

These are usually expressed in terms of the dimensionless length, ξ, and time, η, defined by:

$$\xi = \frac{h\, A'''}{M''_g c_{pg}} x \qquad (2.3\text{-}3)$$

$$\eta = \frac{h\, A'''}{C'''_s} \left[\frac{y}{u_s} - \frac{x}{u_g}\right] \qquad (2.3\text{-}4)$$

In terms of ξ and η, eqns. (2.3-1) and (2.3-2) become

$$\frac{\partial T_s}{\partial \eta} = T_g - T_s \qquad (2.3\text{-}5)$$

$$\frac{\partial T_g}{\partial \xi} = T_s - T_g \qquad (2.3\text{-}6)$$

These describe the heat exchange process in one side of the rotary regenerator. The overall problem of heat exchange within the system requires two sets of these equations for its solution.

In a rotary regenerator the duration of time for which a point in the matrix is affected by a given stream depends upon its distance, x, from the entrance of the fluid. A point in the matrix at x = 0 spends the full heating or cooling periods in the fluid stream, whereas a point at x = 1 stays a shorter time. These variable exposure times result in mathematical boundary conditions which are difficult to handle.

Before the advent of the computer, several workers attempted the solution of the above equations. A complete analytical solution, however, is not available and the particular solutions contained in the literature are, with one exception, obtained by graphical analytical methods (2.11-2.15).

In most studies the overall heat transfer performance of the regenerator is expressed as the heat transfer "effectiveness", ϵ, which, as mentioned previously, compares the actual heat transfer rate to the thermodynamically limited maximum possible heat transfer rate. This definition, for $C_{gc} \leq C_{gh}$, as is the case for the rotary regenerator, results in

$$\epsilon = \frac{1}{t_c} \int_0^{t_c} \frac{T_{gc} - T_{gc\ in}}{T_{gh\ in} - T_{gc\ in}} \qquad (2.3\text{-}7)$$

or alternatively

$$\epsilon = \frac{T_{gc\ out(Avg)} - T_{gc\ in}}{T_{gh\ in} - T_{gc\ in}} \qquad (2.3\text{-}8)$$

where C_g: gas heat capacity rate (J/s K)

t_c: cold gas time period (s)

and superscripts, c,h: refer to cold and hot gas streams

in, out: refer to incoming and outgoing gas

and Avg.: refers to an averaged value.

For design work it was found suitable to express the effectiveness in terms of the following non-dimensional parameters.

$$\epsilon = \phi \left[\frac{C_{gc}}{C_{gh}}, \frac{C_s}{C_{gc}}, \frac{(hA)_c}{(hA)_h}, \left[\frac{hA}{C_g}\right]_c \left[\frac{1}{1 + \frac{(hA)_c}{(hA)_h}} \right] \right] \qquad (2.3\text{-}9)$$

where C_s: solid heat capacity rate (J/s K)

The only rigorous analytical solution available is for the special case of $C_s/C_{gc} = \infty$ when the behaviour becomes identical in form to that of a counterflow direct-type exchanger (2.7)

The graphical-analytical solutions are limited in scope and some disagreement exists between the different design curves proposed. In recent years, however, the partial differential equations of the regenerator have been solved by finite difference methods using digital computers. Lambertson (2.16), Bahnke and Howard (2.17), Maclaine-Cross (2.18), Romie (2.19) and Mondt (2.20) have all developed models of different degrees of complexity and accuracy. In the finite difference method developed by Lambertson the rotary regenerator effectiveness was

computed by considering the metal "stream" in cross-flow with each of the gas streams as two separate but dependent exchangers. The coventional idealisations, mentioned earlier, were again assumed to apply. The effectiveness was thereby obtained for a range of the dimensionless parameters.

The method presented by Bahnke and Howard was similar to the above but the effect of longitudinal heat conduction in the direction of gas flow was accounted for.

The analysis developed by Mondt enabled the study of the effect of longitudinal thermal conduction and variable heat transfer coefficients and also provided temperature distributions as functions of space and time for transients as well as "steady-state".

Maclaine-Cross accounted for the effect on regenerator effectiveness of the fluid remaining within the interstices of the matrix,(i.e. the carry-over), after the end of any period. This effect is, however, negligible when the ratio of matrix to carry-over heat capacity is large.

Kays and London (2.21) summarize in tabular form the thermal effectiveness for rotary regenerators in terms of the usual non-dimensional groups. Their numerical results, based largely on the papers by Lambertson, Bahnke and Howard and Mondt, together give a complete description of the operation of rotary regenerators intended for use with the regenerative gas turbine engine.

For high temperature ceramic rotary regenerators, a mathematical model was recently developed at the British Steel

Corporation (2.6). In this model the heat conduction and, therefore, the temperature gradient within the solid in a direction perpendicular to the gas flow was accounted for by the use of an overall heat transfer coefficient, $\bar{h}$, developed by Hausen (2.11). It is defined so that the total heat transfer between the gas and the adjacent element of ceramic is equal to the product of $\bar{h}$, the effective heat transfer area of the element and the mean of the difference between the gas temperature and the mean temperature of the ceramic of the element.

The Hausen heat transfer coefficient, $\bar{h}$, is given by

$$\frac{1}{\bar{h}} = \frac{1}{h} + \frac{x}{6k}\psi \qquad (2.3\text{-}9)$$

where h is the coefficient for heat transfer by convection and radiation, x is the thickness of the solid wall and k is the ceramic thermal conductivity. The factor ψ expresses the influence of the very rapid changes of the solid temperature at the beginning of the cooling or heating periods. It was found by Hausen that within the solid wall of a regenerator matrix the temperatures during, for example, the cooling period, vary as shown in figure (2.3). As can be seen, at the start of the period the temperatures change rapidly, but gradually the rate of change decreases and becomes constant with time. The value of ψ is given (2.11) as a function of the thickness of the walls, the length of the heating and cooling periods and the thermal diffusivity of the solid. The thicker the walls and the shorter the periods, the more pronounced the effect of the rapid temperature changes. For

thin walls and/or reasonably long periods, $\psi = 1$.

In the B.S.C. model the variation of solid and gas temperatures and, therefore, their physical properties and gas pressures, through the thickness of the matrix, is allowed for by assuming the matrix to be composed of a number of thin discs as illustrated in figure (2.4). Rotation of the circular ceramic matrix is simulated by considering the matrix to be divided into a number of thin radial segments. Within each cell, thus defined, the solid temperature is considered to be uniform and the gas temperature is assumed to rise or fall from its entry to its exit value. Heat balances on both solid and gas phases, within each cell, give the changes in the gas and solid temperatures. The calculation proceeds along a column, concurrently with the gas stream. After all the quantities of interest are obtained from all the cells along a column, the calculation proceeds to the adjacent column on the right or the left, depending on the direction of rotation. The conditions of all the points within the matrix are, therefore, determined. The actual calculation procedure is quite involved and only an outline was presented above. The effect of variations of temperature, carry-over and leakage on the gas flowrates within the matrix and, therefore, the regenerator effectiveness is allowed for in this model.

By using the model, the influence of a number of design parameters on the regenerator effectiveness was determined. The effect of:

(a) Matrix rotational speed (ω),

(b) Matrix passage length to equivalent diameter ratio (l/de)

(c) Cold to hot side matrix frontal area ratio (A_{fc}/A_{fh}),

(d) Matrix passage equivalent diameter and wall thickness (d_e,x)

(e) Hot gas inlet temperature ($T_{gh\ in}$),

on cold gas effectiveness (ϵ_c) were computed to be as follows:

(A) **Effect of matrix rotational speed on cold gas effectiveness**

The main effect of changing the rotor speed, ω. while keeping the other parameters unchanged, is on the value of the solid to the cold gas heat capacity rate ratio, C_s/C_{gc}. With reference to figure (2.5), increasing the ratio C_s/C_{gc} by increasing the rotational speed increases the cold gas effectiveness, ϵ_c, but only up to a certain value of the ratio. Above this value the thermal performance of the regenerator remains virtually unchanged. For the conditions in the British steel regenerator the critical value for the ratio was found to be 2.

Figure (2.5) also shows that increasing the cold gas flux, G_{gc}, (cold gas mass flowrate per unit matrix cold side frontal area) adversely affects the effectiveness.

(B) **Effect of matrix length to passage equivalent diameter on cold gas effectiveness**

Increasing the value of l/de increases the value of ϵ_c. This is demonstrated in figure (2.6), where it is also apparent that the benefit of increasing l/de tends to diminish towards the higher l/de values. Figure (2.6) also shows that increased hot

gas flux, G_{gh}, (hot gas mass flowrate per unit matrix hot side frontal area) results in increased ϵ_c.

(C) **Effect of matrix cold to hot side frontal area ratio on cold gas effectiveness**

Changing the ratio A_{fc}/A_{fh} (i.e. changing the proportion of the matrix frontal area available for flow of the cold and hot gases), but keeping the gas flows constant, changes the values of G_{gc} and G_{gh}, whilst maintaining a constant solid to cold gas capacity rate ratio. Figure (2.7) illustrates how ϵ_c varies with A_{fc}/A_{fh} for two different G_{gc}. For the operating conditions of the British steel regenerator it was found that the maximum ϵ_c was obtained for $A_{fc}/A_{fh} = 1$.

(D) **Effect of matrix passage equivalent diameter and wall thickness on cold gas effectiveness.**

The effect of passage diameter, de, and wall thickness, x, on the performance of the regenerator is shown in figure (2.8) where the cold gas effectiveness of a matrix of 10 mm diameter and 3 mm thickness passages is compared to that for matrices of larger diameters and 5 mm thickness. As can be seen, increasing the passage diameter and wall thickness decreaces ϵ_c. This, however, is only so for small G_{gc} and G_{gh}. The effect is less predictable for large G_{gc} and G_{gh} due to the variation in the nature of the flow through the matrix passages.

(E) **Effect of hot gas inlet temperature on cold gas effectiveness**

The hot gas inlet temperature, as demonstrated in figure (2.9), does influence the regenerator performance and the higher its value the higher the resulting cold gas effectiveness.

In all of the above, gas leakages were ignored, but since they do affect the final level of performance of the rotary regenerator they should be considered and the B.S.C. model does allow for them. As mentioned previously, leakages occur from several points within the regenerator and for this individual leakages will be considered separately.

(a) The hot matrix face cold to hot gas leakage (cold gas at higher pressure) through the central dividing seal partially dilutes the incoming hot gas with hot "cold" gas. This causes the effective G_{gh} to increase and the inlet hot gas temperature to decrease. The net effect on the cold gas effectiveness is consequently dependent on the gas flux levels and the cold gas exit temperature. Figure (2.10) shows the effect of leakage on ϵ_c for a range of G_{gh} and G_{gc}. It can be seen that for low G_{gh} and G_{gc} there is an increase in ϵ_c with cold gas leakage but for higher values ϵ_c decreases.

(b) The cold face cold gas to hot gas leakage through the central dividing seal dilutes the outgoing hot gas and reduces the ingoing G_{gc}. The effect of this leakage on performance is therefore equivalent to reducing G_{gc}.

(c) Cold gas leaking to the atmosphere before passing through the matrix reduces G_{gc} and can, therefore, be treated as (b).

(d) Cold gas leaking to the atmosphere after passing through the matrix does not affect the performance of the regenerator as such.

(e) Hot gas leaking to the atmosphere before giving up heat to the matrix reduces the ingoing G_{gh}.

(f) Hot gas leaking to atmosphere after passing through the matrix has no effect on the regenerator effectiveness.

The effect of the matrix material was also investigated by using the model. It was found that changing from silliminite to a different material such as the alumina bonded silicon carbide made virually no difference to the thermal performance of the regenerator.

The validity of the model was assessed by comparing theoretical results to relevant experimental ones obtained from a pilot plant scale ceramic rotary regenerator (2.6). The results were found to be in good agreement throughout; the correlation coefficient, for example, between predicted and actual exit hot and cold gas temperatures was found to be 0.85. The data from the model can, therefore, be used with confidence for design purposes.

2.4. **Mechanical design of high temperature rotary regenerators**

The basic concept of operation of the rotary regenerator, as already mentioned, is quite simple. A porous matrix is rotated across the flow paths of the hot and cold gases. The energy storage matrix takes the form of a disk rotor and the gas streams are arranged to flow through the rotor in a counter current mode. A number of mechanical problems, however, arise during operation and engineering design plays a very important role in the

successful development of any rotary regenerator.

The nature and severity of the problems is dependent on the operating temperatures and pressures. In the rotary regenerator employed here, the hot products of the combustion of lean methane-air mixtures enter the matrix and impart heat to the mixture, originally at ambient temperature. At the hot face of the matrix, due to final flame temperature of about 1100^{o}C and depending on heat losses, the hot gases are at temperatures of the order of 1000^{o}C. On the opposite side of the matrix, gas at ambient temperature comes in contact with the hot solid. The gas pressures throughout the system are near atmospheric; the mixture inlet pressure (the highest pressure in the system) is only a few centimeters of water above atmospheric.

The ceramic rotary regenerator developed at the British Steel Corporation to preheat air for reheating furnaces and other high output fuel fired furnaces, was designed for operating conditions similar to those of the system evaluated herein. It is, therefore, anticipated that the mechanical problems overcome during the B.S.C. research programme will be similar to those of a large scale, practical, rotary regenerator, forming an integral part of a burner for lean fuel-air mixtures.

The problems associated with the B.S.C. regenerator and the mechanical design necessary to overcome them will be described here (2.6).

(A) **Matrix materials of construction**

The ideal ceramic for the matrix must have certain physical properties.

1. A matrix stress analysis indicated that tensile stresses of 30 MN/m^2 and compressive stresses of 26 MN/m^2 of thermal origin could be expected for their particular design configuration and operating conditions. The material should, therefore, be able to retain its fracture strength well above these limits over the range of operating temperatures.
2. The material must be inert to the air stream and waste gas stream. It must, therefore, be oxidation resistant over the operating temperature range and be able to withstand attack from CO, CO_2, Ferrous oxides, Sulphur oxides and acids, alkali compounds and other contaminants.
3. Along the matrix there are large temperature gradients and due to rotation the matrix is subjected to sudden temperature changes. The material should, therefore, have good thermal shock resistance.
4. To minimise leakage from and within the system, radial and circumferential rubbing seals are required on both sides of the matrix. The matrix material should be more resistant to wear than that of the rubbing seals.
5. Optimum thermal performance dictates the need for passages of diameter and wall thickness that are as small as possible. These, together with the need for a smooth surface finish (for better contact and less friction within rubbing seals), high strength and reasonable cost, due to fabrication difficulties, impose a limit on the range of materials that can be used.

6. For distortion of the matrix surfaces to be avoided the material thermal expension must be low.

After considering a wide range of possible alternatives, an alumino silicate at 45% alumina was successfully employed in the British Steel Corporation high temperature design. Other high temperature ceramics such as boron nitride, have been tried by other equipment developers.

(B) **Rotor design**

The rotor structure, carrying the solid matrix, due to the wide range of operating temperatures and the rotation, are subjected to complex non-symmetric thermal gradients, which result in high hoop and tangential stresses. For this and also for ease of fabrication installation and maintainance, large diameter rotors are usually constructed of a number of matrix elements retained within metallic cage-like structures. In the B.S.C. rotor rectangular heat storage blocks, supported on a metallic grid, form the matrix. Ceramic paper placed between the blocks allows free movement of blocks while at the same time it prevents leakages. The ceramic blocks are supported in the rotor assembly by square sectioned metallic bars which are passed through rectangular grooves in opposing faces of the blocks. Any gaps between the metal bars and the ceramic blocks are filled in with ceramic wool. The metallic supports form a simple parallel bar grid which runs in the rotor plane near the bottom of the rotor where the temperatures are lower. The parallel bar grid is simply supported on the rotor rim ring structure and the entire block assembly is compacted by mechanically or pneumatically actuated

radial compression rams. The assembly is mounted horizontally and is rotated by a drive mechanism acting on the rotor circumference.

High alumina content wear rings placed on both the top and bottom faces of the matrix, where the circumferential rubbing seals touch the matrix, minimised both matrix and seal surface wear.

(C) Sealing system design

Excessive leakage loss from the hot and cold faces of the matrix must be prevented. In the B.S.C. high temperature regenerator, the seal assembly on each face consists of a circumferential barrier against losses to the environment and a radial seal keeping the two streams separate. Thermal expansion of the matrix blocks and irregularities on the matrix faces are allowed for by using barriers composed of assemblies of ceramic seal blocks which are arranged in juxta position along static guide members and are biased into rubbing contact with the rotor face. The seal blocks are made of the same material as the matrix but slightly softer (fired at lower tmepreatures) so that through the rubbing action the seals wear preferentially. The guide members are U-shaped in cross section, they are supported on guide rails and they are cooled by compressed air.

Push rods pass through the guide rails and the U-shaped members, and provide a pivot for flexible motion and with spring assistance enable pressure to be applied to the seal blocks.

During the experiments with a 0.8 m diameter multi-segment ceramic rotor at the B.S.C., air leakages of 0 to 35 percent of the input air were recorded depending on the pressure difference

between the two gas streams. These high leakage rates were due to mechanical problems with the sealing arrangement described above. Even though the concept of the seal design is good, some further development work is required to improve the free movement of the seal block assembly that caused most of the probems during operation.

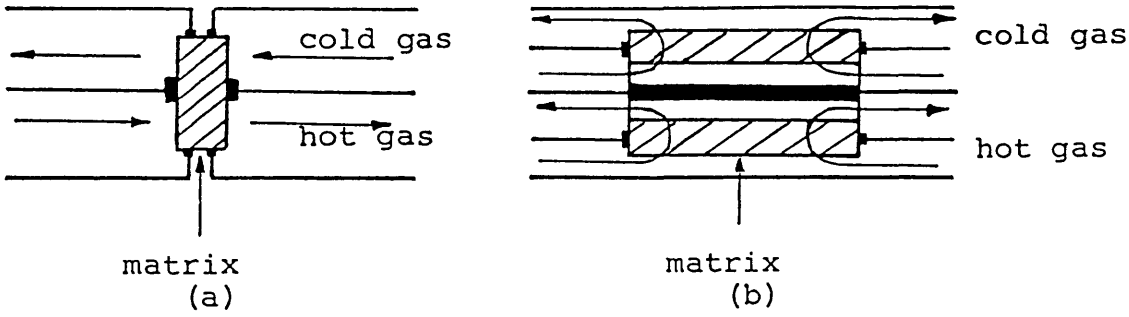


Figure (2.1):
Types of rotary regenerator
(a) disk type
(b) drum type

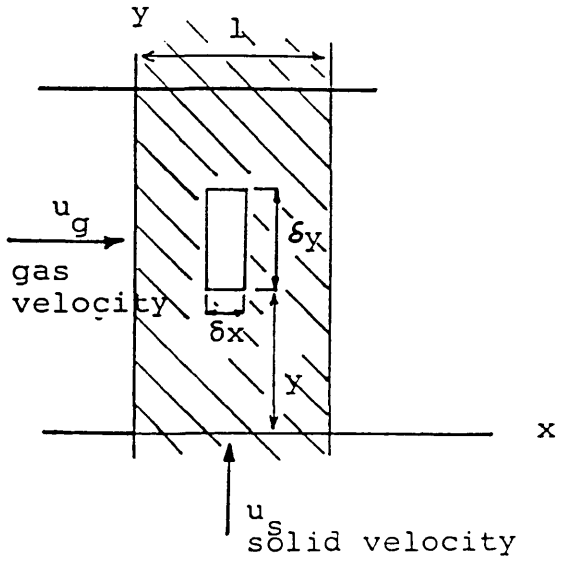


Figure (2.2):
Nomenclature for the plane matrix regenerator

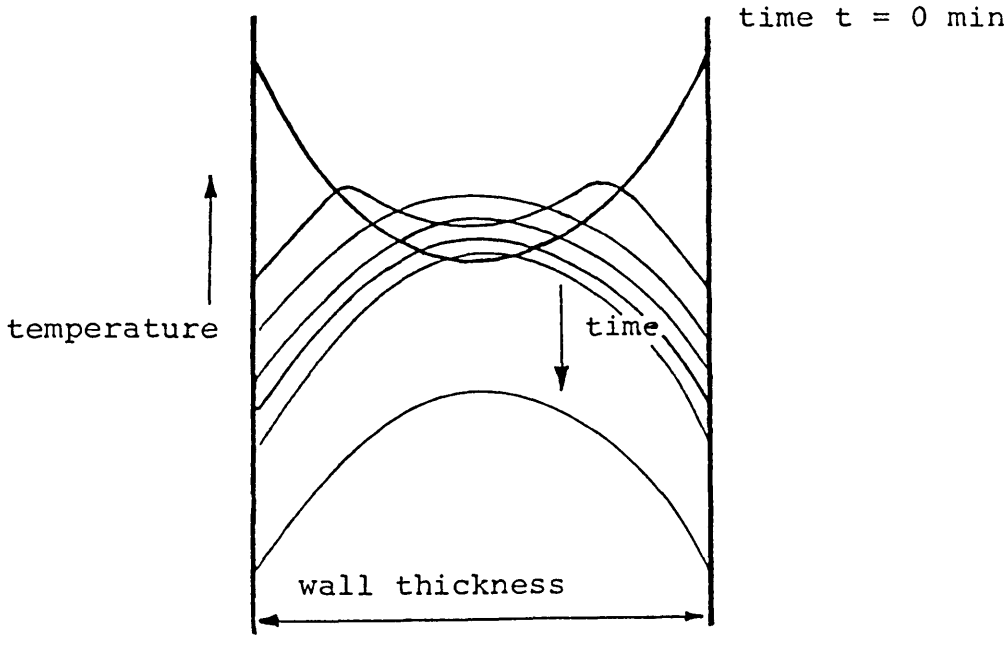


Figure (2.3):
Progress of temperature with time in a thick stone

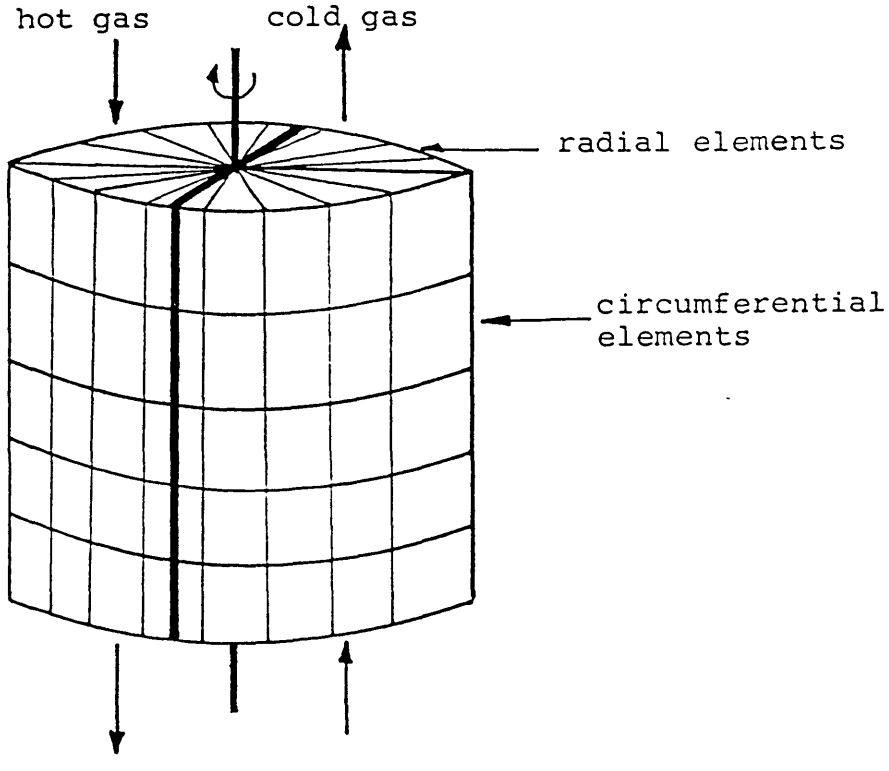


Figure (2.4):
Circumferential and radial elements for modelling of the heat exchange process within the matrix

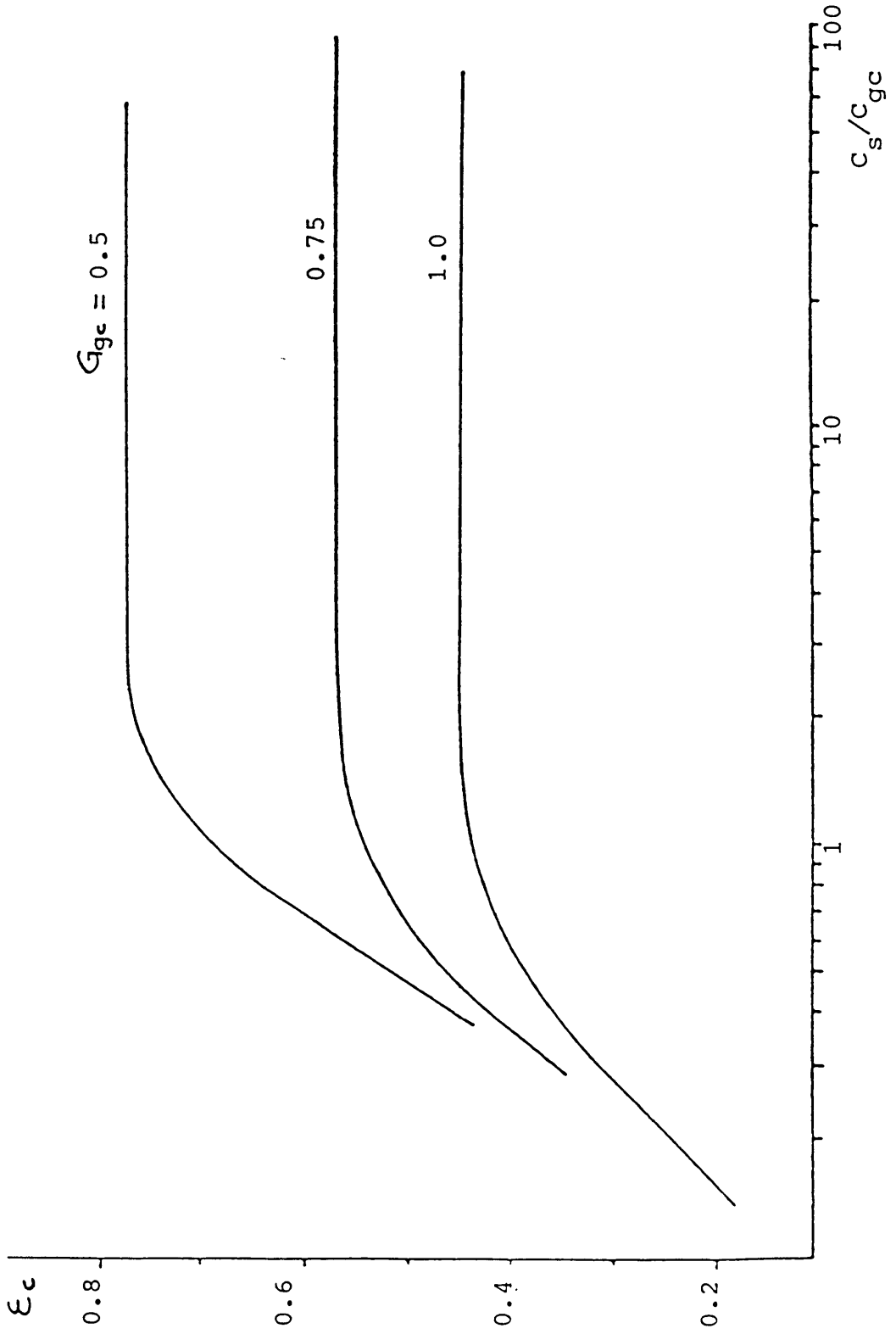


Figure (2.5):
Effect of solid to air capacity rate ratio on cold side effectiveness for B.S.C. regenerator

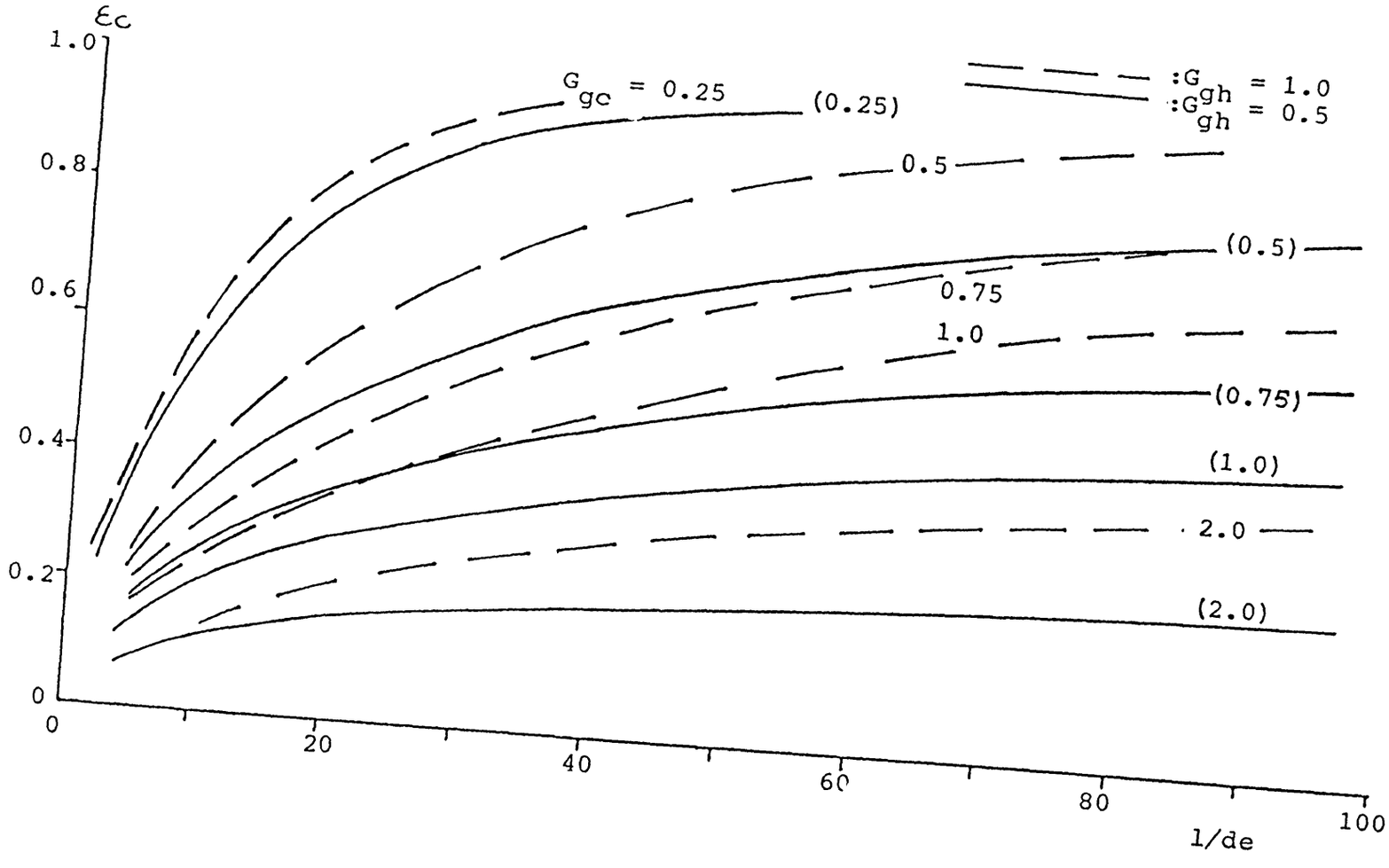


Figure (2.6):
Effect of 1/d on ε_c for G_{gh} = 1.0 and 0.5 for the B.S.C. regenerator

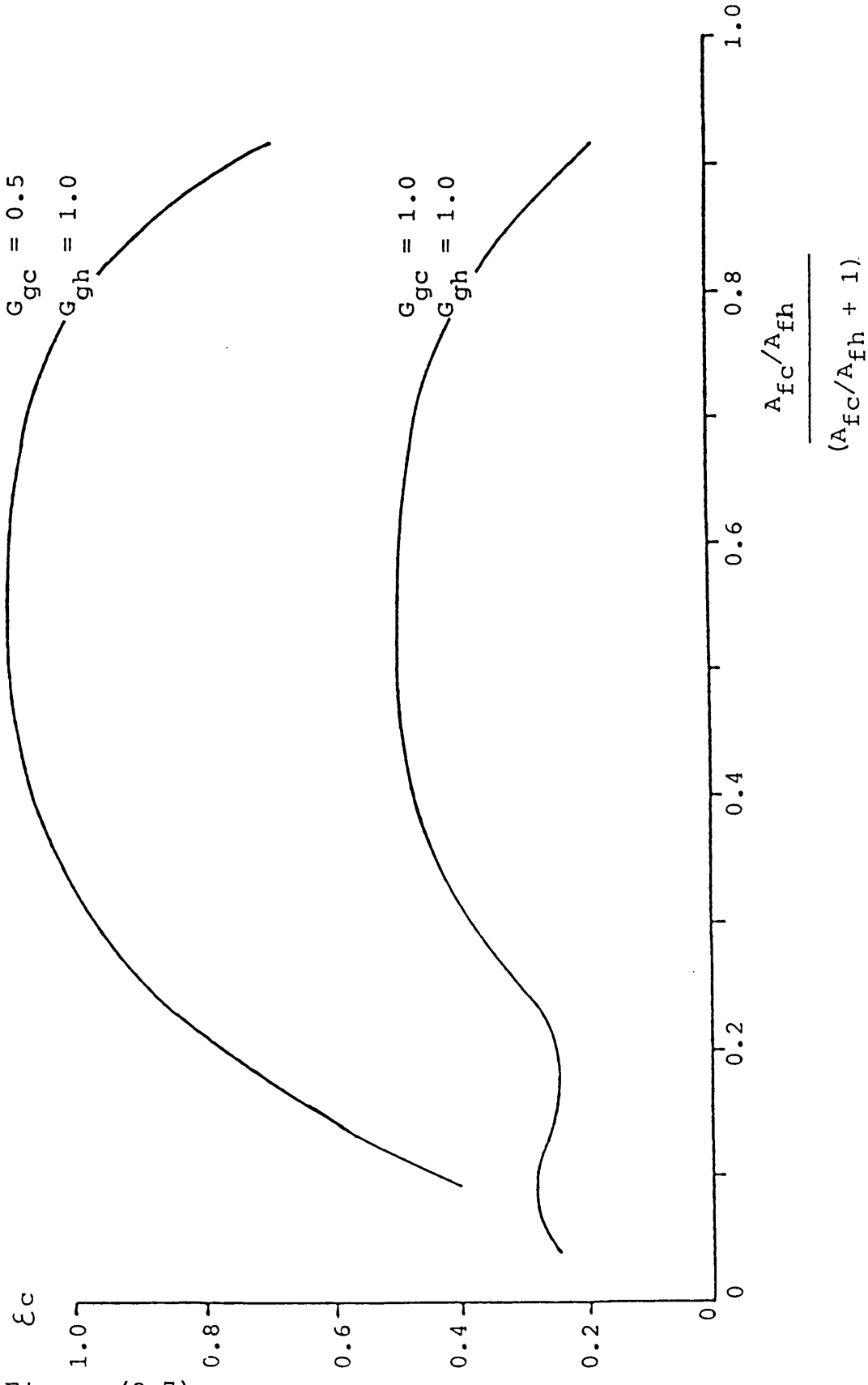
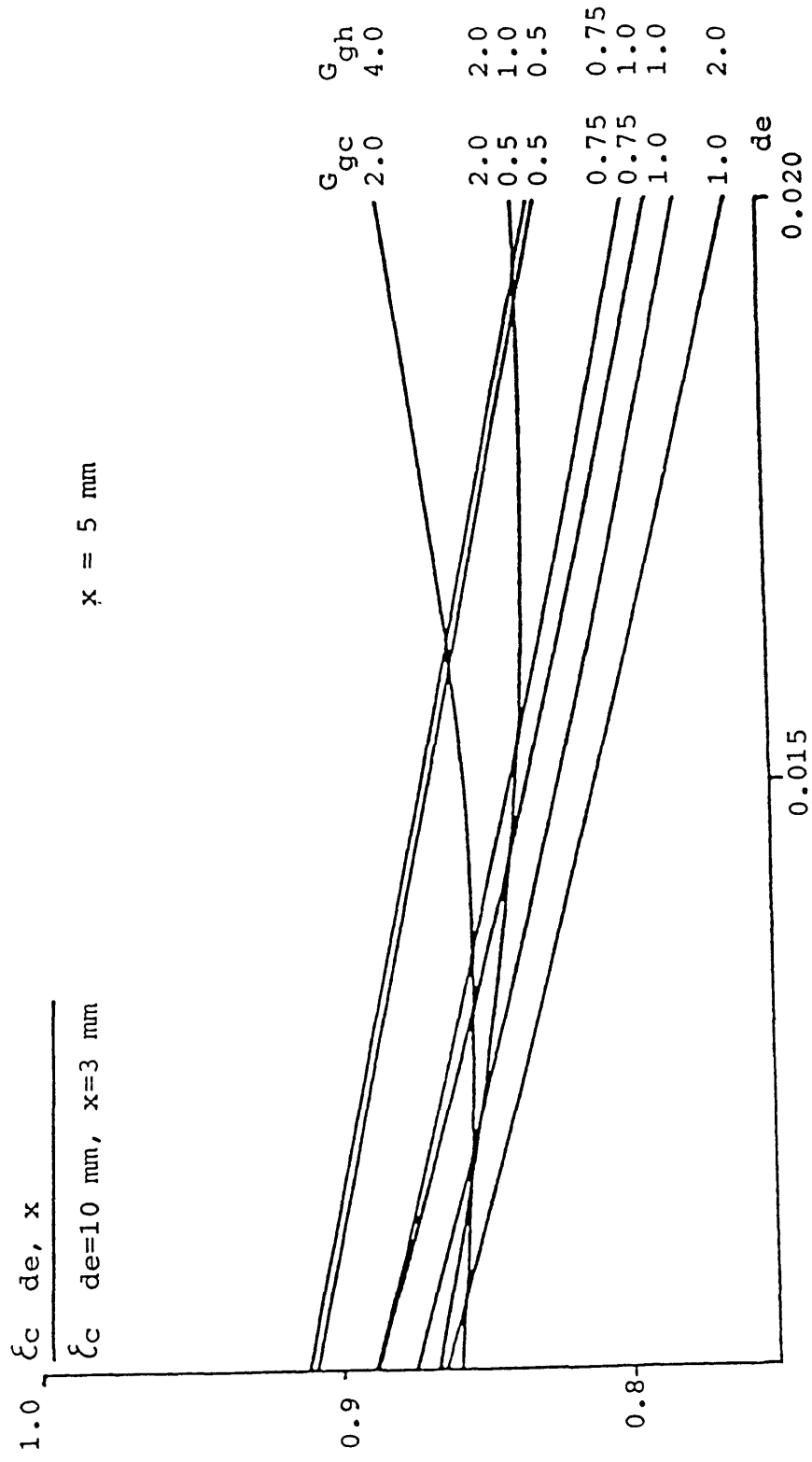


Figure (2.7):

Effect of $\frac{A_{fc}}{A_{fh}}$ on ε_c for G_{gc} = 0.5, 1.0 and G_{gh} = 1.0

for the B.S.C. regenerator



Effect of hole size and wall thickness on ε_c for the B.S.C. regenerator

Figure (2.8)

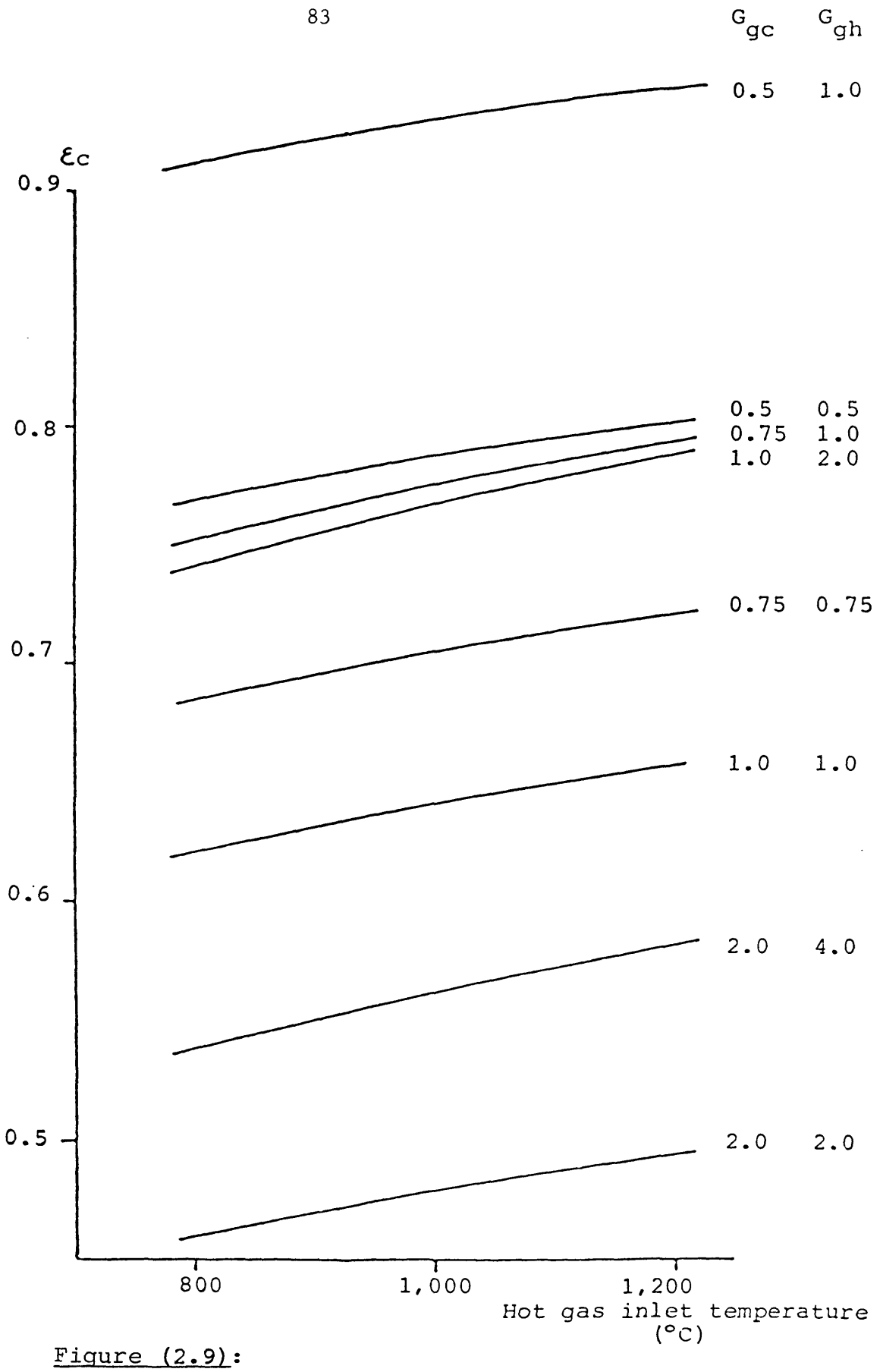


Figure (2.9):
Effect of hot gas inlet temperature on ε_c for B.S.C. regenerator

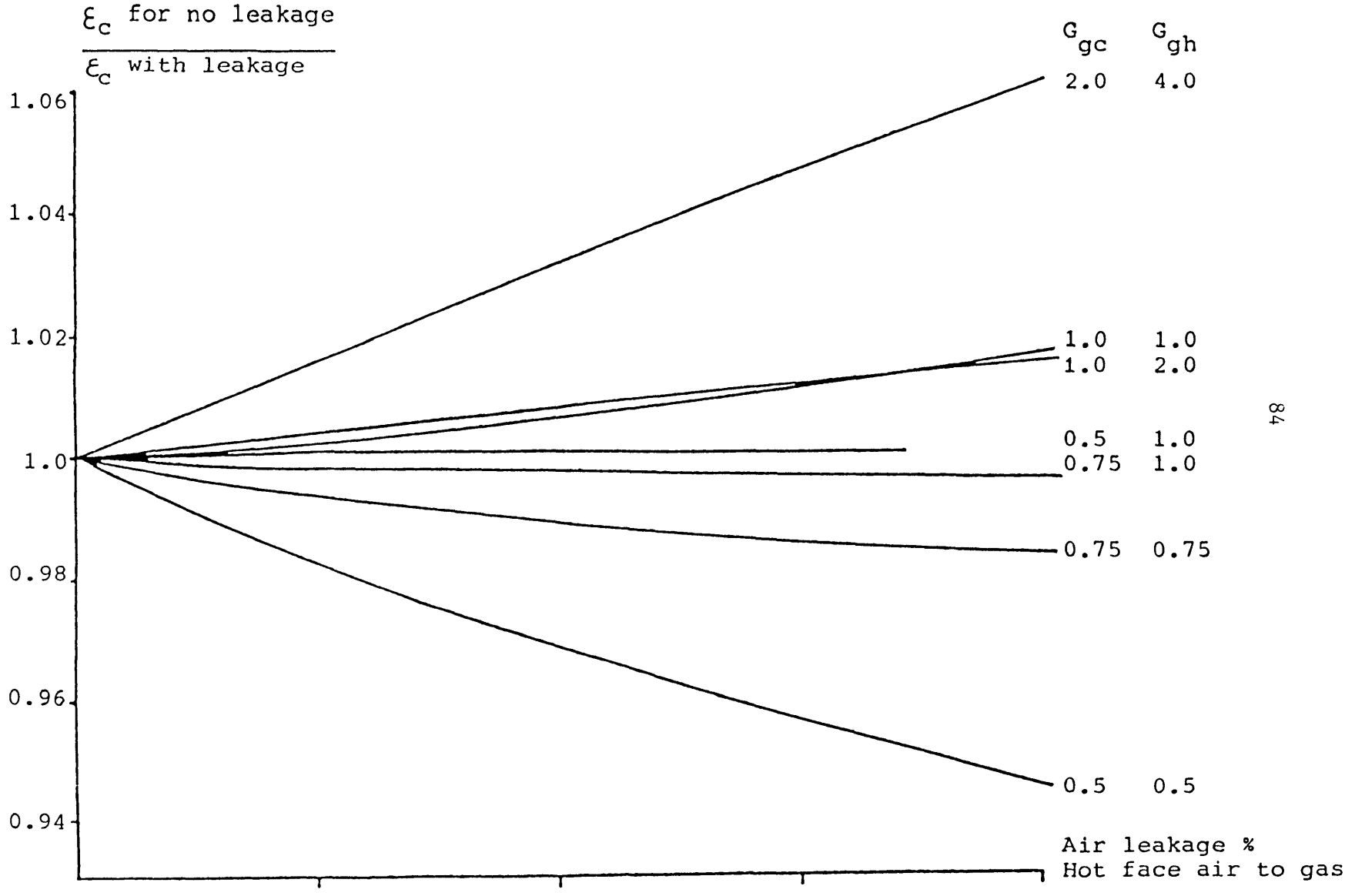


Figure (2.10):
Effect of leakage on ε_c for B.S.C. regenerator

CHAPTER 3

Thermal design, mechanical design and commissioning of the rotary regenerative burner

3.1. Introduction

In the present chapter the design and development of the experimental burner are presented.

The mechanical design of the prototype burner is given by describing the components of the system individually. Special consideration is given to the method of selection, and the thermal design of the matrix, which is the key component of the system.

The way in which certain features of the prototype unit had to be altered to ensure uninterrupted rotation of the matrix for long periods, and without excessive wear of the rubbing surfaces, is then given.

Finally, the leakage results obtained during cold testing of the system are presented.

3.2. Overall design of the rotary regenerative burner

The purpose of this project, as already stated, is the development of a rotary regenerator burner, enabling stable unaided combustion of fuel-air mixtures below their normal lower

flammability limit. In Chapter 1 of this thesis, combustion of such mixtures was proved feasible within burner-heat exchanger systems, that provide for efficient recirculation of heat from the hot products to the cold reactants. In the same Chapter, the selection of a rotary regenerator, as the means of transferring heat from products to reactants, was justifed on the grounds of the large heat transfer area per unit volume inherent in the design of such rotating matrices.

The laboratory scale burner, constructed and investigated in the course of this research programme, is illustrated diagrammatically and pictorially in figures (3.1) and (3.2-3.3) respectively.

Basically, it comprises a vertically mounted rotary regenerator, of the axial flow type. The ductwork, ordinarily essential for directing the hot gas stream towards the matrix, and keeping it and the outgoing heated cold gas stream separate, is replaced by a sealed structure enclosing the upper flat surface of the matrix. The resulting cavity, directly above the matrix, serves as the combustion chamber. The normal lower ducting required for directing the cold gas (the fuel-air mixture in this case) towards the matrix, and preventing it from leaking to the cooled hot gas side (here the cooled combustion products), is retained in the present system.

A rotor houses the solid matrix that effects heat transfer between the hot and cold gas streams, and is the key component of the rotary regenerator-burner system. During operation of the experimental burner, cold fuel (methane was used throughout) - air

mixture enters the system at the base and flows up through one of the two sections of the lower duct. It then enters the rotating matrix where it is preheated by receiving some of the heat stored in the walls of the matrix. The mixture flowing up through half of the matrix emerges from the top of the matrix into the combustion chamber where, provided it has been adequately preheated, it ignites and burns in a premixed flame. Hot combustion products enter the matrix at the top and flow down through its other half, giving up heat to the solid. The cool combustion products leave the burner through the other section of the lower ducting. Austentic stainless steel type 316 was used, almost throughout, for the construction of the different parts of the burner. This grade of steel contains 18 percent Chromium and 1 percent Silicon (3.1) that complement each other's effects and impart to this steel its excellent oxidation resistance. The protective oxide film forming on the surface of stainless steel 316, when it is exposed to hot oxidizing environments, is stable up to a temperature of 900^{o}C (3.1). In addition, welding can be easily performed with this steel and it is readily available and relatively inexpensive. It is, however, very difficult to machine and this, together with several other problems, contributed to the lengthy construction period for the burner system (approximately 9 months).

The different parts comprising the burner are shown schematically in figure (3.1) and they are as follows:

1. The "top hat" structure containing the combustion chamber.
2. The upper sealing ring.

3. The upper compacting ring.

4. The rotor.

5. The lower compacting ring.

6. The lower duct and seal structure.

These are vertically assembled in the order given above.

The lower duct and seal structure is supported and held stationary by three steel supports (7 in fig. (3.1)). They prevent the upper sealing ring and combustion chamber structure from rotating with the matrix by the action of the motor. These supports are welded on a thick steel base plate (see fig. (3.2)) on which the motor, gear box and motor speed controller are also attached.

The design of the above mentioned parts is given in more detail in the following sections.

3.3. Thermal and mechanical design of the rotor and matrix assembly

The rotor, carrying the solid matrix responsible for heat transfer within the regenerator, consists of three concentric 316 stainless steel tubes of identical length (76.2 mm) and outside diameters of 19.0 mm, 63.2 mm and 103.0 mm (see fig. (3.4)).

The matrix occupies the annular space between the two central concentric tubes.

The volume defined by the outer two concentric tubes is loosely packed with "Triton" ceramic fibre to prevent natural

convection currents from setting up and, therefore, reducing heat losses from the hot matrix solid. This volume was completely enclosed by welding, on both the top and botton ends of the two outer concentric tubes, annular 316 stainless steel plates of 103.0 mm outside and 60.0 mm inside diameter and 1.6 mm thickness. The matrix, therefore, is surrounded by a cylindrical steel wall with a low effective thermal conductivity. The only path available for heat conduction is along the tube and plate walls which are only 1.6 mm thick. If the solid temperature, T_s, is assumed to be uniform along the circumference of the matrix and constant in the vertical direction, then, in the case of a matrix surrounded by a solid steel wall of r_i inside, and r_o outside radius, the heat loss rate by conduction would be (3.2)

$$Q_L = \frac{2\pi k_s 76.2 \times 10^{-3}(T_s - T_a)}{\ln \frac{r_o}{r_i}} \qquad (3.3\text{-}1)$$

where k_s: Thermal conductivity of stainless steel (= 25.6 W/mK)

T_a: Ambient temperature (K)

Since, however, in the present system the only possible paths for heat conduction from the matrix to the outside tube are along the two 1.6 mm thick plates, the rate of heat loss, Q_L', is given by

$$Q_L' = 2\,\frac{2\pi k_s\ 1.6 \times 10^{-3}(T_s - T_a)}{\ln \frac{r_o}{r_i}} \qquad (3.3\text{-}2)$$

which means that $Q_L' = 0.04\ Q_L$ or, if the matrix was surrounded by

a solid wall of thermal conductivity k_s', that $k_s' = 0.93$ W/mK.

The innermost tube is packed with "Triton" ceramic fibre in a similar fashion, and sealed at the top and bottom by stainless 316 discs of 19.0 mm diameter. A sealed hollow tube was considered preferable to the possible alternative of a solid bar in order to minimise heat loss by conduction from the upper circular surface which is exposed to hot gases in the combustion chamber.

The area for heat loss by conduction is 1.96×10^{-4} m^2 (thickness of tube wall = 1.6 mm) as opposed to 2.84×10^{-4} m^2 if a solid was employed.

The innermost tube is mounted on the axis of the outer tube assembly and is firmly kept in place by stainless steel pins attached to both tube assemblies. Four pins would have provided the most affective support. However, it was desired to contain within the available space as large a heat transfer surface as possible and, furthermore, the matrix itself supports the core and the stresses in this part of the rotor were not high. Two pins only were used, therefore, and were found to give adequate support.

The matrix, as mentioned previously, is supported within the space between the central rotor core and the outer cylindrical hollow wall. Two entirely different matrix types were tested during experiments. They were

(a) 316 stainless steel flame trap matrix

and (b) A ceramic tube matrix.

These were supported in rotors of identical geometry and dimensions, as described above. Changing from one matrix type to

the other was, therefore, quite straight forward, since no other part of the burner had to be altered.

Metallic matrices, as already mentioned, are not expected to be of use for large industrial burners. The exhaust gas temperatures, even for lean fuel mixtures, are quite high (~1400 K) and the temperature difference between the inlet cold (ambient) and hot gas streams is, therefore, very large. Such temperature differences coupled with the large thermal expansion coefficients of metals, would result in high and non-uniform thermal stresses leading to possible rotor deformation. In addition, the highly corrosive environment would dictate the use of expensive alloys. In a laboratory scale system, however, the matrix need only be quite small, which means that such problems would not be prohibitive. For this reason, and the ease with which metallic matrices can be fabricated, the principle of lean combustion within rotary regenerative burners was initially tested with a metallic matrix. The ceramic matrix, subsequently constructed, was, however, employed for all further experimental work.

During the thermal design of the matrix, the design data available in the literature applied to metallic matrices only. The calculations, therefore, for determining the dimensions of the matrix, and, consequently, the rotor necessary to support it, had to be performend for the metallic matrix. The ceramic matrix was not designed as such but its overall size was dictated by the requirement for identical rotor assemblies with both matrices (i.e. the matrix was constructed to fit the rotor).

(a) **Thermal design and construction of the metallic flame trap matrix**

Stable unaided combustion of very lean fuel mixtures can only be achieved in a heat exchanger-burner system in which:

(1) The preheat imparted to the reactants by the products is large relative to the heat input.

(2) The heat losses from both the combustion chamber and the heat exchanger are small compared to the preheat.

(3) There is no mixing of products with reactants.

The rotary regenerator disk matrix must, therefore, be designed for high effectiveness and small heat losses and the matrix passages must be continuous so that there is no mixing between products and reactants.

In selecting the optimum geometry, and sizing the regenerator matrix for as high an effectiveness as possible, the following must be considered.

(1) The regenerator effectiveness increases with increasing matrix heat transfer area. Large areas can be obtained with matrices of large area per unit volume of matrix ratios and/or matrices of large volumes.

Large area per unit volume of matrix ratios requires that the matrix passages must be of small diameter with thin walls. However, reducing the passage diameter adversely affects the pressure drops of gases flowing through the matrix. Large pressure drops would result in high inlet pressures and large pressure differences between the inlet and outlet sides. These would in turn result in increased

gas leakages from the inlet side both to the environment and the exhaust side of the burner. Since leakages, in this case, are equivalent to heat losses, they should be kept low and a compromise must, therefore, be reached while selecting the optimum matrix geometry.

The volume of a regenerator matrix of the type being considered here (i.e. disk type) can be made large by any of the following three combinations:

(a) Large matrix diameter and short passages.

(b) Long passages and small matrix diameter.

(c) Long passages and large matrix diameter.

Long passage matrices are associated with large pressure drops and, therefore, large leakage rates. Large diameter matrices have external surface areas which are large when compared to those of matrices of the same length but small diameters. Large external surface areas are not desirable due to large heat losses. A compromise would again need to be reached in deciding on the optimum matrix size.

The optimum matrix geometry and dimensions are further constrained by the availability of materials. For the matrix built here, the latter constraint proved to be the governing criteria for geometry selection, and partly for sizing of the matrix.

(2) Larger matrix rotational speeds generally lead to higher regenerator effectiveness. Large rotational speeds, however, result in large carry-over rates (fuel-air mixture, trapped within the passages of the matrix is carried over to the

exhaust side without having given up its combustion energy). These are equivalent to heat losses and should be minimised by maintaining low rotor speeds. In addition, since seals of the rubbing type were used, rotor speeds during operation should be low to avoid excessive surface wear rates.

In designing the metallic matrix for the present system the following were aimed for:

1. Reasonably small diameter passages of thin walls.
2. High effectiveness at low rotational speeds.
3. Matrix geometry for which materials are commercially available.

A flame trap geometry (figure (3.5)) was decided upon and lengths of the plane and corrugated 316 stainless steel strips, necessary for its fabrication, were purchased. Flame trap matrices are easily constructed by winding the plane and the corrugated strips, placed next to each other, round a central cylindrical core. The width of the strips used was 76.2 mm and their thickness 0.05 mm. The corrugations were triangular of 0.41 mm height and 1.31 mm base (see figure (3.6)). The length of the matrix triangular passages was, therefore, fixed at 76.2 mm (it is difficult to reduce the width of the corrugated strip without destroying its corrugations). Design calculations were performed for determining the optimum matrix diameter or alternatively, the optimum number of turns of the plane and corrugated strips of the flame trap matrix, for a regenerator effectiveness of 90 percent. The calculation procedure was repeated for fuel mixture mass flowrates of 9.6×10^{-4} Kg/s (800 cm^3/s at 20^oC and 1 atm absolute

pressure) and 2.4 x 10^{-4} Kg/s (200 cm^3/s).

The effect of increasing the matrix diameter on the rotational speed for maintaining a regererator effectiveness of 90 percent was determined, and the graphs of rotor speed versus matrix diameter, for both mixture mass flowrates, are presented in figure (3.7). As can be seen, the required rotor speed decreases both with increasing matrix diameter and decreasing mixture flowrate. For large diameter matrices (above $\simeq$ 100 mm) the rate of decrease becomes very small and this indicates that a 100 mm diameter matrix would be ideal. It is, however, also evident from figure (3.6) that, over the range of flowrates considered, even the highest rotor speed (2 revs/min) is not excessive. This, combined with consideration of factors such as the linear increase of the matrix external surface area with the matrix diameter (see fig. (3.7)) and the availability of 316 stainless steel tubes, for construction of the rotor, in only a limited range of sizes, resulted in the 40 turn or 60 mm outside diameter matrix being selected as the most appropriate for the experimental system.

For the calculation the following empirical equation, presented by J.E. Coppage and A.L. London (2.7), was employed.

$$\epsilon = \left[\frac{NTU_o}{\frac{1}{2}\left[1 + \frac{C_{gc}}{C_{gh}}\right] NTU_o + 1}\right]\left[1 - \frac{1}{9\left[\frac{C_s}{C_{gc}}\right]^2}\right] \qquad (3.3\text{-}3)$$

where

$$NTU_o = \frac{(hA)c}{C_{gc}}\left[\frac{1}{1 + \frac{(hA)c}{(hA)h}}\right] \qquad (3.3\text{-}4)$$

and ϵ: effectiveness

C_{gc}, C_{gh}, C_s: heat capacity rate of cold gas, hot gas and solid (J/s K)

h_c, h_h: Heat transfer coefficient on cold side and hot side (J/m^2 s K)

A_c, A_h: Heat transfer area on cold side and hot side (m^2)

This simple algebraic equation was shown to provide effectiveness values which are in excellent agreement with others obtained from detailed calculation procedures.

The heat transfer coefficients were computed from the correlation (2.6)

$$St = \frac{0.205}{Re^{(0.55)}} \qquad (3.3\text{-}5)$$

where St: Stanton Number

Re: Reynold's Number

which applies to flame trap matrices of dimensions that are almost identical to those of the matrix considered here, and for Reynold's numbers in the range from 50 to 200. For Re < 50 the Stanton numbers reach the limiting value of 0.024.

In the design calculation (see Appendix A) the effect on regenerator effectiveness of leakages, and heat losses from the matrix solid, were not accounted for. Only a small heat loss from the combustion chamber was allowed for. The calculated results, therefore, are only rough estimates and can at best be considered as indicating actual performance trends. Calculations, for example, to predict the stability characteristics of the 60 mm

diameter metallic matrix burner reveal (see figure (3.8)) that for rotor speeds of 1.38 revs/min, stable combustion would be achieved with mixtures of methane content as low as 1% by volume and at flowrates of 800 cm^3/s (20^oC, 1 atm). Combustion of such lean mixtures has, however, only been realised in systems such as a nine turn spiral enclosed in a Dewar vessel (1.8) and would not be anticipated as feasible for the present system with greater heat leak paths. Indeed, combustion of such lean mixtures was not achieved during testing of the burner. In the calculation (Appendix A) equations (3.3-4) and (3.3-5) were used for estimation of the matrix inlet and outlet gas temperatures and rotational speeds. The combustion was considered solely in terms of a constant limiting final flame temperature of 1400 K. The amount of heat required for raising the temperature of the unburnt preheated mixture from its matrix exit value to 1400 K enabled the calculation of the necessary mixture methane content.

(b) **Construction of the ceramic matrix**

The ceramic matrix (figure (3.9)) was of tubular form and comprised 408 aluminous porcelain tubes that can be used with temperatures of up to 1200^oC. The tubes were of approximately 1.2 mm inside and 2.6 mm outside diameter and 75.0 mm length. They were selected on the basis of the following criteria:

1. The tubes had to be of small inside diameter for as large a heat transfer surface area as possible.
2. The thickness of the tube wall had to be small to permit the fitting of a large number of tubes within the volume available in the rotor.

3. The length of the tubes had to be of the order of 76.0 mm, which is the height of the rotor.
4. The tube material had to be able to withstand high temperatures.
5. The tubes had to be commercially available and of reasonable cost.

During the construction of the ceramic matrix the rotor assembly was placed on a flat surface and the ceramic tubes were inserted one by one in the annular space between the rotor core and its cylindrical outside wall. They were bound together by small quantities of "Autostic" high temperature cement and care was taken in packing them as close together as possible. The tubes were firmly pushed downwards against the flat surface to ensure that they were flush with the bottom rotor surface. When the matrix was complete, the rotor was gradually heated up to a temperature of 200^{o}C over a period of 3 hours to hasten the cement setting process and avoid swelling that would occur with too rapid heating.

Imperfections on the matrix bottom surface were subsequently repaired. Bypass leakage rates at the bottom of the matrix can only be minimised if the matrix surface is flat.

(c) Pressure drop characteristic of the metalic and ceramic matrices

The relationship between pressure drop and volumetric flowrate through both the flame trap and tubular matrices was experimentally determined. The experimental apparatus used in investigating both types of heating surface is shown schematically

in figure (3.10).

Air, obtained from the Departmental supply at a constant 2 bar absolute pressure and variable volumetric flowrate, was passed through half the matrix under test.

The air flowrate was measurd by means of an 18x metric rotameter, and the difference in static pressures upstream and downstream from the test section was measured by a water filled manometer U-tube. The rotameter had been calibrated for air at 2 bar absolute pressure and ambient temperature ($20^{o}C$) by using a bubble meter with the air at 1 bar absolute. The air flowrates, reported here (and also throughout this thesis) are, therefore, for air at 1 bar absolute and $20^{o}C$. The pressure drop measurements were obtained by means of two static taps in equal area duct sections upstream and downstream from the matrix. The entry and exit ducts (see figure (3.10)) used were such that only flow through half the free frontal area of the matrix was possible (they were two symmetrical sections of a cylindrical duct, i.e. similar to the burner entry duct).

In order to avoid leakages from the system, before each test the outlet was closed and the entire apparatus was placed under slight internal pressure. Leakages were thus detected and eliminated.

The pressure drop data obtained for both matrices are presented in graphical form in figure (3.11). For the range of flowrates investigated, the relationship between pressure drop and flowrate for both matrices is linear, and the lines best fitting the experimental data are given by (a) for the flame trap matrix

$\Delta P = 0.30\ V_g$ and (b) for the tubular matrix $\Delta P = 0.17\ V_g$, where ΔP is the pressure drop in N/m^2 and V_g the volumetric flowrate in cm^3/s. Pressure drops in the flame trap matrix are larger due to the smaller size of the passages. The experimental correlations are in good agreement with the relationships obtained from theoretical considerations, i.e. for the flame trap matrix $\Delta P = 0.29\ V_g$ and for the tubular matrix $\Delta P = 0.13\ V_g$.

The above were obtained from the equation giving the pressure drop for laminar flow of incompressible fluids in pipes

$$\text{i.e.} \qquad \Delta P = \frac{64\mu_g l}{2(de)^2 A_{ffp} N} V_g \qquad (3.3\text{-}6)$$

where μ_g: viscosity of air at 20^oC (Ns/m^3)

l: length of passage (m)

de: equivalent diameter of passage (m)

A_{ffp}: frontal free area of each passage (m^2)

N: No. of passages on either the cold or hot side.

The small equivalent diameters of the passages ensure that the flows, even at the high flowrates, are laminar in both matrices and eqn. (3.3-6) would, therefore, apply if the flow was considered incompressible. This is indeed the case here since pressure drops are very small (for the flame trap matrix at $V = 830\ cm^3/s$, $\Delta P = 249\ N/m^2$ and since the pressure at the exit from the matrix is equal to $101325\ N/m^2$, the inlet pressure is, therefore, 0.24%). The ratios of pressure drop to inlet pressure are only fractions of the 10% limit value above which compressible flow must be assumed.

The theoretical relationships, presented above, give values for the pressure drop which are smaller than the measured ones. This can be attributed to the contraction losses of the air entering and leaving the matrix. During actual operation of the burner, the pressure drops for flow through the matrices will be larger due to both the viscosity and the volumetric flowrate increasing with temperature.

It should finally be mentioned here that the uncertainty of the flowrate measurements was estimated as $\pm 0.02\ V_g$ cm^3/s, and that for the pressure drop measurements as ±0.05 cm.

3.4. Combustion chamber design

In the uppermost section of the experimental system the preheated combustible gases are allowed to expand in a cavity which was designed to serve as the burner combustion chamber.

Since the effect of parameters such as combustion chamber volume and configuration on the burner stability characterisation were to be experimentally determined, the top section of the system was designed for allowing flexibility in the chamber size and geometry. The whole section could be easily detached from the rest of the system and combustion chambers of different size and geometry could be readily formed.

Combustion experiments were performed with one flat cylindrical and three hemispherical combustion chambers. The two hemispherical chambers, employed during stability tests, had

refractory walls and were 60.0 mm and 90.0 mm in diameter. The third hemispherical chamber had transparent quartz walls, was 90.0 mm in diameter and was only used to obtain photographic evidence of the combustion within the novel burner.

The flat cylindrical chamber was 15.0 mm in height and 90.0 mm in radius. Its top flat wall was of transparent quartz and it was used both for stability experiments and flame photography.

The design of the above mentioned chambers is given in more detail in the following paragraphs.

1. **Hemispherical chambers with refractory walls** (see figure (3.12)).

These chambers were bounded by the upper surface of the matrix, the cylindrical stainless steel inside wall of the upper sealing ring and a hemispherical concrete dome. The refractory concrete, capable of withstanding temperatures of up to 1800^{o}C, was obtained by mixing cement of 70% alumina content with tabular alumina aggregate and water, in the amounts recommended by the cement manufacturers. The combustion chamber cavity was formed within the refractory dome by casting the concrete in a 316 stainless steel "Top hat" container around a wooden mandril (see figure (3.13) for dimensions). A wooden disk integral with a hemispherical wooden mandril, of diameter equal to that of the chamber being constructed (90 mm or 60 mm) was fixed to the flanged base of this steel container. The concrete was cast through a hole on the flat surface of the "Top hat" container into the void above the mandril. The whole assembly was mechanically

vibrated to ensure the elimination of voidage and to produce a concrete of high density and strength. Following removal of the wooden disk (6 hours after casting) the cast was kept wet for 24 hours to avoid surface drying.

The combustion chamber supporting structure could be firmly attached to the upper surface at the upper sealing ring by means of 10 bolts. Metal to metal contact at this point was eliminated via an insulating gasket. Heat losses by conduction from the combustion chamber structure down to the rest of the system were thus reduced.

Access to the combustion chamber, for initial ignition of the mixture and for temperature measurements during operation, was allowed for by means of three 3 mm i.d. and one 14 mm i.d. tubes in the sides of the "Top hat" container. These access tubes were built into the "Top hat" container prior to casting of the refractory concrete.

2. **Chambers of high purity transparent quartz**

Combustion chambers, partly surrounded by transparent quartz walls, were employed to permit visual study of the flame within the chamber. Two such chambers were used and they were hemispherical and cylindrical in geometry.

For the hemispherical chamber, a high purity quartz dome, 90.0 mm in diameter (i.e. similar to the inside diameter of the upper sealing ring) and 4.0 mm in wall thickness, with a flange round its edge, of 150.0 mm outside diameter and 15.7 mm thickness, was manufactured (figure (3.14)). With the quartz unit in place, on the upper surface of the top sealing ring, a chamber

was formed which was, therefore, bounded by the upper matrix surface, the cylindrical stainless steal sealing ring inside wall and the quartz hemispherical wall.

The quartz dome could be readily secured to the surface of the upper sealing ring via the two segments of a 316 stainless steel ring that were constructed for the purpose. The procedure for assembling the unit was as follows (figure (3.15)).

(a) A gasket of thermal insulating material, 4.0 mm in thickness and inside and outside diameters similar to those of the upper sealing ring (i.e. 90.0 mm and 178.0 mm respectively) was placed on the exposed flat surface of the sealing ring.

(b) The quartz unit was centrally positioned on the exposed flat surface of the gasket. The distance from the edge of the quartz flange to the edge of the gasket and upper sealing ring was 14.0 mm.

(c) A gasket of inside and outside diameters similar to those of the quartz flange (i.e. 98.0 mm and 150.0 mm respectively) was placed on the flat surface of the flange.

(d) The two segments of the stainless steel ring, of outside diameter similar to that of the upper sealing ring and gasket, and inside diameter 20 mm larger than that of the quartz was placed on the surface of the upper gasket so that the holes near its outside periphery were directly above those on the upper sealing ring and gasket.

(e) The two ring segments were finally secured in place by means of 10 bolts which were fastened on the upper sealing ring. The bolts were not in contact with the quartz flange and they

were tightened so that leakages from the combustion chamber to the environment were avoided.

The method, outlined above, of attaching the quartz unit to the stainless steel upper sealing ring, ensured that during combustion experiments, the quartz unit was able to expand quite independently from the rest of the burner. In addition, since the gasket material was softer than either the steel or the quartz and had a low thermal conductivity, effective sealing and reduced heat transfer between the quartz and metal surfaces were achieved.

For the chamber of cylindrical geometry, a high purity quartz disk (150.0 mm diamter, 15.7 mm thickness) was attached by the same method on the upper surface of the sealing ring. A cylindrical volume was, therefore, defined by the circular and flat quartz and matrix surfaces, and the cylindrical sealing ring inside metallic wall.

3.5. The sealing system

Gas leakages are unavoidable from any rotary regenerator system, even the most elaborate. They adversely affect the overall performance of the system and the design of effective seals has been one of the most difficult problems associated with this type of heat recovery device. The rates at which leakages occur depend on the system design and operating conditions; large pressures and pressure differentials between gas streams lead to large leakage rates.

For the rotary regenerative burner, gas leakages, depending on the point in the system from where they occur, are equivalent to heat losses due to either the sensible heat or the heat of combustion carried by the escaping gas. They have, therefore, a detrimental effect on the leaness of a mixture that can be stably burned in the system and should be minimized.

Gases escape from the burner both before and after passing through the matrix. The different types of leakage can be listed as follows.

(a) Leakage of cold fuel-air mixture direct to the atmosphere from the matrix entry section.

(b) Interleakage of cold fuel-air mixture from the matrix entry section to the exhaust side of the system.

Leakages of the above two types result in fuel, which is potentially capable of exothermic reaction, being lost to the environment.

(c) Leakage of hot combustion gases to the atmosphere from the combustion chamber section of the burner.

In this case it is the sensible heat contained in the products that is being wasted.

(d) Carry-over leakages.

These are inherent in the method of operation of the system in that gas trapped within the matrix passages is carried over to the other side due to the rotation of the matrix. Reactants and products are continuously carried over to the burner exhaust and entry sides respectively. In the case of the former, fuel is lost and in the case of the latter, dilution of reactants by products

takes place. Carry-over leakages have undesirable effects on the burner stability characteristics and can only be reduced by employing, as is the case here, matrices of small passages and slow rotor speeds.

The features of the burner, specifically designed to reduce leakages will now be described.

(a) Seal for reduction of leakage from top section of the burner.

A continuous peripheral seal was employed to minimise leakages from the combustion chamber to the atmosphere. The seal was kept in rubbing contact with the rotor surface and, as shown in figure (3.14), was part of a larger cylindrical unit, referred to previously as the upper sealing ring. The cross section of the upper sealing ring is non-uniform and its upper and lower points (see figure (3.16)) have inside diameters 90.0 mm and 126.0 mm respectively.

The peripheral seal is only an extension of the inner surface of the upper part of the sealing ring (5.0 mm in height and 5.5 mm thickness).

During the design stage, high wall temperatures (of the order of $900^{o}C$ to $1000^{o}C$) were anticipated for this part of the burner due to the walls being in contact with conbustion products of temperatures of the order of $1130^{o}C$ (assuming a constant limiting final flame temperature of 1400 K). It was, therefore, deemed necessary to use 316 Stainless Steel for the construction of the sealing ring.

The lower part of the stainless steel ring was made long enough for it to extend by 23.0 mm down the rotor cylindrical

surface. The annular space between the rotor and the sealing ring was tightly packed with "Triton" ceramic fibre thus providing secondary sealing. The fibre was kept in place by a further stainless steal ring that could be attached to the lower flat surface of the sealing ring structure. The inside diameter of the compacting ring was such (104.0 mm) that a 0.5 mm clearance existed between the ring and rotor surfaces. This clearance was allowed in order to avoid contact and, therefore, friction at this point in the system.

During operation the combustion chamber structure, as described previously, was attached to the upper surface of the sealing ring structure and, due to the peripheral seal design, the weight of the combustion and sealing ring assembly was supported by the rotor.

(b) Seal for reduction of leakage from the lower section of the burner (figure (3.17)).

Leakages of reactants to the atmosphere, before they entered the matrix, were reduced by employing a peripheral seal and a sealing ring structure that were almost identical to those described for the upper part of the burner. The only important difference was that the whole unit was not "facing" downwards, as was the case in the upper part of the system, but upwards.

The weight of the rotor and consequently of the entire upper section of the burner, was supported by the peripheral seal.

Since low temperatures were anticipated for this part of the system (of the order of 200^{o} - $300^{o}C$) a polytetrafluoro ethylene (PTFE) stepped bush (13.0 mm wide, 2.0 mm thick) was inserted in a

groove on the inner surface of the compacting ring. There was no clearance between the bush and the rotor surfaces since at this point the requirement was for the rotor to be kept stationary in the horizontal direction while rotating.

Another PTFE bush (3.6 mm wide and 2.0 mm thick) was inserted in a groove on the surface of the peripheral seal to avoid metal to metal contact.

The thermal expansion coefficients of PTFE are considerably larger than those of the stainless steel (100 x 10^{-6} mm/mm ^{o}C and 17.4 x 10^{-6} mm/mm ^{o}C from references (3.1) and (3.3)). To avoid distortion of the PTFE bushes during operation, 1.0 mm clearances were allowed between the groove walls and the bushes. The formula used to estimate the clearance at ambient conditions necessary to avoid contact between PTFE and steel up to a temperature of 250^{o}C was

$$\text{clearance} = \frac{d_{PTFE}(1 + \lambda_{PTFE}\Delta T)}{2(1 + \lambda_{st.st.}\Delta T)} - \frac{d_{PTFE}}{2} \qquad (3.4\text{-}1)$$

where ΔT: Temperature rise above 20^{o}C

λ : Thermal expansion coefficient (mm/mm ^{o}C)

d : Length or diameter of member at 20^{o}C (mm)

and st.st. refers to stainless steel.

It was found that clearances of 1.0 mm were adequate for the assumed temperature rise.

Finally the ducting necessary to keep the inlet and outlet streams separate was welded on the linear surface of the lower sealing ring structure (see figure (3.17)).

(c) Seals for reduction of interleakages

Intleakage of cold reactants from the higher pressure inlet side to the lower pressure exhaust side of the system were reduced by employing a radial contact seal. The seal comprised two elastic metal strips (31.5 mm in length, 9.0 mm in width) and a rectangular 316 stailess steel block (4.0 mm in height and upper surface 9.4 mm x 10 mm).

The strips, under the weight of the rotor and upper sections of the burner, bent and brushed against the rotating matrix lower surface.

The strips and the block were suppoted on a rectangular 316 stainless steel bar which, together with a steel plate, partitioned the lower part of the system in two symmetrical sections.

The rectangular block was positioned in the middle of the bar and it was designed so that its upper surface was both flush with the surface of the peripheral seal and in contact with the rotor central core. The metal strips were long enough for their short sides to be in contact with the inner surface of the peripheral seal and the sides of the central block. Their height was calculated so that when bent, their sides adjacent to the block could only "see" the block. The strips and the rectangular block, therefore, formed a continuous radial seal.

3.6. The rotor drive assembly

A direct current shunt wound (field and armature windings in parallel) electric motor combined with a reduction gear unit (motor: 1000 rpm, output from gear box: 25 rpm) was employed to impart rotation to the regenerator matrix.

Direct current motors are adjustable in speed over a wide range and their efficiency is high over the entire speed range, unlike A.C. motors in which efficiency is roughly proportional to speed. In addition, D.C. shunt wound motors, in contrast to the series wound type, have constant speed characteristics (i.e. speed does not vary with torque required) and the difference between the no load and full load speeds is only small.

Rotation from the motor was transmitted to the matrix via an extended gear wheel that was mounted on the circumference of the rotor (approximately half way up) and which mated with another smaller wheel fitted on the gearbox output shaft (turn down ratio 2.5:1).

The speed of the motor was controlled by a thysistor unit that provided a full wave rectified constant field voltage and variable armature voltage.

Prior to selection of the motor, the torque and, therefore, the power needed to effect rotation of the matrix at the relatively high speed of 10 rev/min were estimated. Rotation is opposed by the frictional forces acting on the upper and lower flat surfaces of the rotor (i.e. where dry slipping contact between the rotating rotor and the stationary seals existed) and

the cylindrical surface of the rotor in contact with the PTFE bearing. The torque and power estimates (see Appendix B) were 3.3 Nm and 3.5 W respectively. In addition the torque necessary to initiate movement of the rotor (due to limiting static friction) was experimentally determined by atatching one end of a string to the rotor gear wheel circumference and the other to a scale pan via a pulley. Small weights were added to the pan until the rotor began to move. The limiting weight was measured to be 6.62 kg. Since the radius of the gear wheel was 85 mm the torque necessary to overcome the limiting frictional force, which is the maximum frictinal force between the surfaces, was 5.52 Nm. The motor-gearbox unit selected was designed to provide 125 W power and a torque of 26 Nm at the maximum speed of 25 revs/min (i.e. 10 revs/min for the rotor). A motor more powerful than required was employed in order to allow for frictional forces increasing with increasing surface wear.

3.7. **Hot commissioning of the rotary regenerative burner**

The initial series of combustion experiments were performed in order to assess the mechanical design of the system and identify and eliminate any feature that would prevent uninterrupted operation during normal burner stability tests.

The mechanical design of the regenerative burner was assessed in terms of the length of time unhindered rotation of the matrix was achieved and the rate and extent of wear suffered by the rotor

and circumferential seals' rubbing surfaces. Methane-air mixtures at flowrates of 500 cm^3/sec (1 atm absolute and 20^oC) and 4.0% by volume in methane were burnt during these experiments. The matrix rotational speed was kept constant at 1.2 rpm and only the metallic flame trap matrix was tested.

The ease or otherwise of matrix rotation was continuously monitored by measuring the current through the motor armature windings. In shunt wound D.C. motors the torque developed is proportional to the armature current (3.4). Increase in the current reading would, therefore, be indicative of the presence of an obstruction to the smooth movement of the rotor under the seals.

The mechanical problems encountered, and the modifications to the design needed to overcome them, were as follows.

(a) The very first test of the system proved disastrous in that unhindered rotation was achieved for less than 10 minutes. Seizing between the stainless steel rotor and upper compacting ring surfaces occured. The allowed 0.5 mm clearance was, therefore, proved inadequate, due to the lateral movememt of the revolving rotor against the walls of the stationary upper sealing ring. The dry contact between the stainless steel surfaces resulted in excessive frictional heat being produced; this melted the metal surfaces and caused them to weld together locally.

The clearance at this point was increased to 2.0 mm and a Phosphor bronze ring was attached to the inside surface of the upper compacting ring as shown schematically in figure (3.16)

When Phosphorous is added to bronze, hard insoluble particles of copper phosphide (Cu_3P) are produced in the microstructure which give the alloy good bearing properties (3.5). Phosphor bronze, however, has a low melting point (750^{o}C from reference 3.3) and is prone to excessive oxidation rates at high temperatures.

Since high temperatures were originally anticipated for the upper parts of the burner, the use of Phospor bronze bearing surfaces was not considered feasible. After the first trial, however, the decision was taken to put its use to the test.

The Phosphor bronze ring (see figure (3.18)) was made slightly oversized since the thermal expansion coefficient of Phosphor bronze (19.44 x 10^{-6} mm/mm ^{o}C) is slightly higher than that of 316 Stainless Steel (18.52 x 10^{-6} mm/mm ^{o}C at 54^{o}C) at the same temperature. Solution of equation (3.4-1) showed that a 0.03 mm clearance between the bronze and steal surfaces would be adequate for temperature rises up to 540^{o}C. The clearance, however, allowed between the surfaces was 0.5 mm.

(b) With the modifications described above, uninterrupted operation of the system for approximately 30 minutes was achieved. The cause of the subsequent rapid increase in the armature current (from 130 mA to ~ 660 mA) was the excessive wear of both the upper circumferential seal and rotor rubbing surfaces. The deep grooves on the surfaces resulted in drastic increase of the frictional force and, therefore, the load on the motor. However, the Phosphor bronze ring on the upper compacting ring was observed to withstand the high temperatures and suffer little corrosion.

It was, therefore, decided to eliminate stainless to stainless contact at the upper part of the system by attaching a Phospor bronze bearing ring on the circumferential seal surface (shown in figure (3.19)). Clearance between the Phospor bronze and stainless steel rings was not necessary in this case as the Phosphor bronze ring was able to expand away from the steel (see figures (3.17) and (3.18)).

(c) Following the installation of the Phosphor bronze bush, unobstructed rotation of the matrix was achieved for the improved, but still insufficient, time period of approximately 2½ hours. Subsequently, however, the load on the motor increased rapidly and operation had to be halted. Examination of the burner, while still hot, revealed that the PTFE bush in contact with the cylindrical surface of the rotor had suffered distortion. This suggested that the 1.0 mm clearance, allowed between the bush and the lower compacting ring was inadequate, probably due to the temperature rising above the maximum anticipated 250^{o}C. To prevent the PTFE bush distorting and, therefore, exerting a braking force on the rotor, the clearance between the PTFE bush and stainless steal compacting ring surfaces was increased by 0.5 mm.

This resulted in continuous and unhindered rotation of the matrix (i.e. armature current almost constant at 140 mA) for approximately 3 hours. Excessive lateral movement of the rotor was then observed and the armature current rose to approximately 450 mA. The PTFE bush, that provided the rotor the only lateral bearing surface, had been exposed to a temperature in excess of

its melting point temperature of 290°C. The bush had melted and the rotor had become eccentric.

Since the Phosphor bronze bushes were proved satisfactory for the considerably hotter upper part of the system, the PTFE bushes in the colder lower part were replaced by two Phosphor bronze rings, one mounted round the circumference of the rotor and the other over and around the lower circumferential seal (see figures (3.20) and (3.21)).

(d) In subsequent trial runs continuous operation for up to 6 hours was successfully attempted. In all the runs the armature current gradually increased from 160 mA at the start to approximately 250 mA. This was due to the increasing wear and, therefore, coefficient of friction of the rubbing surfaces.

The spherical combustion chamber of concrete walls and 60 mm diameter was used during commissioning of the burner. In addition, the attainment of thermal equilibrium within the system was checked by continuously monitoring the gas temperatures, both in the combustion chamber and the outlet from the burner, and the temperature on the outside of the flat combustion chamber structure wall.

Thermal equilibrium was never reached and all the temperatures continued rising even at the end of the 6 hour run. Furthermore it was established, during these experiments, that operating continuously for up to 6 hours resulted in the rate of wear of the Phosphor bronze circumferential seal surfaces being unacceptably high; both Phosphor bronze bushes had to be replaced after approximately 15 hours of operation (i.e. 3 runs). The

large mass and, therefore, weight of the combustion chamber structure (5.47 kg) was responsible for both the long periods of time necessary for thermal equilibrium to be reached and the high rates of wear of the seal surfaces. A reduction in the mass of the combustion chamber would, therefore, be doubly beneficial because

(i) the length of time necessary for the system to reach steady state would be shortened, resulting in shorter runs and, therefore, reduced seal wear per run, and

(ii) the load supported by the rubbing surfaces would be decreased and since, depending on the nature of the surfaces,

$$\text{Wear rate} \propto (\text{load})^{\text{power}} \qquad (2.6)$$

the wear rates would be reduced.

Consequently, the combustion chamber concrete walls were replaced by a much lighter but less durable "Triton" ceramic fibre and Autostic high temperature cement assembly. The hemispherical chamber was formed by loosely packing the "Top hat" structure (see figure (3.22)) with fibre which was supported in place by a 10 mm thickness hemispherical layer of Autostic cement.

The mass of the 60 mm diameter combustion chamber structure was thus reduced from 5.47 to 2.35 kg. In subsequent experiments thermal steady state was reached within 4 hours from start up and the seal surfaces suffered wear at much reduced rates.

To reduce wear even further a graphite based lubricant paste was applied to the lower and upper rubbing surfaces. In the lower

part of the system, following evaporation of the organic substances in the paste, solid graphite layers were deposited on the bronze surfaces. Wear at this part of the system was eliminated. The graphite did not, however, withstand the high temperatures in the upper part of the system. Nevertheless, continuous operation of the system for up to 8 hours and with little wear of the upper seal was achieved.

The performance characteristics of the unit, in terms of rotation of the matrix and wear of the seal surfaces, were considered satisfactory at this point in the development of the design.

3.8. Estimation of bypass and leakage flowrates during cold operation of the rotary regenerative burner

Gas leakages (a) across the upper and lower circumferential seals to the environment and (b) across the radial seal from the entry to the exit section of the burner (see figure (3.24)), can not be eliminated completely and occur due to the following causes:

1) During normal operation of the burner, the surfaces of the circumferential seals and the rotor, even if assumed in perfect contact at start-up (this is not the case in practice), suffer increasing wear which results in deterioration of the quality of contact between them.

2) Since the circumferential seals are rigid, any obstructions in their path cause the loss of contact between large sections of the seal and rotor rubbing surfaces.

3) The radial seal is in contact with the matrix surface which, however, in the case of the flame trap matrix is 80% void and in the case of the tubular matrix is 20% void. The incoming mixture, being at a positive pressure with respect to the outgoing products, enters the passages as soon as they emerge under the radial seal. Part of the mixture, entering the passage, reverses direction and instead of flowing towards the combustion chamber, escapes to the exit side.

4) Imperfections on the matrix surface cause loss of contact between the radial seal and the matrix surface, thus increasing the effective gap size for bypass leakages to occur.

The leakage rates, at all the interfaces of the rotor and the stationary header system, are dependent on the pressure driving force, the gas density and the size of the effective gap between the surfaces. For the burner operating at steady state (i.e. when temperatures and, therefore, pressure differences and gas densities are constant) the leakage rates to the environment increase with operating time due to deterioration of the rubbing surfaces.

To fully characterize the burner, knowledge of the rate at which leakages occur just before flame extinction is necessary. This would, however, require the continuous monitoring of leakage flowrates via continuous meaurement of the exit gas flowrates (to

determine overall loss to the environment) and analysis of the gases in the combustion chamber and the exhaust from the system (to determine interleakage or bypass rates). The additional instrumentation needed to carry out such measurements would, however, influence the performance of the system by increasing the pressure drops (constrictions in outlet) and heat losses (probe in combustion chamber) and by altering the flow characteristics in the combustion chamber (probe). For the reasons outlined above, the bulk of data for the estimation of leakage flowrates were obtained during cold operation of the system; these were then compared to a limited number of data obtained during normal operation by approximate overall leakage measurements after extinction (for comparison of overall leakage rates). During hot operation (a) the gas densities are lower, (b) the gas volumetric flowrates and, therefore, pressure drops and pressure differences between the entry and exit streams and between the system as a whole and the environment are higher and (c) the effective gap between surfaces is larger. Leakage rates determined during cold tests are, therefore, low and can only be considered as indicating actual trends.

The cold tests performed to determine leakage flowrates were as follows:

1. Determination of dependence of bypass flowrate, V_{by}, on pressure drop across the radial seal.

Air from the Departmental supply was passed through the burner, as is schematically shown in figure (3.25). The upper surface of the matrix was blocked by several layers of insulating

tape and all the air leaving the burner, V_{by}, had, therefore, been forced to bypass the radial seal. The volumetric flowrate of the emerging air was measured by means of a 7x metric air rotameter that had been calibrated for air at 1 atm and ambient temperature ($20^{o}C$). Static pressure taps in the inlet (P_{in}) and outlet (P_{out}) sections of the system connected to the two sides of an inclined water filled U-tube enabled the measurement of ($P_{in} - P_{out}$).

Experiments were performed for a range of V_{by}, both with the flame trap and the tubular matrix, and for rotor speeds of 0 revs/min and 4 revs/min. The data obtained is presented in graphical form in figure (3.26). As can be seen the relationship between V_{by} and ($P_{in} - P_{out}$), for both matrices, is of the form $V_{by} \propto \sqrt{(P_{in} - P_{out})}$, which applies to flows through an orifice. The resistance offered to the flow of air between the flame trap matrix surface and the radial seal is considerably smaller than that offered when the tubular matrix is in contact with the seal. This can be explained in terms of the longer voidage fraction of the flame trap matrix. The effective gap size for the flame trap matrix - radial seal contact was calculated (see appendix C) as 0.7 mm, while for the tubular matrix-seal contact as 0.4 mm.

Rotation of the matrix does not appear to have any influence on the effective gap size for either matrices; this can be attributed to the uniform distribution and the large number of the voids on the matrix surfaces.

2. **Determination of leakage and interleakage flowrates**

The rates at which leakages to the environment and interleakages occured during cold operation of the regenerative

burner were deduced from flow and pressure measurements obtained over a range of air inlet flowrates. The experimental arrangement was as shown in figure (3.25). The flowrates of air entering and leaving the burner were monitored by an 18x and a 7x rotameter respectively. The 18x rotameter had been calibrated to provide the equivalent air flowrate at 1 atm absolute pressure when the actual air through the rotameter was at 2 atm absolute pressure. The pressure, therefore, of the air through the rotameter was kept constant at 2 atm absolute and its flowrate was controlled via the two valves before and after the rotameter. The smaller rotameter (7x) at the exit from the system, was calibrated for air at 1 atm absolute which was also the pressure of the air stream emerging from the burner.

Two static pressure taps, one in the inlet duct and one in the outlet duct of the system, provided data for the pressure difference across the radial seal.

The difference between the measured inlet and outlet flowrates was equal to the flowrate of air escaping to the environment both from the lower and upper rotor and ducting interfaces.

The measured pressure difference, used in conjunction with the previously obtained graph of bypass flowrate against pressure difference, enabled the estimation of bypass flowrate.

The leakage flowrates thus calculated and expressed as percentages of the inlet flowrates, are presented in figures (3.27) and (3.28) and tables C.1 to C.4 of Appendix C. For both matrices and for both types of leakages, the percentage leakage

decreases with increasing inlet flowrate. On the basis of these cold tests, it can, therefore, be assumed that leakage losses would affect the performance of the flame trap matrix and tubular matrix regenerative burners to a lesser extent the larger the inlet mixture flowrate.

For the system incorporating the flame trap matrix, and over the range of inlet flowrates investigated (100 cm^3/s to 800 cm^3/s), the percentage leakage to the ouside varies from 13% to 27%. For the tubular matrix system and the same range of inlet flowrates, percentage leakages from 10% to 24% were recorded. The bypass leakages for the flame trap matrix and tubular matrix systems were estimated as 21% to 44% and 9% to 24% of the inlet flowrate respectively. For identical operating conditions, therefore, the overall leakage rates from the tubular matrix system compare favourably to those from the flame trap matrix system. This can be attributed to the following characteristics of the systems:

(a) The pressure drops associated with flow through the flame trap matrix were found (see section (3.3)) to be larger than those with flow through the tubular matrix. For the same inlet flowrates, the gas pressures both in the inlet section and the combustion chamber of the flame trap matrix system, are, therefore, higher than those in the tubular matrix system. Consequently the pressure driving forces for leakage flow across the upper and lower circumferential seals and the radial seal are larger and leakages occur at a faster rate.

(b) The size of the effective gap between the radial seal and the flame trap matrix surface was estimated to be almost double that for the tubular matrix due to the large voidge of the flame trap matrix. The radial seal is, therefore, less effective in the flame trap matrix system and bypass leakage flowrates are larger.

In the experiments described above, the uncertainty of the volumetric flowrate measurements, V_g, was estimated as $\pm 0.02 V_g$ cm^3/s and that for the pressure measurements as ± 0.05 cm.

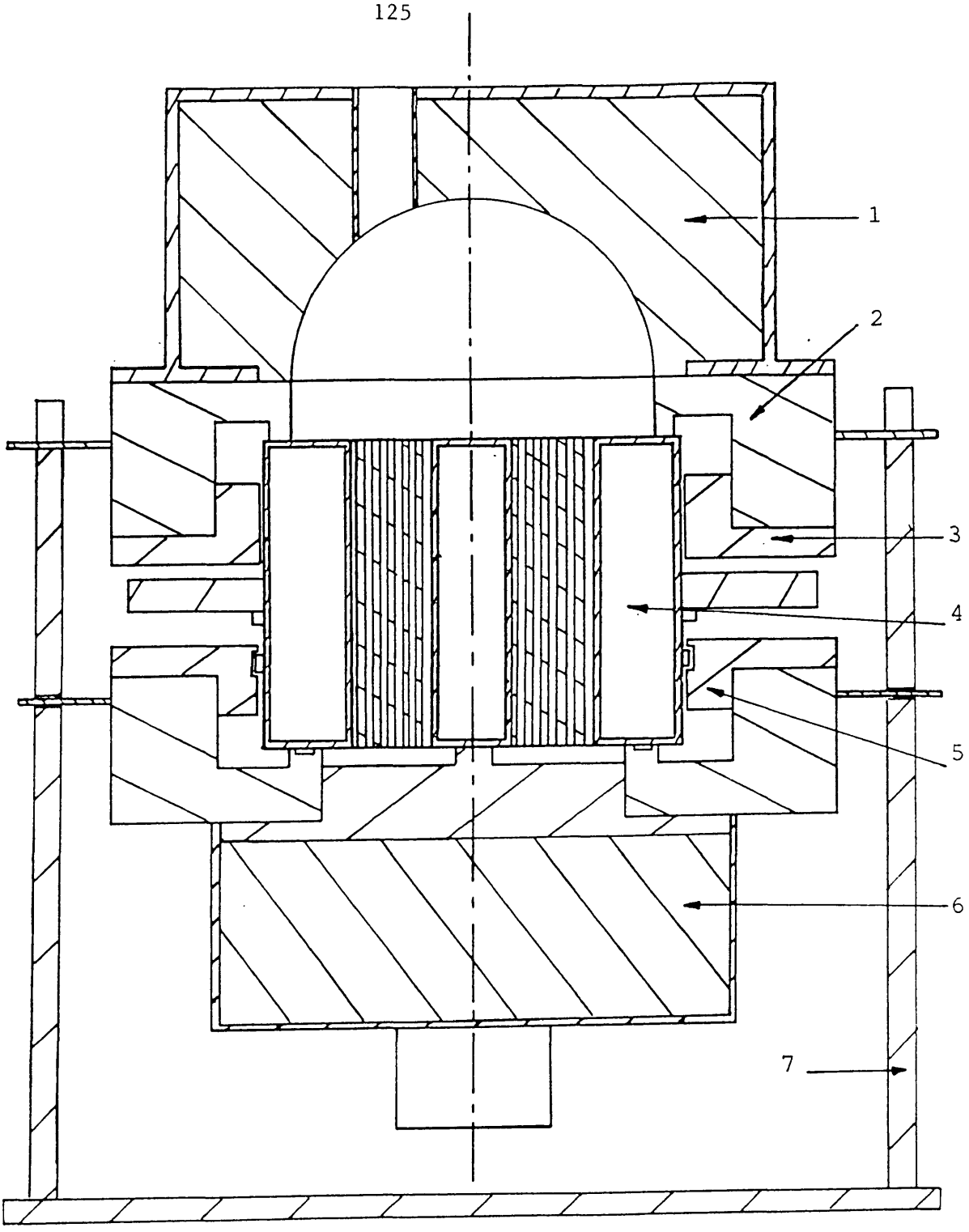


Figure (3.1): The rotary regenerator burner (schematic representation).

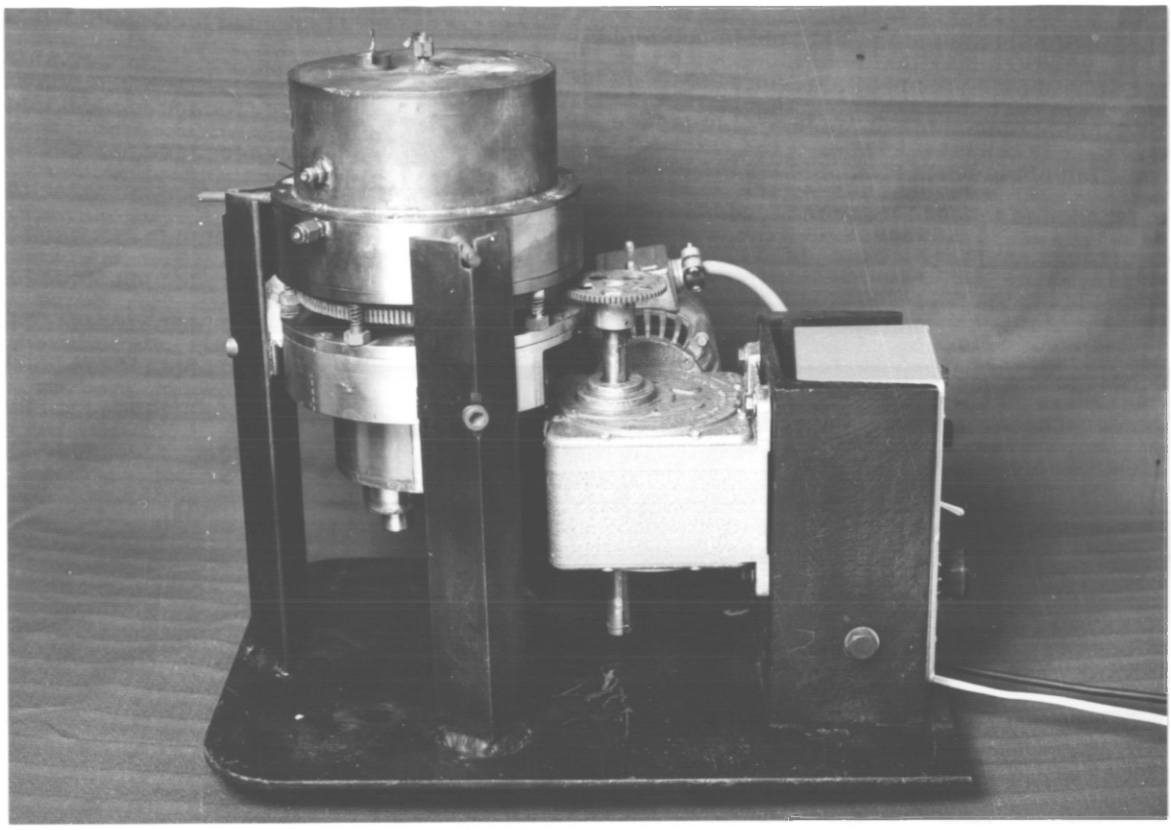


Figure (3.2): The rotary regenerative burner.

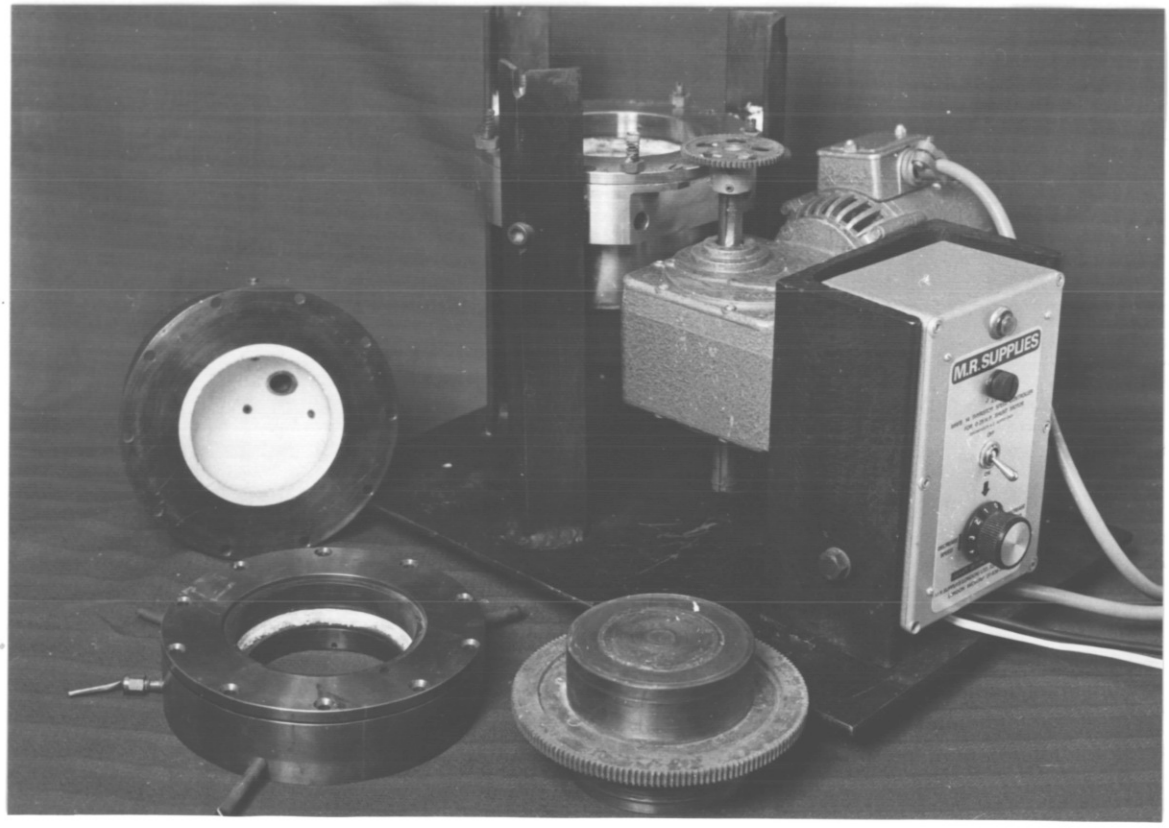


Figure (3.3): The parts of the rotary regenerative burner.

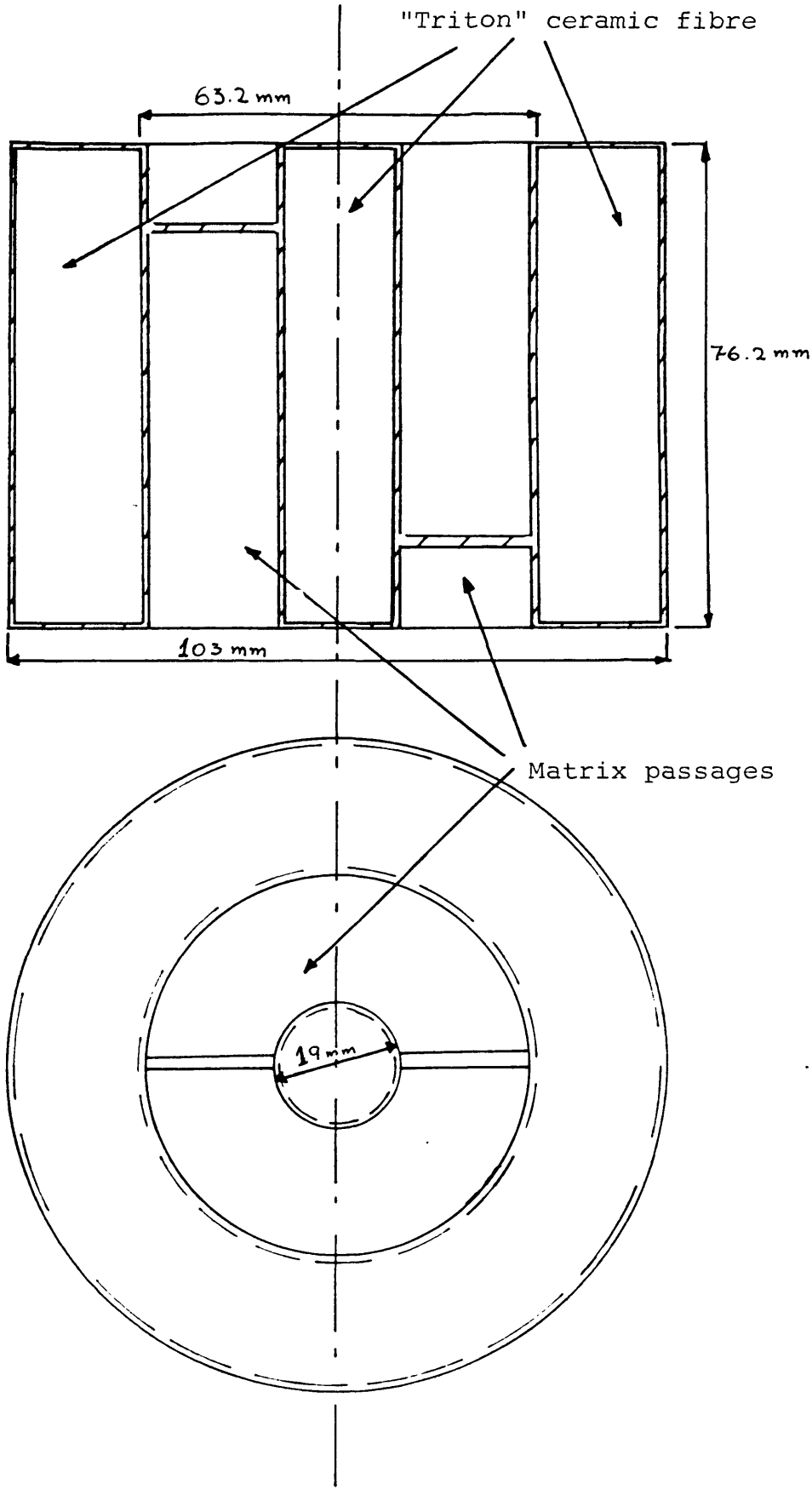


Figure (3.4): The regenerator rotor.

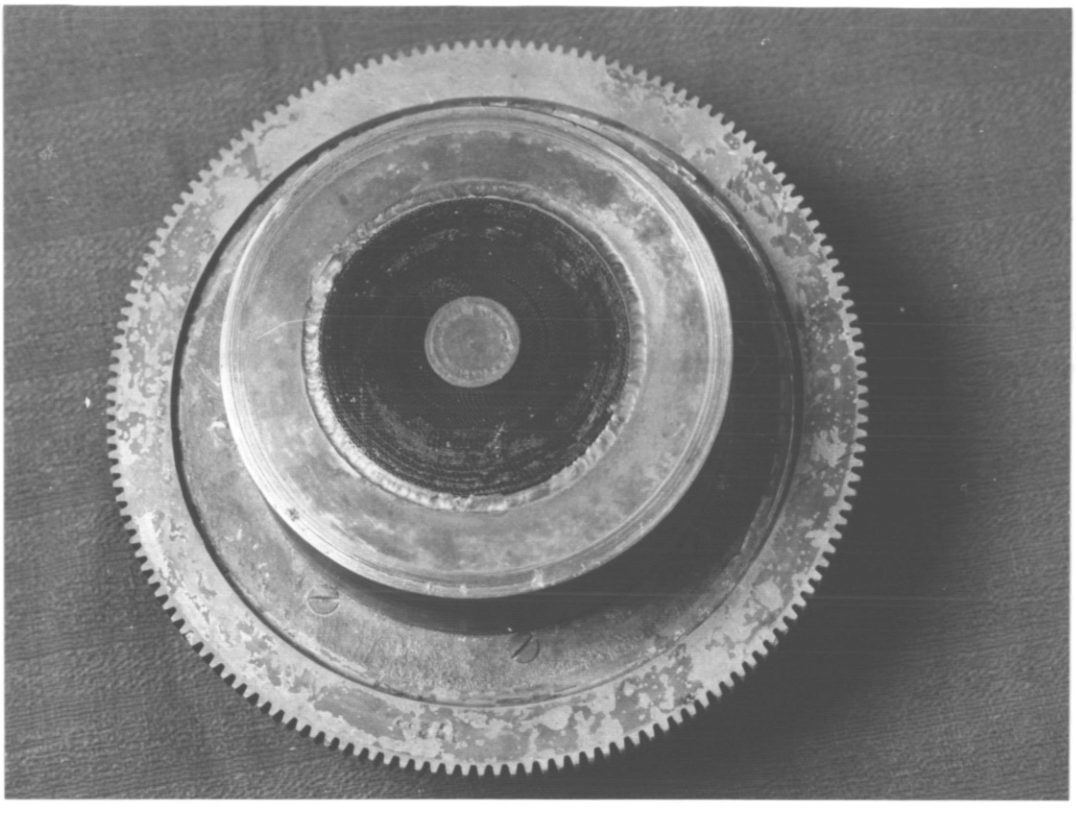


Figure (3.5): The metallic matrix rotor.

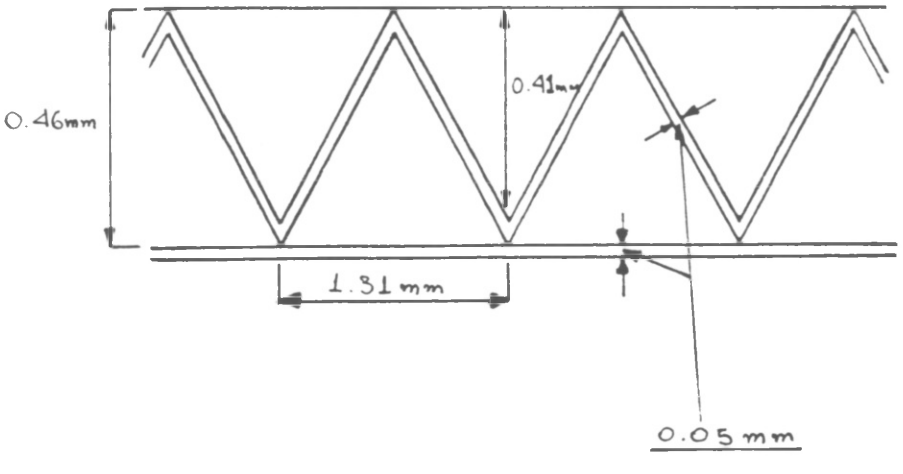


Figure (3.6): Dimensions of the flame trap matrix.

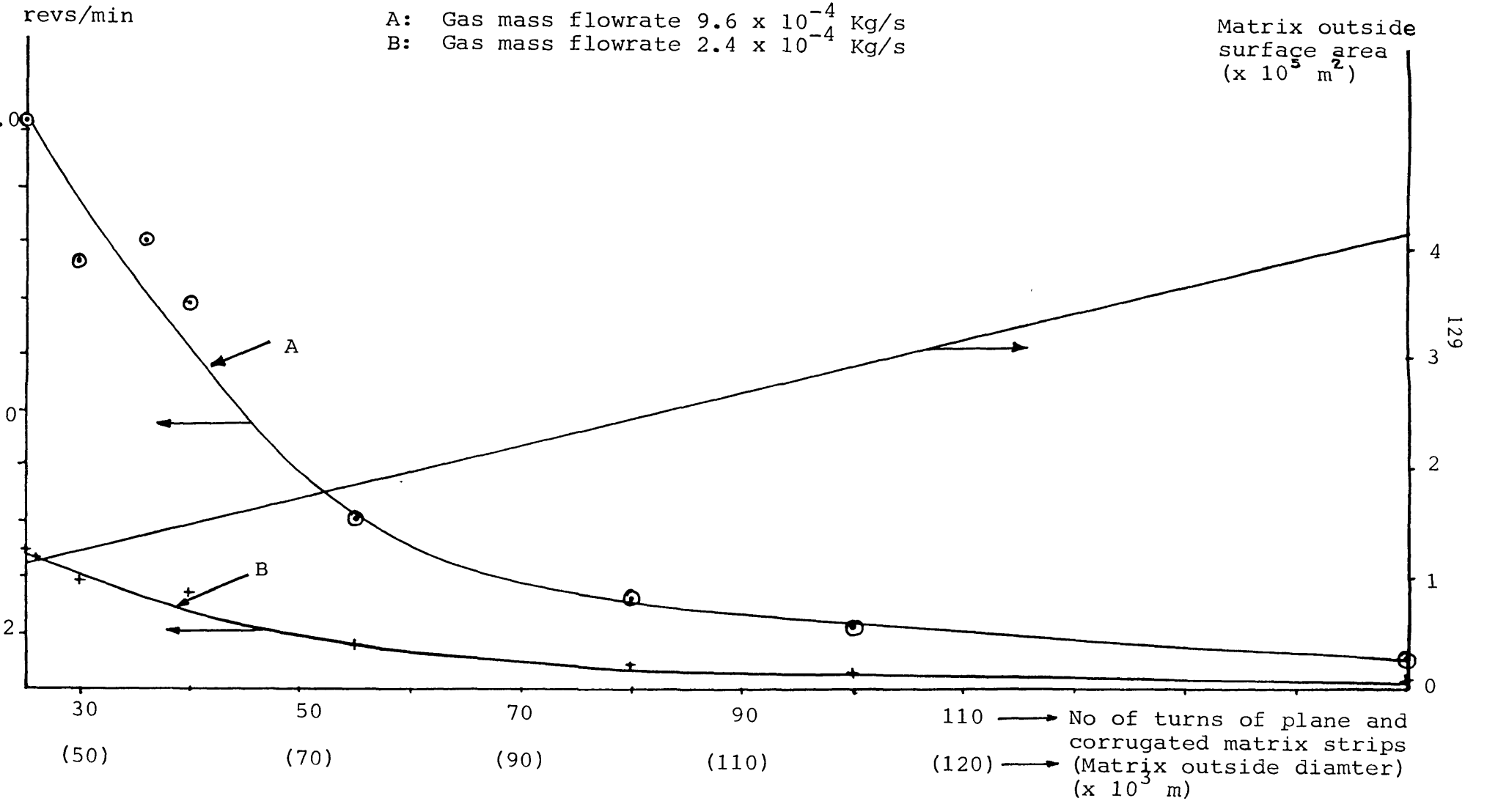


Figure (3.7): Matrix rotational speed against matrix size for 90% effectiveness. Matrix surface area against matrix diameter.

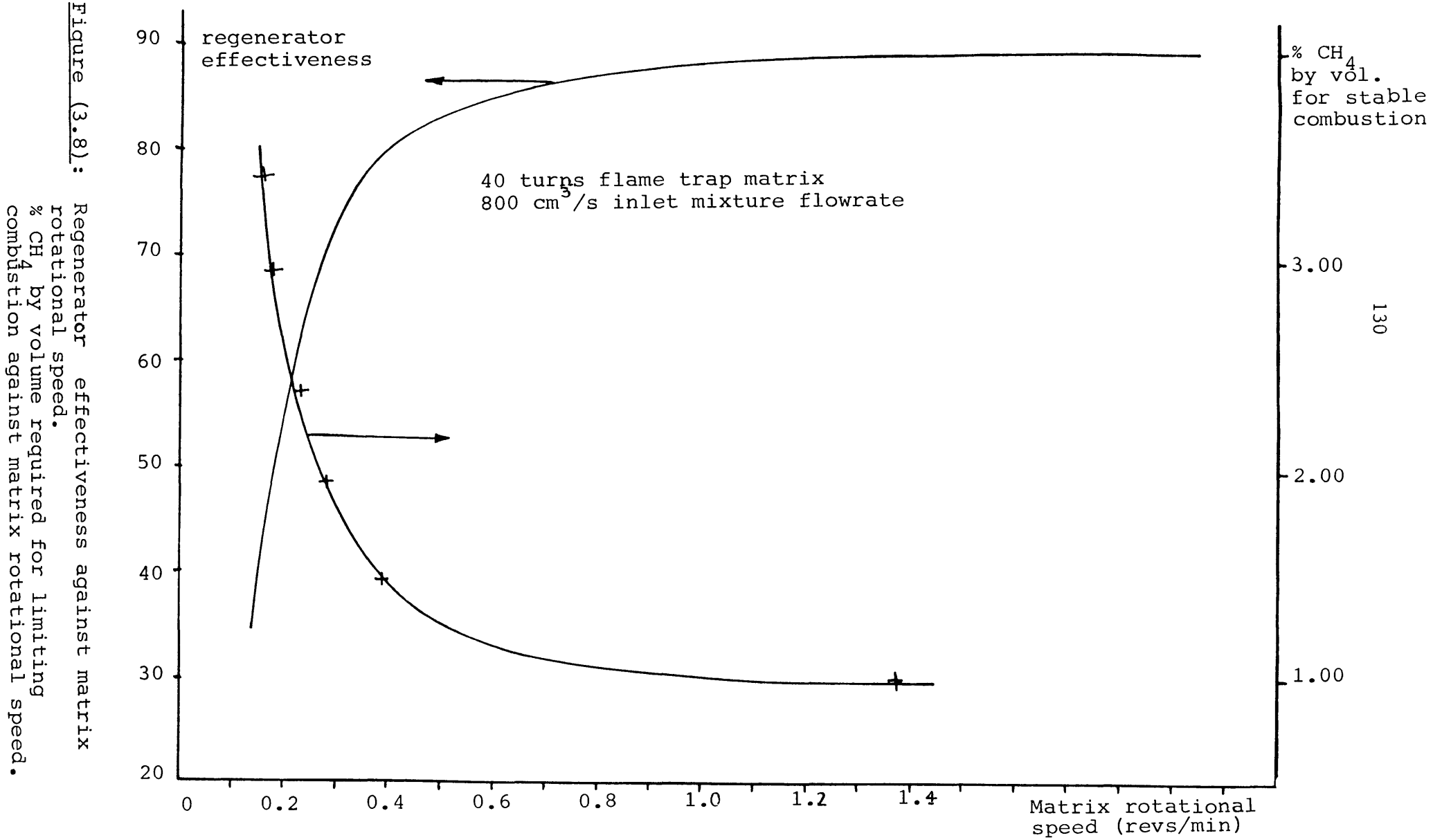


Figure (3.8): Regenerator effectiveness against matrix rotational speed.
% CH_4 by volume required for limiting combustion against matrix rotational speed.

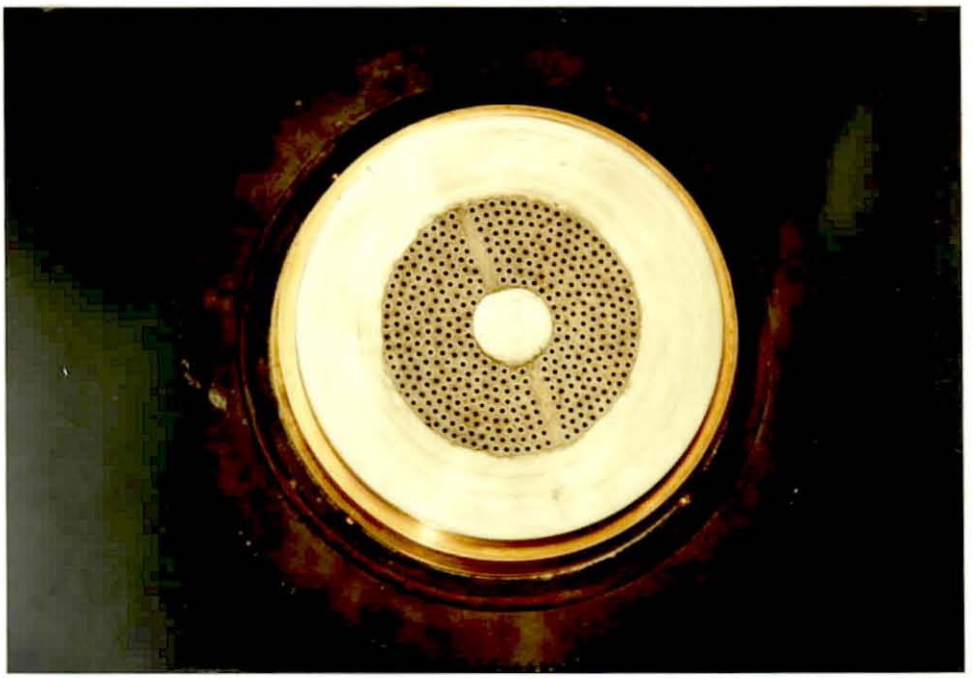


Figure (3.9): The ceramic matrix.

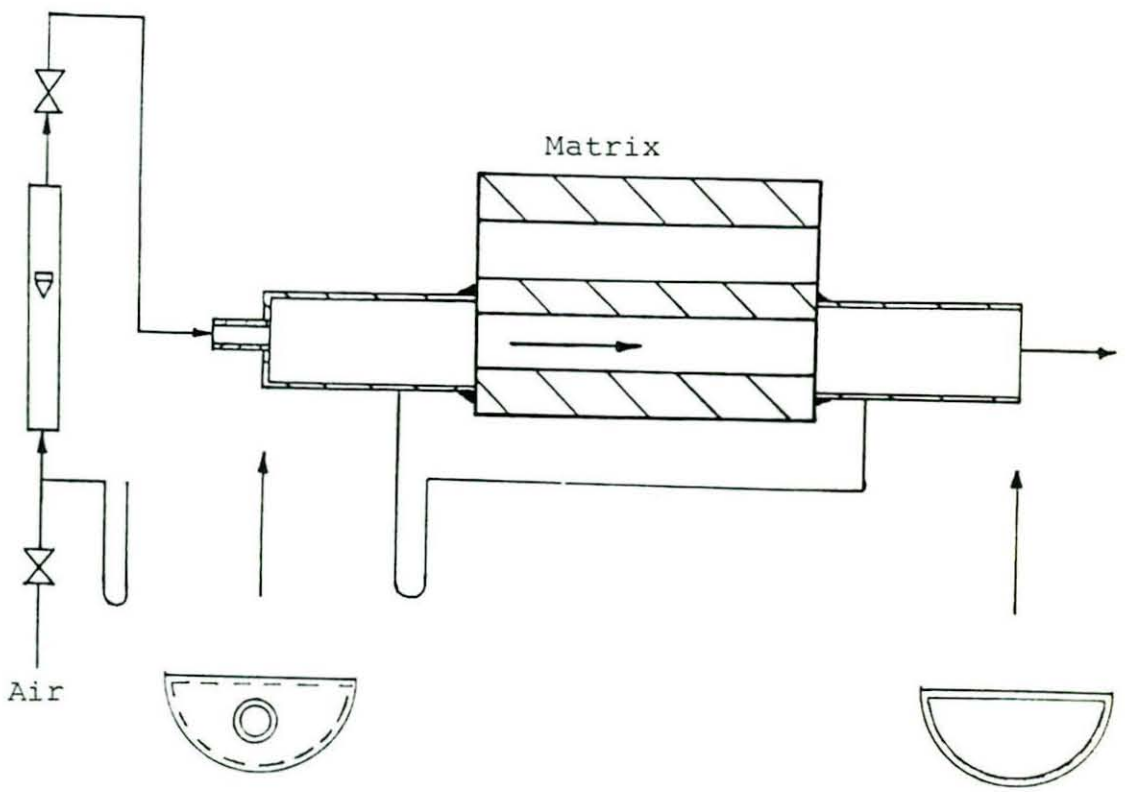


Figure (3.10): Schematic representation of equipment for measurement of pressure drop through half the matrix.

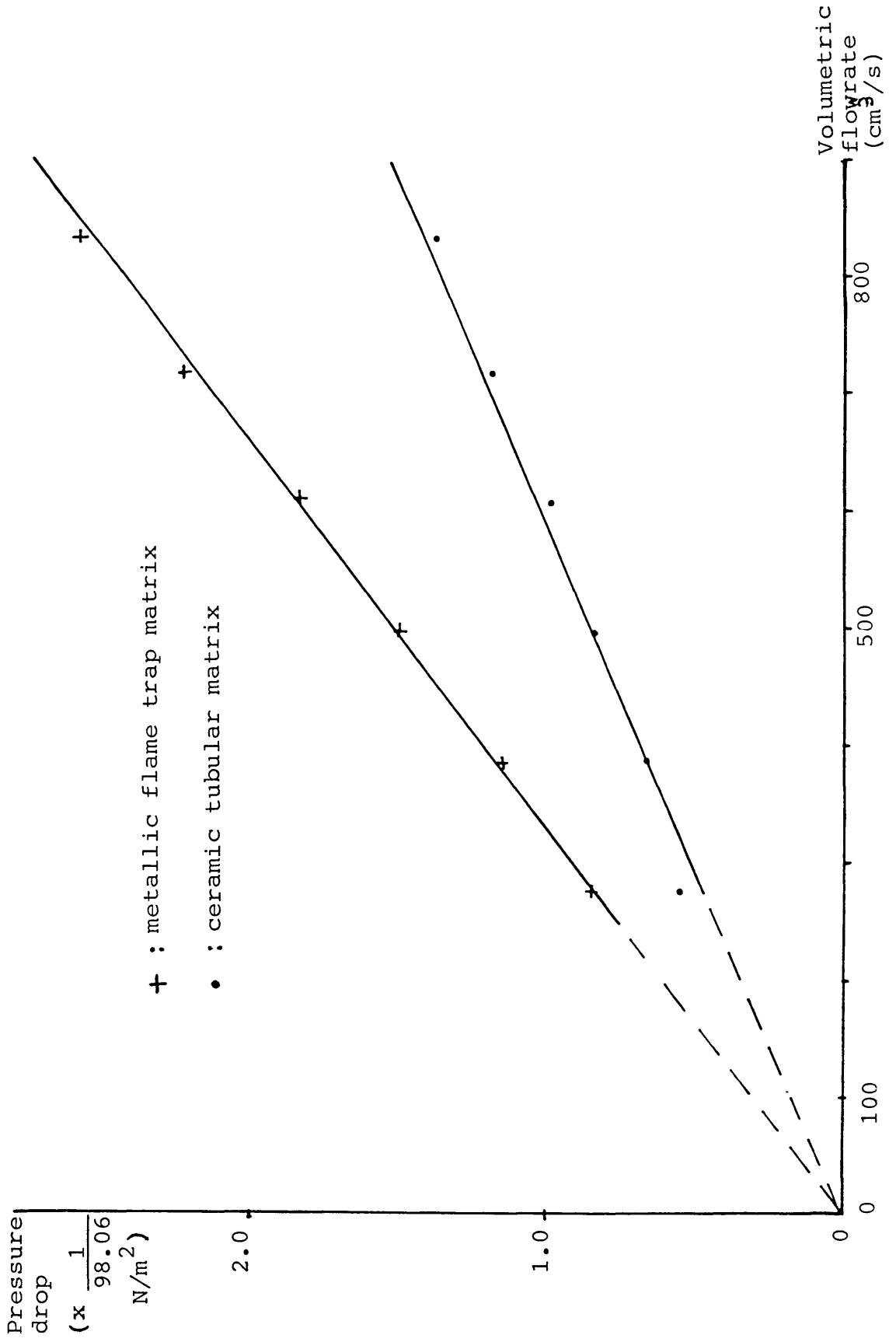


Figure (3.11): Pressure drops for flow through
(a) the metallic matrix
and (b) the ceramic matrix .

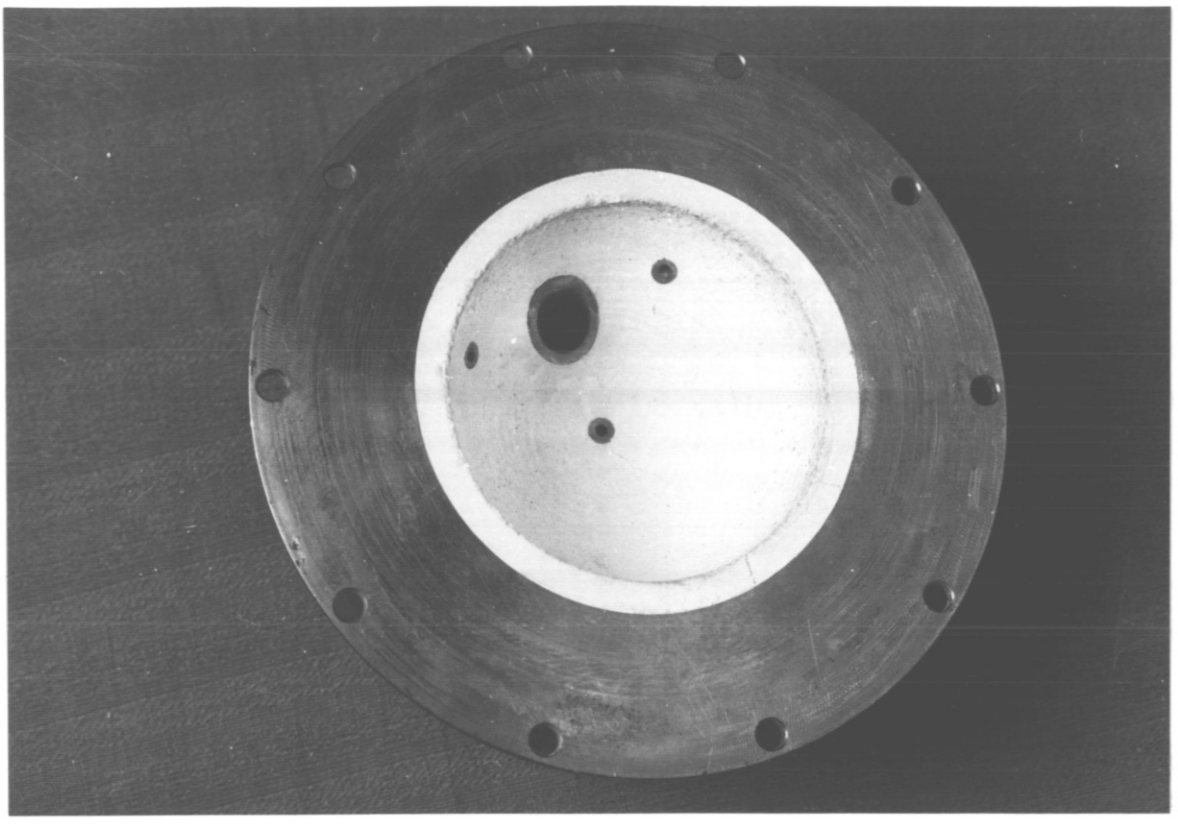


Figure (3.12): The 90 mm i.d. hemispherical chamber of concrete walls.

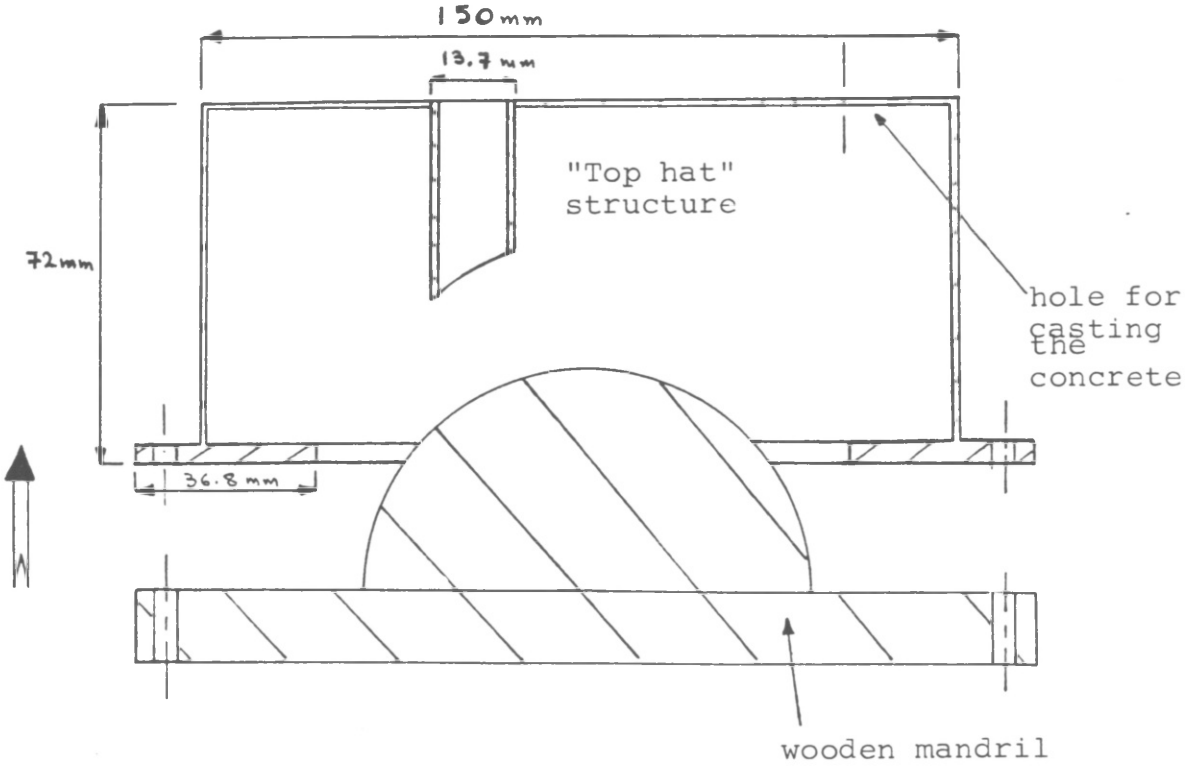


Figure (3.13): The "Top hat" structure and the wooden mandril for construction of the 90 mm i.d. chamber.

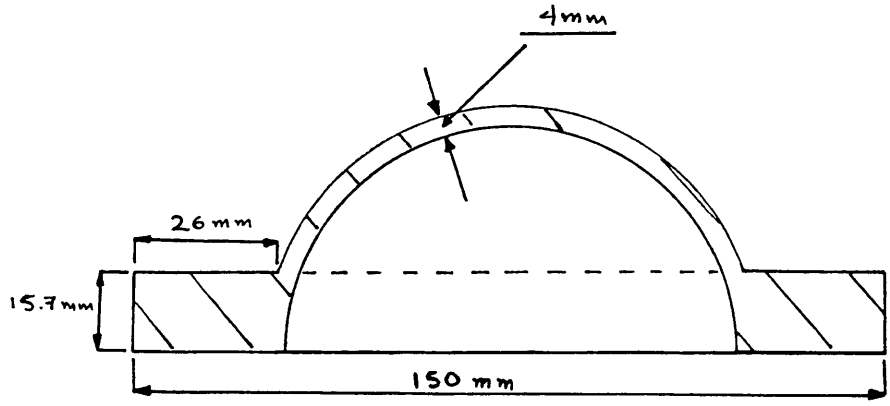


Figure (3.14): The transparent quartz 90 mm i.d. dome.

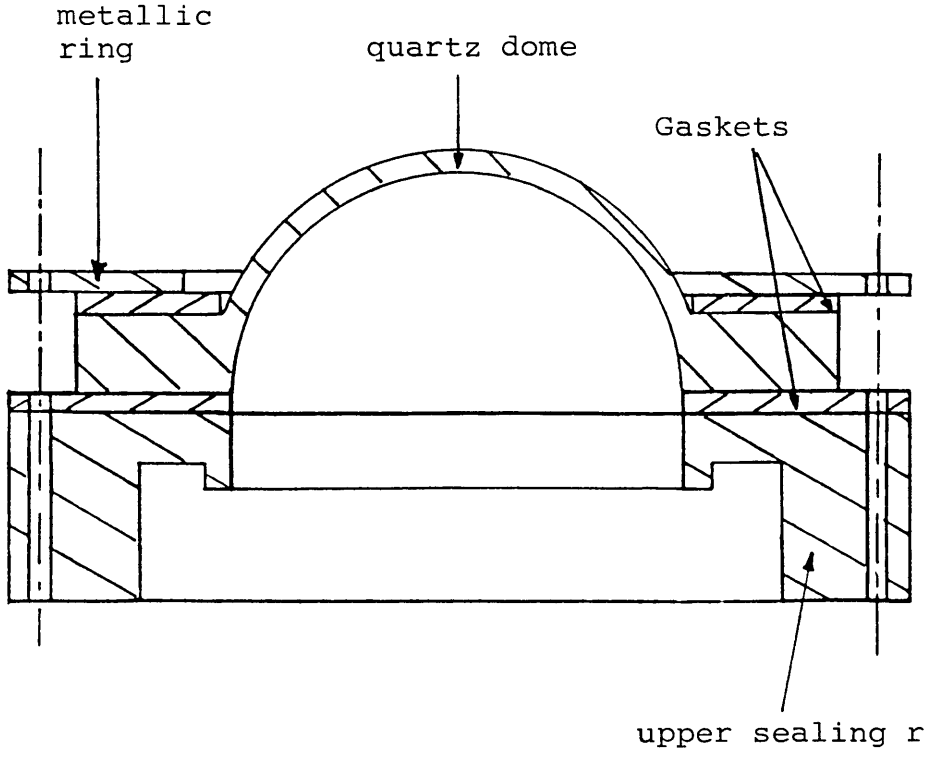


Figure (3.15): The quartz dome attached on the upper sealing ring (bolts not shown).

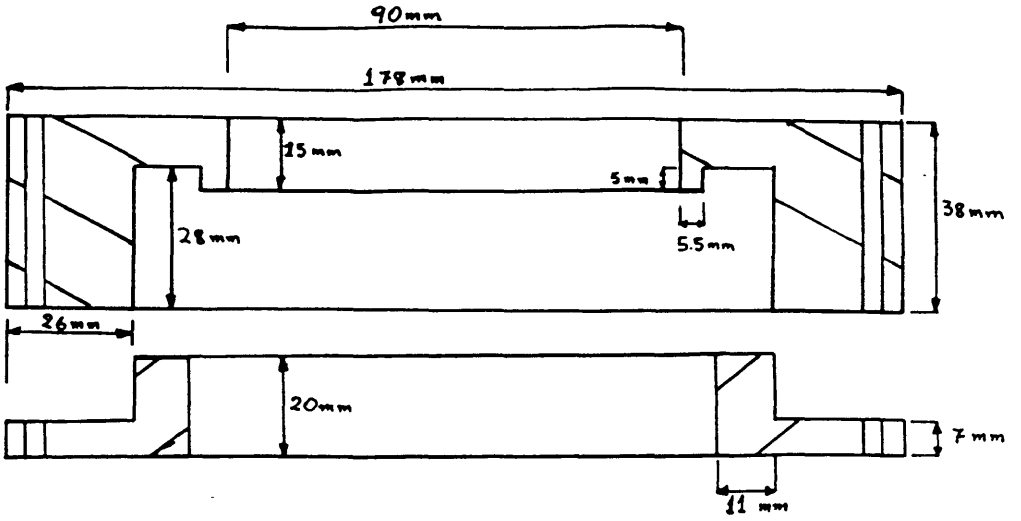


Figure (3.16): The upper sealing and compacting rings of the prototype unit.

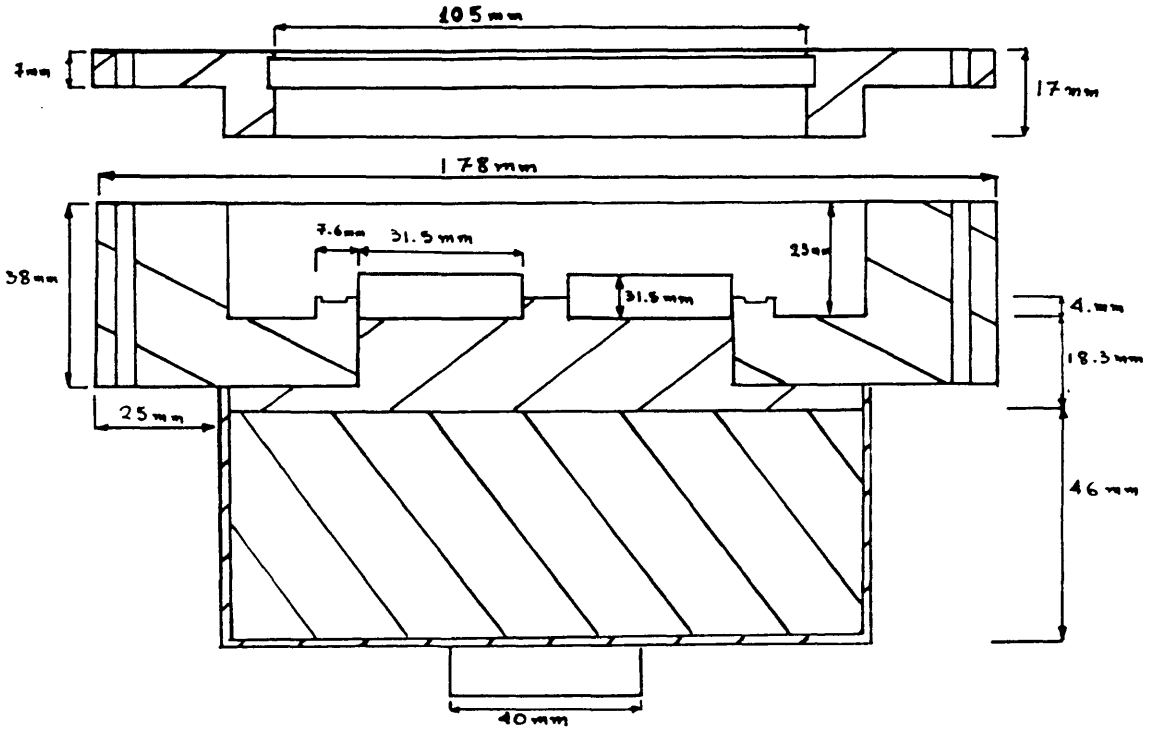


Figure (3.17): The lower section of the prototype unit.

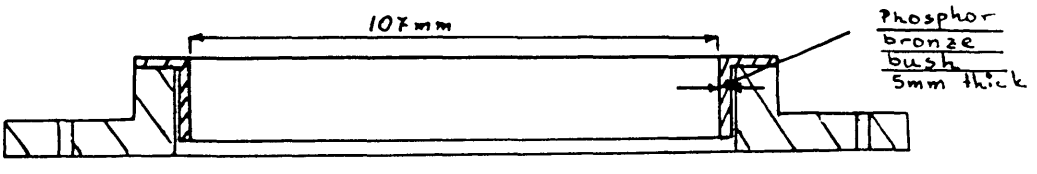


Figure (3.18): The upper compacting ring of the modified unit.

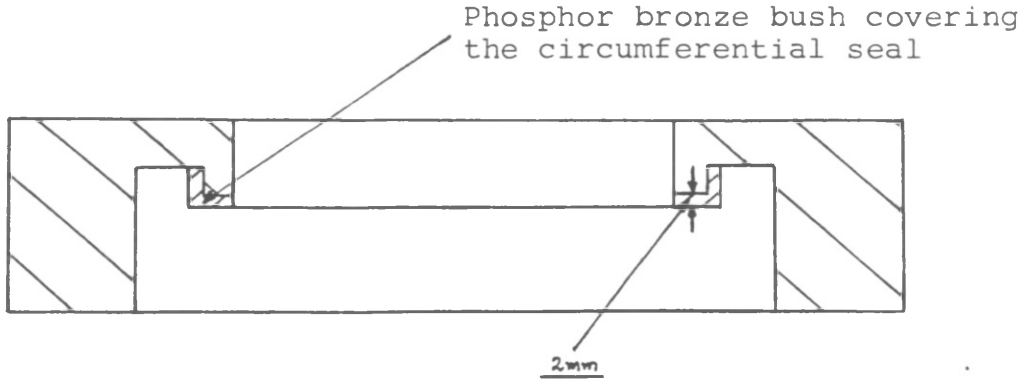


Figure (3.19): The upper sealing ring of the modified unit.

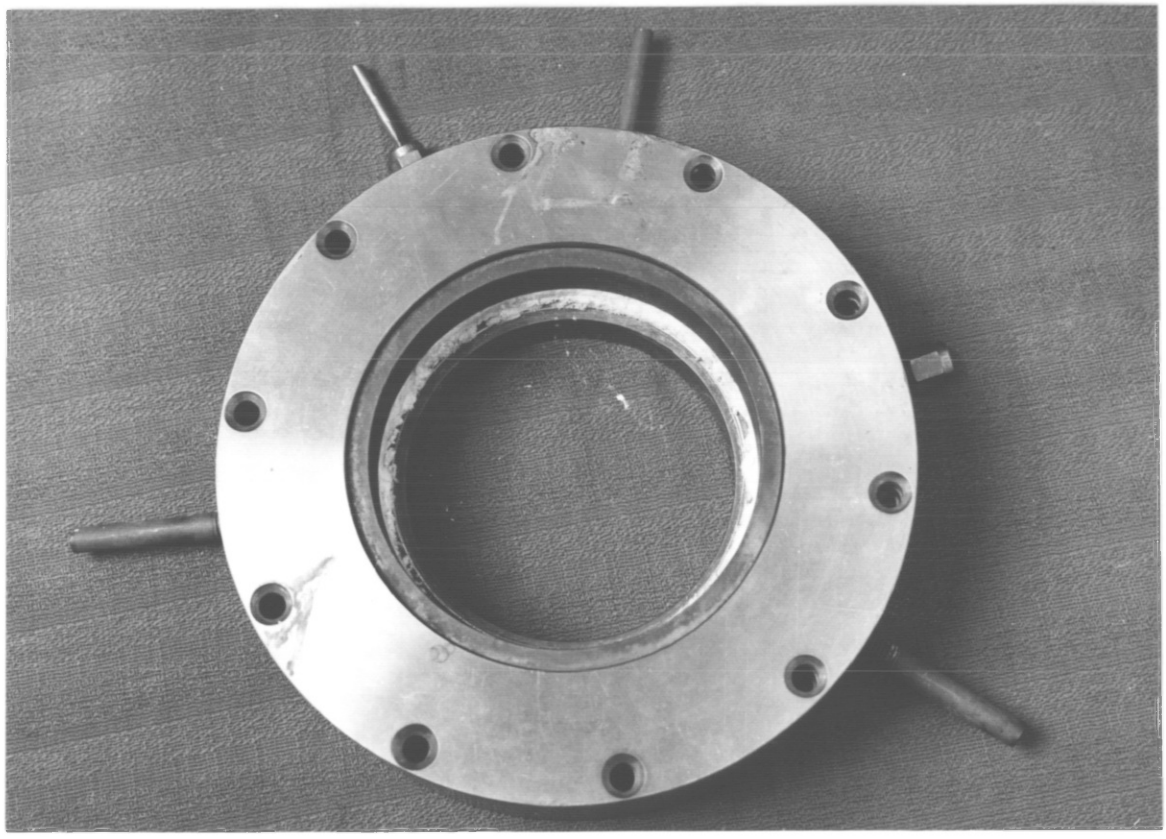


Figure (3.20): The upper sealing and compacting ring of the modified unit.

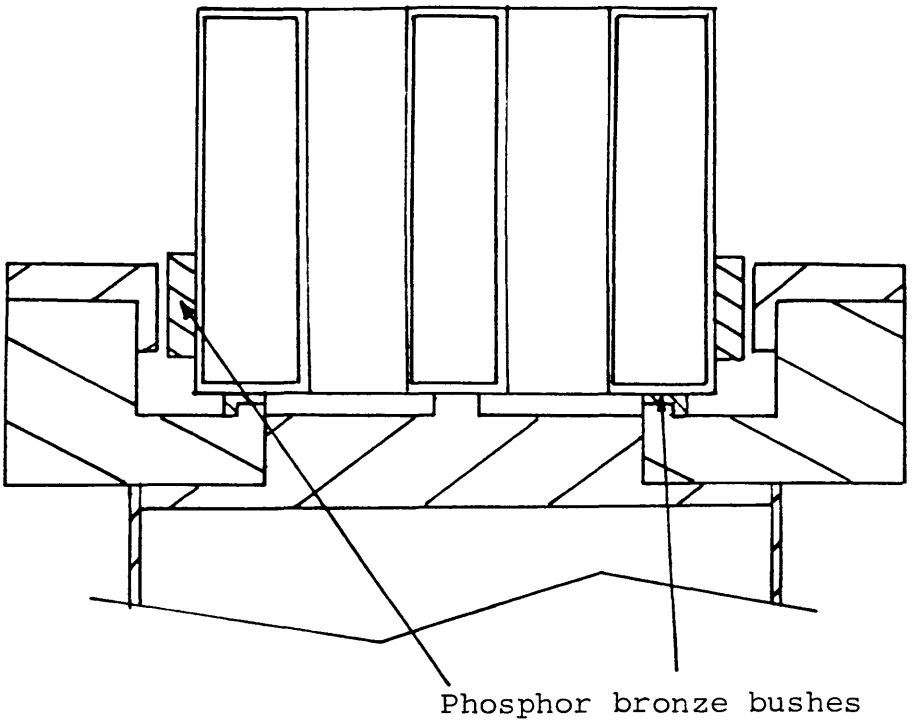


Figure (3.21): Lower section of the modified unit.

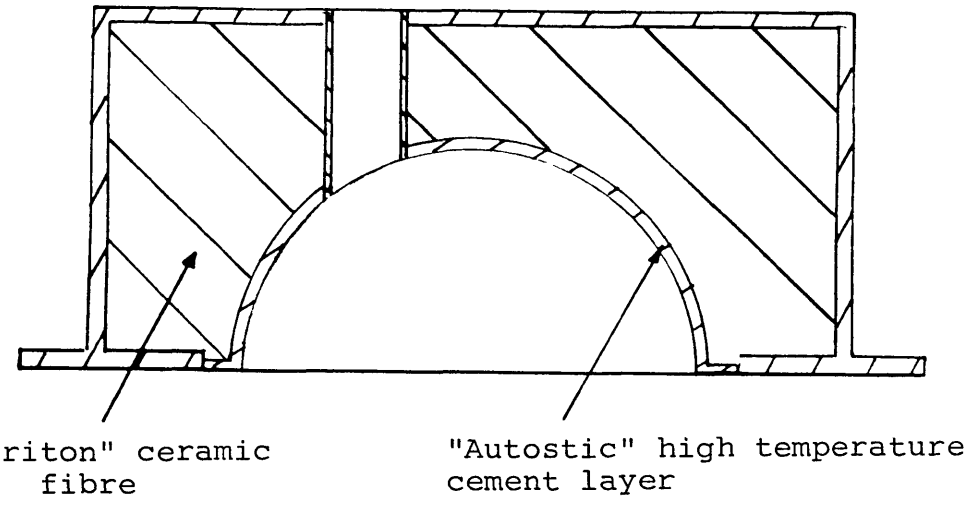


Figure (3.22): The lighter combustion chamber structure.

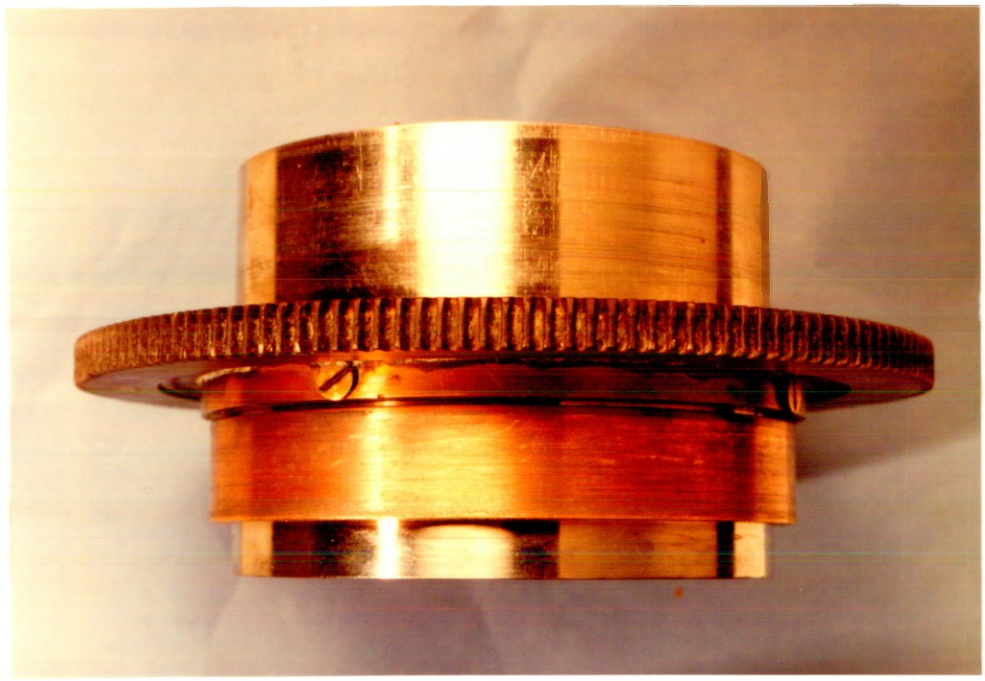


Figure (3.23): The rotor of the modified unit.

$$V_l = \sum_{i=1}^{4} V_{l_i}$$

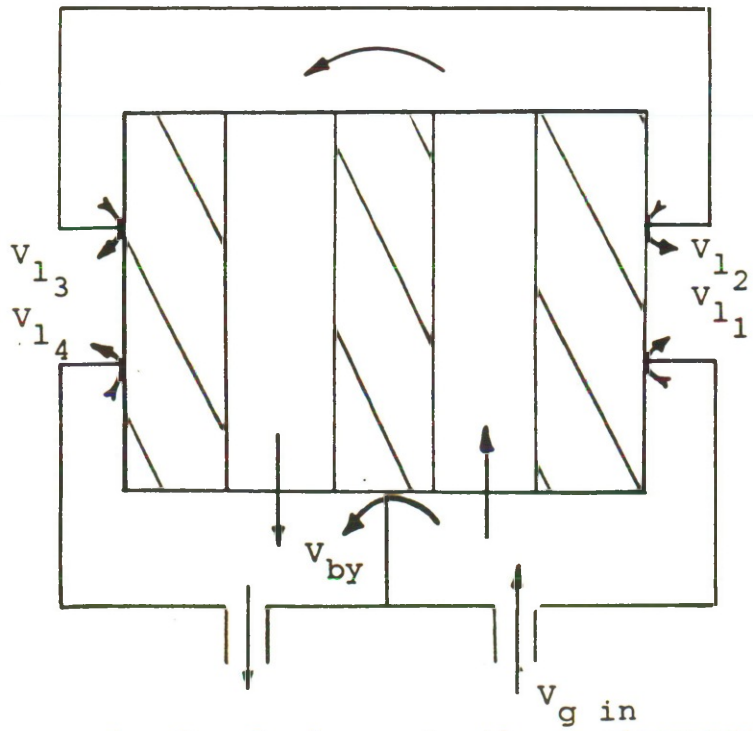


Figure (3.24): Paths for leakages to the environment, V_l, and bypass leakages, V_{by}.

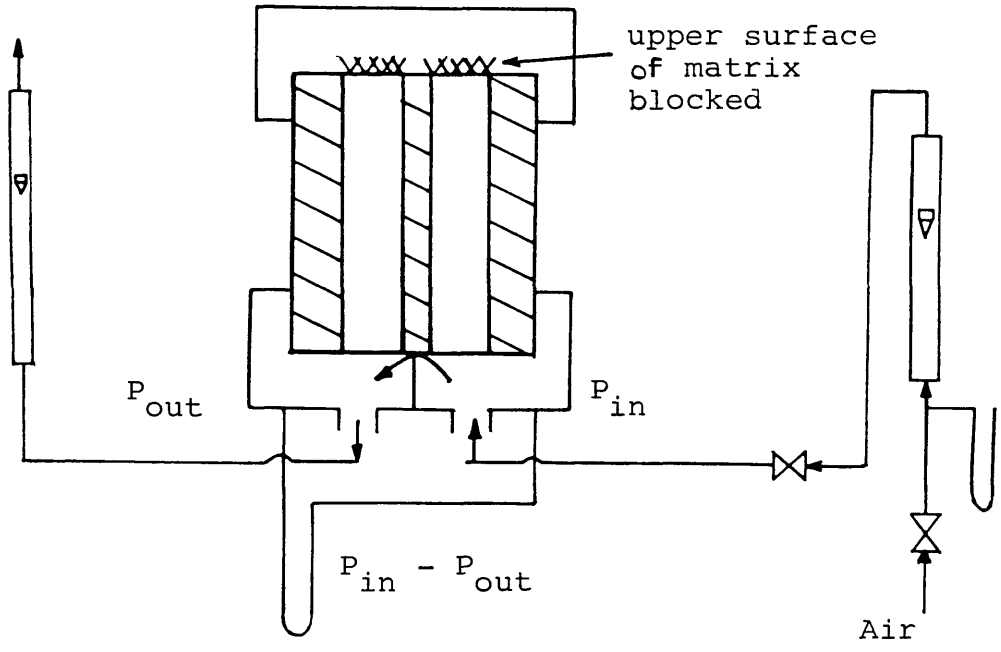


Figure (3.25): Schematic representation of equipment for obtaining relationship between $P_{in} - P_{out}$ and V_{by} (bypass leakage rate).

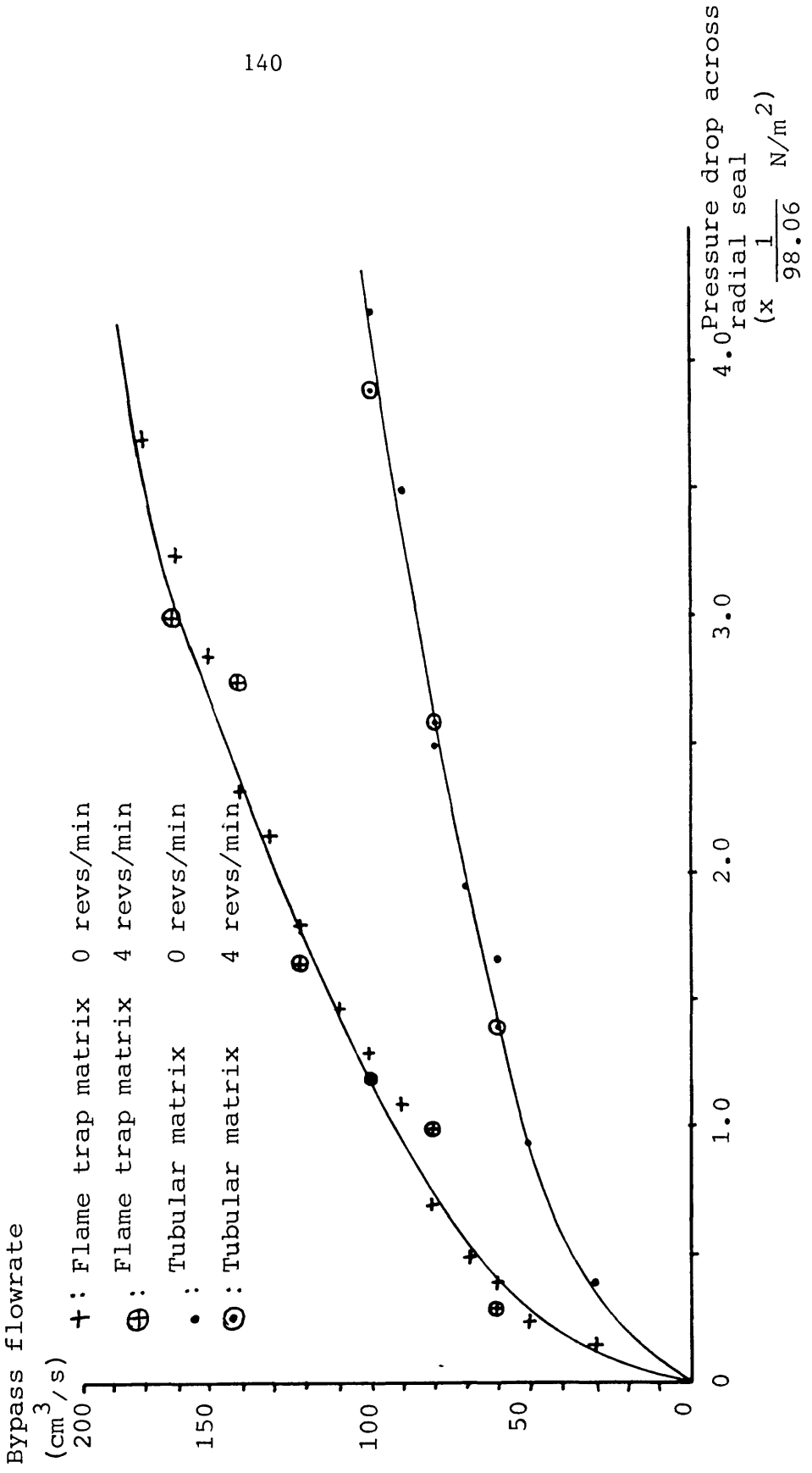


Figure (3.26): Variation of the bypass leakage rate with the pressure difference across the radial seal .

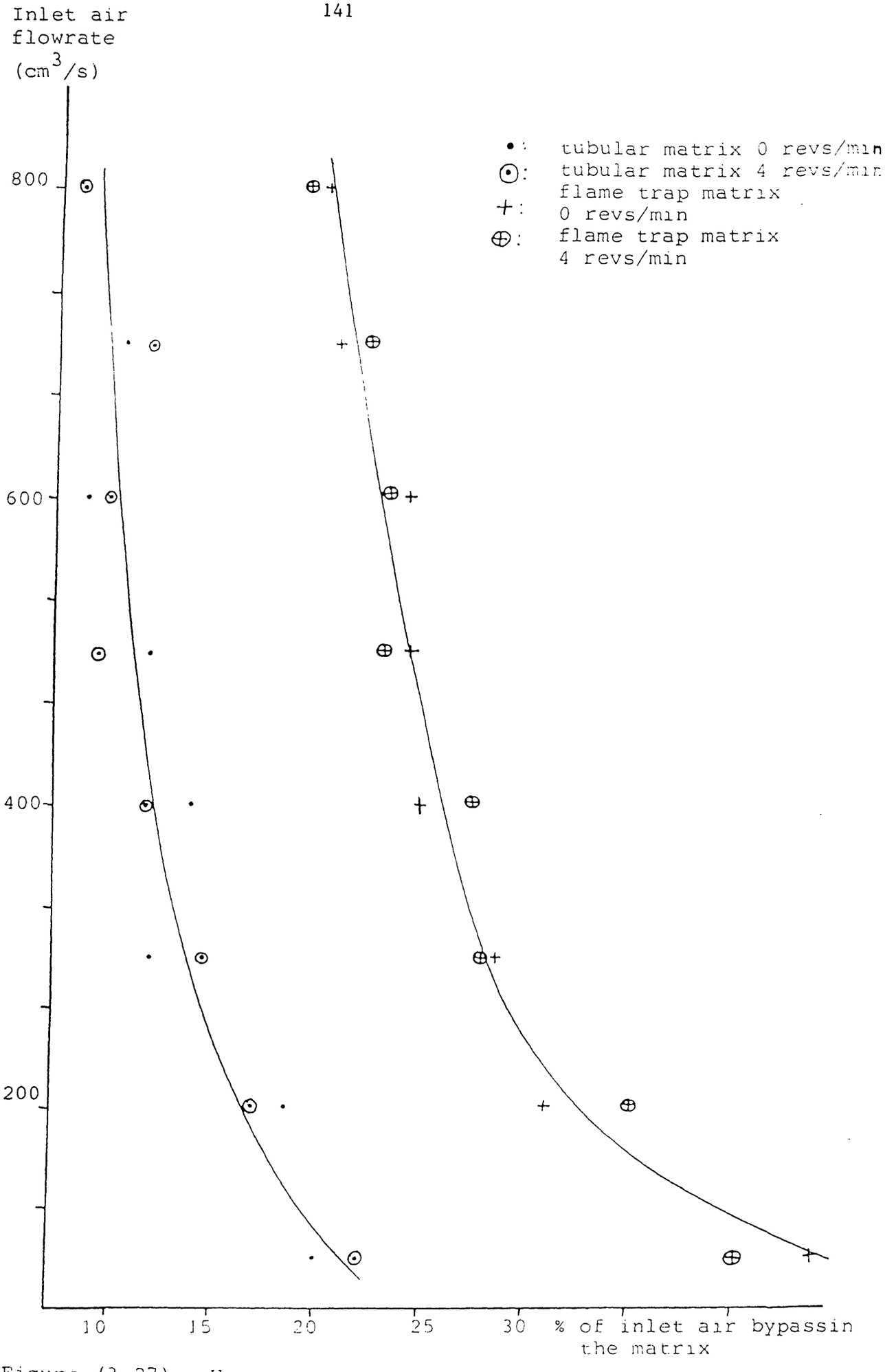


Figure (3.27): Variation of bypass flowrate with inlet flowrate

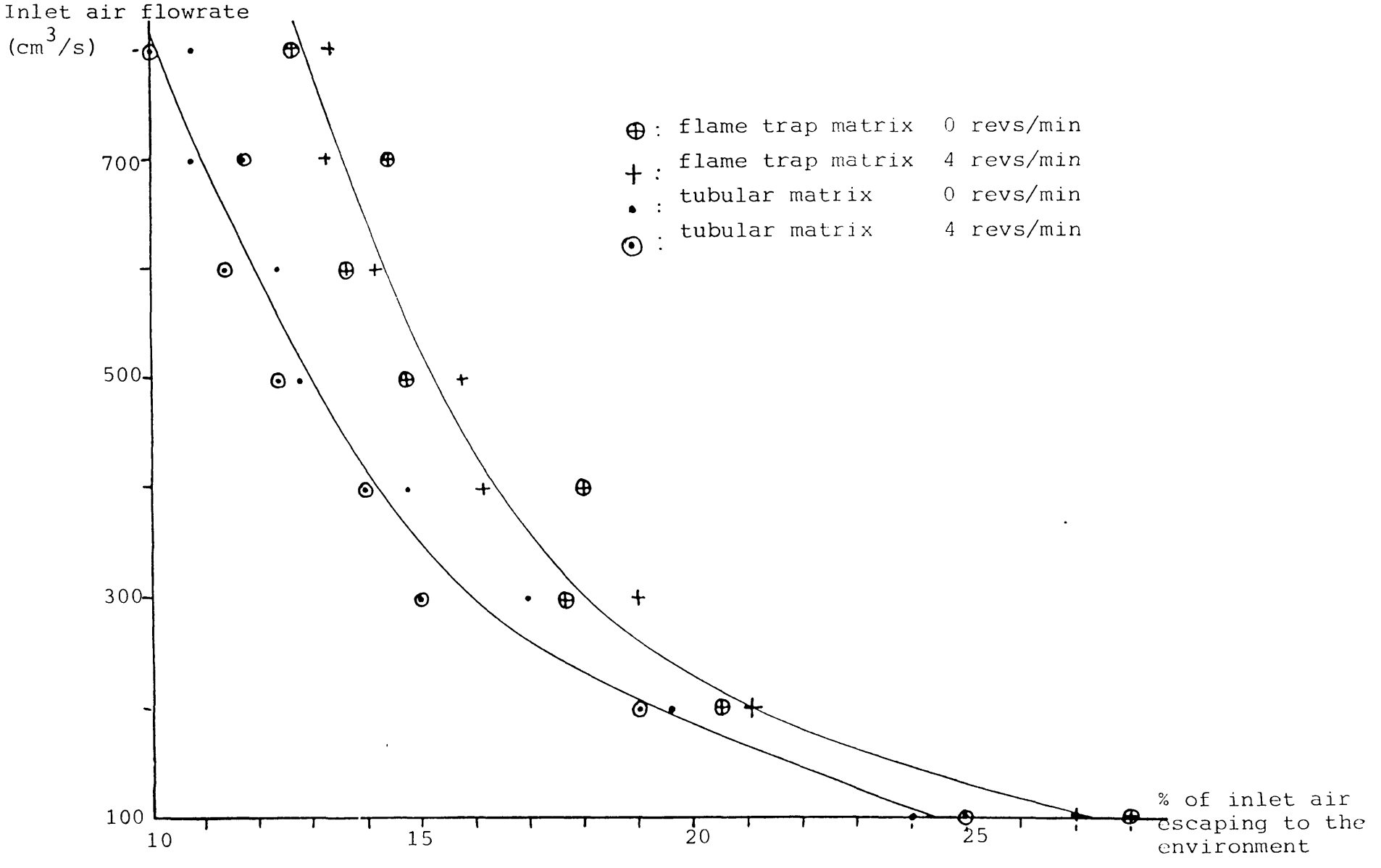


Figure (3.28): Variation of the leakage rate to the environment with the inlet flowrate.

Chapter 4

Mathematical modelling of combustion within the rotary regenerative burner

4.1. Introduction

In the present Chapter an approximate model is developed for the prediction of the stability characteristics of the experimental burner with the ceramic matrix and hemispherical combustion chambers of 60 mm and 90 mm diameter.

The assumptions and method, involved in modelling the combustion and heat recirculation processes, are presented. The description of the computer program, that was written to solve the equations of the model, follows and, finally, the predicted results are presented in graphical form, and discussed.

4.2 General philosophy of modelling of the rotary regenerative burner

The development of a mathematical model that predicts the stability characteristics of the rotary regenerative burner was considered essential, and formed an integral part of the experimental study.

Such a model could be usefully employed in design studies, in

as much as it would provide an understanding of the effects of the large number of parameters, on the final level of performance of the system.

The combustion and heat transfer processes within the burner are interdependent and complex. A rigorous model that included every phenomenon down to microscopic detail would have been extremely time consuming or even impossible. A compromise, therefore, between the rigorous model and one that gives acceptable results was reached.

The model was based on a theory that described the processes within heat recirculating burners of a type similar to that of the rotary regenerator burner. In all the burners, of the type under consideration, preheated, fast moving reactants emerge from a heat exchanger into a relatively large combustion chamber where the gases are almost stationary. These heat recirculating burners for combustion of lean fuel mixtures below their lower flammability limit, were shown in Chapter 1 to be characterized by similar "L" shaped stability curves. The theory predicting the performance of such systems was of a general form and its keystone was the experimental observation that temperature remained sensibly constant for one fuel, irrespective of flow velocity, heat losses or fuel concentration. In order to quantify the rotary regenerative burner, the precise dependence of the heat transfer process on the parameters of the burner had to be established before the general analysis could be used.

A number of simplifying assumptions had to be made in formulating the model and a computer program was written. The

model was evaluated by comparing predicted results to results obtained during the experimental study. The assumptions involved in modelling the combustion and heat transfer processes within the different parts of the burner are included in the following sections.

4.3. **Modelling of processes within the combustion chamber**

Preheated reactants, discharging from half the upper matrix surface, enter the combustion chamber where, provided they are hot enough, combustion takes place. The combustion chamber of hemispherical refractory cement walls is considered throughout the analysis presented here. Since the effective channels from which reactants enter and products leave the chamber are semicircular (i.e. the two symmetrical sections of the circular matrix) the optimum chamber geometry for avoiding dead spaces within the volume available for combustion, and for minimizing the wall area through which heat losses can occur, is the hemispherical geometry. In addition, a chamber of refractory cement walls would be of greater practical interest than say a chamber of quartz walls.

The reactant streams flowing through the matrix passages receive heat from the hot matrix walls and emerge at high temperatures and, with exit velocities that depend on the radial and angular position of the passages involved. The temperatures of the walls surrounding the passages near the central rotor core

and near the outside rotor cylindrical wall are lower than those of passages which are positioned in between. This is due to the large thermal conductivitiy of and, consequently, large heat loss through, the metal rotor walls. Lower wall temperatures mean smaller driving force for heat transfer and, therefore, lower preheat temperatures.

The temperatures of the solid walls surrounding the passages also depend on the angular displacement of the passages from the "hot products stream-cold reactants stream" interface. The solid temperature (throughout the matrix length) is maximum at the "hot-cold" gas interface and minimum at the "cold-hot" gas interface (rotation is clockwise (see figure (4.1)). There is, therefore, an angular variation of the temperature of the reactants emerging into the chamber.

The variation of the temperature of the individual streams with the radial and angular position of the passages from which they emerge, in conjunction with the geometry of the matrix and combustion chamber assembly, render the flow within the chamber very difficult to treat rigorously.

The complexity of the flow field within the chamber increases with increasing inlet gas flowrate. At very low flowrates the gas stream entering the chamber flows upwards, towards the part of the chamber wall directly above the matrix entry section. The stream is then forced to flow along the remaining wall surface and is eventually subjected to a 180^{o} change of direction. The gases then enter the exit passages without difficulty and flow down through the matrix.

For high inlet flowrates the gas stream emerging from the matrix impinges as a jet on the chamber wall and only a small part of it flows along the wall surface. Due to the small size of the exit passages, at such high flowrates, vortexing and, therefore, mixing occurs within the central section of the chamber. This, depending on the position of the flame, probably leads to some mixing of products and reactants. During cold testing of the burner the flow field was investigated by employing the transparent hemispherical 90 mm diameter quartz chamber and by injecting talcum powder in the air stream. Vortexing was observed for inlet flowrates exceeding 500 cm^3/s. The tests were performed with the tubular matrix and, if a 20% overall loss is assumed, the flowrate above which vortexing occured was $400cm^3/s$, i.e. for flows of Reynold's numbers greater than 458 (see Appendix D). During normal operation of the burner the volumetric flowrates in the combustion chamber are higher than those at the inlet. If the gases are assumed to be ideal and the inlet flowrate at 20^oC is $V_{g\ in}$(at 1 atm. absolute) the combustion chamber flowrate, V_{gcc}, (gases almost at 1 atm absolute) at the limit (assuming a constant limiting flame temperature of 1400 K) is given by

$$V_{gcc} = (1 - \%\ \text{loss})\ \frac{1400}{293}\ V_{g\ in} \qquad (4.3\text{-}1)$$

If vortexing is assumed to occur for flows at Reynold's numbers greater than 458, the inlet flowrate must be greater than 630 cm^3/s for the 90 mm diameter chamber and 420 cm^3/s for the 60 mm diameter one (see Appendix D).

For the combustion chambers of 60 mm and 90 mm diameters, assuming a constant final flame temperature of 1400 K, it can be shown that, for inlet flowrates of up to 1833 cm^3/s and 2749 cm^3/s respectively, the Reynold's numbers characterizing the flow within the chamber are below 2000 (i.e. flow is laminar and since there is vortexing it is unsteady).

The heat , loss associated with operation of the rotary regenerative burner mainly originates from the combustion chamber section of the system. The combustion chamber inside wall receives heat (a) by convection from the preheated reactants and the combustion products within the chamber and (b) for higher inlet flowrates (i.e. when heat recirculation rate is large compared to the heat loss rate) by radiation from the matrix upper surface. Since very lean fuel-mixtures are considered here, the reactant and product gases in the chamber are mainly air and do not, therefore, emit or absorb energy in appreciable amounts. For higher inlet flowrates the matrix surface temperature must be higher than that of the chamber wall. The hot gases giving up heat to the matrix solid walls flow through the matrix passages with higher velocities than in the relatively large combustion chamber and the convective coefficient for heat transfer to the matrix walls must, therefore, be larger than the one for heat transfer to the chamber wall. Furthermore, since for higher inlet flowrates the heat recirculation to heat loss rate ratio is expected to be large, the temperatures of the hot product gases entering the matrix must be apprieciable. The opposite must be true during operation with low inlet flowrates.

When the system is at equilibrium the heat received by the combustion chamber wall is conducted through the metal wall of the burner and is lost to the environment by natural convection from the surface of the insulating layer surrounding the system.

The processes described above are interdependent and directly affect the combustion process. If, in predicting the stability characteristics of the burner for a given set of parameters, an entirely fundamental approach was to be used, the mass, momentum, energy and species conservation equations would have to be solved simultaneously. This would be impossible as the detailed kinetics of individual reaction steps for hydrocarbon combustion are not known in detail. The approach used here, even though it appears simplistic, is based on an experimental observation. As previouslly mentioned, the lean combustion stability limits for the family of burners, in which the rotary regenerator burner appears to belong, were found to behave as the flammability limits in stationary gases, i.e. that the decrease in fuel required to maintain the mixture at the limit, when the initial temperature is raised is such that the decrease in heat of combustion exactly balances the increase in thermal enthalpy. The constant flame temperature is of the order of 1400 K for methane-air mixtures.

In modelling the processes within the combustion chamber the following assumptions were made.

(a) The flame front is very thin and complete combustion occurs before the preheated reactants have time to lose any of their sensible heat to the combustion chamber wall. This would only be the case if the flame is stabilized on the matrix.

(b) The heat of combustion, due to the fuel contained in the preheated mixture, is used in its entirety in heating the exhaust gases to the constant final flame temperature of 1400 K for methane. This is quite reasonable as temperatures are low and dissociation can be ignored.

(c) The temperature of the combustion chamber wall is uniform. This might be the case depending on whether the flame is stabilized on the matrix or spread throughout the combustion chamber.

(d) The temperature of the exhaust gases is uniform throughout the chamber (at 1400 K for methane). This again will only be so if the flame zone is spread throughout the combustion chamber.

(e) There is a discontinuity at the exit from the chamber in that the exhaust gases leave at a temperature which is lower than 1400 K due to the sensible heat they give up to the chamber walls.

(f) Heat transfer to the combustion chamber wall is only by convection from the exhaust gases at 1400 K. In practice heat is also received by radiation from the matrix surface which, depending on the surface temperatures might be appreciable. Its inclusion would, however, complicate the model, and the processes within the combustion chamber and the rotating matrix would have to be considered simultaneously.

(g) The temperature on the surface of the metal walls of the burner is assumed to be equal to the combustion chamber

inside wall temperature and all the heat lost from the system is assumed to originate in the combustion chamber. Since the walls of the burner are metallic and, therefore, of high thermal conductivity, and the matrix solid (from where heat losses also occur) is surrounded by hollow walls of low effective thermal conductivity, the above are reasonable approximations of the actual conditions within the system.

For methane-air mixtures the percentage of methane by volume required for stable combustion just before extinction, f, is given in terms of the limiting final flame temperature, 1400 K, the averaged preheat temperature of the reactants entering the chamber, $T_{gc\ out(Avg)}$, and the heat of combustion per unit volume of methane (at 20°C, at 1 atm absolute), q, as follows:

$$f = \frac{\rho_{g_{20}}\ c_{pg}\ (1400 - T_{gc\ out\ (Avg)})}{q} \qquad (4.3\text{-}2)$$

where $\rho_{g_{20}}$: mixture density at 20°C (kg/m^3)

c_{pg} : mixture specific heat at arithmetic mean between 1400 K and $T_{gc\ out}$ (J/kg K)

The mixtures under consideration are mainly air and the physical properties used here are, therefore, those for air.

Since $\rho_{g_{20}} = 1.2\ kg/m^3$ and $q = 32.5 \times 10$ J/M^3

$$f = 4 \times 10^{-8}\ c_{pg}\ (1400 - T_{gc\ out(Avg)}) \qquad (4.3\text{-}3)$$

The heat lost by the exhaust gases, Q_L, is given by

$$Q_L = A_{cc}U_{cc}(1400 - T_a) \qquad (4.3\text{-}4)$$

where A_{cc}: chamber wall surface area (m^3)

U_{cc}: overall heat transfer coefficient (J/m^2 s K)

T_a : ambient temperature (K).

An approximate overall heat transfer coefficient is used here and it is given in terms of the thermal resistances for (a) heat transfer by forced convection from the exhaust gases to the chamber wall, (b) heat transfer by conduction through the layer of insulation surrounding the burner and (c) heat transfer by natural convection from the surface of the insulating layer to the environment.

The overall heat transfer coefficient in terms of the chamber radius, r_{cc}, and the convective coefficient for transfer from the exhaust gas to the chamber wall, h_{cc}, is obtained in Appendix D as

$$A_{cc}U_{cc} = \frac{1}{(3.141r_{cc}^2 + 11.1 \times 10^{-3})h_{cc}} + 2.269 \qquad (4.3\text{-}5)$$

The conective heat transfer coefficient, h_{cc}, between the exhaust gas and the combustion chamber wall was obtained from the predictions for uniform heat flux in a curved pipe when flow is laminar and fully developed (4.1). The analysis applies to flows

of large Dean numbers, De, where

$$De = Re\sqrt{r/\beta} \tag{4.3-6}$$

and Re: Renold's number

r: radius of pipe (m)

β: radius of curvature of pipe axis (m)

When De is large, the central part of the fluid in a curved pipe is driven towards the outer wall by centrifugal forces. The fluid then changes direction and flows along the wall surface to the inner wall. This secondary flow increases the rate of convective transfer and the coefficient becomes larger than that for flow of the same Reynold's number in a pipe of the same dimensions, but straight.

The Nusselt number for such flows was obtained from theoretical considerations and was then compared to experimental results. The theoretical predictions and the experimental results were found to be in good agreement.

For Prandtl number $Pr \geq 1$ the Nusselt number is given by

$$Nu = 0.864\frac{De^{1/2}}{\zeta} x \frac{1}{1 - \frac{37.05}{\zeta}\left[\frac{\zeta}{12} + \frac{1}{24} - \frac{1}{120\zeta} - \left[\frac{4}{3^3\zeta} - \frac{1}{3\zeta} + \frac{1}{15\zeta}\right]\frac{1}{20Pr}\right]De^{-1/2}} \tag{4.3-7}$$

where

$$\zeta = \frac{1}{5}\left[2 + \left[\frac{10}{Pr^2} - 1\right]^{1/2}\right] \tag{4.3-8}$$

The hemispherical chamber and the effectively semicircular matrix channelsof the rotary regenerator burner can be considered as a curved semicircular duct of equivalent radius, r_e, given by

$$r_e = \frac{2\pi r_{cc}}{2 + \pi} \qquad (4.3\text{-}9)$$

and radius of curvature $\beta = r_e$.

In the combustion chamber, as previously mentioned, vortexing occurs but in a direction perpendicular to that of vortices that would be set up under the influence of centrifugal forces. Since, however, the effect of both types of secondary flow is to augment the convective coefficient, it was assumed that eqn. (4.3-7) could be employed to estimate the values of h_{cc}. This assumption can only be evaluated by performing accurate measurements for the determination of the actual temperature profiles through the chamber wall and within the combustion chamber. This was, however, beyond the scope of the present study.

The convective heat transfer coefficient for air at 1400 K, expressed in terms of the Dean number, De, and the combustion chamber radius, r_{cc}, is given by (see Appendix D)

$$h_{cc} = \frac{0.0597}{r_{cc}} \frac{0.692De^{\frac{1}{2}}}{1 - 1.948De^{-\frac{1}{2}}} \qquad (4.3\text{-}10)$$

Due to the heat loss, Q_L, the temperature of the hot exhaust gases

entering the matrix is given by

$$T_{gh\ in} = 1400 - \frac{Q_L}{M_{gcc}\ c_{pg}} \qquad (4.3\text{-}11)$$

The exhaust gas mass flowrate, M_{gcc}, is smaller than the mixture mass flowrate entering the system due to the bypass leakages and leakages to the environment. For the model, leakages were assumed to occur entirely from the entry section of the system at an overall rate of 15% of the inlet volumetric flowrate. Actual values are expected to be higher depending on the degree of wear of the rubbing surfaces.

The exhaust gas specific heat, c_{pg}, is that for air between $T_{gh\ in}$ and 1400 K. Since $T_{gh\ in}$ is unknown, c_{pg} was taken for air between 775 K and 1400 K (1157 J/kg K). From eqns. (4.3-4, 5, 10 11), $T_{gh\ in}$ can be evaluated and used for the estimation of the average preheat temperature of the rectants entering the chamber, $T_{gc\ out(Avg)}$. With this known (from the model for heat exchange within the matrix), the limiting percentage methane content by volume, f, in the inlet mixture can be calculated from eqn. (4.3-2).

4.4. Modelling of heat transfer within the rotating matrix

Several models, of varied degrees of complexity and, therefore, accuracy, have been developed for computing the rotary regenerator effectiveness. The model employed here need not be

very complex as the values for the hot inlet gas temperatures it uses are predicted by the model described in the previous section and are, therefore, of limited accuracy.

The model developed here applies to the ceramic tubular matrix; ceramic, as opposed to metallic matrices are more suitable for high temperature applications.

The idealization assumed in the rotary matrix heat exchange model are as follows:

(a) The thermal conductivity of the matrix solid is zero in the direction of the gas and "matrix" flows. It is infinite in the other direction normal to the gas flow. Since the matrix passages are of low thermal conductivity aluminous porcelain and their thickness is small, this idealization must be close to the real situation in the matrix.

(b) Entering gas temperatures are uniform over the flow inlet cross-section and constant with time. In practice this is only true for the cold mixture entering the matrix. The temperature of the hot exhaust gas does vary over the inlet cross-section.

(c) The linear velocity of the gas through the passages is constant. The volumetric flowrate and, therefore, the linear velocity of the gas does in practice vary with temperature.

With these assumptions, a typical element (see figure (4.2a)) from the cold side of the matrix can be represented schematically as shown in figure (4.2b). Each of these elements can be regarded as a cross-flow exchanger with a gas and a "metal" stream.

For simple unmixed cross-flow with uniform temperatures across the inlets, and averaged temperatures across the outlet, the equations for heat exchange within each element are

$$\frac{M_g c_{pg}}{n_c}(T_{gc\ out} - T_{gc\ in}) = \frac{M_s c_{ps}}{n_r}(T_{sh\ in} - T_{sh\ out})$$

$$= \frac{hA}{2n_c n_r} \Delta T_{avg} \qquad (4.4\text{-}12)$$

where M_g, M_s: gas and solid mass flowrates within the matrix (kg/s)

T_{gc}, T_{sh}: gas and solid temperatures within the cold side of the matrix (solid hotter than gas) (K)

c_{pg}, c_{ps}: solid and gas specific heats (J/kg K)

n_c, n_r: no. of subdivisions of the gas and "solid" streams

h: convective heat transfer coefficient from gas to solid (J/s m^2 K)

A: heat transfer area available within the matrix

and in, out: refer to solid or gas entering or leaving the element

For a small enough element the arithmetic-mean temperature difference, ΔT_{avg}, may be assumed to be valid,

$$\text{i.e.} \qquad \Delta T_{avg} = \left[\frac{T_{sh\ in} + T_{sh\ out}}{2}\right] - \left[\frac{T_{gc\ in} + T_{gc\ out}}{2}\right] \qquad (4.4\text{-}3)$$

From eqns. (4.4-1, 2, 3) the outlet temperatures may be obtained

in terms of the inlet temperatures as

$$T_{gc\ out} = T_{gc\ in} + \frac{n_c}{M_g c_{pg}} \frac{C_1}{C_2} \qquad (4.4\text{-}4)$$

$$T_{sh\ out} = T_{sh\ in} - \frac{n_r}{M_s c_{ps}} \frac{C_1}{C_2} \qquad (4.4\text{-}5)$$

where

$$C_1 = T_{sh\ in} - T_{gc\ in} \qquad (4.4\text{-}6)$$

$$C_2 = \frac{2n_c n_r}{hA} + \frac{n_r}{2M_s c_{ps}} + \frac{n_c}{2M_g c_{pg}} \qquad (4.4\text{-}7)$$

Similar equations can be obtained for $T_{gh\ out}$ and $T_{sc\ out}$, i.e. the exit gas temperatures of an element on the hot side of the matrix.

The matrix and gas streams can be subdivided in any number of such elements and for illustration purposes in figure (4.3) both streams have been subdivided in two equal substreams. The shaded areas represent the cold gas/hot gas interfaces and the left edge is physically the same as the right edge, i.e. $T_{sh}(2,1) = T_{sc}(1,3)$ and $T_{sh}(1,1) = T_{sc}(2,3)$. .This has been referred to as the "reversal" condition. The inlet and outlet solid and gas temperatures for each element can be calculated from the following recurrence relationships obtained from eqns. (4.4-4 and 4.4-5)

For the cold side

$$T_{gc}(r + 1,\ c) = T_{gc}(r,c) + \frac{n_c}{M_g c_{pg}} \frac{T_{sh}(r,c) - T_{gc}(r,c)}{C_2} \tag{4.4-8}$$

and

$$T_{sh}(r,c + 1) = T_{sh}(r,c) - \frac{n_r}{M_s c_{ps}} \frac{T_{sh}(r,c) - T_{gc}(r,c)}{C_2} \tag{4.4-9}$$

For the hot side

$$T_{gh}(r + 1,c) = T_{gh}(r,c) + \frac{n_c}{M_g c_{pg}} \frac{T_{gh}(r,c) - T_{sc}(r,c)}{C_2} \tag{4.4-8'}$$

and

$$T_{sc}(r,c + 1) = T_{sc}(r,c) - \frac{n_r}{M_s c_{ps}} \frac{T_{gh}(r,c) - T_{sc}(r,c)}{C_2} \tag{4.4-9'}$$

With reference to figure (4.3), the mixture inlet temperature (assumed $20^{o}C$) is equal to $T_{gc}(1,2)$ and $T_{gc}(1,1)$. Calculation of the temperatures for element 1 requires $T_{gc}(1,1)$ and the unknown $T_{sh}(1,1)$. For the calculation to start, a temperature profile must be assumed for the right edge. The calculation can then proceed in the order indicated by the element numbers. For calculation of elements 5 and 7, $T_{gh}(1,1)$ and $T_{gh}(1,2)$ are required. These are equal to the known exhaust products temperature $T_{gh\ in}$ (see previous section).

If the assumed solid temperature profile on the right edge is duplicated on the left edge, i.e. if the reversal condition is satisfied, the calculation can be stopped. If, however, this is not the case, the temperature distribution calculated for the left edge is assumed for the right edge and the procedure is repeated until the reversal condition is met to the required accuracy.

Before a solution can be accepted the heat balance error, i.e. (heat received by cold gases/heat given up by hot products) must be close to unity.

Since the gas flowing through the matrix passages contains little or no carbon dioxide and water, heat transfer from the gas to the solid is solely by convection. In addition, due to the small size and large number of passages in the matrix, the flow through the passages is laminar even for high inlet gas flowrates (for air at ambient conditions, Re = 2000 if V_g = 6670 cm^3/s). For fully developed laminar flow and uniform heat flux along a tube, the Nusselt number has been shown to reach an assymptotic value of 4.364 (4.2). The length along the tube required for the flow to become fully developed, i.e. the so called thermal entry length x, is given by

$$x \simeq 0.05 \, Pr \, Re \, d \qquad (4.4\text{-}10)$$

Since in our case Re and d are small, x is very small. For V_g = 800 cm^3/s, Re = 69 and x = 3 mm, i.e. 4% of the tube length.

The convective heat transfer coefficient used is, therefore,

given by

$$h = \frac{4.36k_g}{d} \qquad (4.4\text{-}11)$$

where k_g: gas thermal conductivity (J/s m K)

d: tube inside diameter (m).

The gas thermal conductivity, k_g, and specific heat, c_{pg}, are evaluated at $\frac{T_{gc\ in} + T_{sh\ in}}{2}$.

4.5 Computer program and predicted stability characterictics

A computer program (see Appendix E for a copy of the Fortran 77 program), based on the combustion and heat exchange models developed in the preceeding sections, was written. The objective of the program was to predict the stability characteristics of the rotary regenerative burner, used in the experimental study, with a combustion chamber of hemispherical cement walls and a ceramic matrix of geometric configuration and dimensions identical to those of the experimental ceramic matrix. The stability characteristics were computed for methane as the fuel and over a range of values of the remaining burner parameters, i.e. inlet mixture flowrate, combustion chamber radius and matrix rotational speed.

The program basically consisted of three sections for the calculation of

(a) the combustion products temperature

(b) the temperature of the preheated reactants and

(c) the percentage of methane by volume required for stable combustion under limiting conditions.

Before any of these calculations were performed the selected number of subdivisions for the matrix gas and solid streams, and values for the gas flowrate, combustion chamber radius and matrix rotational speed were read. In addition, four two-dimensional arrays for the gas and solid temperatures on both sides of the matrix, and one one-dimensional array for the difference between the respective solid temperatures on the left and right edges of the grid were defined. The air specific heat and thermal conductivity were finally given as second order functions of temperature correlating the data for air given in reference (3.2)

The computations performed in each of the program sections can be outlined as follows:

(a) Calculation of hot products temperature

- The Dean number is calculated for the given gas mass flowrate and combustion chamber radius.
- The Nusselt number for heat transfer from the product gases to the combustion chamber wall is calculated from the known Dean number.
- The convective heat transfer coefficient is calculated from the known Nusselt number.
- The heat lost by the product gases is calculated.
- The temperature of the product gases leaving the combustion chamber is calculated.

- If the calculated product gas temperature at the exit from the combustion chamber is smaller than 20°C, which is the assumed temperature of the mixture at the inlet to the burner, the gas flowrate is too low for stable combustion and calculation is stopped.
- The first raw elements of the two-dimensional matrix for the gas temperatures on the "heating-up" side of the matrix are equated to the products temperature at the exit from the combustion chamber.

(b) Calculation of the temperature of the preheated reactants.

- The inlet gas temperature is equated to 20°C.
- The first column solid temperatures on the "cooling-down" side of the matrix are given initial values.
- The solid and gas temperature distribution throughout the matrix is calculated.
- The reversal condition is checked by comparing the differences between the estimated solid temperatures on the right edge (see figure (4.3)) and the respective calculated ones, to some acceptable value.
- If the reversal condition is satisfied the procedure is terminated. The printed value for the heat balance error is checked and if not satisfactory, the program is rerun for improved accuracy of the solid temperatures.
- If the reversal condition is not satisfied the iteration for the gas and solid temperatures is continued.
- If after every iteration the error in the heat balance does not improve to the required extent (i.e. if the convergence is slow), the new values for the solid temperatures are equated to the

calculated ones but increased by a multiple of the difference between the calculated and the estimated values.

(c) Calculation of the limiting fuel percentage.

- The average mixture preheat temperature is used for the calculation of the percentage of fuel by volume for stable combustion just before extinction.

The stability characteristics (i.e. plots of limiting mixture flowrate versus composition) of the burner with the 60 mm diameter combustion chamber were computed for matrix rotational speeds of 0.6, 1.2, 2.4 and 4.8 revs/min. The predicted stability curves are of the expected general "L" shape for heat recirculating burners, and,as shown in figure (4.4), for inlet flowrates above 150 cm^3/s the leaness of the limiting mixtures increases with increasing matrix rotational speed. At low inlet flowrates, the heat loss to heat recirculation rate ratio is large and the performance of the burner is, therefore, controlled by the rate at which heat losses occur. Since the heat loss rate is independent of the matrix rotational speed, for low inlet flowrates the performance of the burner remains unchanged irrespective of the matrix speed. At higher inlet flowrates, however, heat losses become less important in favour of the rate at which heat is being exchanged between products and reactants, and since, as shown in figure (4.5), the regenerator effectiveness increases with increasing rotational speed, the leaness of the limiting mixtures increases with increasing rotational speed. For an inlet mixture flowrate of 800 cm^3/s the regenerator effectiveness, as demonstrated in figure (4.5), reaches a maximum value of

approximately 79% the a rotor speed of 4.8 revs/min. In the same figure, the effect of the inlet flowrate on the regenerator effectiveness is also shown. The effectiveness decreases monotonically with increasing mixture flowrate and this explains the shape of the stability curves in figure (4.6). In this, the stability characteristics of the burner with both a 60 mm and a 90 mm diameter combustion chamber are presented for inlet flowrates up to 2,000 cm^3/s. At about 700 cm^3/s and 600 cm^3/s for the burner with the 60 mm and 90 mm diameter chamber respectively, the leaness of the limiting mixtures is at a maximum. Increased flowrates, however, result in some increase of the fuel content of the limit mixtures. This suggests that for high inlet flowrates, heat recirculation, in addition to heat losses, plays an increasingly unimportant role.

From figure (4.6) it is also apparent that leaner mixtures can be stably burned in the 90 mm combustion chamber burner. This is due to the combustion chamber burner volume being larger which in turn means lower linear velocities for the products gases in the chamber and, therefore, lower values for the convective heat transfer coefficient and overall heat losses from the system. This is despite the fact that the area available for heat transfer to the 90 mm chamber is 2.35 times that to the 60 mm chamber.

In Chapter 6 of this thesis the predicted stability data, presented here, are compared to data obtained during the experimental study.

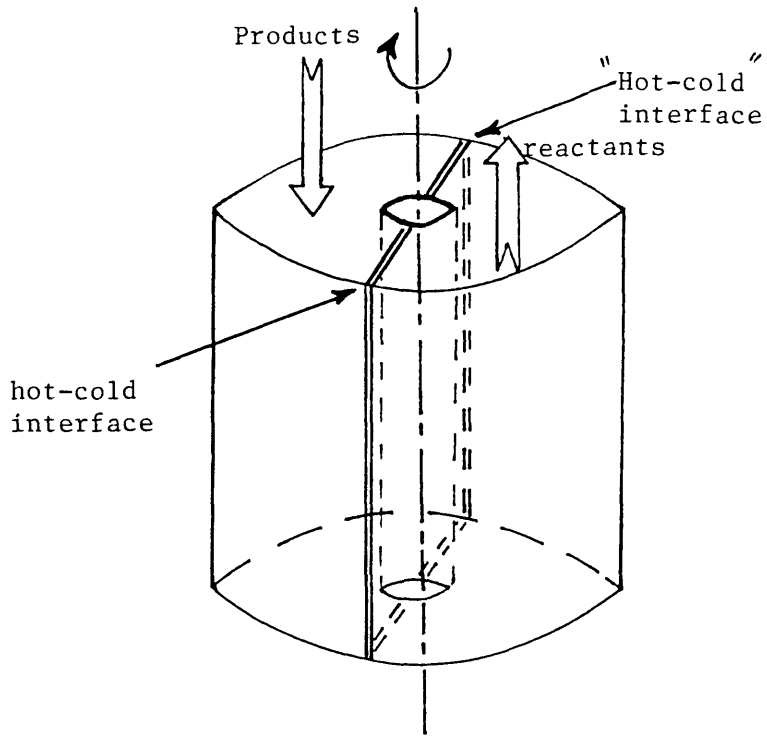


Figure (4.1): The matrix interfaces for the case of clockwise roration.

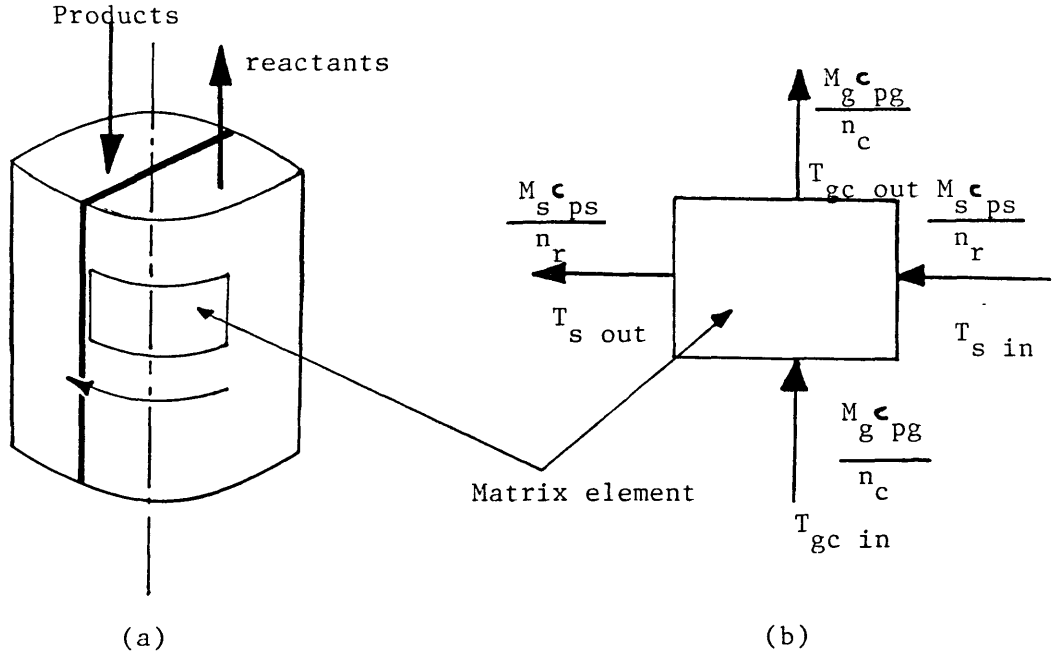


Figure (4.2): Matrix element for modelling of heat transfer within. the regenerator

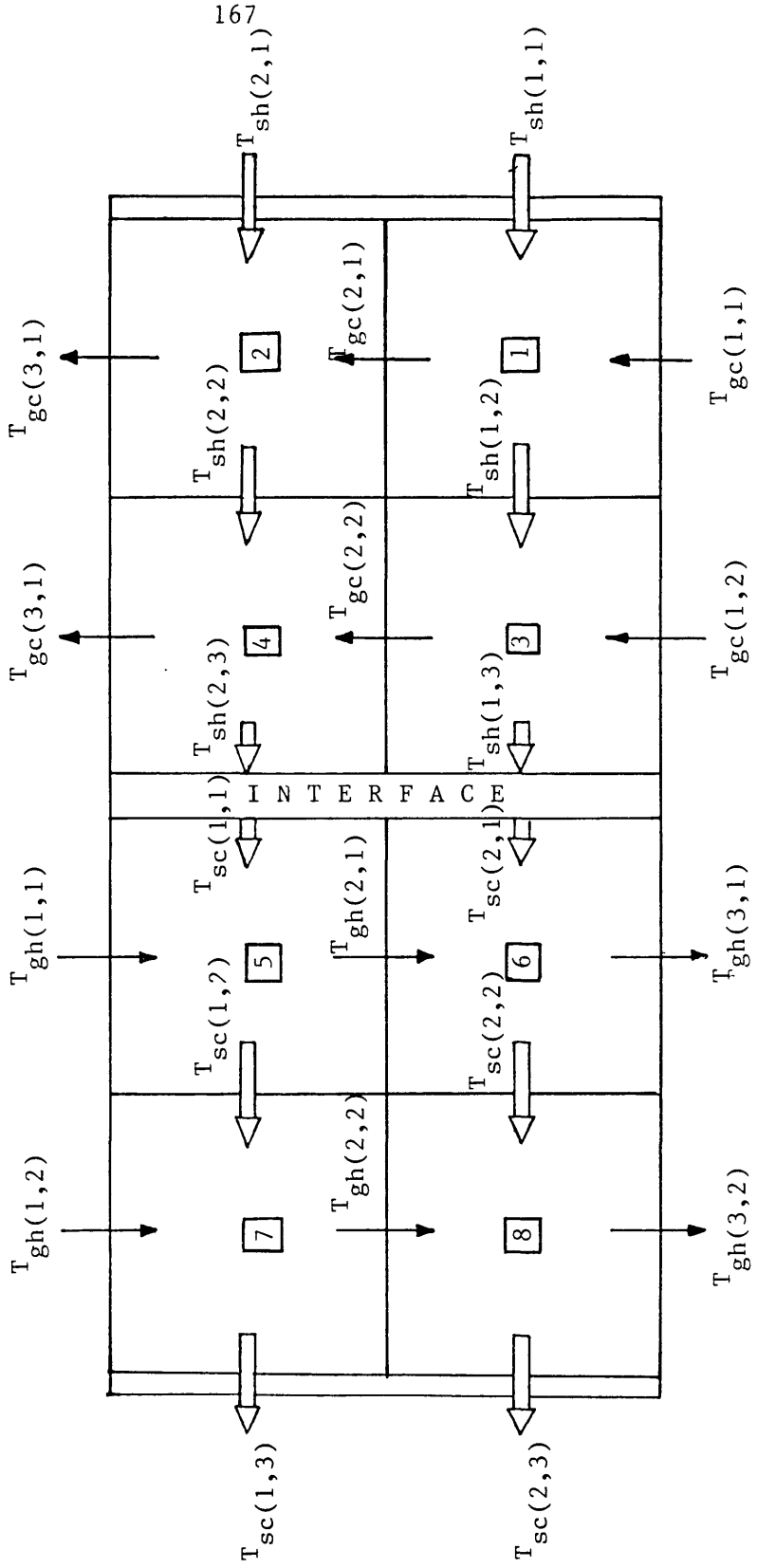


Figure (4.3): Solid and gas temperatures within a 2x2 grid of elements for modelling of heat transfer in the matrix.

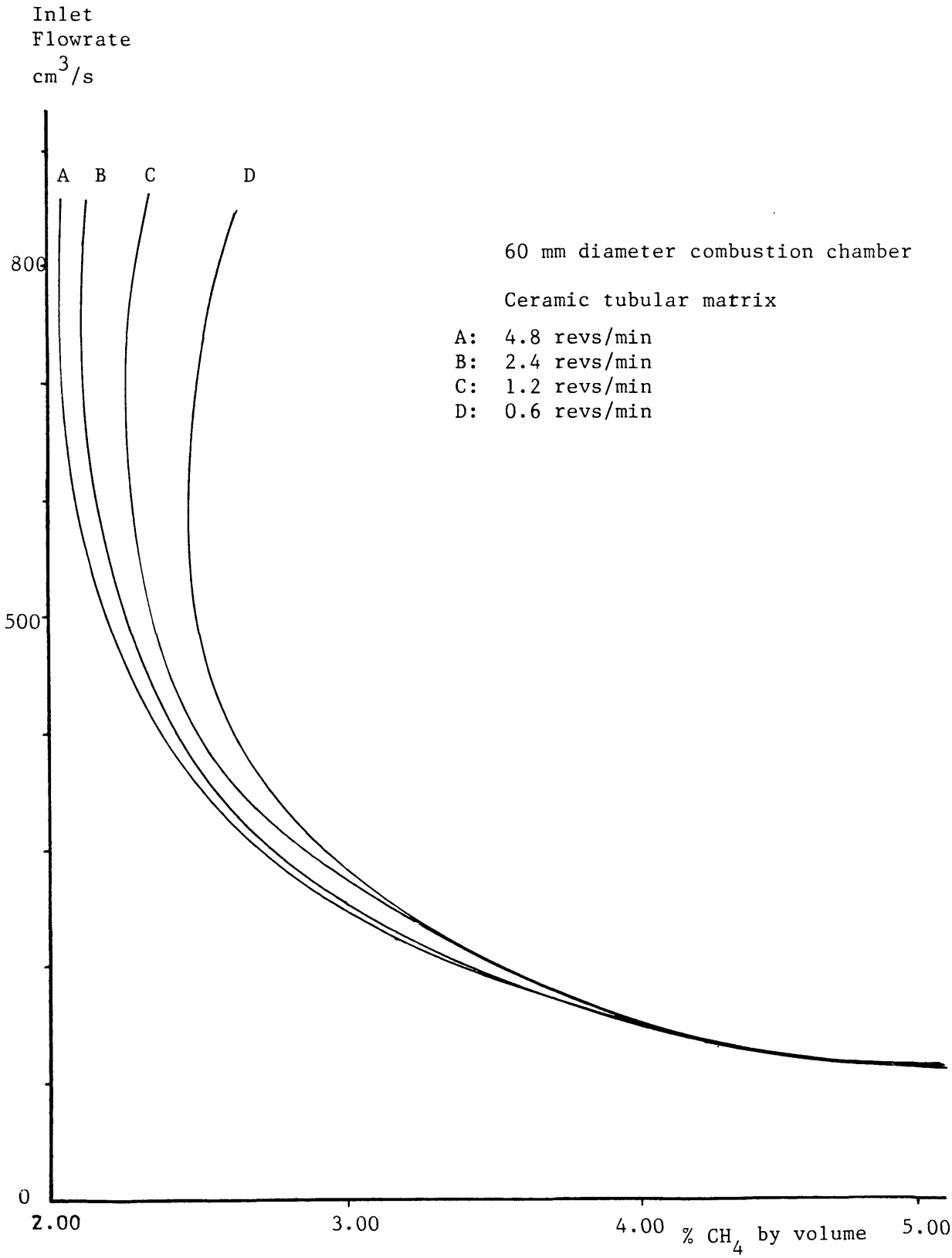


Figure (4.4): Burner predicted stability characteristics.

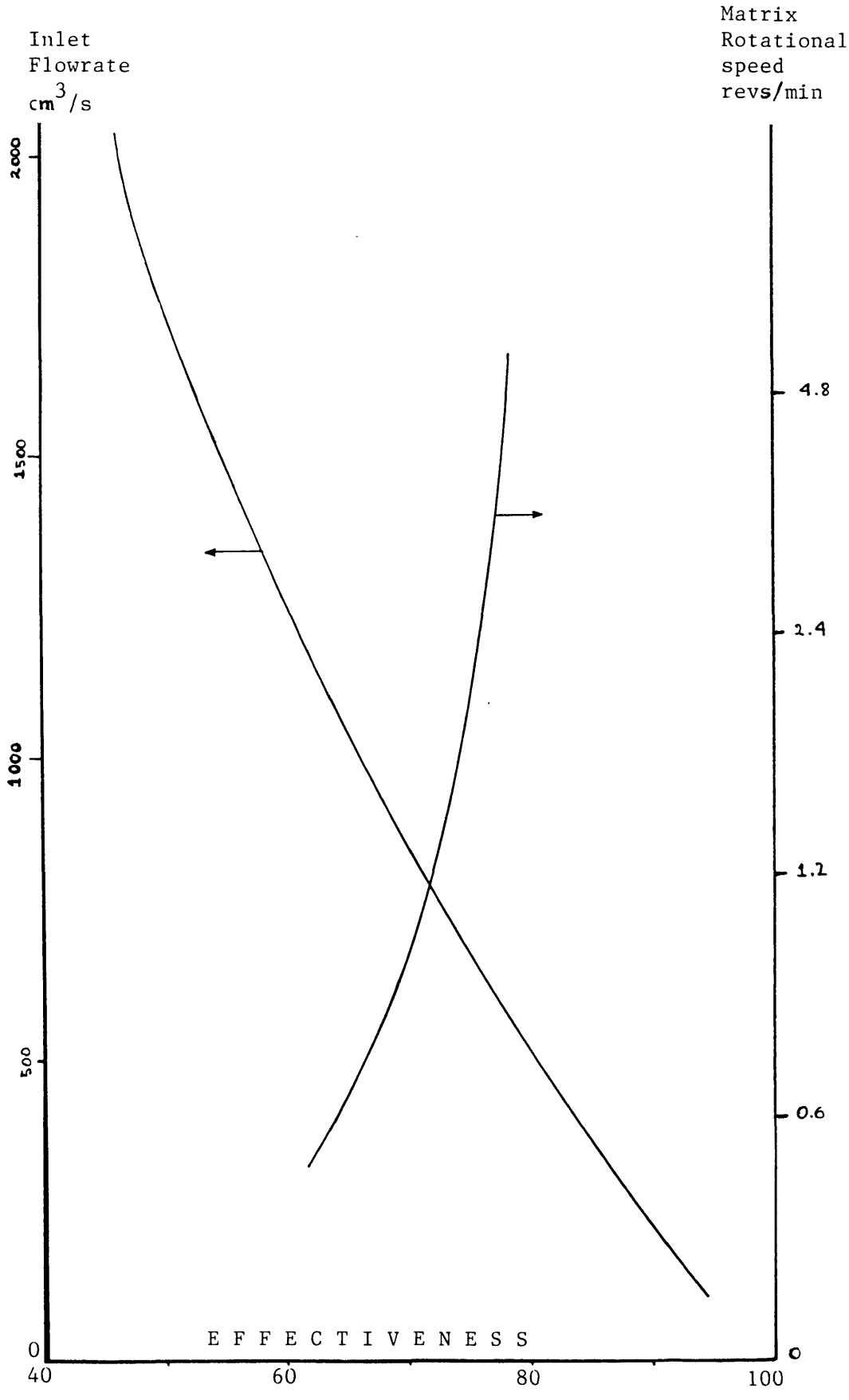


Figure (4.5): Effectiveness vs inlet flowrate (1.2 revs/min) and Effectiveness vs rotational speed (800 cm^3/s).

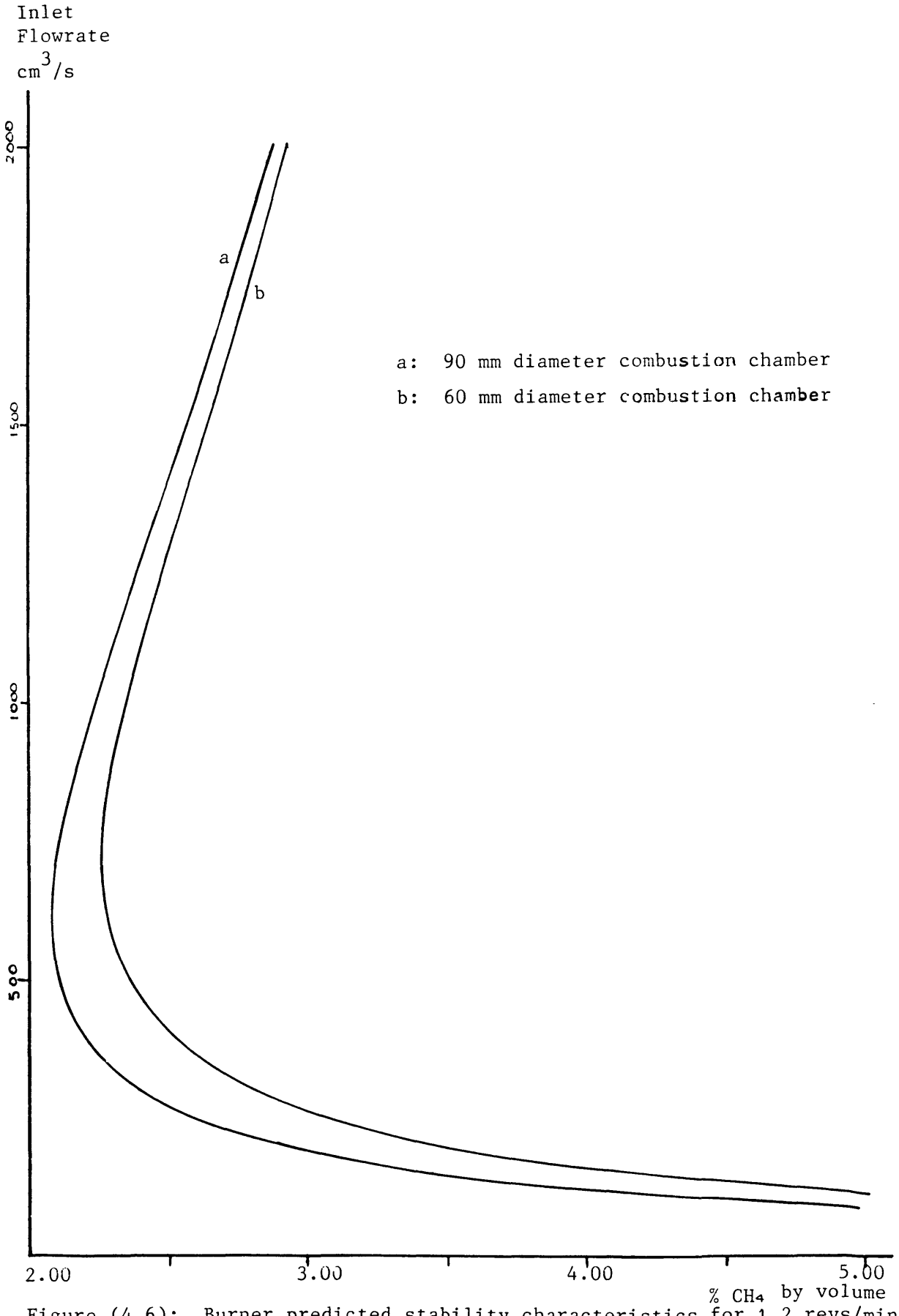


Figure (4.6): Burner predicted stability characteristics for 1.2 revs/min.

Chapter 5

Experimental apparatus and techniques

5.1. Introduction

In the present chapter the series of experiments completed in the course of this research programme and the equipment necessary for the purpose are described.

The wear suffered by the individual burner parts during operation and, therefore, the repairs that had to be carried out, prior to every experimental run, are given in detail.

Finally the procedures for igniting the burner and for obtaining the limiting points for stable combustion within the system are described.

5.2. The experimental programme

The experimental programme, as previously stated, included work on both the metallic and ceramic matrix regenerative burners. The feasibility of burning lean methane-air mixtures in such systems was first investigated by employing the metallic flame-trap matrix as the regenerator heat exchange medium. The experiments were performed with the system incorporating the 60 mm diameter hemispherical combustion chamber of refractory cement

walls, and over a range of matrix rotational speeds. For each rotor speed, plots of the limiting mixture flowrate against composition were obtained. Furthermore, data for the estimation of the leakage rates to the enviroment were collected at the end of each run.

On completion of this series of tests, experimental work was initiated on the ceramic tubular matrix system. Owing to the envisaged limited practical applicability of the matallic matrix system at high temperatures, the ceramic matrix was employed in all the experimental runs that ensued.

Stability curves for the ceramic matrix system were obtained as for the metallic matrix one, over a range of matrix rotational speeds, for methane as the fuel and with the 60 mm diameter refractory cement dome as the combustion chamber. The effect of the rotor speed and, therefore, the regenerator effectiveness, on the overall level of performance of the system was, thus, established.

In the experiments that followed, the influence of the combustion chamber geometric configuration and size on the combustion chamber process, and, consequently, the system stability characteristics, were investigated. Stability curves were obtained for one matrix rotational speed and (a) a 90 mm diameter hemispherical combustion chamber of refractory walls (i.e. a chamber of similar geometry and construction, but of larger size than the one used up to that point) and (b) a 90 mm diameter and 15 mm height cylindrical combustion chamber with

walls partly of 316 stainless steel and partly of high purity quartz.

The processes within the combustion chamber of the rotary regenerator burner were investigated for the case when the inlet mixture flowrate and composition were close to the limiting ones for the particular set of operating and geometric configuration parameters of the system. Investigation proceeded by sampling, and, subsequently, analysing the combustion chamber and exhaust gases, and by measuring the temperature of the combustion chamber gases via a suction pyrometer. Sampling and temperature measurements were carried out on the system with a 60 mm diameter hemispherical chamber, for one matrix rotational speed and over a range of inlet mixture flowrates.

A photographic record of combustion within (a) the 90 mm diameter hemispherical chamber of transparent quartz walls and (b) the 90 mm diameter 15 mm height chamber of transparent quartz upper flat wall, was then obtained, again for one rotor speed and a range of inlet mixture flowrates.

Finally, lean combustion with controlled heat abstraction from the combustion chamber was attempted.

5.3 The experimental apparatus

The mechanical design features of the individual components of the experimental rotary regenerative burner were described in detail in Chapter 3 of this thesis. During the experiments for

the determination of the stability characteristics of the burners with the refractory cement domes as the combustion chambers, the system was almost entirely surrounded by a uniform, 76.0 mm thick, layer of "Triton" ceramic fibre insulation. A small gap had, of course, to be allowed where the rotor and the motor gearbox-shaft gears were in contact. During the stability experiments with the cylindrical combustion chamber, the thickness of the "Triton" fibre layer on the exposed flat surface of the quartz disk was 114 mm. Choice of this thickness meant that the insulation layer over the cylindrical chamber was similar in magnitude to that surrounding the refractory cement domes. In the construction of the hemispherical chambers a thin cement layer supported "Triton" ceramic fibre packing contained within the "Top hat" structure.

The thickness of the insulation layer proved quite adequate for both the hemispherical and cylindrical combustion chamber systems and, depending on the mixture inlet flowrate, the temperatures on the surface of the insulation varied only between $30^{o}C$ to $59^{o}C$.

The torque developed by the motor and, therefore, the ease with which the rotor moved between the seals, was monitored during experimental runs by continuous measurement of the armature current. In motors of the type used here (D.C. shunt wound), as mentioned previously, the armature current is proportional to the torque developed. A digital milliammeter was used for the purpose.

During operation of the burner, the product gases from the exit section of the system were discharged to the atmosphere via

the horizontal and vertical sections of a 60 mm i.d. PVC tube, and the laboratory exhaust duct. Tubing of large inside diameter was employed in order to eliminate additional pressure drops in this part of the system. A leak proof joint between the 60 mm i.d. PVC tube and the 42 mm o.d. burner exit port was achieved by packing "Triton" ceramic fibre in the annular void between the plastic and metallic tubes. The insulating "gasket" also helped to minimise damage to the PVC tube by reducing the rate of conductive heat transfer from the hot metal surface of the burner exit port. The "horizontal" section of the PVC tube was so inclined that water vapour condensing on the inside surface of the PVC tubing was collected in a catch pot at the lowest point of the tubing arrangement.

The methane - air mixtures were supplied to the burner at flowrates and compositions that were monitored and controlled through the flow system that is depicted in figure (5.1). The air was obtained from the Departmental air supply and the methane from a pressurized cylinder. Technical grade methane was used, which is guaranteed as 97.8% methane. The air and methane pressures were measured by means of two mercury manometers. The pressure for both the methane and air entering the system was reduced, via two regulator valves, down to 2 atm absolute, which can be accurately measured on mercury manometers.

The air flowrate was monitored by an 18x metric air rotameter and the methane flowrate by a methane rotameter, with a range of up to 117 cm^3/s of methane at 1 atm absolute and 15^oC.

The methane and air flowrates were controlled via the valves A and B shown in figure (5.1). The gas streams were brought together and mixed downstream from the valves A and B in a glass vessel packed with wire gauge. The packing was included both to enhance the mixing and to act as a flame trap in case of ignition of the mixture or flame flash-back. The premixed gas emerging from the mixing vessel could flow towards the experimental burner or an auxilliary burner. The proportion of the flow that was directed towards the main burner was controlled by adjusting the valves C and D.

The flowrate of the mixture flowing towards the auxilliary burner was measured by means of an 18x metric air rotameter. The pressure of the gas flowing through this rotameter varied little with flowrate since the pressure drop for flow through the length of plastic tubing from the auxilliary burner (and, therefore, to the atmosphere) was very small. The flowrate to the main burner was equal to the difference between the total mixture flowrate and and the flowrate to the auxilliary burner. Inclusion of the auxilliary burner also allowed the flowrate to the main burner to be altered while the mixture composition remained constant. A diffusion flame was stabilized on the auxilliary burner in order to maintain complete combustion of the excess gas received by it. The pressure of the mixture entering the main burner was measured by a water manometer.

Reinforced PVC tubing was used throughout the system and Jubilee clips and wire fastening were used to strengthen the junctions between the flexible and metal or glass tubing.

Needle valves were used because of their ability to allow small changes in the flow to be made. The air, mixture and methane rotameters were calibrated for air and methane at 1 atm absolute and ambient temperature of 22^{o}C.

The gas temperatures at several points within the combustion chamber volume and the exit and entry sections of the burner were measured by means of thermocouples supported by twin bore fused quartz tubes. The high temperatures within the combustion chamber were measured by three Pt/Pt 87% Rd 13% thermocouples. The thermocouple wires were passed through the two parallel channels of three insulating quartz tubes 180 mm in length and 3 mm in outside diameter. The thermocouple junctions were kept clear of the quartz rod surface and they were covered by a thin film of "Autostic" high temperature cement in order to prevent any catalytic effect they might have had on the methane oxidation reaction (see figure (5.2)). The quartz tubes could be inserted in the combustion chamber through the three access tubes in the sides of the "Top hat" container. Compression fittings were used to minimize leakages through the annular gaps between the quartz rods and the metal tubes. The precise positions of the access tubes and, therefore, the thermocouple measuring stations are indicated in the diagram of figure (5.3). The thermocouple leads emerging from the quartz tubes were inserted in flexible insulating sleaves to prevent them from short circuiting, and were attached on a permanent terminal remote from the burner system. The lengths of the thermocouple leads were such that it was possible to move the quartz rods and, therefore, the thermocouple

junctions from the point where they entered the combustion chamber to the one diametrically opposite. The two wall temperatures, and the gas temperatures along the path of the junctions, could be measured.

The entry and exit gas temperatures, which were considerably lower, were measured by Chromel - Alumel thermocouples. The thermocouple leads were again supported by twin bore quartz tubes, but in this case only short lengths were necessary. The thermocouple junctions were again kept at a distance from the tube surface and were permanently positioned in the middle of the PVC entry and exit tubes, immediately before and after the burner. The gas streams were accessed through holes on the sides of the PVC tubes; the quartz tubes carrying the thermocouples partly penetrated the tube wall and were firmly sealed in place by "Araldite" adhesive.

Finally the upper flat metallic surface temperature was measured by a Chromel - Alumel thermocouple. The thermocouple junction was kept in close contact with the wall by "Autostic" cement.

The Pt/Pt 87% Rd 13% leads were connected via compensating cables and a multiswitch to a Pt/Pt Rd digital thermometer. In the case of the Chromel - Alumel leads, compensating cables were not necessary and the thermocouples were directly connected through a multiswitch to a Chromel - Alumel digital thermometer.

The bare thermocouples, employed here for measurement of the gas temperature, are of the simplest form possible and did not measure the true gas temperature. This is especially true for the

Pt/Pt Rd thermocouples which were required to measure the temperatures of very hot gases surrounded by walls at lower temperatures. When a thermocouple junction is exposed to a hot gas it receives heat by convection from the gas but it also exchanges radiant heat with the chamber walls which it can "see". If the walls are at a lower temperature they will absorb radiant heat from the junction and the thermocouple E.M.F. reading will be lower than that correponding to the true gas temperature. Since the rate at which radiant heat exchange occurs between a thermocouple junction and a wall is proportional to the difference of the forth power of their temperatures, the radiation loss will be large when both the absolute values of the temperatures and their difference are high. At $600^{o}C$ and above, radiation effects result in a junction radiating a significant proportion of the heat it receives to the chamber walls (5.1), (5.2). The Pt/Pt Rd thermocouple junctions were exposed to gas temperatures of the order of $1127^{o}C$ and were, therefore, subject to large errors due to high radiative losses. The Chromel - Alumel thermocouple junctions in the exit and entry streams were exposed to gases of much lower temperatures (of the order of 200 - $300^{o}C$ and 20 - $30^{o}C$ respectively) and their reading can, therefore, be considered as representative of the true gas temperatures.

In the discussion above, consideration of the additional heat loss suffered by thermocouple junctions because of conductive heat transfer along the thermocouple leads was omitted. The thermocouples employed here, were of very fine wires and their hot junctions were not in contact with the quartz tubes. The rate,

therefore, of heat loss by conduction was very small and its effect on the thermocouple reading can be neglected.

The small size of the combustion chambers, and the desire to avoid any effects on the combustion process, prevented the use of elaborate thermocouple systems (such as multi-shield or heated shield thermocouples) during the stability experiments. The bulk of the combustion gas temperature data was, therefore, obtained by means of bare thermocouples and can only be used for comparison purposes. Since, however, the applicability or otherwise of the constant limiting final flame theory for the rotary regenerative burner needed to be established, a separate series of combustion experiments were performed with the express purpose of accurately measuring the gas temperature in the combustion chamber. The measurements were obtained by means of a single shield suction pyrometer. As illustrated in figure (5.4), a Pt/Pt 87% Rd 13% thermocouple, supported by a twin-bore quartz tube 150 mm in length and 1.2 mm o.d. was contained within a single-bore fused quartz tube 180 mm in length, 1.8 mm i.d. and 3 mm o.d. This outer tube was blocked at one end and had one 0.8 mm hole 3 mm from its blocked end and two 0.5 mm holes 10 mm from its open end and could be inserted in the combustion chamber through one of the access tubes. The tube carrying the thermocouple was inserted in the support tube, with the thermocouple junction near the blocked end. The Pt/Pt Rd leads emerged from the two 0.5 mm diametrically opposed holes, and the quartz tube open end was firmly attached by "Autostic" cement to one end of a 100 mm long 3 mm i.d. copper tube.

Care was taken during construction of the pyrometer for the thermocouple junction not to be in contact with either the rod or the inside surface of the tube and for its distance from the 0.8 mm hole to be such that the junction could not "see" any outside surfaces. The holes through which the thermocouple leads emerged were sealed with "Autostic" cement and the length of the leads was again such that the pyrometer could be traversed in a straight line within the chamber. As shown in figure (5.4), the pyrometer was connected via lengths of PVC tubing to a vacuum pump and a bubble flowmeter. The pressure downstream from the pyrometer was meaured by means of a mercury manometer and the suction rate and, therefore, flowrate through the pyrometer could be controlled by a needle valve upstream from the pump.

In the suction pyrometer the gas, the temperature of which is to be measured, is forced to flow over the thermocouple junction by means of the vacuum pump. The rate of the convective heat transfer from the gas to the junction is increased and the thermocouple is thereby caused to read more accurately. According to the theory of suction pyrometry (5.2) the thermocouple reading with no flow past the thermocouple, i.e. no suction, will be considerably removed from the true gas temperature due to the very small coefficient of convective heat transfer. As the suction, and, therefore, flowrate is increased the thermocouple reading increases until a point is reached when the rate of convective transfer is so great that the radiative and conductive losses are very small in comparison. Further increases in the gas flow result in no appreciable temperature rise, thus indicating that

the true gas temperature has been reached by the hot junction. All the results recorded from the suction pyrometer tests relate to this condition.

The combustion process, as mentioned in section 5.2, was further investigated by analysis of the combustion chamber and exhaust gases. Gas samples were obtained by means of a fused quartz probe that could be inserted in the exhaust side, and the combustion chamber (through one of the access tubes on the side of the "Top hat" container) of the system. The probe was similar in dimensions and geometric configuration to the suction pyrometer, described above, but with the inner quartz tube and thermocouple absent and only one 0.8 mm diameter hole 3 mm from its blocked end. The probe was connected to a vacuum pump and a bubble flowmeter as indicated in figure (5.5). Gas samples were collected in a cylindrical glass vessel with two valves (C and D in figure (5.6)) on either of its open ends. The flow through the probe could be started or interrupted instantaneously by the valves B and E and with these open the suction rate could be controlled by the needle valve A. The hot gas emerging from the probe was expanded and cooled in a catch-pot which was contained in a vessel filled with water at $0^{o}C$. The water vapour, carried by the product gas, was, therefore, condensed and removed from the gas in this part of the flow system. The pressure within the sample vessel could be made positive with respect to the atmospheric pressure by diluting the gas sample with inert gas (H_2 and He) from a pressurized cylinder. With the valves C, D and F open and B and E closed, inert gas from the cylinder could flow in

the sample vessel until the required pressure, indicated by a mercury manometer, was reached. The sample vessel, with its valves closed, could be easilly detached from the rest of the flow system and connected to the Perkin-Elmer Model 8310 Gas Chromatograph for gas analysis. Positive pressures within the sample vessel were essential for forcing the gas sample through the Chromatograph columns.

In the final series of experiments, heat was abstracted from the combustion chamber of the burner by means of a stream of water flowing through the turns of a copper coil. The stability characteristics of the burner were determined for each of two coils with similar configuration but different number of turns. The coils were constructed by rolling 484 mm (8 turns) and 238 mm (4 turns) of copper tubing (4.4 mm o.d. and 2.6 mm i.d.) into 17 mm diameter curved helices as illlustrated in figure (5.6).

The inlet and outlet sections of the coils were straight extensions of the coil tubing, they were conveniently located side by side, and were perpendicular to the planes of the coil axes. The coils were secured within the 60 mm diameter hemispherical combustion chamber by passing the inlet and outlet tubes through the vertical access tube and by bending them, at the point where they emerged from the top of the tube, through an angle, just sufficient for them to be in contact with the access tube rim; vertical movement of the coils during operation was thus prevented. The planes of the coil axes were kept parallel to the upper surface of the matrix by tightly packing the void left in the access tube with "Triton" ceramic fibre. This also ensured

that introduction of the coils did not give rise to leakages from this part of the system.

The water inlet and outlet temperatures were measured by two Chromel - Alumel thermocouples. The thermocouple leads were passed through the two parralel channels of two 10 mm long quarz tubes. These tubes were inserted into the copper tubes through holes that were drilled near their ends. "Araldite" adhesive was used to prevent water leakages. The coil inlets were connected, via a valve and a 7x metric calibrated water rotameter, to the Departmental water supply.

Prior to the combustion experiments the air, methane and excess rotameters were calibrated by means of two bubble flowmeters. The air rotameter was calibrated by connecting a large inside diameter bubble meter via a length of rubber tubing to the outlet of valve A of figure (5.1). Since the air static pressure during normal operation was to be maintained at 2 atm absolute, the air rotameter was calibrated by varying the air flowrate over the rotameter range but keeping its pressure, between the main supply regulator valve and valve A, constant at 2 atm absolute. The air volumetric flowrates through the bubble meter, estimated by recording the time for a soap bubble to travel a distance corresponding to a known volume, were, however, for air at approximately 1 atm absolute. From the calibration chart, (i.e. plot of volumetric flowrate versus rotameter reading), thus obtained, the volumetric flowrate for air at 1 atm absolute could be read directly even though the actual pressure of the air flowing through the rotameter was 2 atm absolute.

For the methane rotameter a smaller inside diameter bubble meter was connected to valve B of figure (5.1) and a diffusion flame was stabilized by means of wire gauze on top of the bubble meter tube. The calibration was for methane at 2 atm absolute and from the calibration chart the volumetric flowrates for methane at 1 atm absolute could be obtained.

For the mixture rotameter the large bubble meter was connected where the mixture emerged from the flow system, just before the excess burner, and the excess mixture flowrate was varied by adjusting valves C and D of figure (5.1).

The inaccuracy associated with the calibration results is due to errors in measuring the times, and starting and stopping the chronometer when the soap bubble passes the two reference points within the meter tube. The readings were always repeated and the arithmetic average taken. Further errors, however, between the actual and measured flowrates, arose during operation of the system due to the following:

(a) The ambient and consequently the inlet gas temperatures varied over the experimental period and differed, therefore, to a greater or lesser extent from those ($22^{o}C$) during the calibration experiments.

(b) Gases are compressible and due to the additional pressure drop for flow through the burner (a function of geometric configuration, flowrate and temperatures within the burner), the actual flowrates through the rotameters for the gases at a measured pressure of 2 atm absolute were smaller than when the same gas pressure was applied with flow through the

bubble meter tube only.

The exact errors cannot be estimated, but since both the temperature variation (from ~20°C to ~30°C) and the pressure drop for flow through the burner (of the order of a few centimeters of water) were small, the errors must have been small, i.e. within ±2%.

5.4. Experimental operating procedure

Throughout the experimental study the following procedure had to be repeated prior to igniting the burner:

(a) The flow system was tested for leaks by subjecting the tubing and flow measuring equipment, with the inlet (A, B) and outlet valves (C,D) shut off, to a pressure of 2 atm absolute. Inability of the system to maintain the pressure was indicative of the existence of leaks that had to be located and eliminated. The leaks were located by applying films of soap solution to all the junctions round the flow system; non leak-proof junctions were detected by the bubbles of increasing volume rising through the film.

(b) Before each experimental run the parts of the burner were examined and it was ensured that the rubbing surfaces were clean and smooth and the matrix passages were free from blockages.

During operation the Phosphor bronze bush, covering the surface of the upper circumferential seal, suffered oxidation

to varying degrees, depending on the mixture inlet flowrate and, therefore, the rate at which heat was transferred by convection from the combustion gases to the combustion chamber walls. Following runs with high inlet flowrates (~ 800 cm^3/s) the oxide layer was always quite thick (~ 0.5 mm) and completely detached from the body of the bush. During operation with low inlet flowrates (~ 100 cm^3/s) the bush suffered negligible oxidation. During the whole of the experimental programme, however, the bush only had to be replaced (due to cracking) four times.

The Phosphor bronze surfaces in the lower part of the system (i.e. of the Phospor bronze ring roung the rotor periphery and the bush on the lower circumferential seal) suffered no oxidation (due to lower temperatures) and after a few runs they were completely covered by uniform layers of self-lubricating graphite. The graphite, as previously mentioned, was deposited due to evaporation of the organic substances contained in the lubricant paste. To avoid very thick graphite layers from building up after the initial series of experiments, no further graphite paste was applied to the lower rubbing surfaces.

In the upper part of the system the graphite paste did not withstand the temperatures and had to be reapplied before each experiment.

Before applying the lubricant, the upper rubbing surfaces (both of the rotor and the seal) were thoroughly cleaned and polished by different grades of abrasive paper.

In the process of the above the "Triton" fibre packing, serving as a secondary seal, was always damaged and had to be replaced.

The cement walls of the hemispherical combustion chambers, due to the successive heating and cooling cycles (even though the burner was always allowed to cool slowly overnight), did suffer some cracking. The cracks were limited in number but quite deep and were repaired by further layers of cement.

Both the ceramic and metallic matrices withstood the temperatures and stresses well. In the case of the ceramic matrix some damage of the upper surface was observed.

(c) Following reassembly of the burner, either the old or a new outer insulation layer was placed round the system. The organic binder within the insulating material evaporated during operation and after prolonged usage the insulation integrity deteriorated, requiring replacement.

With the burner operational, the fan in the laboratory exhaust channel was switched on and the auxilliary burner lit. No combustible mixture was allowed to accumulate in the laboratory under any circumstances. The burner was almost always ignited through the large access tube with moderate mixture flowrates, and fuel-air mixtures below stoichiometric, but above the lower flammability limit. Rapid heating to very high temperatures during the initial stages was thereby avoided.

During the experiments with the cylindrical combustion

chamber and the cooling coils for heat abstraction, a flame was stabilized on the matrix without the upper part of the system in place. After successful ignition the upper sealing ring, and the combustion chamber containing structure, were slowly lowered onto the rotor surface.

After ignition, the thermocouples were inserted in the combustion chamber and they were traversed within its volume. The gas temperatures were always observed to vary with position and with the exception of the maximum temperature, they exhibited an erratic variation with time. The maximum temperature was always recorded by thermocoulpe A with the hot junction between positions 2 and 3 of figure (5.3). The combustion stability during the initial stages was checked by continuously monitoring the relatively steady maximum temperature.

For 30 minutes after ignition the burner was operated with the same mixture flowrate and composition, and without rotation of the matrix. It was found that starting the motor immediately after ignition, more often than not, resulted in extinction of the flame. Following the initial 30 minute time period, the motor was switched on and the matrix rotational speed was gradually increased, over a further 30 minute period, from a low initial value to the one required; the mixture flowrate and composition were not altered during this time.

During the first 30 minutes the maximum temperature was always observed to increase slowly with time. After the motor was switched on the maximum temperature exhibited an initial rapid increase, which was, however, subsequently followed by a decrease. If too high an initial rotational speed of rate of increase of

speed was applied, the maximum temperature decreased rapidly and the flame was extinguished.

During the first 60 minutes of operation an almost flat hemicircular flame was observed, via the ignition access tube, to be stabilized over the matrix inlet section. With the matrix stationary, since the mixture was flammable, the premixed flamelets over each matrix passage were propagated by means of the ordinary processes of heat transfer and diffusion of active species from the reaction zone back to the emerging mixture. The heat losses suffered by the flame (initially very high due to the low temperatures of the combustion chamber walls) decreased with time, due to the heating up of the burner walls; this explains the initial increase of the maximum gas temperature within the chamber.

When the matrix was being rotated, ignition of the preheated mixture emerging from those passages crossing the "hot-cold" interface (see figure (3.5a)) was due to heat transfer and diffusion of active species from the flamelets stabilized over the adjacent passages. Since the "exit" matrix passages had been preheated for 30 minutes, rotation of the matrix resulted in an immediated increase of the maximum gas temperature because of the higher unburnt gas temperatures achieved initially (i.e. temperature of preheated mixture before combustion took place). However, after completion of the first half revolution, the gas temperature dropped, since the passages crossing the "hot-cold" interface had only been heated for a much shorter period (= half the time required for a complete revolution). With excessive rotational speed, the heat stored in the matrix walls became

insufficient to preheat the mixture to the unburnt temperature required for successful ignition of the mixture emerging from the passages crossing the "hot-cold" interface. The initially hemicircular flame was, on several occasions during the initial stages of the experiments, observed to rotate with the matrix and gradually diminish in size. If at this point the motor was switched off, the flame was gradually re-established over the whole of the inlet section of the matrix.

After the required rotational speed was reached, the air, methane and excess flowrates were gradually (over periods of time of approximately 60 minutes) adjusted so that the mixture flowrate and composition were as required.

Since "L" shaped stability curves were always expected, the critical points (i.e. last point at which there is combustion, and first point at which there is no combustion) at high flowrates were determined by keeping the inlet mixture flowrate constant and gradually reducing the methane content until extinction occured. This required the air flowrate to be held constant and the methane flowrate to be reduced.

The critical points on the horizontal section of the stability curves were obtained by keeping the methane percentage constant and reducing the inlet mixture flowrate. In this case both the methane and air flowrates were kept constant, while the flowrate to the auxilliary burner was gradually increased.

Before any of the operating conditions were altered, the system was always allowed to reach thermal equilibrium in terms of the exhaust gas temperature and the solid temperature on the outside of the "Top hat" container metallic flat wall. As

illustrated in figures (5.7) and (5.8), 4 to 6 hours were required for the initial steady state to be reached. Shorter times (~ 1 hour) were required for subsequent steady states to be reached due to the mixture flowrate or composition only being changed by small increments. The time required for steady state to be reached was a function of the mixture flowrate and, therefore, the convective heat transfer coefficients for heat transfer between the combustion chamber and matrix passages walls, and the reactant and product gases.

The exhaust gas temperatures, as shown in figure (5.8), initially increased with time, which indicates that the initial rate of heat loss from the system decreased with time. Decreasing the mixture flowrate or compostion resulted in a decrease of the exhaust gas temperature. This does not, however, mean that the heat loss rate increased but is merely indicative of the decrease in the heat input to the system. The existance of combustion inside the burner was checked by continuously monitoring the highest combustion chamber temperature, as during the initial stages of the experiments. Rapid decrease in the temperature reading indicated flame extinction.

During the experiments for determination of the stability characteristics of the rotary regenerative burner, whenever a thermal steady state was reached, the combustion chamber temperatures were recored at 10 mm intervals along the lines of traverse of the thermocouples. This procedure was repeated until the first point at which no stable combustion was reached.

During the experiments for the accurate measurement of the combustion chamber temperature, the system was allowed to reach its final steady state before extinction, and the suction pyrometer was inserted in the combustion chamber through the access tube for thermocouple A (see figure (5.3)).

The suction rate through the pyrometer was increased until the thermocouple reading stopped increasing with the suction rate. This was repeated at several points along the line of traverse of the pyrometer.

In the series of experiment for the determination of the composition of the chamber and exhaust gases, gas samples were withdrawn from the combustion chamber and the exhaust during steady state operation of the system both well before and just before the extinction point. The sampling rate was always quite slow, in order not to disturb the system, and sampling always proceeded for approximately 15 minutes.

In the experiments involving heat abstraction, the critical points were determined by a procedure similar to that for determination of the ordinary stability characteristics, but the water inlet and outlet tempertures were also recorded.

During the experiments with the transparent quartz flat and hemispherical tops for photographing the flame, the same basic procedure was repeated. However, at the various steady states of interest, the insulation above the combustion chamber was removed briefly to permit the flame to be photographed.

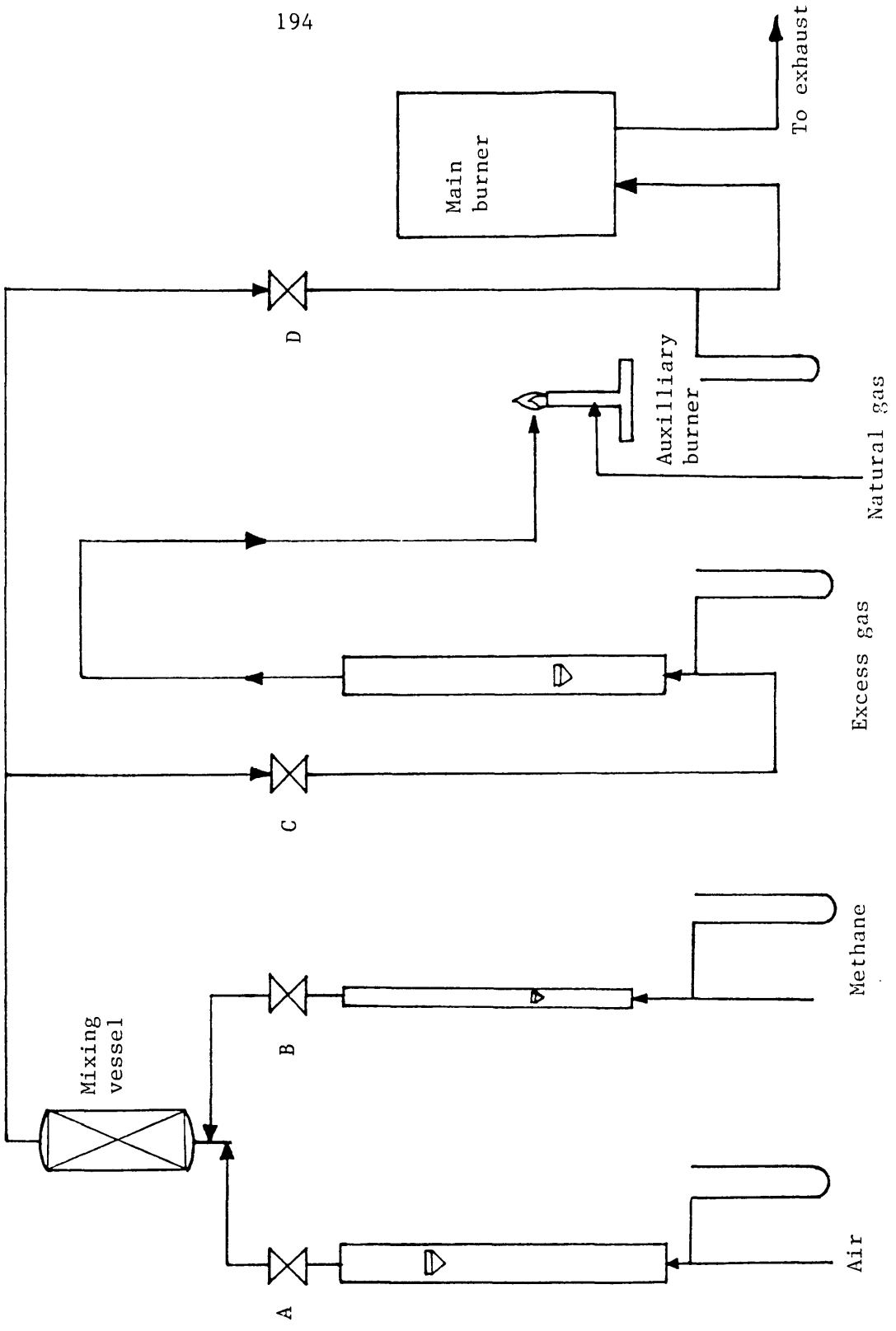


Figure (5.1): The flow measuring equipment.

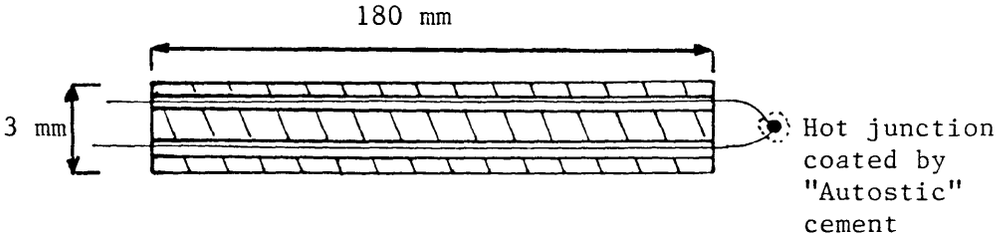


Figure (5.2): The thermocouple and support quartz rod.

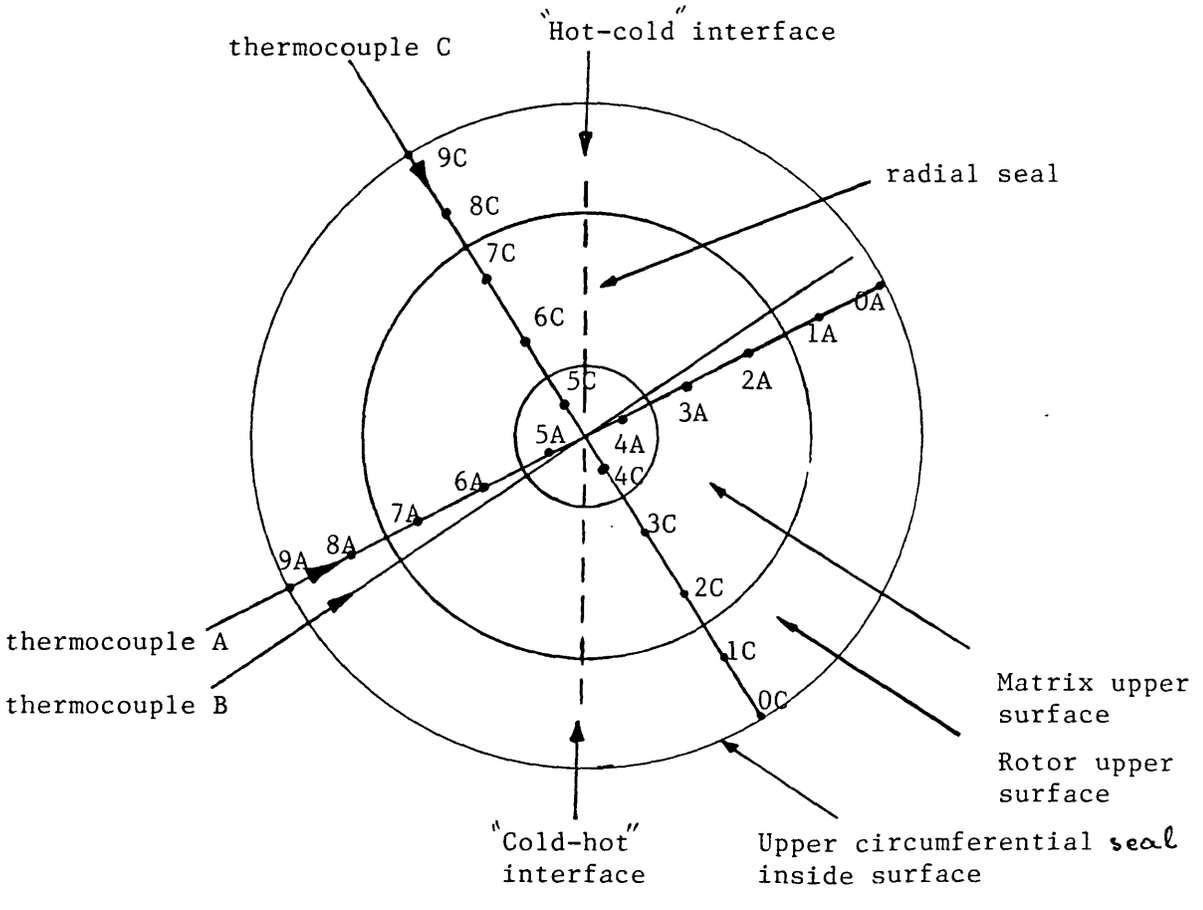


Figure (5.3)a: Thermocouple positions in relation to the two sections (entry and exit) of the matrix.

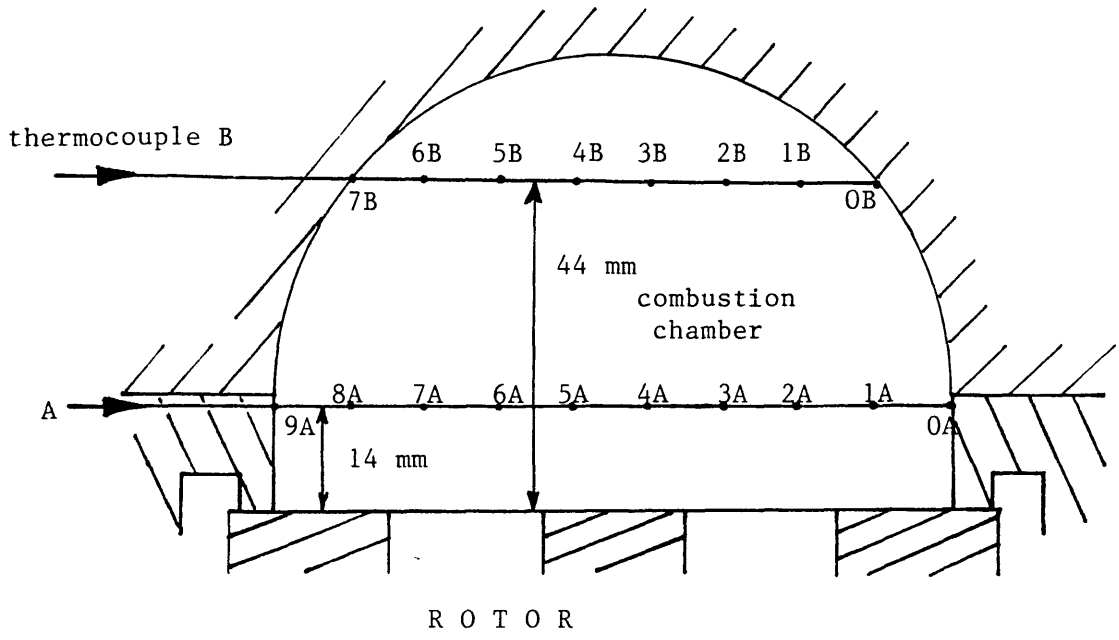


Figure (5.3)b: Distance of thermocouples (A,B) from the matrix upper surface (90 mm diameter combustion chamber)

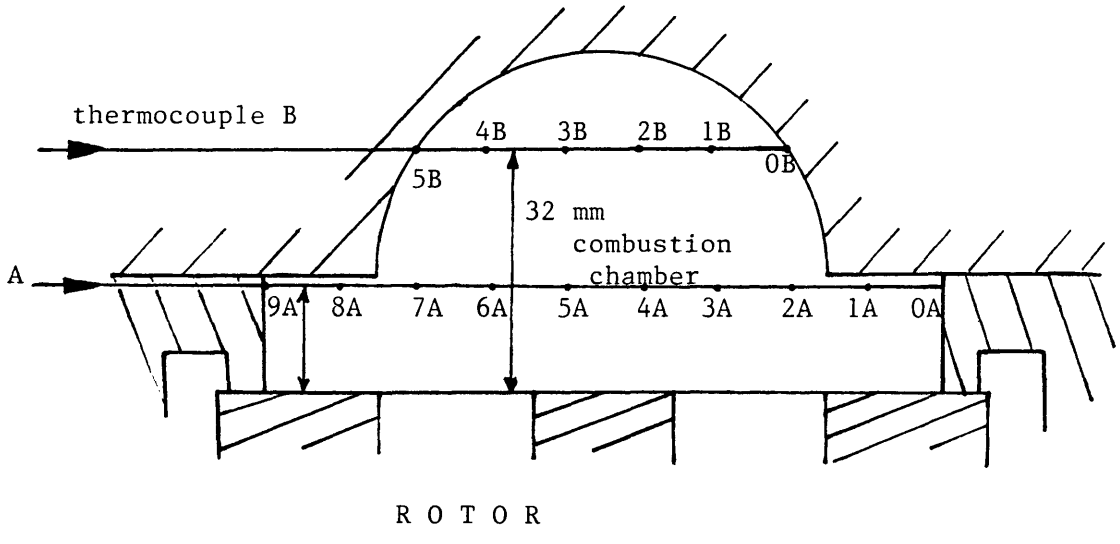


Figure (5.3)c: Distance of thermocouples (A,B) from the matrix upper surface (60 mm diameter combustion chamber)

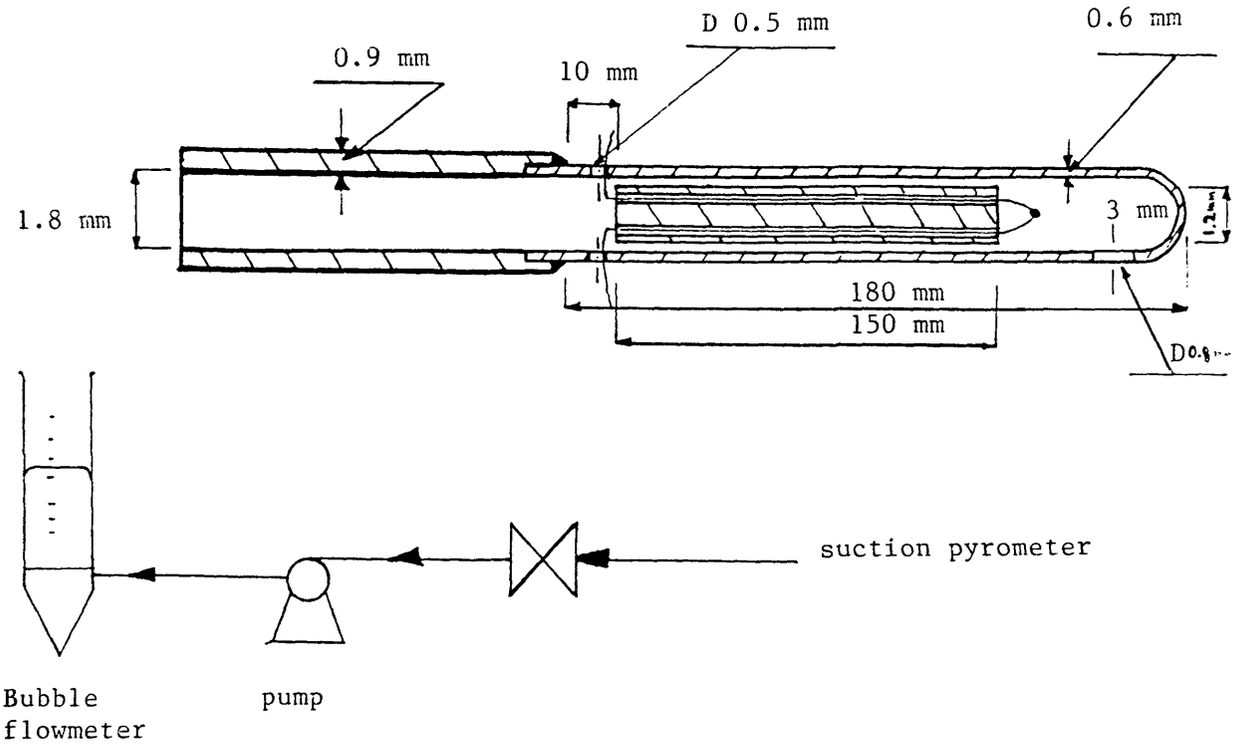


Figure (5.4): The suction pyrometer and the flow measuring equipment for temperature measurement

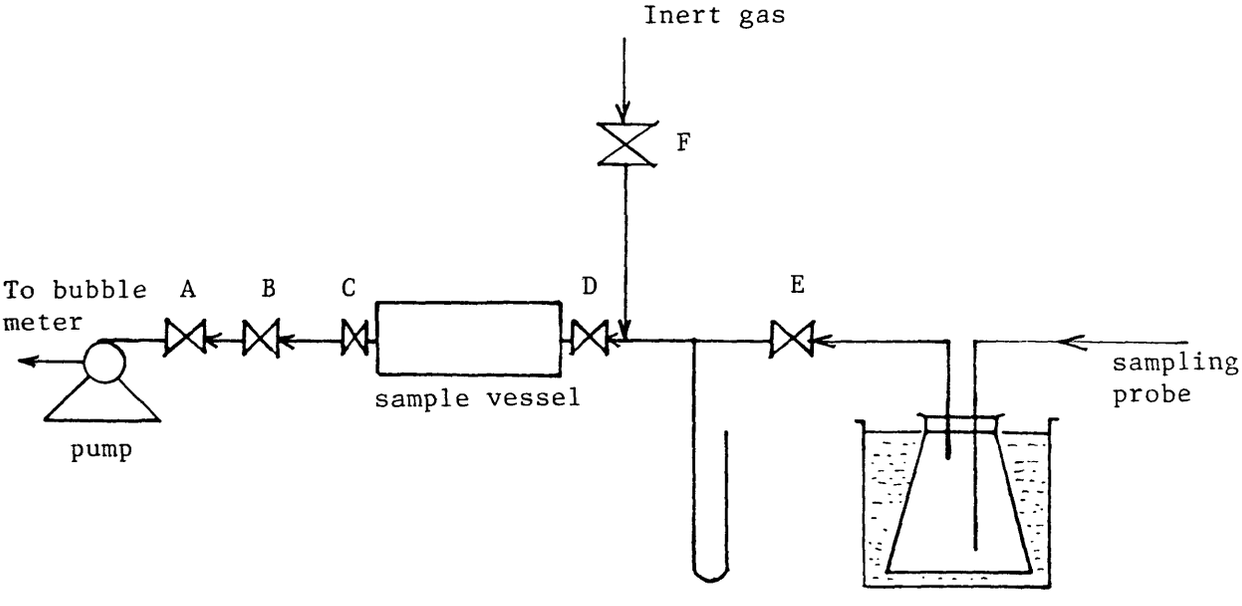


Figure (5.5): The flow measuring equipment for gas sampling

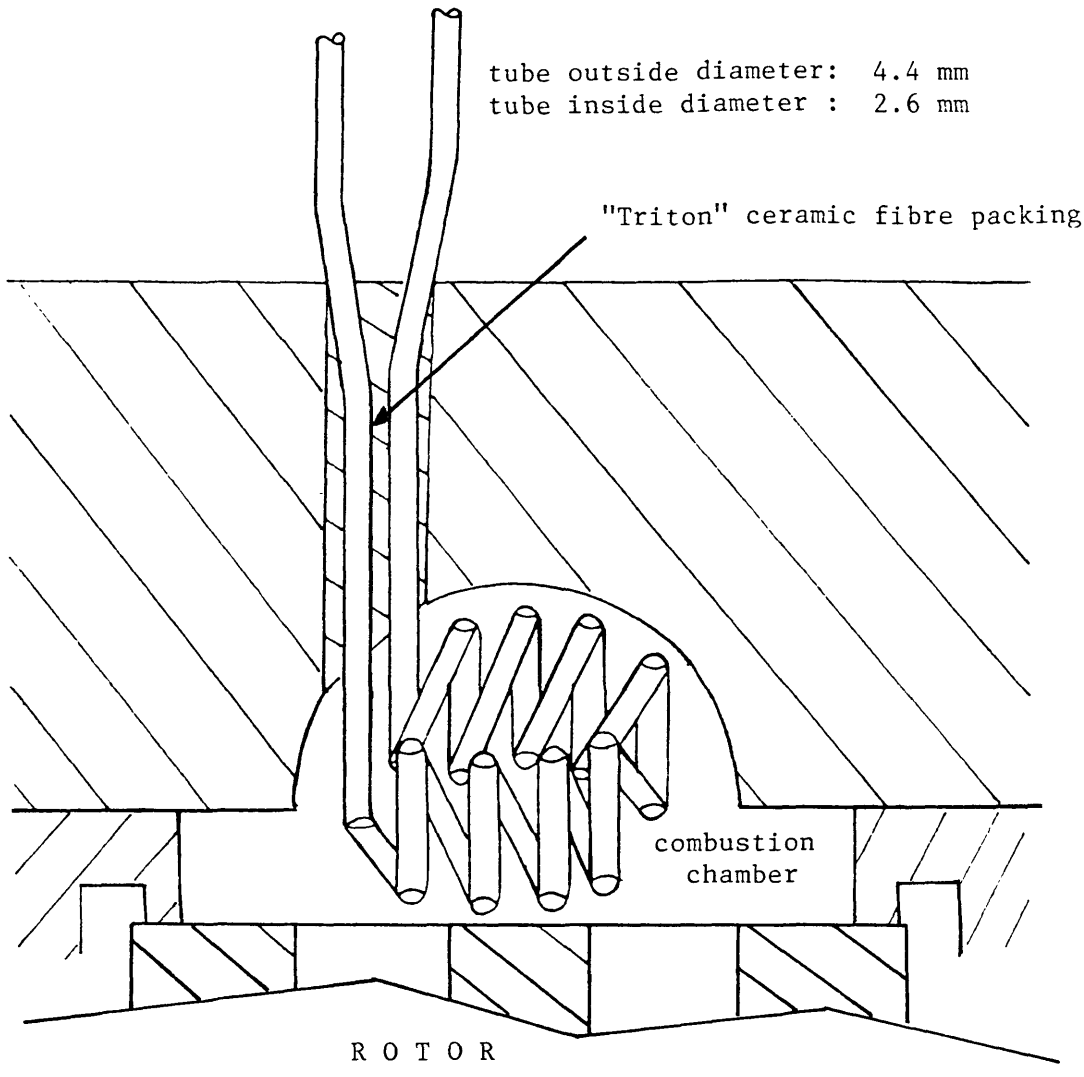


Figure (5.6): The 8 turn coil within the 60 mm diameter combustion chamber

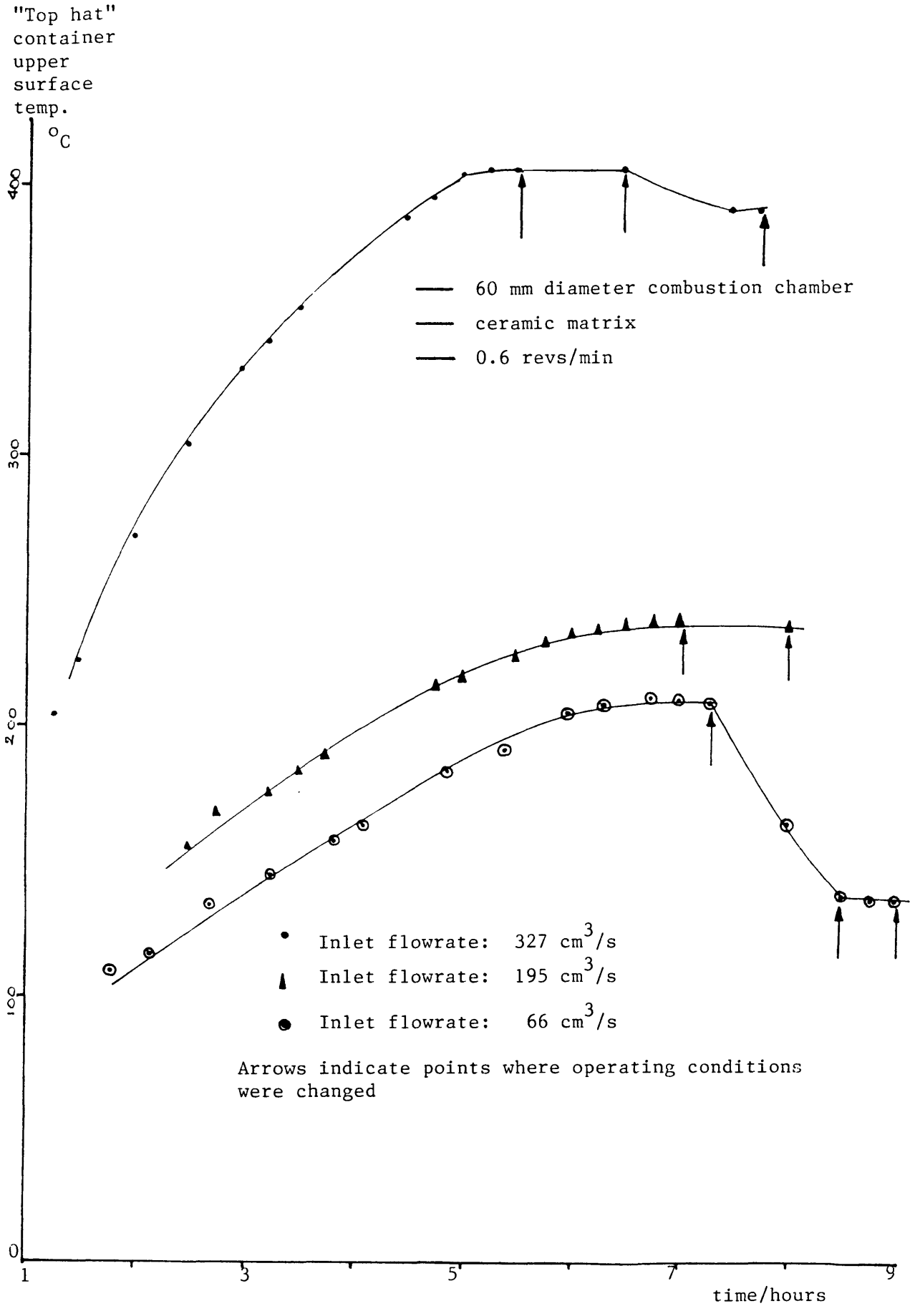


Figure (5.7): Variation of "Top hat" container upper surface temperature with time during three experimental runs.

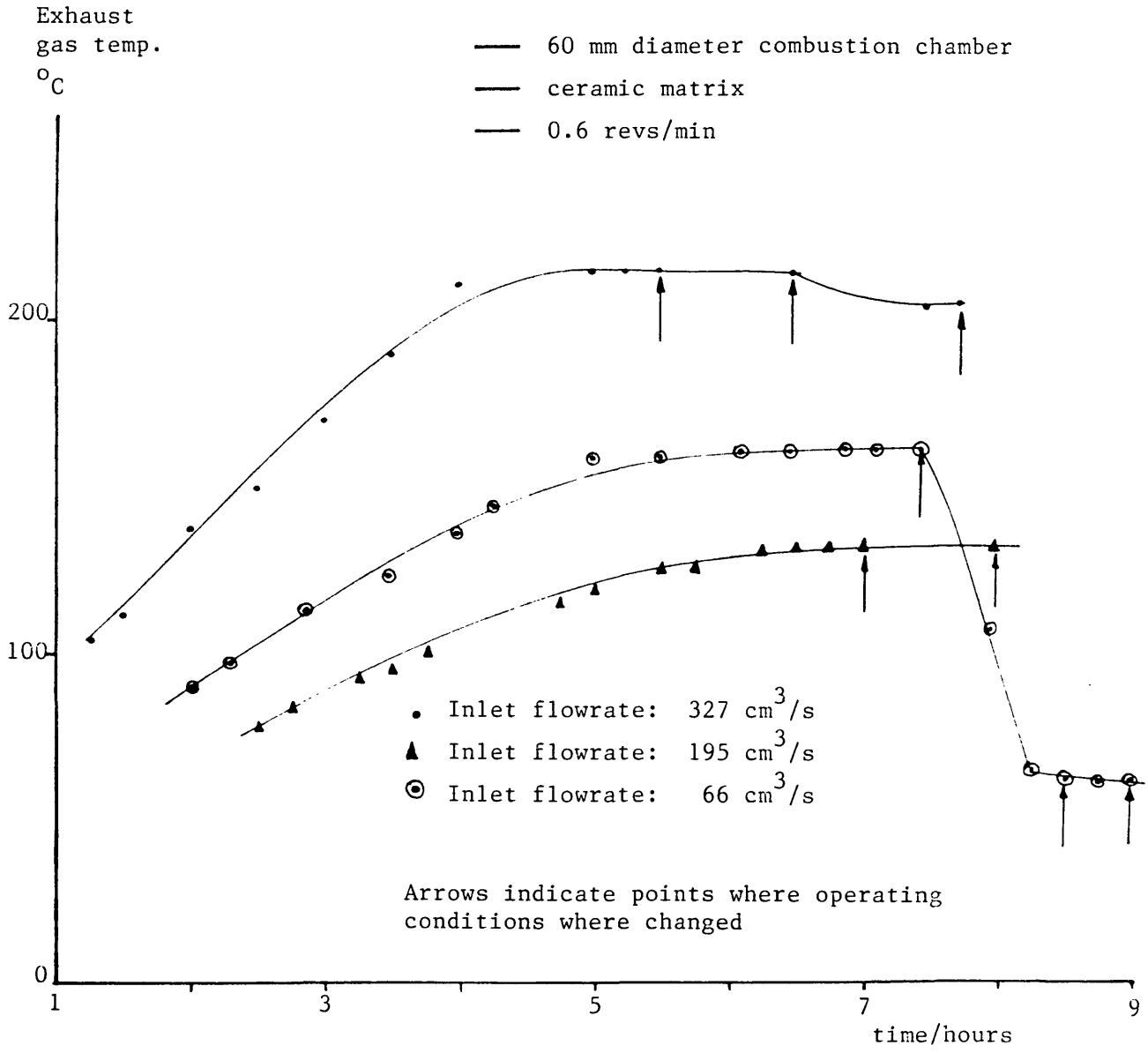


Figure (5.8): Variation of exhaust gas temperature with time during three experimental runs

Chapter 6

Experimental results and discussion

6.1. Introduction

The stability characteristics for both the metallic and ceramic matrix regenerative burners are presented and the ceramic matrix burner is shown to be the most efficient.

The experimental stability characteristics for the ceramic matrix are then contrasted to the ones predicted by the model. The experimental and predicted characteristics are found to be in reasonable agreement.

Information about the flame position within the combustion chamber is extracted from the temperature data and the suggestions, thus, made are verified by photographic evidence.

The flame stability criteria within the present system are discussed on the basis of the accurately measured combustion chamber gas temperatures and are shown to be different from those governing stability within the ""Swiss roll" burner.

The gas analysis results are presented, and it is shown that complete combustion within the system was rarely achieved.

Finally, the stability characteristics of the system with heat abstraction from the combustion chamber are given, and it is shown that lean combustion is still attainable.

6.2. Experimental results for methane combustion in the metallic matrix burner

The flame stability characteristics of the metallic matrix rotary regenerative burner with the 60 mm diameter hemispherical combustion chamber were obtained for the matrix rotational speeds of 0 revs/min, 0.6 revs/min, 1.2 revs/min, 2.4 revs/min and 4.0 revs/min.

The limiting mixture points were obtained for methane - air inlet mixture flowrates of up to 1100 cm^3/s (at 1 atm absolute, ambient teperature), which was the highest flowrate measurable by the flow system rotameters.

The stability curves for the burner, as previously mentioned, were obtained by gradually reducing the flowrate or the composition of the reactant stream directed to the burner and, therefore, finding the compositions and flowrates that corresponded to the last point for stable combustion and the first point for no combustion. Before any of the operating conditions were altered, adequate time was allowed for the system to reach thermal equilibrium and, depending on the mixture initial flowrate and composition, several such stable combustion steady states (5 - 3) were always reached before the final one was established.

The experimental data necessary for the determination of the burner stability curves are presented in Table (F.1) of Appendix F. The inlet, combustion chamber and exhaust gas temperatures and the upper wall surface temperature recorded by the *in situ* and traversing bare thermocouples, when the final stable combustion

steady state was reached, are also presented in Table (F.1).

The experimental mixture flowrates and compositions, representing extinction and stable burning points, are given in graphical form in the figures (6.1) to (6.5). The curves therein are the best boundaries between the limiting points and they are characteristic of the ability of the metallic matrix burner to sustain stable unaided combustion in lean methane-air mixtures. The stability curves, as expected, have a similar "L" shape, irrespective of the matrix rotational speed, but their vertical limbs are not as well defined as those for the "Swiss roll" burner (see figure (1.8)). It is, however, apparent that higher flowrates would lead to curves of more prominent vertical sections.

As can be seen from figure (6.6), in which the family of stability curves are for comparison purposes presented together, the leaness of the mixtures that can be stably burnt depends on the matrix rotational speed; increasing the speed leads to leaner mixtures. The curves, however, for 2.4 revs/min and 4.0 revs/min are almost identical and for this reason higher rotational speeds were not investigated. Mixtures as lean as 3.15% of methane in air by volume could be burnt for a matrix rotational speed of 4.0 revs/min and for a mixture inlet flowrate of approximately 1000 cm^3/s. It is in addition evident from figure (6.6), that irrespective of the matrix rotational speed, the lowest mixture inlet flowrate for stable combustion was approximately 150 cm^3/s.

The combustion chamber gas and wall temperatures, recorded by the bare Pt/Pt Rd traversing thermocouples (see figure (5.3a,b)) are presented in Table (F.1) of Appendix F. The measured gas temperatures, as indicated in Chapter 5, are not the true gas temperatures but can, however, be used to obtain information concerning the position of the flame within the chamber.

It is apparent from Table (F.1) that, irrespective of the matrix rotational speed and mixture inlet flowrate, there was a distribution in the wall and gas temperatures. The wall temperatures (positions 0 and 9 of thermocouples A and C, and 0 and 5 of thermocouple B) were not uniform and the highest values were always recorded on the section of the wall adjacent and directly above the matrix inlet section. The highest values for this section of the wall were almost always measured in its upper part (by thermocouple C), i.e. where the gases impinged after emerging from the matrix.

The temperatures in the lower part of the wall (measured by thermocouples A, C), which was the inside cylindrical surface of the metallic upper sealing ring, were quite uniform over its two symmetrical sections adjacent to the inlet and exit hemicircular sections of the matrix. For low inlet mixture flowrates the temperatures in the two sections were quite different but for high flowrates they were more uniform. A similar effect was observed for the hemispherical ceramic upper part of the combustion chamber wall.

The highest gas temperatures within the combustion chamber were always recorded by the thermocouples nearest the matrix

surface (i.e. thermocouples A and C). Of these the highest were always at positions 2 and 3 of thermocouple A, which were the two measurement stations directly above the matrix inlet section closest to the "hot-cold" interface (see figure (5.3a)).

For low inlet mixture flowrates the gas temperatures were quite low, typically 700^{o}C. They were widely distributed within the chamber and the highest values were measured by the thermocouples A and C when positioned directly above the matrix entry section. For high inlet flowrates the gas temperatures were more uniformly distributed and the highest temperatures were recorded by the thermocouples A and C when positioned directly above the matrix inlet and exit sections respectively.

In order to more fully characterize the burner, the rates at which leakages to the environment occured during operation were experimentally determined as described in Appendix F. The leakage test results (see Table (F.2)) are presented in the plot of figure (6.7) as percentages of the inlet volumetric flowrate. The equivalent results obtained during cold testing of the system are replotted for comparison purposes in the same figure. As expected, the hot operation leakage rates were higher than the cold operation ones, but the lower the inlet flowrate the smaller the difference between the two. Furthermore, it can be observed from figure (6.7) that, as in the case of the cold operation leakage rates, the hot operation leakage rates did not vary with the matrix rotational speed.

6.3. Discussion of the results for combustion in the metallic matrix burner

The shape of the flame stability curves of figure (6.6) have already been explained by the general theory for heat recirculating burners described in Chapter 1. At low flowrates the heat loss rate was large compared to the heat recirculation rate, and increasingly rich mixtures were required for stable combustion. With increasing flowrates, however, the heat losses became less significant and leaner mixtures could be burnt.

The relative position of the stability curves for the matrix rotational speeds investigated, can also be explained in terms of the heat loss to heat recirculation ratios. At low flowrates, since the heat losses were controlling and they were independent of the matrix speed, the curves coincide. At high flowrates, however, heat recirculation was controlling and, since it occured at rates that increased with the regenerator effectiveness or alternatively the matrix rotational speed, the higher the speed the leaner the mixtures that could be combusted. This, however, only appears to apply for rotational speeds slower than 2.4 revs/min and, as can be seen in figure (6.6), the stability curves for 2.4 revs/min and 4.0 revs/min are almost identical. A maximum in the regenerator effectiveness must, therefore, be reached at a rotational speed larger than 1.2 revs/min and equal or smaller than 2.4 revs/min. This critical rotational speed was calculated for the metallic matrix system (Appendix A) by employing the empirical equation (3.3-3). In the calculation procedure the heat

losses from the matrix solid and the gas leakages were ignored and a value for the heat loss from the combustion chamber gases was assumed. The critical speed was calculated as 1.38 revs/min and it corresponded to an effectiveness of 90% (see figure (3.8)). With such high regenerator effectiveness, it was calculated (see figure (3.8)) that mixtures as lean as 1.0 % of methane in air by volume could be stably burnt at inlet flowrates of 800 cm^3/s. Since, however, the leanest mixture with which stable combustion was achieved in practice was 3.3% of methane in air by volume, at the same inlet flowrate, the actual maximum regenerator effectiveness must have been considerably lower than the calculated one.

The empirical equation (3.3-3) describing the heat transfer process within the matrix has been shown to predict results which are comparable to ones obtained from more involved and accurate analyses and the combustion model was based on the proven theory of a constant limiting final flame temperature. Therefore, for the predicted results to be more realictic, the assumptions of no heat losses from the matrix solid and more importantly, no leakages and a small heat loss from the combustion chamber, would have to be modified.

Examination of the flame stability results, obtained for the burner with the matrix stationary, reveals that, even though the regenerator effectiveness was zero in theory, stable unaided combustion of mixtures leaner than 5.3% methane in air by volume were feasible at inlet florwrates in excess of 170 cm^3/s. Furthermore, mixtures as lean as 4.26% were burnt at the high

flowrates of 900 cm^3/s. These were not that different from the 3.86% methane in air by volume mixtures combustible at the same flowrate in the burner with the matrix rotating at 0.6 revs/min. The observations above lead to the conclusion that in the metallic matrix rotary regenerative burner heat recirculation from the products to the reactants was effected, not solely by heat being stored in and removed from the matrix solid, but by some additional means and at rates which were significant proportions of the total.

The flame trap matrix, under discussion, had walls which were metallic and, therefore, of high thermal conductivity and they were continuous both in the perpendicular and parallel directions to the gas flow. It was, therefore, by conduction through the walls in the direction of the "metal" flow that additional heat was transferred from the products to the reactants side. It must, however, be mentioned that such conduction proceeds together with longitudinal conduction which results in equalization of the temperatures along the matrix length and reduction, consequently, of the regenerator effectiveness (2.21).

The flame stability curves considered so far are characteristic of the overall heat-exchanger burner system together with its inherent gas leakages to the environment and the bypass leakages from the entry to the exit section. They do not, therefore, solely reflect on the regenerator effectiveness but also on the rates at which gas leakages occured. The total gas leakages to the environment were measured to occur (see figure (6.7)) at rates that ranged from 13% to 23% of the inlet

volumetric flowrates of 1000 cm^3/s and 150 cm^3/s respectively. Figure (6.7) shows that the leakages during hot operation were only slightly higher than those during cold operation and the difference decreased with decreasing inlet flowrates. The hot bypass leakages could not be measured but it is anticipated that they also were only slightly higher than those during cold operation.

Consideration of the gas temperature distribution in the combustion chamber provides information concerning the position of the flame within the chamber volume. The gas temperatures above the inlet section of the matrix and near the "hot-cold" interface were always found to be the maximum within the chamber. This is not surprising since the matrix wall temperatures were maximum near this interface and the reactant streams emerging from the matrix passages did so with preheat temperatures that decreased with increasing angular displacement from the "hot-cold" interface. The flame stabilized in this part of the chamber was, therefore, the most stable and acted as a "pilot" for the remaining flame.

The lower gas temperatures, observed at low inlet mixture flowrates, can be entirely attributed to the lower film coefficients for convective heat transfer from the gas to the thermocouple hot junction. The wide temperature distribution and the fact that high temperatures were recorded above the whole of the inlet section of the matrix suggest that, at low mixture flowrates, the limiting flame was stabilized over the matrix inlet section.

At high flowrates, however, the temperature distribution was more unifrom and the temperatures were largest over the parts of the matrix inlet and exit sections on either side of the "hot-cold" interface, i.e. where the solid and gas temperatures were maximum. At high inlet flowrates, therefore, the indications are of a flame diffused through the part of the chamber volume in close proximity to the "hot-cold" interface.

The arguments above were further substantiated by the photographic evidence obtained from the systems with the chambers of transparent quartz and presented in section 6.8 of this chapter.

6.4. Experimental results and discussion for methane combustion in the ceramic matrix burner

The stability characteristics of the rotary regenerative burner with the ceramic matrix and the 60 mm diameter hemispherical combustion chamber were obtained for the matrix rotational speeds of 0 revs/min, 0.6 revs/min, 1.2 revs/min and 2.4 revs/min.

The combustion experiments were performed, as with the metallic matrix system, with mixtures of methane in air but at mixture inlet flowrates which, in order to avoid excessive wear of the Phosphor bronze bush covering the surface of the upper circumferential seal, were kept lower than 800 cm^3/s (1 atm absolute, ambient temperature).

The rate of wear was found to increase with increasing inlet mixture flowrate, and for flowrates higher than 800 cm^3/s it was quite high resulting in a drastic increase of the load on the motor. If the final limiting flame temperature was, as expected, constant irrespective of the mixture flowrate, the above can be explained in terms of the convective coefficient for heat transfer, and ultimately the wall temperatures, increasing with increasing gas flowrates.

The experimental results are presented in tabular form in Appendix F and in graphical form in figures (6.8) to (6.11). The stability curves are again "L" shaped and as can be seen from figure (6.12) the methane content of the leanest combustible mixture (i.e. at high inlet flowrates) decreases with increasing rotor speed and, therefore, regenerator effectiveness. Figure (6.12), however, also shows that increasing the speed above 1.2 revs/min did not greatly affect the effectiveness, and the stability curves for 1.2 revs/min and 2.4 revs/min are almost identical. For the ceramic matrix system, operation with speeds higher than 2.4 revs/min did not, therefore, need to be investigated. The same effect was observed with the metallic matrix system but the critical rotational speed for maximum effectiveness was somewhat higher (between 1.2 and 2.4 revs/min).

At mixture inlet flowrates of 800 cm^3/s and a matrix speed of only 2.4 revs/min, combustion of mixtures as lean as 2.60% of methane in air by volume was possible in the ceramic matrix system. Stable combustion of such lean mixtures was never attained in the metallic matrix burner and, as is apparent from

figure (6.12), with the exception of the case when the ceramic matrix was stationary, the performance of the ceramic matrix burner compares favourably to the metallic matrix one over the whole range of the rotational speeds investigated. Furthermore, it is evident from figure (6.12) that the mixtures combustible within the ceramic matrix system, when the matrix is only rotated at 0.6 revs/min, are leaner than those combustible in the metallic matrix system, even for the matrix rotational speed of 4 revs/min when the effectiveness of the system is maximum. The higher efficiency of the ceramic as compared to the metallic matrix burner can be attributed to superior thermal performance of the matrix, and lower leakage rates. The pressure drops arising during flow through the flame trap matrix were found to be higher (see Chapter 3) than those arising during flow through the tubular matrix. The pressure differentials, therefore, between the metallic matrix system (both the combustion chamber and the inlet section) were higher and, since seals of identical configuration were used in both systems, the gas leakage rates from the metallic matrix system were higher. Furthermore, since in the metallic matrix burner both the pressure difference between the inlet and outlet sections and the effective gap size (see Chapter 3) between the matrix surface and the radial seal were larger, the bypass leakage rates within the metallic matrix system were higher than those within the ceramic matrix system. Both types of leakages were equivalent to heat losses due to (a) loss of potentially combustible fuel and (b) loss of sensible heat contained in combustion gases.

The higher rates at which gas leakages within and from the metallic matrix burner occured also explain the ceramic matrix burner's ability to sustain combustion in mixtures at lower inlet flowrates. In both systems (a) the areas available for heat losses to occur were the same, (b) the limiting flame temperatures are expected to have been similar and (c) the heat losses were controlling during operation with mixtures at low inlet flowrates. Thus, irrespective of how effective each individual matrix might have been, the heat losses, and, consequently, the level of performance, of both systems should have been similar. The effective heat losses, however, from the metallic matrix system were in fact increased due to the higher leakages.

The effectiveness of rotary regenerators has been shown to increase both with increasing solid to gas capacity rate ratio and increasing passage length to equivalent diameter ratio. The solid capacity rates, C_s, for the ceramic and metallic matrices employed here, can be obtained in terms of the matrix rotational speed, ω, from the following:

For the ceramic matrix $C_s = M_s c_{ps} \omega = 0.279 \times 800 \times \omega$

$= 218\ \omega$

and for the metallic matrix $C_s = 0.305 \times 501 \times \omega = 153\ \omega$. For any gas capacity rate and any matrix rotational speed, therefore, the ceramic matrix solid to gas capacity rate ratio was always larger, which indicates that the ceramic matrix regenerator effectiveness would tend to be higher. Conversely, however, the metallic matrix had passages of larger length to diameter ratios

(for the matallic matrix 75/0.378 and for the ceramic matrix 75/1.2), which would have the opposite effect on the effectiveness.

In order to accurately determine the ceramic to metallic matrix effectiveness ratios the matrix effectivenesses should be determined by measurement of the temperatures of the reactants emerging from the matrix and the products entering the matrix. Such measurements were not feasible with the traversing thermocouples and more refined methods of temperature measurement would have been very difficult to apply to the experimental system. Considering, however, that the ceramic matrix effectiveness, as opposed to the metallic matrix one, was not subject to the deleterious effect of high thermal conductivity walls, it can be anticipated that, for the same operational conditions, the ceramic matrix regenerator effectiveness was higher than that of the metallic matrix regenerator.

Combustion in mixtures of composition below the normal low flammability limit, as figure (6.12) shows, could still be achieved when the ceramic matrix was stationary, even though the regenerator effectiveness was zero as such (no heat was being transferred from the products to the reactants by storage in and removal from the matrix solid). Since, in contrast to the metal walls of the flame trap matrix, the thermal conductivity of the ceramic walls of the tubular matrix was only small, it can be assumed that the reactants were preheated mainly by the radiative heat received by the matrix solid from the combustion chamber walls. Only relatively rich mixtures (minimum 4.32% of methane in

air by volume) were combustible, however, and this means that only a small fraction of the sensible heat contained in the products was recirculated to the reactants. This can be attributed to the following:

(a) The matrix solid thermal conductivity was low and only a small proportion of the radiative heat it received was disperced throughout its length.

(b) The convective coefficient for heat transfer from the matrix walls to the reactants was small due to the small diameter of the matrix passages and the consequent laminar flow therein.

Most of the heat received by the matrix was, therefore, stored in its upper part and thermal equilibrium was achieved very quickly. The rapid tendency towards richer mixtures, as the inlet mixture flowrate is increased (see figure (6.12)), provides further support for the arguments presented above; the rate at which heat was recirculated increased only slowly with increased flowrate whilst the preheat temperatures decreased rapidly.

The gas temperature trends recorded within the combustion chamber of the ceramic matrix burner, during the experiments with the matrix in rotary motion, were similar to those recorded within the chamber of the metallic matrix burner (see section 6.2). The temperature trends again suggest that

(a) the part of the flame stabilized above the matrix inlet section and on the side of the "hot-cold" interface was the most stable and acted as a "pilot" for the rest of the flame.

(b) at low flowrates the flame was stabilized over the matrix inlet section and

(c) at high flowrates the flame was diffused through a part of the chamber nearest the "hot-cold" interface.

During operation with the matrix stationary, for all but the smallest flowrates, the high gas temperatures were uniformly distributed over the whole of the matrix exit section, indicating that the flame was stabilized in the part of the chamber directly above the matrix exit section.

The highest gas temperatures within the ceramic matrix combustion chamber were generally higher than the equivalent ones (i.e. for the same inlet mixture flowrate) in the metallic matrix burner. This can be explained in terms of the higher actual gas flow velocities through the combustion chamber of the ceramic matrix burner (due to the lower leakages from this system) and, consequently the higher convective coefficients for heat transfer from the chamber gases to the thermocouple hot junction.

In Chapter 4 of this thesis a mathematical model that predicts the stability characteristics of the ceramic matrix burner was developed. Due to the complexity of the processes within the burner, and the large number of parameters affecting its performance, several idealizations had to be made in developing the model. In order to evaluate the model, the predicted results will now be compared to the experimental ones.

In predicting the stability curves of figure (4.4) the overall gas leakage rate had to be estimated. Since the estimate used (15% of the inlet mixture flowrate) was experimentally found to be unrealistic, the predicted curves were corrected, as described in Appendix F. The improved stability curves are

presented together with the experimental ones in figure (6.13). As can be seen the predicted stability characteristics, despite the crudity of the model, are in reasonable agreement with the experimentally determined ones. For high inlet flowrates the model predicts stable combustion with mixtures leaner than the experimental and the % error between the predicted and experimental limiting mixture compostions is of the order of 25%. For low inlet flowrates, the predicted inlet mixture flowrates for stable combustion are higher than the experimental ones and the % error between the two is of the order of 50%.

Since the performance of the burner, as predicted by the model, is affected by a large number of necessary idealizations, determining the ones that need to be altered in order to improve the model would be difficult. Several of the said idealizations, such as the assumption of a very thin flame zone near the matrix inlet section, and uniform combustion chamber wall and gas temperatures, were shown experimentally not to hold.

Examination of the predicted and experimental stability curves of figure (6.13) reveals that

(a) for low inlet flowrates, since heat losses are controlling, the heat loss rate predicted by the model is higher than the actual and

(b) for high flowrates, since heat recirculation is controlling, the rate of heat recirculation predicted by the model is higher than the actual.

To improve the model, therefore, the idealizations affecting the above should be altered.

6.5. Experimental results and discussion for methane combustion in the ceramic matrix burner with combustion chambers of different size and configuration

To determine the effect of the combustion chamber size and geometry on the performance of the ceramic matrix burner the stability characteristics were obtained for a matrix rotational speed of 1.2 revs/min and both for a large (90 mm diameter) hemispherical chamber and a cylindrical chamber (90 mm diameter 15 mm height) burner. The experimental results presented in Table (F.1) of Appendix F, are plotted in figure (6.14). The experimental stability curve of the burner with the smaller size hemispherical chamber (same matrix speed) is included in figure (6.14) for comparative purposes.

Even though the volumes of the 90 mm diameter and 60 mm diameter hemispherical combustion chambers are 3 and 1.6 times larger than the volume of the cylindrical chamber, the levels of performance of the three systems do not appear to have been greatly different. Figure (6.14) does, however, show that at high flowrates, the leaness of the limiting mixtures increased with increasing combustion chamber volume. For the cylindrical and larger hemispherical chamber systems this trend persisted over the whole of the inlet flowrate range. The 60 mm diameter hemispherical combustion chamber system was, however, the most efficient for inlet flowrates lower than 500 cm^3/s.

For the burners of hemispherical chambers, increasing the volume of the chamber results in the following:

(a) The chamber wall surface area is increased. The chamber walls are not perfectly hemispherical but include a cylindrical section 90 mm in diameter and 15 mm in height (i.e. inside surface of the upper circumferential seal) that cannot be altered. Increasing the diameter of the hemispherical section from 60 mm to 90 mm resulted, therefore, in a chamber of overall wall surface area only 1.3 times larger.

Increasing the wall surface area leads to higher rates of convective heat transfer from the combustion gases to the wall and ultimately larger heat losses from the system.

(b) For a given inlet mixture flowrate the flow velocities through the chamber are decreased. Lower flow velocities result in a lower convective coefficient for heat transfer from the hot gases to the walls. The effect of the larger heat transfer area on the overal heat loss rate from the system is, therefore, counteracted by the reduced coefficients, but to an extent that depends on the relative magnitude of the two processes. Lower gas flow velocities also result in larger residence times for the reactants entering the combustion chamber. So far it has been assumed that complete combustion always takes place irrespective of the system operating conditions. However, as will be shown in section 6.7, this is not the case in practice for mixtures of limiting composition, and for combustion within the 60 mm diameter combustion chamber. Thus, increasing the residence time would improve the efficiency of the combustion process and, consequently, of the burner as a whole.

For the hemispherical chamber systems, it is apparent from figure (6.14), that for low inlet flowrates the controlling heat losses were larger in the case of the system with the larger chamber. Larger flowrates were necessary here for stable combustion. For high inlet flowrates, however, the larger chamber system was more efficient and combustion in leaner mixtures was sustained. Since at high flowrates heat recirculation was controlling, and the parameters governing the rate at which it occured were the same in both systems, the better efficiency of the larger chamber system can be attributed to the longer residence times and, therefore, the higher combustion efficiency within its chamber.

The volume of the chamber of the cylindrical chamber burner was the smallest and for any inlet flowrate the flow velocities and, therefore, the convective coefficients within the chamber were the highest. For low inlet flowrates, however, the performance of the burner was identical to that of the burner with the 90 mm diameter hemispherical chamber. The effect of the increased flow velocities on the overall rate of heat losses from the system was, therefore, entirely counteracted by the reduced chamber wall surface area.

The lower efficiency of the cylindrical combustion chamber burner, when the inlet flowrates were high, can again be attributed to the shorter residence times of the reactants in the chamber and, therefore, their less efficient combustion.

It should finally be mentioned that the gas temperature trends within the chambers of the larger hemispherical and

Table (6.1)

Sampling position	Inlet flowrate cm^3/s	% CH_4 inlet	% O_2 by vol.	% N_2 by vol.	% CH_4 by vol.	% CO by vol.	% CO_2 by vol.
3A	158	5.05	12.73	82.82	-	-	4.45
7A	158	5.05	12.82	82.70	0.05	0.05	4.38
exhaust	158	5.05	14.68	80.50	1.52	0.02	3.28
3A	83	5.05	13.42	81.95	0.52	0.19	3.91
7A	83	5.05	12.99	82.48	0.23	0.13	4.17
exhaust	83	5.05	15.08	79.97	1.88	0.05	3.01
3A	180	5.85	10.94	82.87	-	-	6.18
7A	180	5.85	11.00	82.80	-	-	6.20
exhaust	180	5.85	13.56	80.38	1.55	-	4.51
3A	55	5.85	12.07	81.95	0.46	0.24	5.27
7A	55	5.85	11.57	82.41	0.19	0.20	5.63
exhaust	55	5.85	14.44	79.65	1.98	0.13	5.49
3A	303	3.60	13.06	81.98	-	-	4.96
7A	303	3.60	12.88	82.00	-	-	5.12
exhaust	303	3.60	15.19	79.84	1.42	-	3.55
3A	292	3.37	14.99	81.16	-	-	3.85
7A	292	3.37	15.65	80.64	0.27	0.15	3.28
exhaust	292	3.37	16.65	79.63	1.01	0.02	2.70

Table (6.1) (continued)

3A	354	3.50	14.92	81.02	-	-	4.05
7A	354	3.50	15.29	80.76	0.12	0.11	3.72
exhaust	354	3.50	16.06	79.97	0.70	0.02	3.25
3A	333	3.40	15.65	80.53	0.03	0.01	3.67
7A	333	3.40	16.12	80.29	0.31	0.16	3.11
exhaust	333	3.40	16.42	79.92	0.60	0.03	3.04
3A	430	3.31	15.40	80.79	-	-	3.87
7A	430	3.31	15.86	80.48	0.18	0.12	3.36
exhaust	430	3.31	16.76	79.72	0.81	-	2.71
3A	428	3.18	16.91	79.76	0.07	0.07	2.56
7A	428	3.18	16.17	80.32	0.27	0.13	3.10
exhaust	428	3.18	19.98	79.60	0.84	0.03	2.54
3A	585	3.12	15.72	80.76	-	-	3.53
7A	585	3.12	16.10	80.36	0.08	0.10	3.35
exhaust	585	3.12	17.10	79.35	0.78	0.01	2.76
3A	583	2.98	16.12	80.47	0.05	0.02	3.33
7A	583	2.98	16.50	80.17	0.21	0.14	2.97
exhaust	583	2.98	17.11	79.52	0.76	0.02	2.58
3A	807	2.85	15.81	80.74	-	-	3.45
7A	807	2.85	15.99	80.62	0.05	0.04	3.30
exhaust	807	2.85	17.25	79.32	0.88	0.01	2.54
3A	807	2.61	16.56	80.46	-	0.02	2.95
7A	807	2.61	17.56	79.31	0.74	0.05	2.52
exhaust	807	2.61	17.05	79.31	0.76	0.02	2.86

cylindrical chamber burners were similar to those described previously for the small hemispherical chamber burner and the flame position was not, therefore, affected by the size or configuration of the chamber.

6.6. Gas analysis and combustion chamber gas temperature measurement results and discussion

To determine the combustion efficiency of the burner the combustion chamber and exhaust gases from the burner were analysed for N_2, O_2, CH_4, CO and CO_2. The 60 mm diameter hemispherical chamber system was employed in the process, and the ceramic matrix was rotated at 1.2 revs/min. The burner was operated over a range of inlet mixture flowrates and gas samples were obtained under steady state conditions, both far from and quite near the previously determined limiting conditions. The sampling rates were always kept quite low (below 5% of the inlet flowrate) and, with reference to figure (5.3a), the combustion chamber gas samples were drawn from the positions 3A and 7A (i.e. from above the matrix inlet section on the side of the "hot-cold" interface and above the matrix exit section on the side of the "cold-hot" interface).

From the analysis results, presented in Table (6.1), the overall conclusion can be drawn that the idealisation of complete combustion within the system did not apply in practice. Traces of CO were almost always found in the exhaust gas and this was

especially so when the system was operated with mixtures of composition approaching the limiting value. Reduction in the fuel content and mixture inlet flowrate were generally found to adversely affect the combustion efficiency.

The combustion chamber gas composition was, as expected, found to vary with position. With non-limiting mixtures it was found that in the part of the chamber above the matrix inlet section and near the "hot-cold" interface, i.e. where the mixture preheat temperatures were highest, complete combustion always occured and no traces of CH_4 of CO were ever detected. In most instances, however, this was not true within the part of the chamber above the matrix exit section and near the "cold-hot" interface, where both CH_4 and CO were detected.

Since the reactants emerged from the matrix passages with preheat temperatures that decreased with increasing angular displacement from the "hot-cold" interface, the rate of reaction within the chamber also decreased with increasing angular displacement from the "hot-cold" interface and the available residence time was not adequate for complete reaction of the colder reactants. The presence of CO can be explained in terms of the finding (6.1) that oxidation of CO is inhibited in very lean preheated methane - air mixtures by the presence of CH_4. Once all the CH_4 has been consumed, CO combustion is rapidly completed.

For the limiting mixtures, due to the reduced heat input, incomplete combustion occured even in the part of the chamber which the reactants entered with the maximum preheat temperatures.

The exhaust gas composition, in addition to the burner combustion efficiency , also depends on the rates at which the leakages from and within the system occured. The actual exhaust gas emerging from the matrix passages into the burner exit section, was diluted by the inlet methane - air mixture bypassing the matrix. The relatively large amounts of methane present in the exhaust gas, even when combustion within the burner was complete, can, therefore, be attributed partly or in total to the methane contained in the bypassing gas.

Gas sampling from the system at the final steady state before extinction, was followed by the accurate measurement of the combustion chamber temperatures via the suction pyrometer described in detail in the previous chapter. The suction rate was, as previously mentioned, always increased until a maximum temperature reading was reached. This was repeated at several positions along the path of the pyrometer (identical to that of thermocouple A in figure (53a)).

A maximum temperature was always recorded at the position directly above the matrix inlet section and almost halfway between the matrix inside and outside periphery. This was again the position along the pyrometer path were the reactants, emerging from the matrix passages below, had the highest preheat temperatures.

Since, as illustrated in the diagram of figure (5.3a), the pyrometer measuring stations directly above the matrix inlet section were at an angular displacement of 30^{o} from the "hot-cold" interface, where the reactants preheat temperatures achieved their

Table (6.2)

Inlet mixture flowrate cm^3/s	% CH_4 by vol.	Gas Temperatures ^oC 1A	2A	3A	4A	5A	6A	7A	8A
158	5.05	365	502	923	697	570	570	543	502
83	5.05	-	-	-	-	-	-	-	-
180	5.85	406	550	746	526	508	515	513	480
55	5.85	-	-	-	-	-	-	-	-
303	3.60	586	860	1127	1078	1036	890	850	800
292	3.37	-	-	-	-	-	-	-	-
354	3.50	595	790	1140	1070	1025	801	865	797
333	3.40	-	-	-	-	-	-	-	-
430	3.31	632	812	1170	1082	1046	805	812	793
428	3.18	-	-	-	-	-	-	-	-
585	3.12	700	839	1184	1054	847	802	890	817
583	2.98	-	-	-	-	-	-	-	-
807	2.85	720	895	1210	1123	898	813	848	841
807	2.61	-	-	-	-	-	-	-	-

true maximum, the recorded maximum temperatures must be smaller than the actual maximum within the chamber.

It is apparent from Table (6.2), in which the temperature measurement results are presented, that the maximum temperature increased with increasing inlet mixture flowrate. At low inlet flowrates the rate of increase was rapid but at higher flowrates it was only gradual, and in the range from 292 cm^3/s to 807 cm^3/s the maximum temperature only increased from 1400 K to 1483 K. At low inlet flowrates the maximum temperatures were low and increasing the inlet flowrate from 155 cm^3/s to 83cm^3/s increased the temperatures from 1019 K to 1196 K.

The observed trends for the maximum recorded combustion chamber gas temperatures can be explained in terms of the flame position relative to the pyrometer. At low inlet flowrates, since the temperatues are low, it can be safely assumed that they do not correspond to the true flame temperatures. The flame must have been thin and stabilized over the matrix inlet section. This would also explain the initial rapid increase in the recorded temperatures due to lifting of the flame with increasing flowrate.

At higher inlet flowrates, however, since the recorded temperatures are high and similar to the constant limiting flame temperature recorded in the "Swiss roll" burner (1403 ± 39 K) they can be assumed to correspond to the true flame temperatures for the flame stabilized in the region of the chamber in immediate proximity to the pyrometer measuring position.

Since the recorded flame temperatures for inlet flowrates in the range from 300 cm^3/s to approximately 500 cm^3/s are similar to

the constant limiting flame temperature (~ 1400 K for methane) which represents stable combustion in preheated quiescent methane - air mixtures, it can be assumed that for such inlet flowrates in the present system, as in the case of the "Swiss-roll" burner, stability was governed by criteria similar to those that apply to the flammability limits in quiescent mixtures. The continuous increase, however, in the recorded flame temperatures would suggest that stability within the system was governed by further criteria, of importance increasing with increasing inlet flowrate.

The reactants, as previouly mentioned, emerged from the matrix passages with preheat temperatures that decreased with increasing distance from the "hot-cold" interface. The part of the flame, therefore, stabilized in the hottest reactants acted as a "pilot" for the colder ones. The preheat temperature distribution can be assumed to have been wider for higher inlet flowrates, when the heat losses from the system were not controlling and the heat recirculation rate was quite high. The necessity, therefore, for a hotter "pilot" flame to sustain combustion in the colder reactants must have been greater the higher the inlet mixture flowrate.

6.7. Experimental results and discussion for combustion with heat abstraction

The flame stability characteristics of the 60 mm diameter hemispherical chamber burner, with the ceramic matrix, being

Table (6.3)

Inlet mixture flowrate cm^3/s	% CH_4 by vol.	No. of turns of coil	Water flowrate Kg/min	Water inlet temp. ^oC	Water outlet temp. ^oC	Heat removed by water J/s	Heat input to burner J/s	% of heat input removed by H_2O
670	4.09	4	0.175	22	45	280	891	31.4
668	3.92	4	0.175	-	-	-	-	-
449	4.44	4	0.175	20	37	204	648	31.4
447	4.27	4	0.175	-	-	-	-	-
262	4.95	4	0.175	24	35	134	421	31.8
259	4.65	4	0.175	-	-	-	-	-
678	4.79	8	0.175	23	57	414	1055	39.2
677	4.61	8	0.175	-	-	-	-	-
439	4.95	8	0.175	25	48	280	706	39.6
440	4.77	8	0.175	-	-	-	-	-
266	5.53	8	0.175	21	36	183	478	38.3
264	5.25	8	0.175	-	-	-	-	-

rotated at 1.2 revs/min, and with heat abstraction from the combustion chamber gases, are presented in figure (6.15) together with those corresponding to the system from which heat was not abstracted.

Removing heat from the combustion chamber gases is equivalent to increasing the overall heat losses from the system and, as can be seen from figure (6.5), larger limiting inlet mixture flowrates and richer mixtures are required for stable combustion. Mixtures of concentrations below or just above the low flammability limit, depending on the coil heat transfer area, were, however, burned in the system. Flame blowout due to high flow velocities within the chamber was not observed even at the highest flowrates investigated.

The heat removed by the water flowing through the cooling coil was found to be independent of the water flowrate. For the range of water flowrates investigated the coefficient (both convective and radiative) for heat transfer to the coil outside wall must have been controlling. The proportions of the heat input to the burner lost to the water, when the conditions within the burner corresponded to those of the final steady states before extinction, were computed for the inlet flowrates investigated and for both coils and they are presented in Table (6.3). The salient feature correlating the various percentages of heat input removed by the water is very simple; near the stability limit, and for a cooling coil of a given geometric configuration the proportion of heat input to the burner lost to the water remains constant. The proportion increased with increasing cooling coil heat transfer

area and was approximately 31.5% for the 4 turn coil and 39.0% for the 8 turn coil.

Doubling the size of the coil did not, therefore, greatly increase the heat losses from the system. Considering, however, the degree to which flame stability was affected when the heat abstraction rate was increased from 0% of the heat input to 31.6% of the heat input, it is apparent from figure (6.15) that increasing the heat abstraction rate from 31.5% to 39% of the heat input resulted in disproportionaly large deterioration of the burner stability characteristics. The shear presence of the cold coils within the chamber must, therefore, have had an adverse effect on the burner flame stability characteristics due to reduction of the chamber volume and quenching of the flame on the cold coil surface.

6.8. Photographic evidence of combustion within the rotary regenerative burner

Information about the flame position within the combustion chamber was obtained from the temperature data, accumulated in the course of the experimental study. The suppositions thus made were verified by obtaining a photographic record of the combustion process within both the hemispherical and cylindrical chambers of transparent quartz walls.

Combustion experiments were performed with inlet mixture flowrates of 790 cm^3/s, 384 cm^3/s, 168 cm^3/s and 81 cm^3/s. The

ceramic matrix was rotated at 1.2 revs/min and the flames were observed and photographed at several steady states of the system prior to flame extinction. The flames observed in the hemispherical and cylindrical chamber, when the system operating conditions were of a similar nature, were observed to be identical and were not distinguishable in the photographs taken.

The ceramic matrix, as depicted in the photographs herein, was rotated in the clockwise sense and the right hand side half section was its inlet section.

For low inlet flowrates, when flame extinction was not imminent, the flame comprised small flamelets stabilized over the individual matrix passages. The flame zone, as shown in the photograph of figure (6.16), was thin and covered the whole of the matrix inlet section. However, for operating conditions corresponding to those of the last final steady state before extinction, the flame, as can be seen in the photograph of figure (6.17), was not anchored on the matrix but hovered above a large part of its inlet section. Round the matrix outside edge, where the preheat temperatures were lower due to larger heat losses from the matrix walls to the rotor metallic walls, the flame had lifted. The matrix upper surface was no longer visible due to the lower temperatures of the solid.

For higher inlet flowrates (~ 384 cm^3/s) of mixtures with non-limiting compositions, as can be seen in the photograph of figure (6.18), individual flamelets were again stabilized on all the passages of the matrix inlet section. The flames in this case were quite tall and the solid appeared white hot over a small area

in the proximity of the "hot-cold" interface.

Decreasing the mixture methane content to just above the limiting composition, resulted in the flames becoming much taller (figure (6.19)) especially round the matrix outside and inside edges. The matrix solid temperatures decreased and near the "cold-hot" interface the matrix solid was no longer red hot.

Decreasing the mixture composition to the limiting one caused the flame to become even taller and, as can be seen from the photograph in figure (6.20), to be stabalized only over a part of the matrix area near the "hot-cold" interface. A large section of the matrix solid in the vicinity of the "cold-hot" interface appeared dark and was, therefore, much cooler than the rest of the solid.

During combustion of lean, but not limiting mixtures, at high inlet flowrates, the flame was obsereved to be diffused through most of the combustion chamber volume (figure (6.21)). The majority of the matrix solid appeared white hot and only the areas in close proximity to the "cold-hot" interface, and the matrix inside and outside walls, appeared red hot. When the mixture composition was reduced to the limiting one the flame was observed to be diffused through a part of the combustion chamber volume on the side of the "hot-cold" interface, (figure (6.22)) where the matrix solid appeared white hot. Over the inlet section of the matrix, only a part of the solid, almost halfway between the inside and outside edges of the matrix, appeared white hot.

The suggestions concerning the flame positions, which were made in the previous sections on the basis of the information provided by the temperature data, have been entirely justified by the photographic evidence presented above.

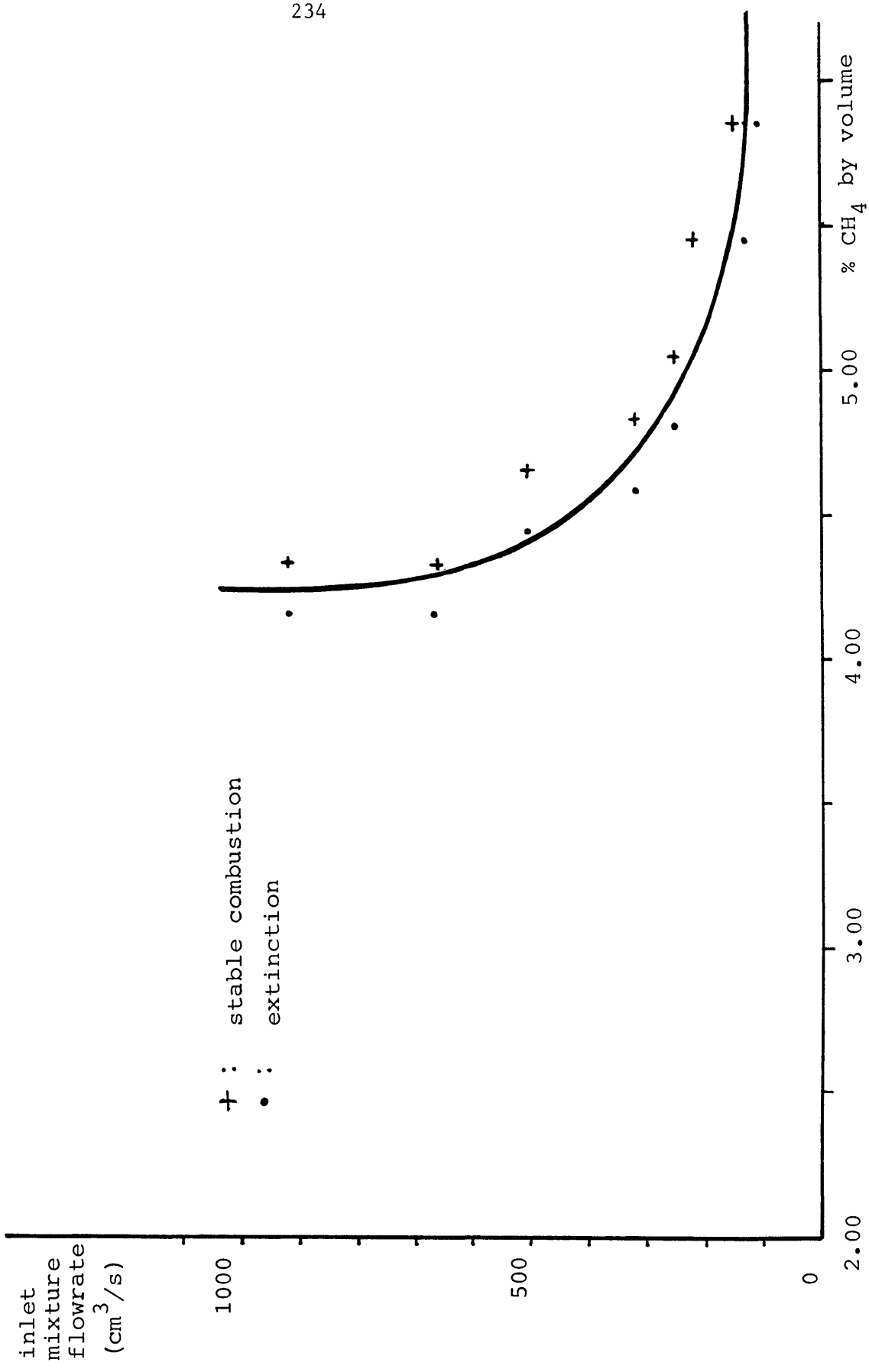


Figure (6.1): Flame stability characteristics for metallic matrix system and 60 mm diameter hemispherical chamber
0 revs/min matrix rotational speed.

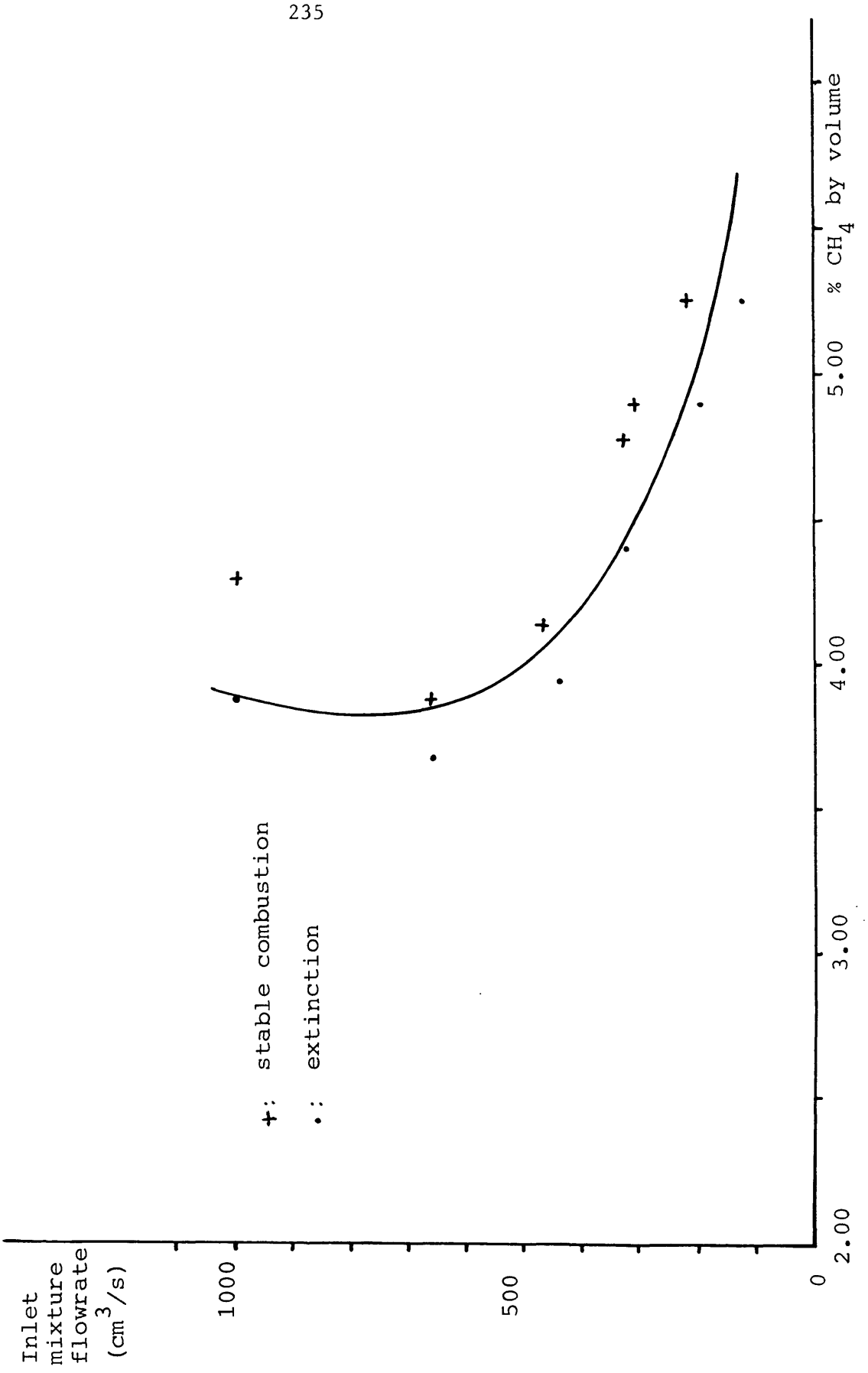


Figure (6.2): Flame stability characteristics for metallic matrix system and 60 mm diameter hemispherical chamber (0.6) revs/min matrix rotational speed.

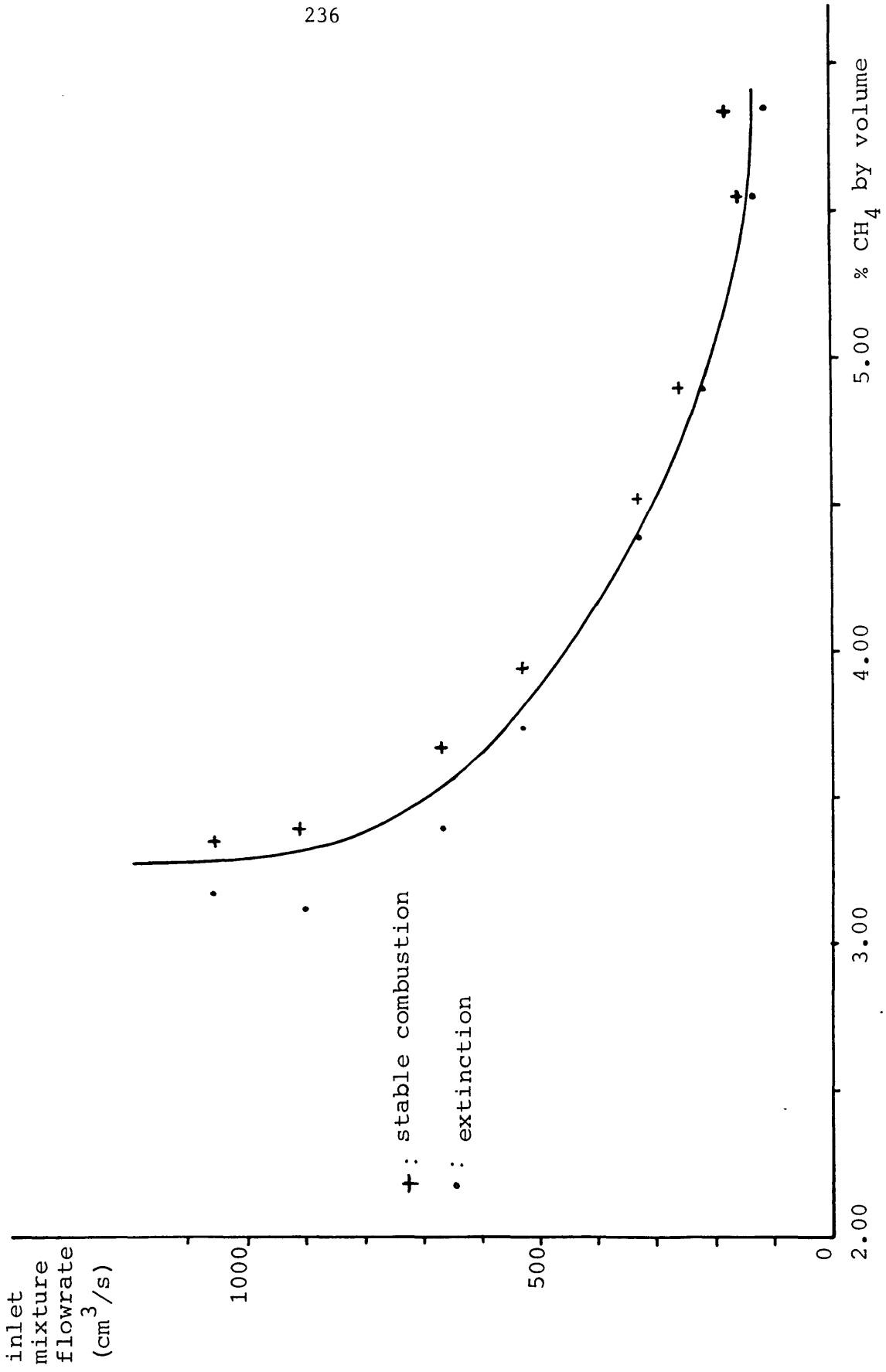


Figure (6.3): Flame stability characteristics for metallic matrix system and 60 mm hemispherical combustion chamber
1.2 revs/min rotational speed.

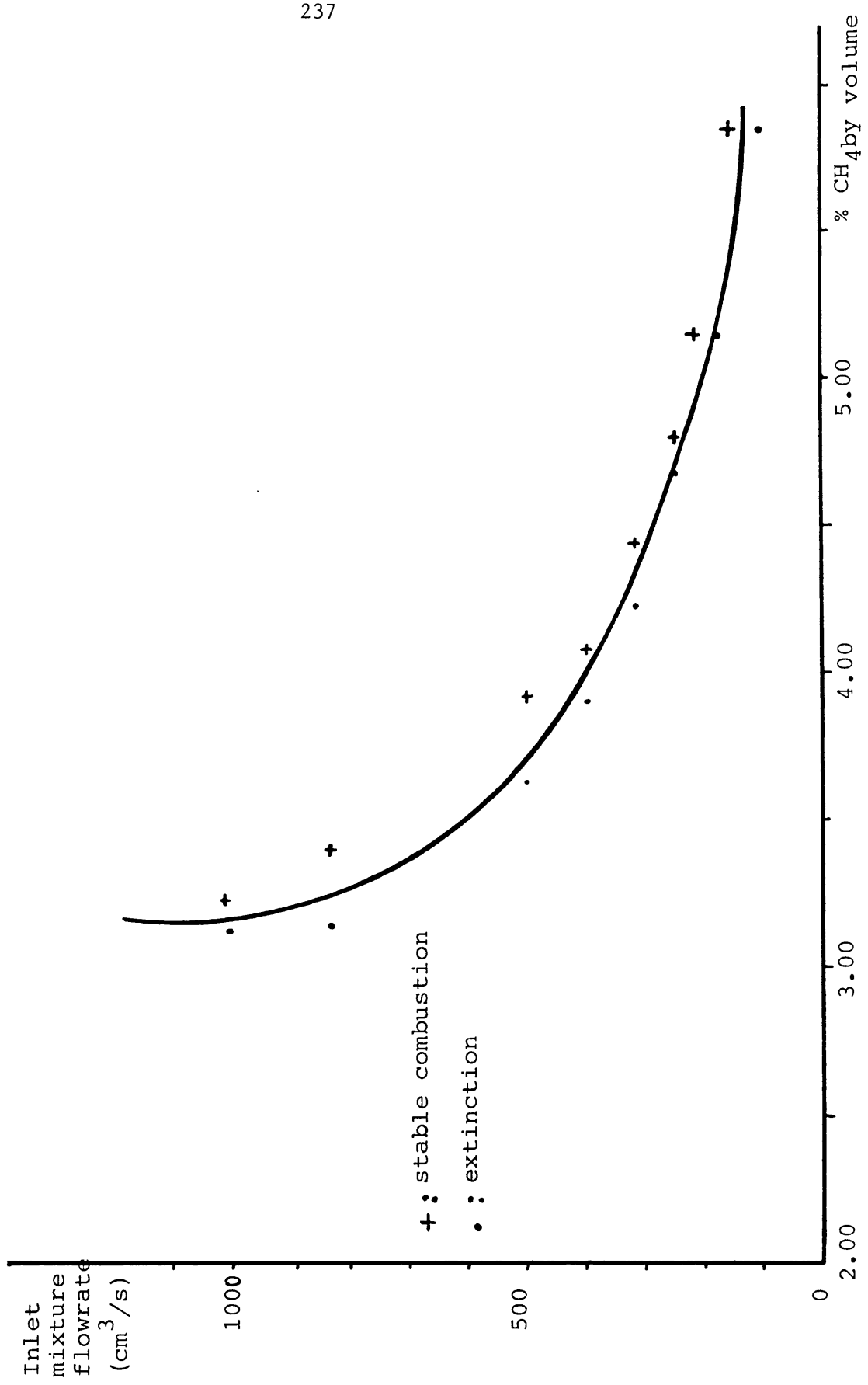


Figure (6.4): Flame stability characteristics for the metallic matrix system and 60 mm diameter hemispherical combustion chamber
2.4 revs/min matrix rotational speed.

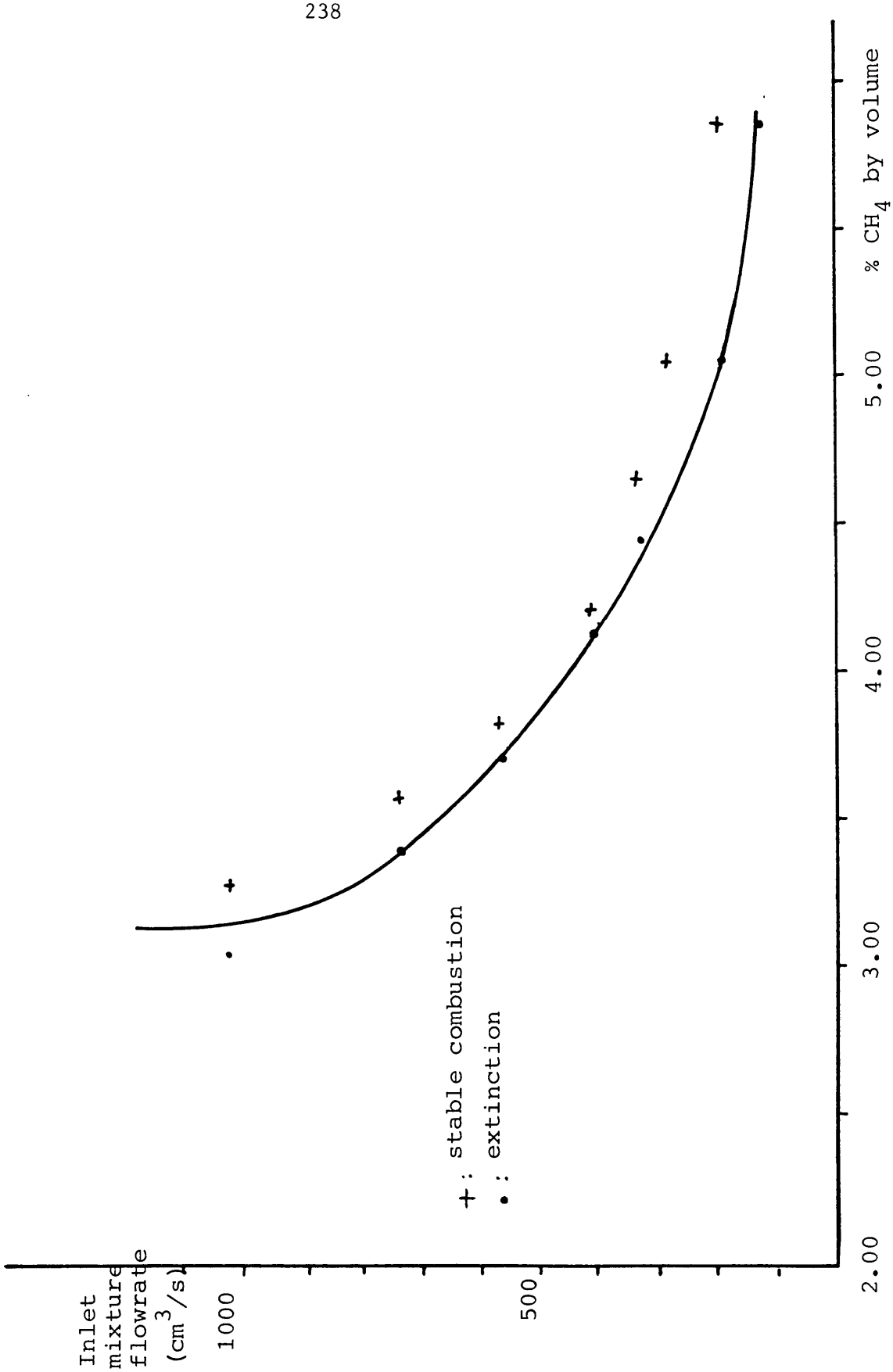


Figure (6.5): Flame stability characteristics for the metalic matrix system and 60 mm diameter hemispherical combustion chamber
4 revs/min matrix rotational speed

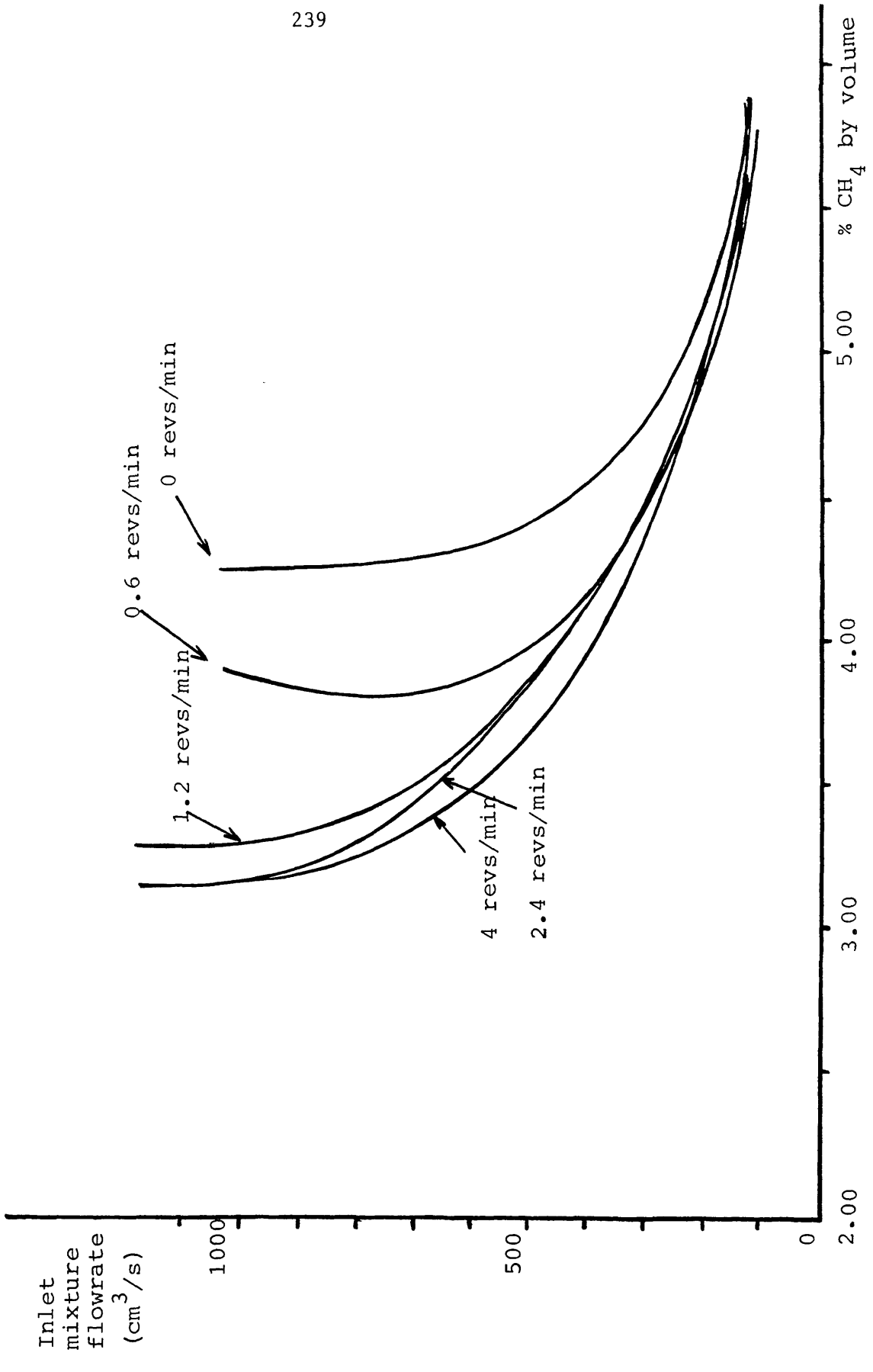


Figure (6.6): Effect of matrix rotational speed on the metallic matrix system stability characteristics (60 mm i.d. hemispherical combustion chamber).

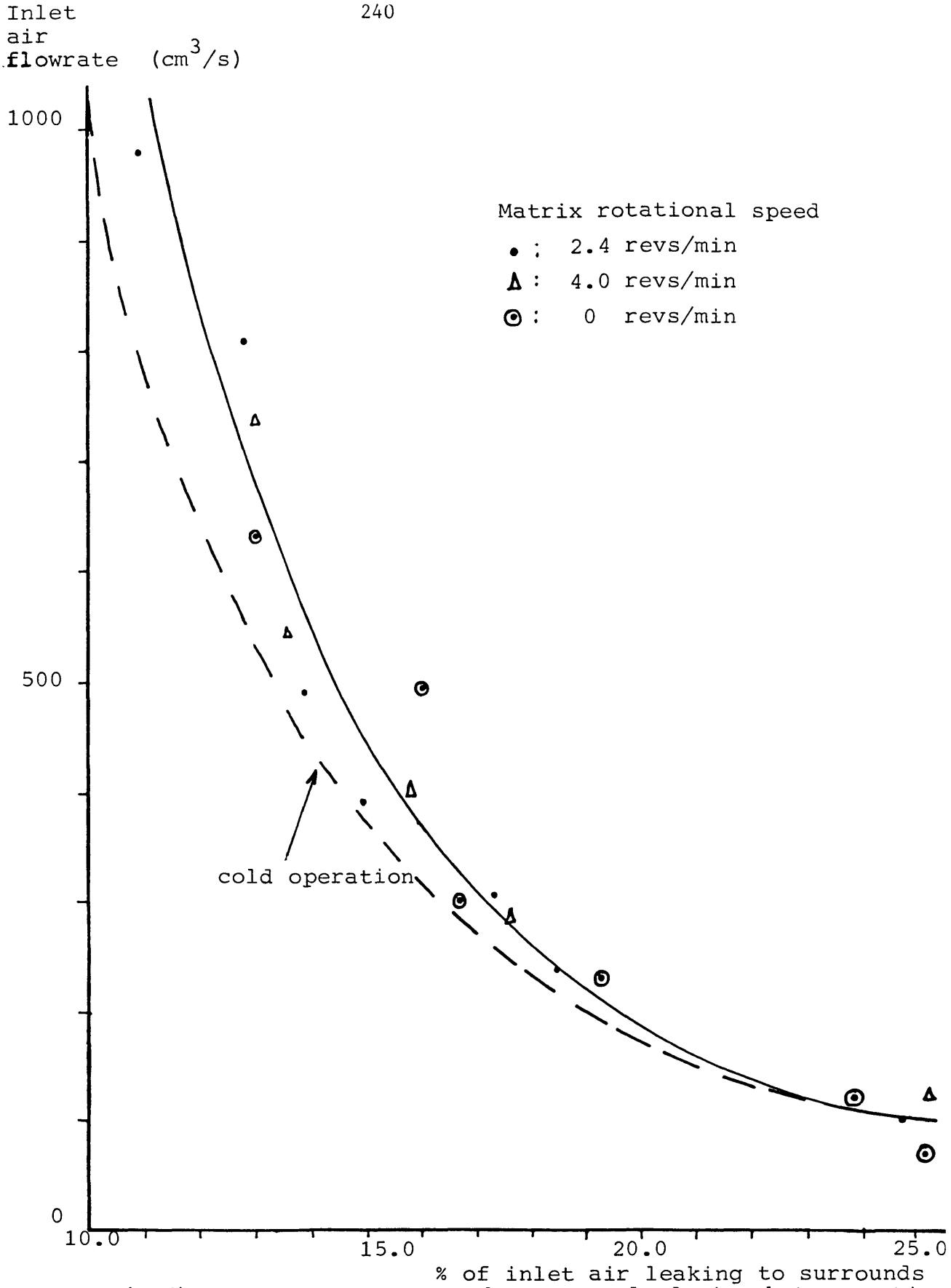


Figure (6.7): Leakage rates to the surrounds during hot operation of the metallic matrix system.

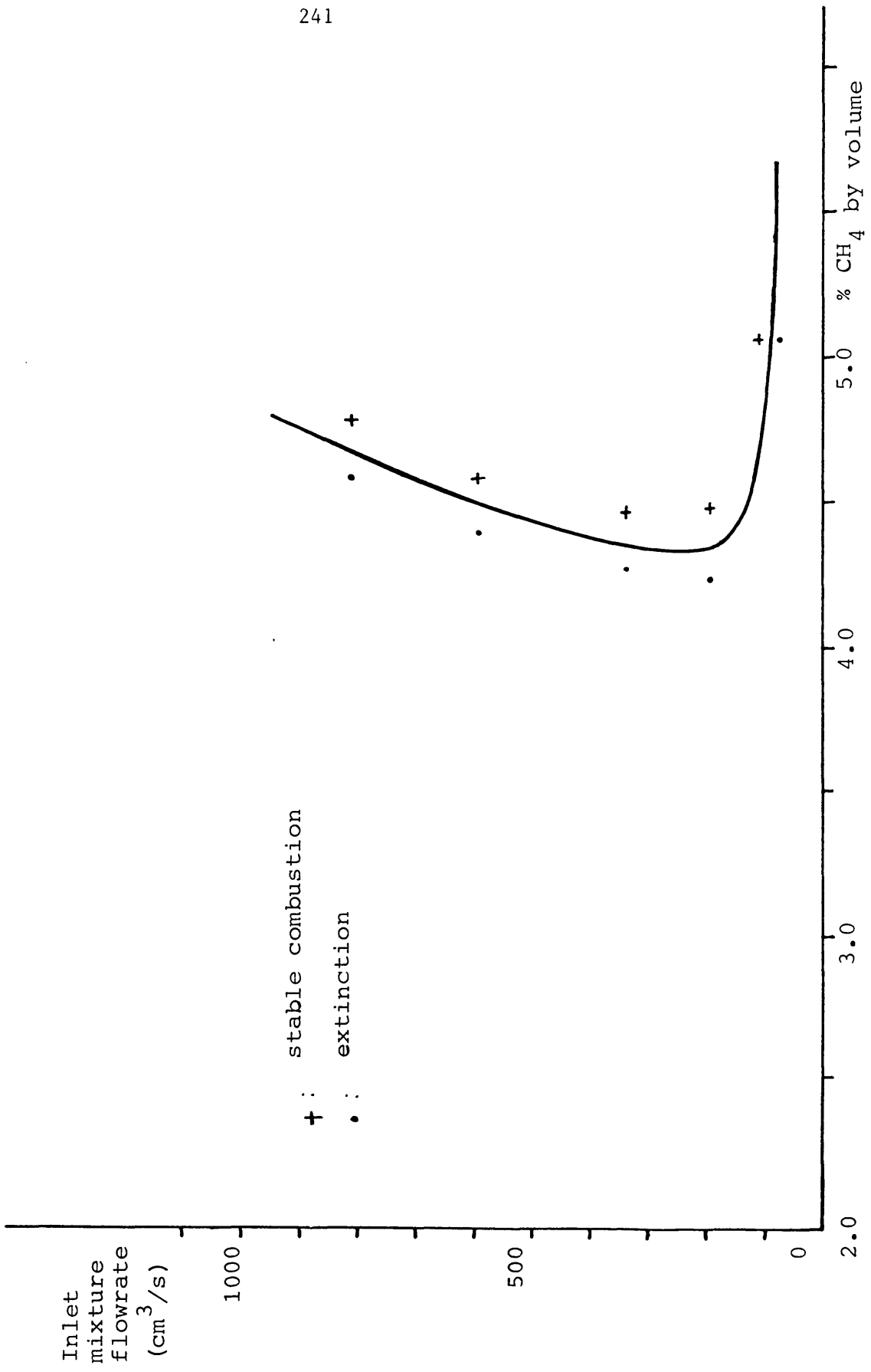


Figure (6.8): Flame stability characteristics for the ceramic matrix system and 60 mm id hemispherical combustion chamber
0 revs/min matrix rotational speed.

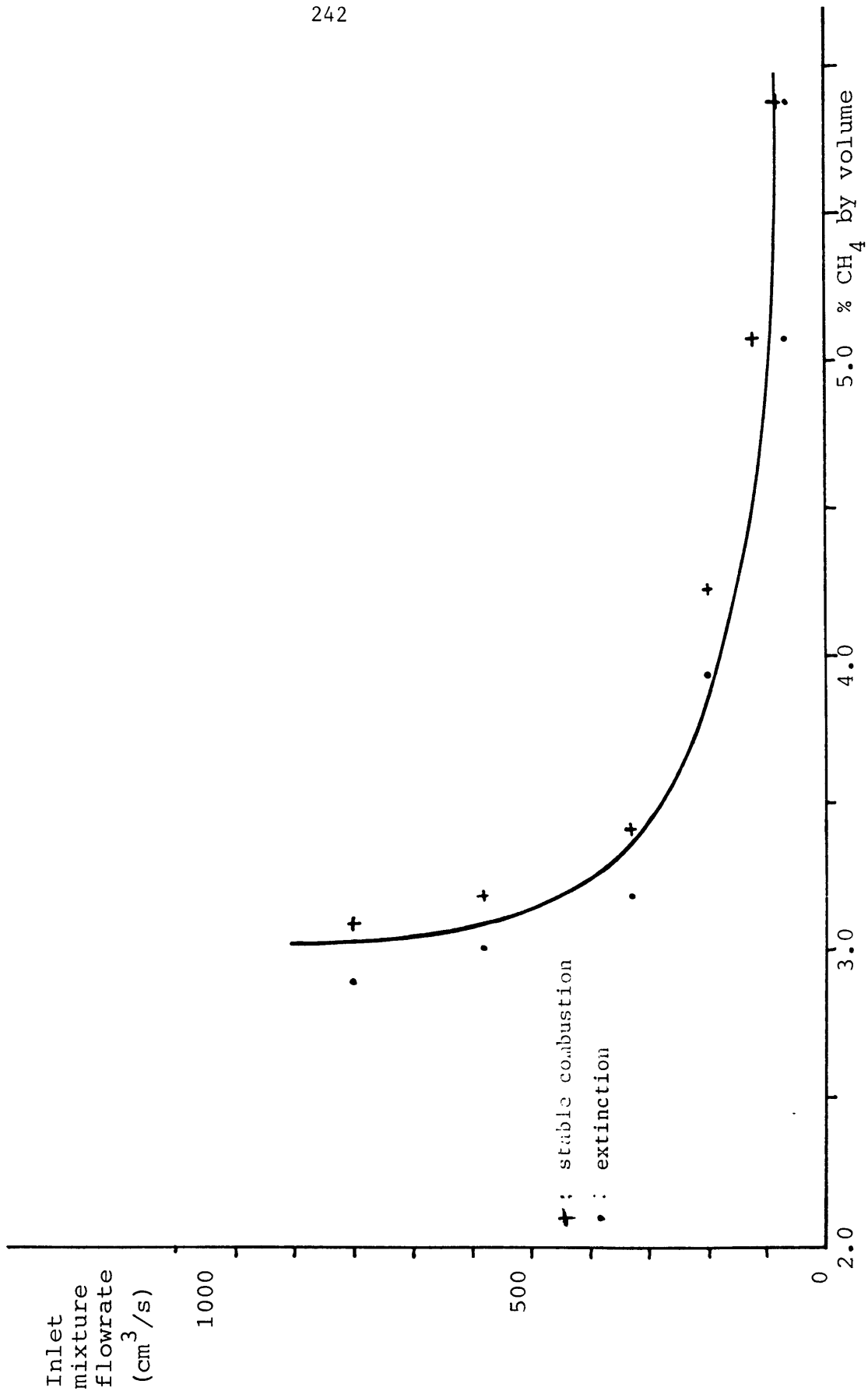


Figure (6.9): Flame stability characteristics for the ceramic matrix system and 60 mm diameter hemispherical combustion chamber

0.6 revs/min matrix rotational speed

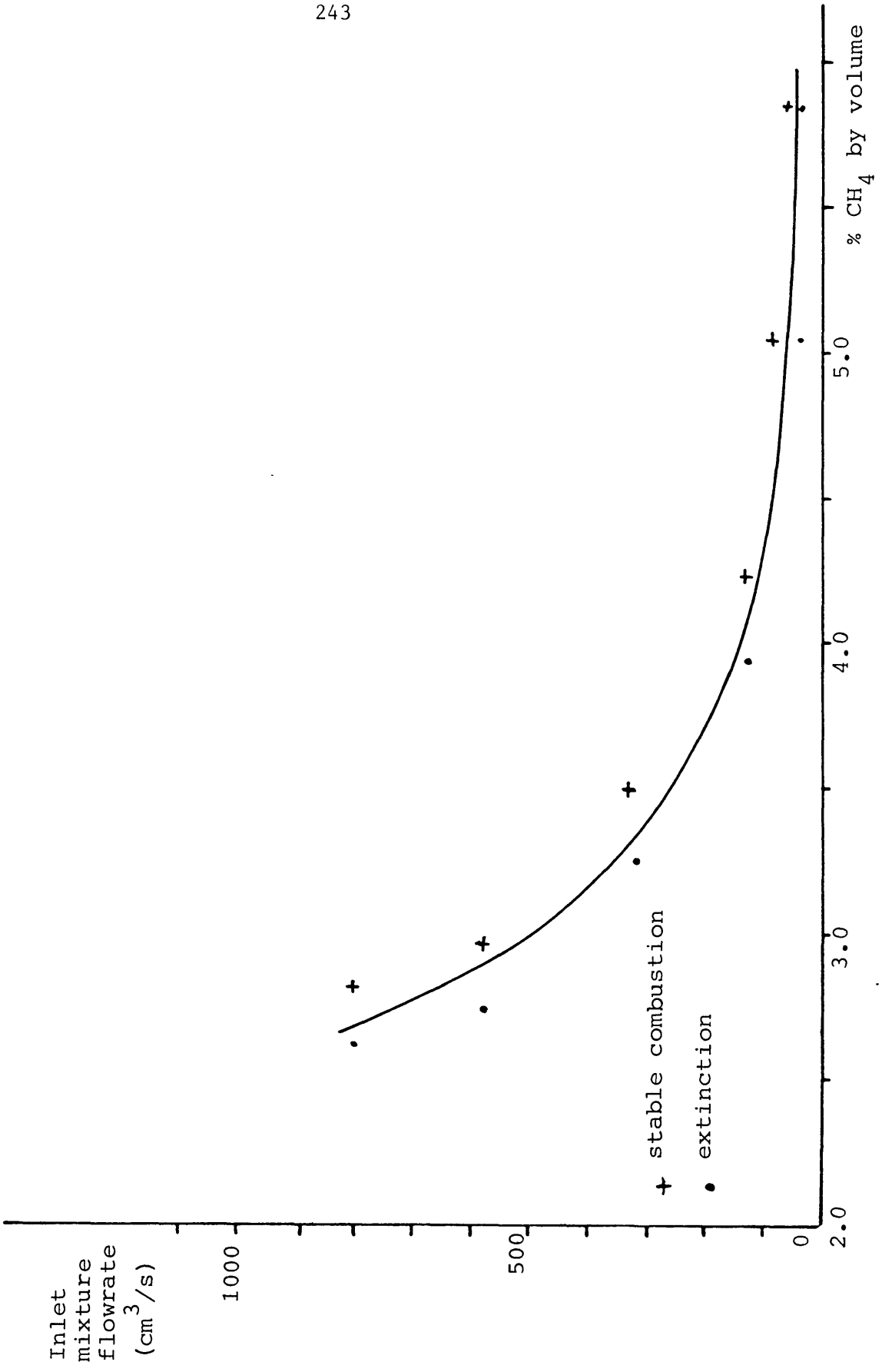


Figure (6.10): Stability characteristics for ceramic matrix systems and 60 mm diameter hemispherical combustion chamber
1.2 revs/min matrix rotational speed

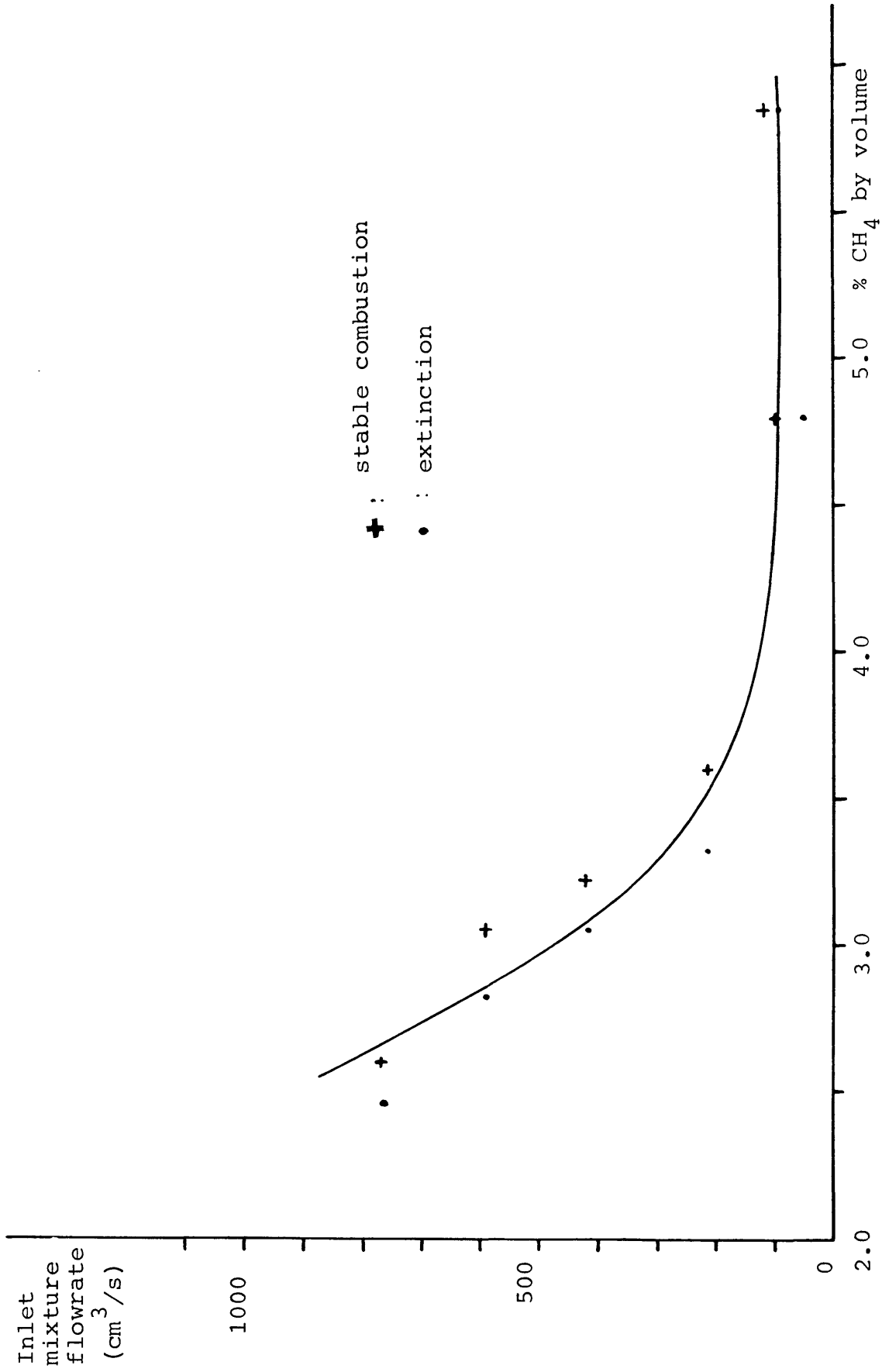


Figure (6.11): Stability characteristics for ceramic matrix system and 60 mm diameter hemispherical combustion chamber
2.4 revs/min matrix rotational speed

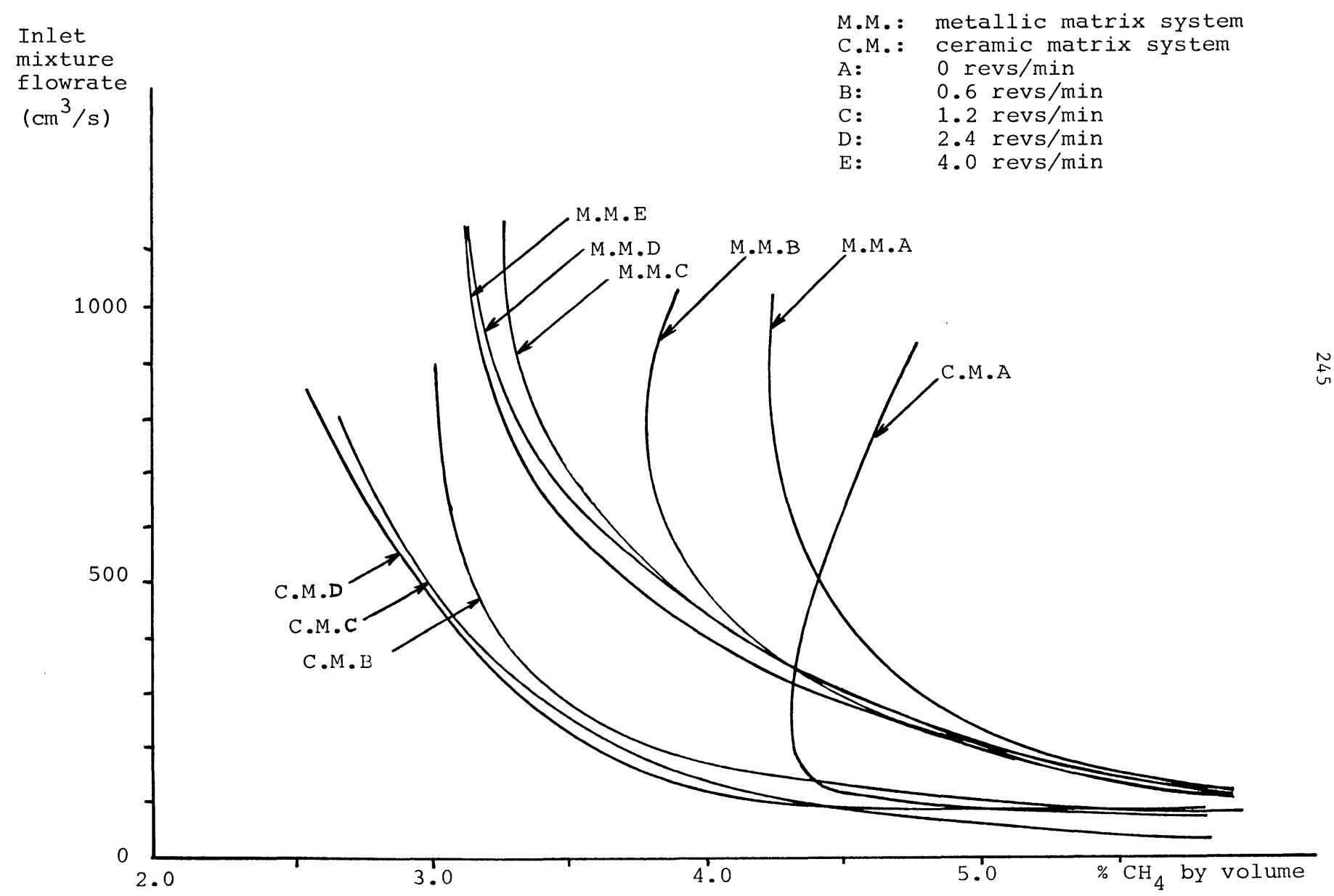


Figure (6.12): Effect of matrix material and geometric configuration on the stability characteristics.

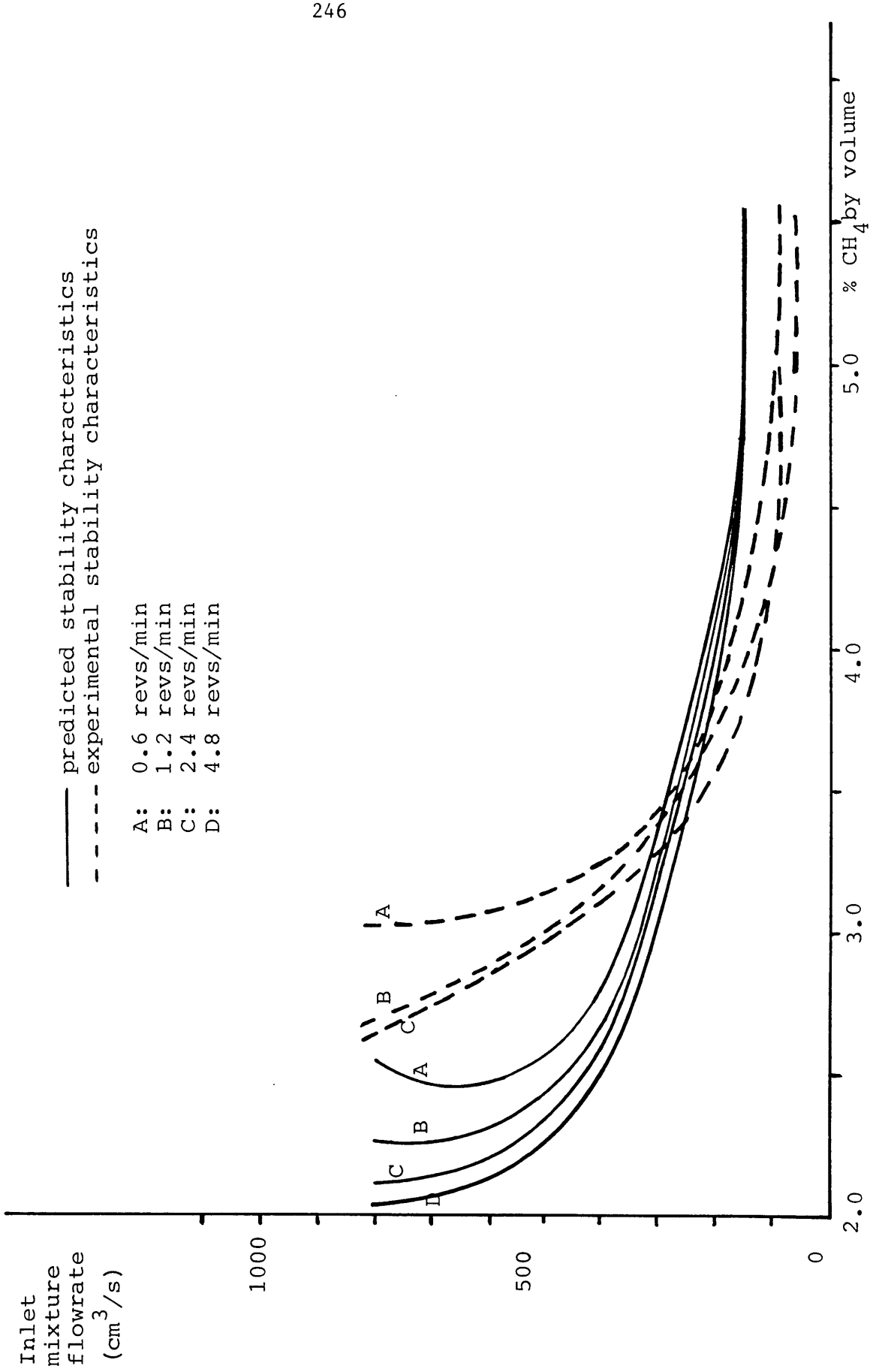


Figure (6.13): Predicted and experimental stability characteristic for the ceramic matrix system with the 60 mm hemispherical combustion chamber.

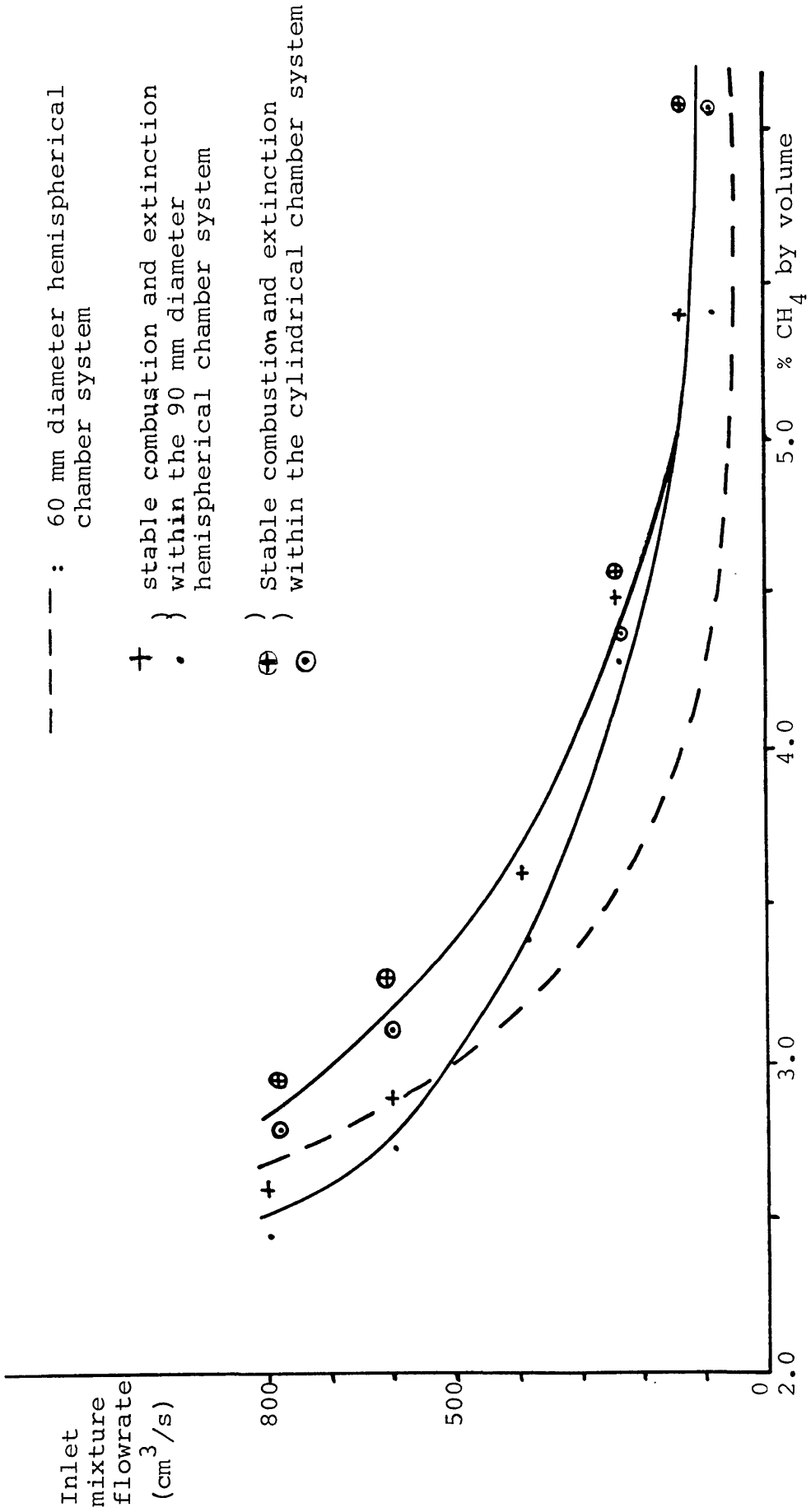


Figure (6.14): Effect of combustion chamber size and geometric configuration on the ceramic matrix system stability characteristics (1.2 revs/min case).

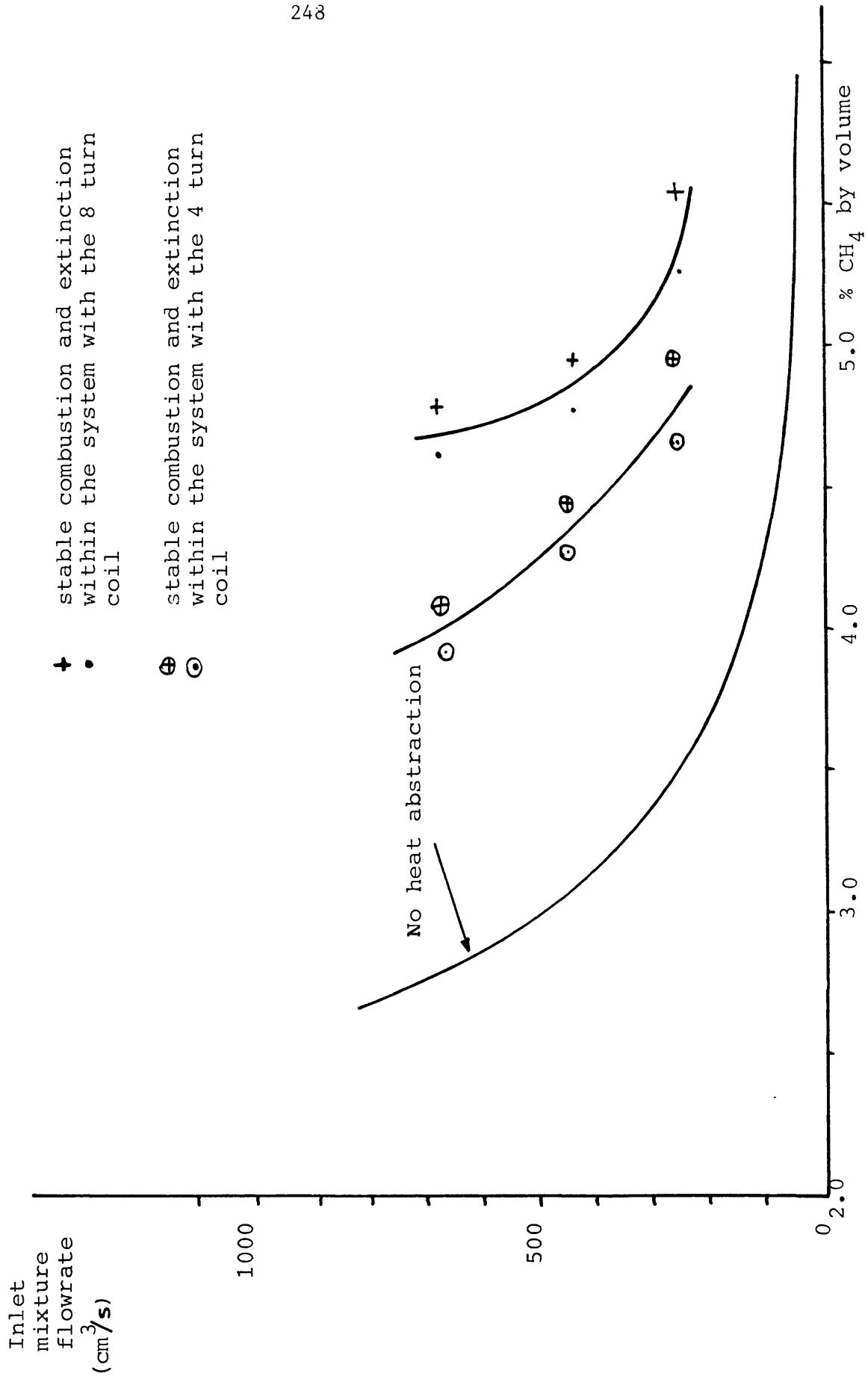


Figure (6.15): Effect of heat abstraction on the stability characteristics of the ceramic matrix, 60 mm diameter hemispherical combustion chamber, system (1.2 revs/min).

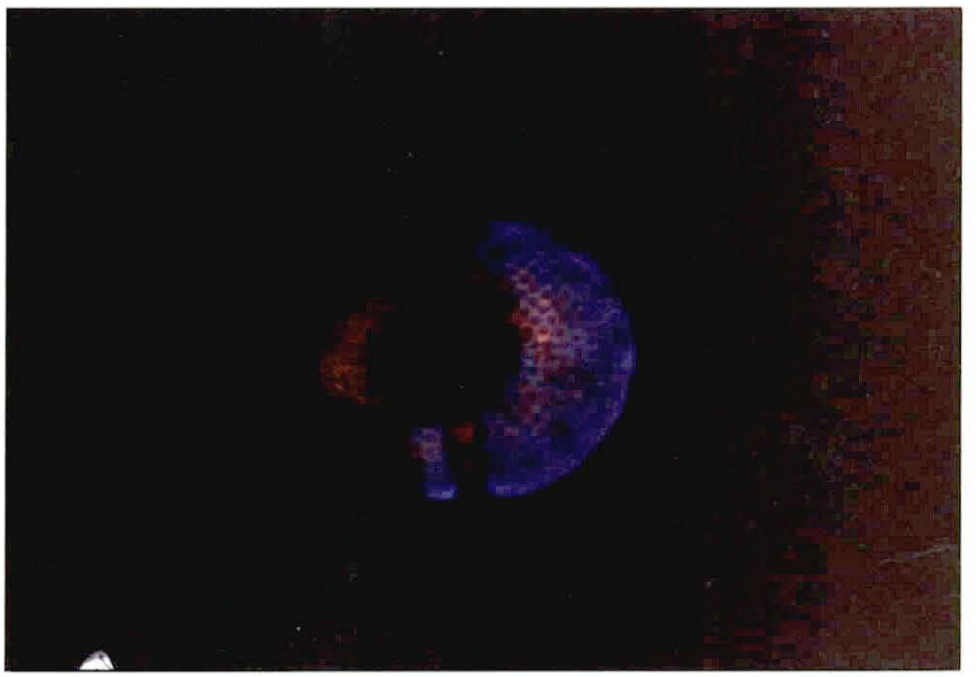


Figure (6.16): Flame for inlet flowrate of 168 cm^3/s and non-limiting mixture.



Figure (6.17): Flame for inlet flowrate of 81 cm^3/s and limiting mixture.

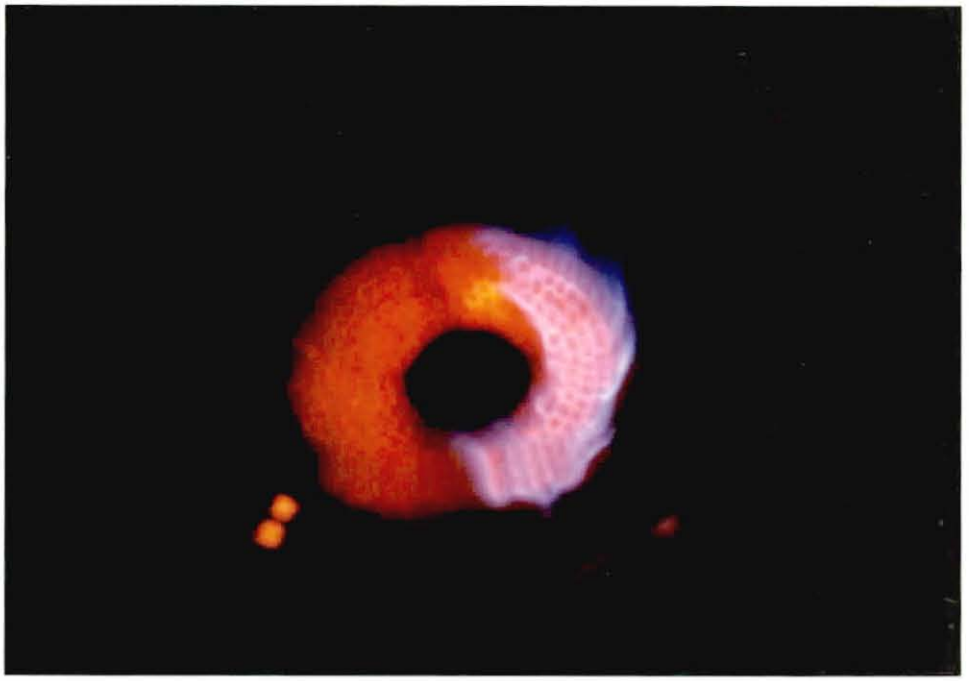


Figure (6.18): Flame for inlet flowrate of 384 cm^3/s and non-limiting mixture

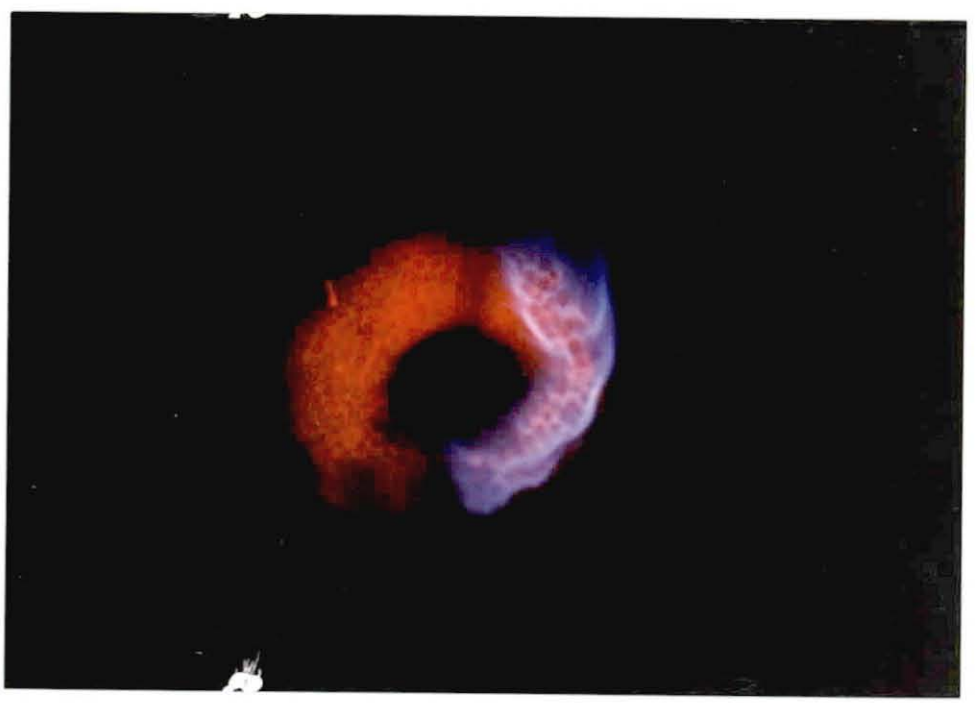


Figure (6.19): Flame for inlet flowrate of 384 cm^3/s and mixture composition approaching the limiting



Figure (6.20): Flame for inlet flowrate of 384 cm^3/s and limiting mixture

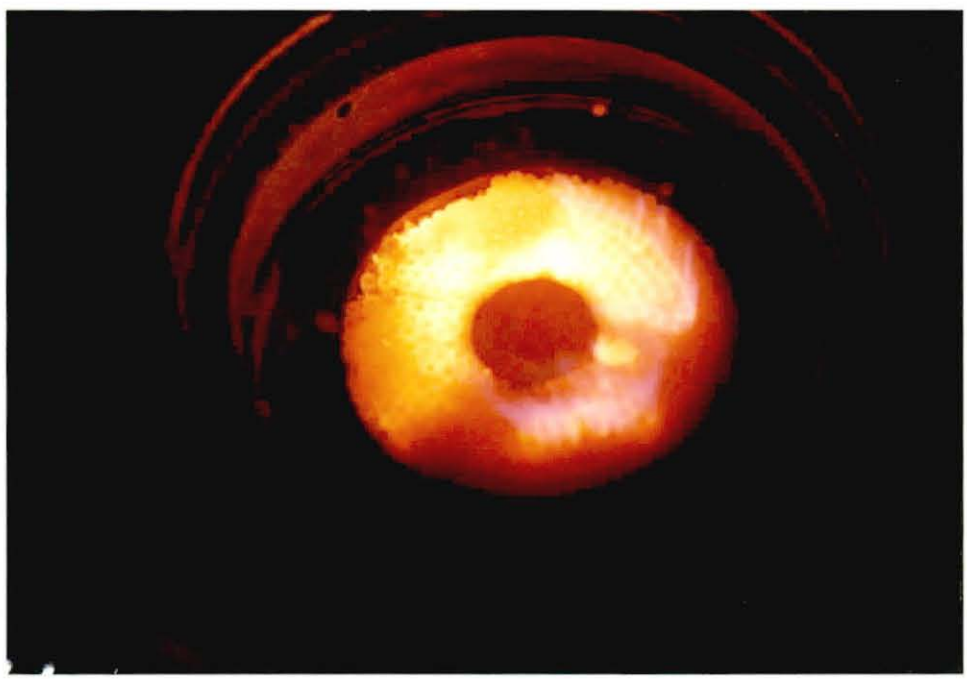


Figure (6.21): Flame for inlet flowrate of 790 cm^3/s and non-limiting mixture

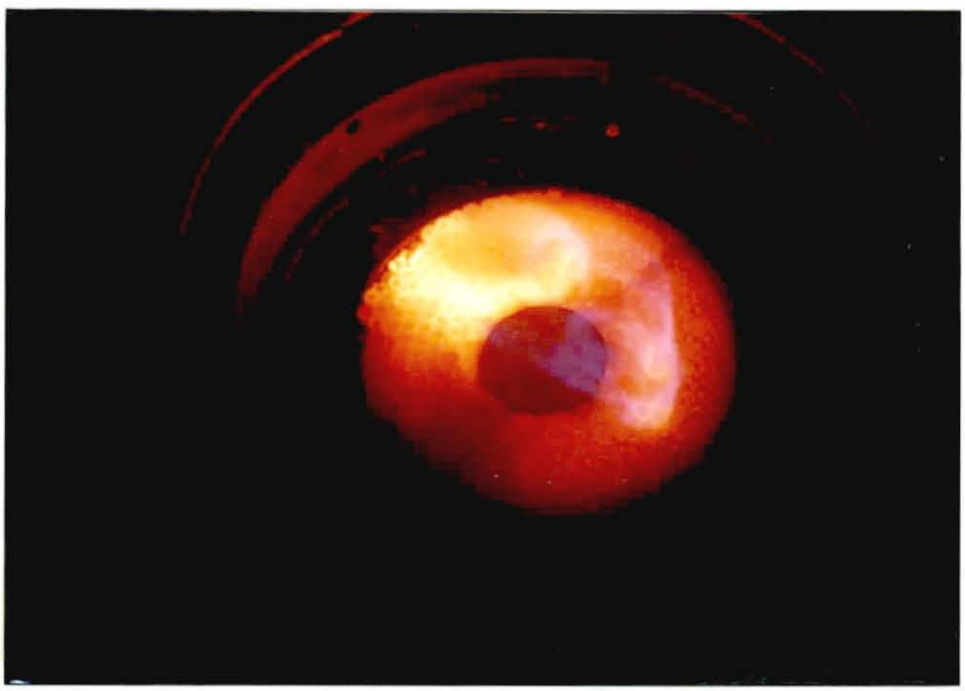


Figure (6.22): Flame for inlet flowrate of 790 cm^3/s and limiting mixture

Chapter 7

Summary and conclusions

Combustion in fuel-air mixtures of composition below that of their lower flammability limit cannot normally be sustained due to the adverse effect of the diluent heat capacity on the reaction temperature and consequently, the reaction rate. If the prereaction temperature of the reactants is, however, increased, by heat recirculated from the hot reaction products, stable unaided combustion in such mixtures can be achieved.

A common method of recycling heat from the products to the reactants is by direct mixing of products with reactants. In the process, however, the reactants are diluted by the products, and the effect of increasing the temperature on the reaction rate is partly counteracted by the reduction in the fuel concentration; the leaness of the mixtures combustible is, therefore, limited.

To effect combustion in very lean gaseous fuel-air mixtures, which was the purpose in the present research effort, heat recirculation must proceed between products and reactants that are kept separate. Combustion must, therefore, take place within a burner that incorporates a heat exchanger. Several such systems have so far been investigated and have been shown to be able to sustain combustion in lean mixtures and at appreciable inlet mixture flowrates. The majority of these, however, were at the laboratory scale and considerable effort and investment would be necessary for the development of durable industrial units

operating on the same principles. Because of this, a burner incorporating a heat exchanger of proven design was evaluated in the course of this research programme. In the present experimental burner, the heat exchanger was a disk rotary regenerator.

In disk rotary regenerators heat is transferred by storage in and recovery from, a porous matrix which is rotated about its vertical axis across the flow paths of the hot and cold streams flowing in a counter-current mode. The rotary regenerator burner basically comprised a rotary regenerator with the upper ducting replaced by a structure containing a cavity that served as the combustion chamber.

The following conclusions have been derived from this project:

1. A design study has been undertaken and a prototype unit constructed. Two matrices of different geometric configuration and materials of construction (i.e. a metallic flame trap matrix and a ceramic tubular matrix) have been built and tested with the system. Both matrices withstood well the high temperatures and the thermal stresses they were subjected to during the combustion experiments. Three combustion chambers have been tested, i.e. two hemispherical chambers of 60 mm and 90 mm i.d. and one cylindrical chamber 60 mm in diameter and 15 mm in height.
2. During the commissioning of the burner several modifications in the mechanical design were found necessary. The problems encountered were mainly due to excessive wear of the rubbing surfaces between the rotor and the stationary header system,

and inadequate clearances for differential thermal expansion of the parts of the system reaching different temperatures during operation. Use of Phosphor bronze for the rubbing surfaces throughout the system, increased clearances and a lighter combustion chamber structure resulted in a unit that could be operated continuously for at least 9 hours.

3. The gas leakage rates across the upper end lower circumferential seals of the metallic matrix system to the environment were measured during both cold and hot operation. The leakages during hot operation were found to be only slightly higher than those during cold operation and in both cases the percentage of the inlet flow escaping to the atmosphere decreased with increasing inlet flowrate (27% at 100 cm^3/s and 15% at 800 cm^3/s). For the ceramic matrix system the leakage rates to the environment were lower and were measured during cold operation to be in the range from 24% to 10% for inlet flowrates from 100 cm^3/s to 800 cm^3/s. Bypass leakages across the radial seal from the inlet to the exit section of the system could only be determined during cold operation, but, as in the case of the leakages to the environment, they must have been only slightly higher during hot operation. Again they were higher in the metallic matrix system (45% to 20% as opposed to 22% to 9% for inlet flowrates in the range from 100 cm^3/s to 800 cm^3/s) and the percentage of the inlet gas bypassing the matrix decreased with increasing inlet flowrate.

4. A mathematical model, describing the interdependent combustion and heat transfer processes within the ceramic

matrix - hemispherical combustion chamber system, was developed for prediction of the system flame stability characteristics. The combustion process was modelled in terms of the constant limiting final flame temperature (1400 K for methane) theory that was experimentally found to apply to heat recirculating burners in which flow velocities within the combustion chamber are low. The heat exchange process within the rotating matrix was modelled by assuming the matrix to be composed of a number of elements that can be considered as cross-flow exchangers with a "metal" and a gas stream. The convective coefficients for heat transfer from the combustion gases to the chamber walls were assumed to be similar to those within a curved pipe.

5. The flame stability characteristics for both the metallic and ceramic matrix, 60 mm i.d. hemispherical combustion chamber, systems have been obtained over a range of inlet methane - air mixture flowrates and for a number of matrix rotational speeds. Stable unaided combustion of methane - air mixtures of composition below that of their normal lower flammability limit (5.3% of CH_4 in air by volume) has proved possible within both systems. Flame blow-off due to excessive inlet flowrate was never observed, even at the highest inlet flowrates investigated. The stability curves obtained were of the shape (i.e."L" shaped) predicted by the constant limiting, final flame temperature theory, indicating that at low inlet flowrates heat losses were contolling, and at high inlet flowrates heat recirculation was controlling. The ceramic matrix system was generally found to be more

efficient than the metallic matrix one. Combustion in mixtures as lean as 2.6% of CH_4 in air by volume at inlet flowrates of 800 cm^3/s was achieved in the ceramic matrix system as opposed to 3.3% in the metallic matrix system. With the matrix stationary, however, leaner mixtures were burnt in the metallic matrix system due to the larger thermal conductivity of the matrix metallic walls.

6. The thermal efficiency of both systems was found to increase with increasing matrix rotational speed, but only up to a certain value. Above this limiting speed the efficiency remained constant (for the metallic matrix system between 1.2 revs/min and 2.4 revs/min, and for the ceramic matrix system between 0.6 revs/min and 1.2 revs/min).

7. The thermal efficiency of the ceramic matrix system was also shown, for high inlet flowrates, to increase with increasing combustion chamber volume. For low inlet flowrates, however, the large hemispherical chamber (90 mm i.d.) and the cylindrical chamber systems (of the smallest volume) were found to require the same limit mixture flowrates for stable combustion while the smaller hemispherical chamber system (60 mm i.d.) required smaller flowrates. The observed trend for high inlet flowrates was attributed to the reactants residence time and, therefore, combustion efficiency increasing with the combustion chamber volume. For low inlet flowrates, since heat losses were controlling, the observed behaviour was attributed to the dependence of the rates of convective heat transfer from the combustion gases to the chamber walls, both on the walls surface area (increasing

with increasing chamber volume) and the convective coefficient (decreasing with increasing chamber volume).

8. The stability characteristics for the ceramic matrix burner predicted by the theoretical model were found to be in reasonable agreement with those determined by experiment. The system performance predicted by the model was, however, (a) better than the actual for high inlet flowrates by about 20% and (b) worse than the actual for low inlet flowrates by about 50%. Both heat recirculation and heat losses are, therefore, overestimated by the model.

9. Combustion in lean mixtures was also attempted with simultaneous heat abstraction from the combustion chamber gases. Heat was removed by means of water flowing through a copper coil. The heat abstraction rate could only be varied by varying the coil outside heat transfer surface area (overall coefficient for heat transfer to the coil was controlling). With two heat abstraction rates, of 31% and 39% of the heat input to the system, combustion in mixtures of concentrations below or just above the normal lower flammability limit proved possible with the ceramic matrix, 60 mm diameter hemispherical chamber system.

10. Analysis of the combustion chamber and exhaust gases from the system showed that the conditions within the chamber were far from uniform, and that complete combustion, when the conditions were limiting, was never achieved. For stable combustion, however, with mixtures of inlet flowrate and composition not corresponding to the limiting value, complete combustion was always found to occur in the part of the

chamber above the marix inlet section, on the side of the "hot-cold" interface, where the reactants emerged with the highest preheat temperatures. This, together with the combustion chamber gas temperature trends recorded by the bare thermocouples, indicated that the flame in this part of the chamber was the most stable and acted as a "pilot" for the remaining reactants. A maximum temperature was always recorded above the matrix inlet section and on the side of the "hot-cold" interface, due to the reactants emerging from the matrix passages with preheat temperatures decreasing with increasing angular displacement from the "hot-cold" interface.

11. The recorded combustion chamber gas temperatures also indicated that for limiting conditions (a) at low inlet flowrates, the flame was stabilized over the matrix inlet section and was quite thin, and (b) at high inlet flowrates, the flame was diffused through the part of the chamber in the proximity of the "hot-cold" interface. These conditions were verified by the photographic evidence obtained during combustion experiments in the hemispherical and cylindrical combustion chambers of transparent quartz walls.

12. Accurate measurement, finally, of the gas temperatures within the combustion chamber indicated that the flame temperature, in the region of the chamber where the reactants emerged with the highest preheat temperatures, was close to the constant limiting final flame temperature, but increased slowly with increasing inlet flowrate (from 1400 K at ~100 cm^3/s up to ~1490 K at 800 cm^3/s). Stability within the regenerative

burner was not, therefore, just governed, as in the case of the "Swiss roll" burner, by criteria similar to those that apply to the flammability limits in quiescent mixtures. Since the reactants emerge from the matrix passages with temperatures that decrease with increasing distance from the "hot-cold" interface, at the limit, the temperature of the most stable part of the flame must be higher than the equivalent one in the "Swiss roll" burner, in order to be able to sustain combustion in some of the colder reactants. Since the distribution of preheat temperatures is expected to increase with increasing inlet flowrates the necessary temperature for the "pilot" part of flame must also increase with increasing flowrate.

In summary, the project has successfully demonstrated the concept of burning gaseous fuel - air mixtures, both with and without heat abstraction, at concentrations leaner than the normal lower flammability limit, using a heat recirculating burner incorporating a rotary regenerator. Furthermore, a detailed characterisation of the combustion performance of the novel burner system has been provided.

Appendix A

Calculation of the matrix rotational speed for the required effectiveness ϵ and estimation of the stability characteristics of the experimental metallic matrix

Calculation of the matrix rotational speed for achieving the required effectiveness ϵ

Calculation of the speed, ω, requires 5 stages, as follows.

(a) Calculation of gas temperatures at inlets and outlets of the matrix for a given effectiveness ϵ

The temperature of the cold mixture at the inlet to the matrix, $T_{gc\ in}$, is always constant and equal to the ambient temperature, taken here as $20^{o}C$. A constant limiting final flame temperature of $1127^{o}C$ is assumed for the combustion chamber. It is further assumed that 10% of the heat content of the hot product gases is lost to the environment. The temperature of the hot products at the inlet to the matrix, $T_{gh\ in}$, can, therefore, be calculated from the following:

$$0.1\ c_{px}(1127 - 0) = c_{py}(1127 - T_{gh\ in}) \qquad (A\text{-}1)$$

where c_{px} and c_{py} are the gas specific heats evaluated at the arithmetic mean temperatures.

$$T_x = \frac{1127 + 0}{2} \text{ and } T_y = \frac{1127 + T_{gh\ in}}{2}$$

From eqn. (A-1) and taking c_{px} = 1110 J/kg K, $T_{gh\ in}$ = 1023°C. For the required cold gas side effectiveness ϵ to be achieved, the temperature of the preheated mixture emerging from the matrix must, therefore, be as evaluated from the following relationship for the effectiveness.

$$\epsilon = \frac{T_{gc\ out} - T_{gc\ in}}{T_{gh\ in} - T_{gc\ in}} \qquad \text{(A-2)}$$

In the case of ϵ = 0.90, $T_{gc\ out}$ = 923°C.

Similarly for ϵ = 0.8 $T_{gc\ out}$ = 822°C

ϵ = 0.7 $T_{gc\ out}$ = 722°C

ϵ = 0.6 $T_{gc\ out}$ = 622°C

ϵ = 0.5 $T_{gc\ out}$ = 501°C

ϵ = 0.4 $T_{gc\ out}$ = 401°C

(b) Gas physical properties

The gas physical properties, necessary for the calculation of the rotor speed are

(a) gas viscosity, μ_g

(b) gas thermal conductivity, k_g

(c) gas specific heat, c_{pg}

(d) gas density, ρ_g

The viscosity, thermal conductivity and specific heat are evaluated at a temperature which is 60% of the way between the average matrix wall temperature and the arithmetic average gas temperature. The average wall temperature is taken to be the

arithmetic average cold and hot gas temperature,

i.e.

$$T_{s\ Av} = \frac{T_{gh\ Av} + T_{gc\ Av}}{2}$$

For an effectiveness of 90%:

$$T_{gh\ Av} = 580^{o}C$$

$$T_{gc\ Av} = 471^{o}C$$

Therefore $$T_{s\ Av} = 526^{o}C$$

The physical properties are therefore evaluated at the temperatures given by:

For the cold side $526 - 0.6(526 - 471) = 493$ (A-3)

For hot side $526 - 0.6(526 - 580) = 558$ (A-4)

The gas density is evaluated at the arithmetic mean temperature.

Since the fuel-air mixtures considered only contain small quantities of fuel the physical properties used throughout are those of pure air (mostly from references 3.1 and 3.2).

Property	Cold side	Hot side
ρ_g (Kg/m^3)	0.474	0.414
c_{pg} (J/Kg K)	1089	1104
μ_g x 10^5 (Kg/m s)	3.53	3.71
k_g (W/m K)	55.9	59.3
Pr	0.687	0.691

where P_r is the Prandtl number.

The physical properties for other regenerator effectivenesses can be similarly evaluated.

(c) Calculation of the physical characteristics of the flame trap matrix

Flame trap matrices can be constructed by winding a plane and a corrugated strip round a central core. For the matrices considered here, the diameter of the core is 19 mm and the dimensions of the plane and corrugated strips are included in figure (3.6). It can be shown that, in terms of the number of turns, n, the required lengths for the plane, l_{pl}, and corrugated, l_{cr}, strips are given by

$$l_{pl} = \frac{\pi}{2}\left[38n + 0.51(1 + 2n)n\right] \times 10^{-3} \qquad \text{(A-5)}$$

$$l_{cr} = \frac{\pi}{2}\left[19(2n - 1) + 0.51(2n - 1)n\right]\frac{2 \times 0.786}{1.31} \times 10^{-3} \qquad \text{(A-6)}$$

where n: Number of turns round the central core

and 0.786 mm = length of the side of the equilateral triangle

1.31 mm = length at the base of the triangle.

The total length of metal strip used, l, is, therefore, given by

$$l = l_{pl} + l_{cr} \qquad \text{(A-7)}$$

The matrix total frontal area, $2A_f$, is given by

$$2A_f = \frac{\pi}{4}\left[(19 + 2(0.51n))^2 - (19)^2\right] \times 10^{-6} \qquad \text{(A-8)}$$

The matrix total occupied frontal area, $2A_{foc}$, is given by

$$2A_{foc} = 2A_f - 1 \times 0.05 \times 10^{-3} \qquad \text{(A-9)}$$

The matrix total free frontal area, $2A_{ffr}$, is given by

$$2A_{ffr} = 2A_f - 2A_{foc} \qquad \text{(A-10)}$$

The heat transfer areas for the cold, A_c, and hot, A_h, sides of the matrix are equal and are given by

$$A_c = A_h = \frac{1 \times 76.2 \times 10^{-3}}{2} \qquad \text{(A-11)}$$

where 76.2×10^{-3} m = width of strips.

The number of passages available for gas flow on the hot, N_h, and cold, N_c, sides of the matrix are equal and are given by

$$N_h = N_c = \frac{2A_{ffr}}{2 \times 0.27 \times 10^{-6}} \qquad \text{(A-12)}$$

where 0.27×10^{-6} m^2 = free frontal area of each triangular passage.

TABLE (A.1)

No. of turns	5	10	20	25	26	30	36	40	55	80	100	150
Length of plane strip (m)	0.343	0.765	1.851	2.514	2.656	3.257	4.254	4.983	8.174	15.093	22.071	45.123
Length of corrugated strip (m)	0.366	0.863	2.147	2.932	3.101	3.815	4.491	5.270	9.667	17.922	26.257	54.824
Total length of strip (m)	0.709	1.628	3.998	5.446	5.757	7.072	8.745	10.253	17.841	33.015	48.328	99.947
Frontal area ($\times 10^4$ m^2)	1.726	3.861	9.357	12.72	13.44	16.49	21.55	25.25	41.46	76.65	121.1	229.0
Occupied area ($\times 10^5$ m^2)	3.54	8.14	2.00	2.72	2.88	3.54	4.37	5.13	8.92	16.51	24.16	500
Free area ($\times 10^4$ m^2)	1.37	3.05	7.36	10.00	10.6	12.9	17.2	20.1	32.5	60.1	87.98	179

Table A.1 (continued)

No. of turns	5	10	20	25	26	30	36	40	55	80	100	150
No. of passages	510	1,438	3,485	3,723	3,933	4,823	6,398	7,493	12,119	22,398	32,767	66,667
Heat transfer area ($\times 2^{-1} m^2$)	0.054	0.124	0.300	0.415	0.439	0.539	0.666	0.781	1.36	2.52	3.68	7.62
Mass of matrix (kg)	0.021	0.048	0.119	0.162	0.171	0.211	0.260	0.305	0.531	0.983	1.439	2.980
Outside matrix diamter (m)	0.024	0.029	0.039	0.045	0.045	0.050	0.056	0.060	0.075	0.101	0.121	0.172
Outside matrix surface area ($\times 10^5 m^2$)	-	-	0.94	1.08	1.09	1.20	1.34	1.44	1.79	2.42	2.90	4.12

The mass of the matrix , m_s, is given by

$$m_s = 1 \times 2A_{foc} \times 76.2 \times 10^{-3} \times 7817 \qquad \text{(A-13)}$$

where 7817 Kg/m^3 = density of stainless steel 316.

Finally, the outside diameter of the matrix, d, is given by

$$d = 19 + 2(0.51n) \qquad \text{(A-14)}$$

The values for the above were evaluated for matrices in the range from 5 to 150 turns and are given in table (A.1)

(d) Calculation of required rotor speeds

The rotor speed, ω, in revs/min can be calculated from the solid capacity rate, C_s, which is given by

$$C_s = m_s \frac{\omega}{60} c_{ps} \quad (c_{ps} = 501 \text{ J/Kg K}) \qquad \text{(A-15)}$$

C_s for a given matrix gas flowrate and required effectiveness can be calculated from

$$\epsilon = \left[\frac{NTU_o}{\frac{1}{2}\left[1 + \frac{C_{gc}}{C_{gh}}\right]NTU_o + 1}\right]\left[1 - \frac{1}{\left[\frac{C_s}{C_{gc}}\right]^2}\right]$$

where $$NTU_o = \frac{(hA)_c}{C_{gc}}\left[\frac{1}{1 + \left[\frac{(hA)_c}{(hA)_h}\right]}\right]$$

The gas heat capacity rates, C_{gc}, C_{gh} are given by

$$C_{gc} = M_{gc}\ c_{pgc} \tag{A-16}$$

$$C_{gh} = M_{gh}\ c_{pgh} \tag{A-17}$$

The heat transfer coefficients can be calculated from

$$St = \frac{0.205}{Re^{0.55}} \tag{A-18}$$

for $50 < Re < 200$

and

$$St = 0.0224 \tag{A-19}$$

for $Re < 50$.

The Stanton number, St, is given by

$$St = \frac{Nu}{Re\ Pr}$$

where Nu: Nusselt no. $= \frac{h\ de}{k_g}$

and de: equivalent diameter of matrix passages $= 3.78 \times 10^{-4}$m

Therefore, $$h = \frac{St\ Re\ Pr\ k_g}{Re\ Pr} \tag{A-20}$$

The Reynold's number is calculated from

$$Re = \frac{M_g\ de}{0.27 \times 10^{-6}\ \mu_g N} \tag{A-21}$$

TABLE (A.2)

(values in parentheses are for 200 cm^3/s)

No. of turns	5	10	20	25	26	30	36	40	55	80	100	150
Re_c	149.8 (37.5)	53.1 (13.3)	21.9 (5.5)	20.5 (5.1)	19.4 (4.9)	15.8 (4.0)	11.9 (3.0)	10.2 (2.6)	6.3 (1.6)	3.4 (0.9)	2.3 (0.6)	1.2 (0.3)
Re_h	142.3 (35.6)	50.5 (12.6)	20.8 (5.2)	19.5 (4.9)	18.5 (4.6)	15.0 (3.8)	11.3 (2.8)	9.7 (2.4)	6.0 (1.5)	3.2 (0.8)	2.2 (0.5)	1.1 (0.3)
Nst_c	0.013 (0.024)	0.023 (0.024)	0.024 (0.024)	0.024 (0.024)	0.024 (0.024)	0.024 (0.024)	0.024 (0.024)	0.024 (0.024)	0.024 (0.024)	0.024 (0.024)	0.024 (0.024	0.024 (0.024)
Nst_h	0.013 (0.024)	0.024 (0.024)	0.024 (0.024)	0.024 (0.024)	0.024 (0.024)	0.024 (0.024)	0.024 (0.024)	0.024 (0.024)	0.024 (0.024)	0.024 (0.024)	0.024 (0.024	0.024 (0.024)
h_c (J/s m^2 K)	198.6 (91.7)	125.1 (32.5)	53.6 (13.4)	50.2 (12.5)	47.5 (11.9)	38.7 (9.7)	29.2 (7.3)	24.9 (6.3)	15.4 (3.8)	8.4 (2.1)	5.7 (1.4)	2.9 (0.7)

Table A.2 (continued)

No. of turns	5	10	20	25	26	30	36	40	55	80	100	150
h_h	207.4	130.1	54.4	50.9	48.2	39.3	29.6	25.3	15.6	8.4	5.8	2.9
(J/sm^2 K)	(92.9)	(32.9)	(13.6)	(12.7)	(12.0)	(9.8)	(7.4)	(6.3)	(3.9)	(2.11)	(1.44)	(0.8)
NTU_o	5.16	7.47	7.76	10.03	10.05	10.07	9.37	9.35	10.09	10.12	10.10	10.65
	(5.16)	(7.47)	(7.76)	(10.03)	(10.05)	(10.07)	(9.37)	(9.35)	(10.09)	(10.12)	(10.10)	(10.65)
C_r	-	-	-	2.72	2.71	2.70	3.48	3.51	2.68	2.66	2.67	2.40
(J/K)	(-)	(-)	(-)	(0.68)	(0.68)	(0.67)	(0.87)	(0.88)	(0.67)	(0.66)	(0.67)	(0.6)
W	-	-	-	2.01	1.90	1.53	1.60	1.38	0.60	0.32	0.22	0.1
(revs/min)	(-)	(-)	(-)	(0.50)	(0.47)	(0.38)	(0.40)	(0.34)	(0.15)	(0.08)	(0.05)	(0.02)

Table (A.3)

Turns	40	40	40	40	40	40	40
ϵ	0.95	0.80	0.70	0.60	0.50	0.40	0.90
Re_c	10.08	10.19	10.72	11.02	11.42	11.77	
Re_h	9.83	9.44	9.23	9.05	8.84	8.67	
h_c (J/s m^2 K)	25.03	24.96	24.62	24.47	24.30	24.08	
h_h (J/s m^2 K)	25.21	25.33	25.67	25.83	25.99	26.15	see
C_c (J/K)	1.048	1.045	1.044	1.026	1.019	1.014	
C_h (J/K)	1.056	1.069	1.075	1.082	1.090	1.095	previous
NTU_o	9.36	9.39	9.41	9.56	9.63	9.66	
C_r (J/K)	-	0.99	0.72	0.58	0.46	0.41	tables
ω (Revs/min)	-	0.39	0.28	0.23	0.18	0.16	
f (%)	-	1.44	1.92	2.35	2.92	3.37	1.00

The rotor speeds were evaluated for 90% effectiveness, mass flowrates of 9.6×10^{-4} Kg/s (800 cm^3/s) and 2.4×10^{-4} Kg/s (200 cm^3/s) and for a number of matrices in the range from 5 to 150 turns. The results are presented in Table (A.2).

Estimation of the stability characteristics of the 40 turn or 60 mm diameter matrix for a methane-air mixture flowrate of 800 cm^3/s and different regenerator effectivenesses

In estimating the stability characteristics of the burner it is assumed that the heat required for raising the temperature of the preheated mixture leaving the matrix, $T_{gc\ out}$, to the assumed constant limiting final temperature, 1400 K, is entirely supplied by the methane gas contained in the mixture. The percentage by volume methane content of the mixture, f, is given by:

$$f\ V_g\ q = M_g\ c_{pg}\ (1127 - T_{gc\ out})$$

Therefore
$$f = \frac{\rho_g\ c_{pg}}{q}\ (1127 - T_{gc\ out}) \qquad \text{(A-22)}$$

where ρ_g: gas density at inlet conditions (1.2 Kg/m^3)

c_{pg}: specific heat capacity of gas at $\frac{1127 + T_{gc\ out}}{2}$ (J/Kg K)

q: Methane heat of combustion per unit volume of fuel (= 32.5×10 J/m^3)

The results from the calculation for the 40 turn matrix and mixture flowrate of 800 cm^3/s (20^oC, 1 atm) are presented in

Table (A.3) for regenerator effectivenesses of 95%, 90%, 70%, 60%, 50% and 40%.

APPENDIX B

Calculation of torque and power necessary for rotation of the matrix at 10 revs/min

In order to determine the magnitude of the torque, M_r, required to maintain steady angular motion of the rotor, the friction torques opposing the motion due to slipping and, therefore friction between (a) the PTFE bearing and rotor cylindrical surfaces, M_{br}, and (b) the upper and lower stainless steel seals and the flat upper and lower rotor surfaces, M_{sr}, must be determined.

For steady rotational speeds the applied torque, M_T, must be in equilibrium with the friction torques. Therefore,

$$M_T = M_{br} + M_{sr} \qquad \text{(B-1)}$$

The power, P, necessary for the matrix to be rotated at a steady speed ω = 10 revs/min, can be calculated from

$$P = 2\pi\omega M_T \qquad \text{(B-2)}$$

(a) Calculation of bearing and rotor friction torque, M_{br}

When the burner is cold the internal diameter of the PTFE bearing is identical to the rotor outside diameter. During combustion experiments, however, due to the thermal expansion

coefficient of PTFE being greater than that of stainless steel, the PTFE bearing inside diameter is larger than that of the rotor. Figure (B.1a) shows a free body diagram of the rotor when at rest, i.e. with no forces acting on the rotor in the plane perpendicular to the rotor. The forces in the parallel plane (i.e. weight of upper part of burner on the rotor and reactions on the circumferential seals) are not shown. The radial clearance between rotor and bearing has been exaggerated in the figure.

If a small torque is applied tending to rotate the rotor, the rotor is forced against the bearing wall. If the torque is increased the rotor rolls against the bearing until the magnitude of the torque is such that equilibrium is reached and the friction between the surfaces is the limiting friction. If the torque is increased further, slipping occurs and the rotor moves back to a new eqiilibrium position as shown in figure (B.1b).

For steady angular motion the total reaction, F_R, which is equal to the vector sum of the frictional force, F_f, and the radial force, F_N, must be equal to the force, F_W, applied by the gear mounted on the motor. The angle ϕ_K, since the rotor is turning at a constant speed, is given by

$$\tan\phi = \mu \qquad \text{(B-3)}$$

where μ: coefficient of friction between PTFE and stainless steel in this case

The friction torque applied by F_f is, therefore, given by

$$M_{br} = F_f \frac{d}{2} = \sin\phi \; F_W \frac{d_{rotor}}{2}$$

$$= \frac{\sin(\tan^{-1}\mu) d_{rotor}}{d_{gear}} M_W \qquad \text{(B-4)}$$

since $\mu = 0.04$, $d_{rotor} = 103$ mm and $d_{gear} = 170$ mm

$$M_{br} = 0.024 M_T$$

(b) Calculation of friction torques between seals and rotor surfaces

The friction torque, M_{sr}, opposes the angular motion of the rotor due to the dry slipping contact between the rotor upper and lower surfaces and the upper and lower circumferential seals. M_{sr} is equal to the sum of the individual friction torques acting on the lower and upper surfaces of the rotor. The individual friction torques, with reference to figure (B.2) and assuming that the load is evenly distributed over the area of contact, are given by

$$M = \frac{\mu F_N}{\pi(R_2^2 - R_1^2)} \int_0^{2\pi} \int_{R_1}^{R_2} r^2 dr d\theta$$

or

$$M = \frac{2}{3}\mu F_N \left[\frac{R_2^3 - R_1^3}{R_2^2 - R_1^2}\right] \qquad \text{(B-5)}$$

For the upper rotor surface the normal force, F_N, is equal to the sum of the weights of the combustion chamber structure (the 60 mm diameter concrete walls chamber, i.e. the heaviest structure to be used is considered here) and the upper sealing ring,
i.e.

$$F_N = 11.03 \times 9.81 = 108N$$

Since the surfaces in contact are both of 316 stailess steel, $\mu = 0.5$, and since $R_1 = 50.5$ mm and $R_2 = 45.0$ mm for the upper part, from eqn. (B-5)

$$M = 3.0 \text{ Nm}$$

For the lower rotor surface the load, supported by the seal in this case, is equal to that supported by the upper rotor surface plus the weight of the rotor itself,
i.e.

$$F_N' = 15.41 \times 9.81 = 151N$$

The surfaces in contact are PTFE and stainless steel, $\mu = 0.04$, and $R_1' = 41.8$ mm and $R_2' = 38.2$ mm.
Therefore

$$M' = 0.2 \text{ Nm}$$

The frictional torque is therefore

$$M_{sr} = M + M' = 3.2 \text{ Nm}$$

From eqn. (B-1), the total friction torque acting on the rotor is given by

$$M_T = 3.2 + 0.024M$$

i.e. $$M_T = 3.3 \text{ Nm}$$

The power required for rotating the matrix at a constant speed of 10 revs/min is, therefore,

$$P = 2 \times \pi \times 3.3 \times \frac{10}{60} = 3.49 \text{ Watts.}$$

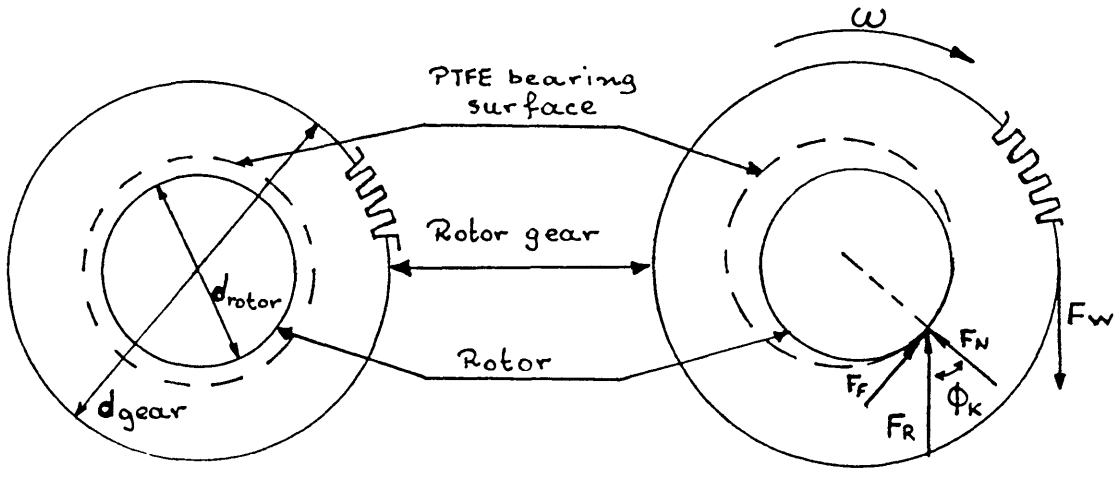


Figure (B.1): Forces acting on the rotor in the horizontal plane (forces in the vertical plane are not shown).

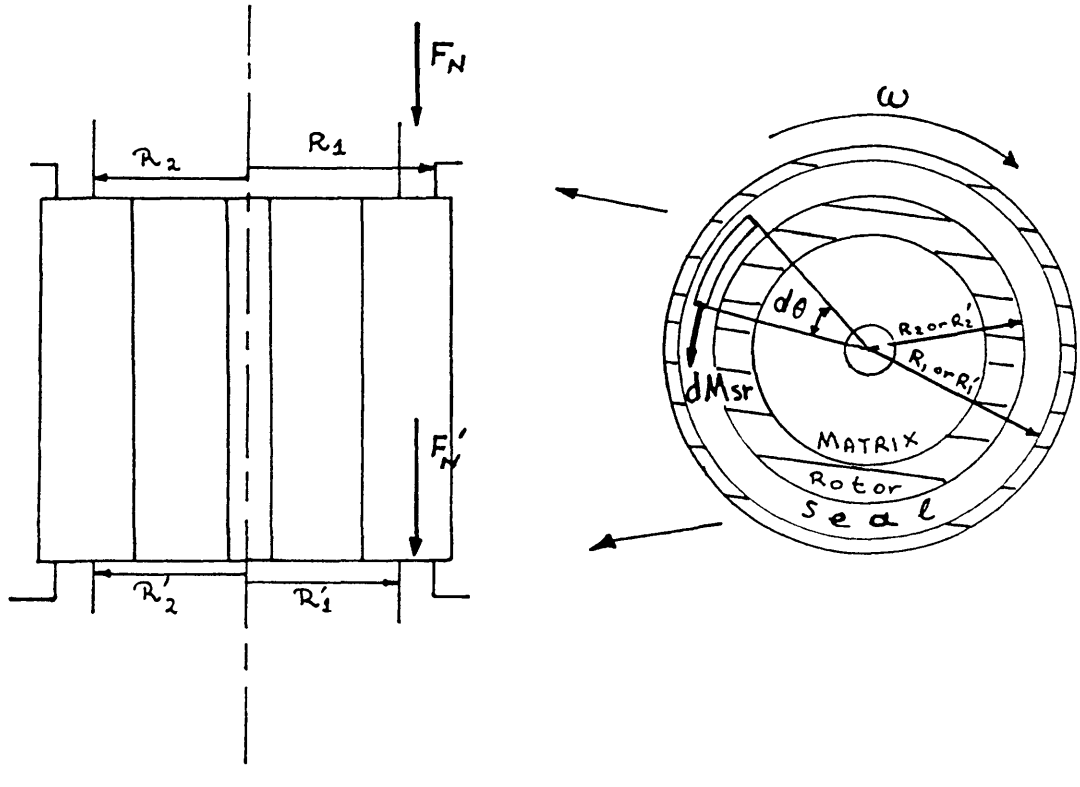


Figure (B.2): Frictional forces acting between the upper and lower circumferential seals and the rotor upper and lower surfaces respectively.

APPENDIX C

Calculation of size of effective gaps between matrix surface and radial seal and leakage flowrates data

The equation for flow of an incompressible fluid through an orifice of diameter, d_o, and area A is

$$V = C_D A \sqrt{\frac{2(\rho_w - \rho)\Delta Z}{\rho\left[1 - \left[\frac{d_o}{d}\right]^2\right]}} \qquad (C\text{-}1)$$

where V: volumetric florate (cm^3/s)

C_C: discarge coefficient

A: Area of orifice (m^2)

ρ_W: water density (Kg/m^3)

ρ: fluid density (Kg/m^3)

ΔZ: pressure drop in cm H_2O

d_o: orifice diameter (m)

d: diameter from which flow contracts (m)

From figure (3.26) for the flametrap matrix for V_{by} = 160 cm^3/s, $P_{in} - P_{out}$ = 3.2 x 98.06 N/m^2 and for the tubular matrix for V_{by} = 100 cm^3/s, $P_{in} - P_{out}$ = 4.0 x 98.06 N/m^2.

Since for both $P_{out} \approx 101325$ N/m^2 for the flame trap matrix, P_{in} = 101640 and

$$\frac{P_{in} - P_{out}}{P_{in}} = 0.003$$

and the tubular matrix $P_{in} = 101717$ and

$$\frac{P_{in} - P_{out}}{P_{in}} = 0.004$$

i.e. in both cases flow can be considered as incompressible as density changes are only significant if

$$\frac{P_{in} - P_{out}}{P_{in}} > 0.10$$

For the "orifice" in question the pressure recovery is very poor and $C_D = 0.5$ is assumed (for an orifice meter $C_D = 0.6$).

Since $d_o \ll d$, $1 - \left[\frac{d_o}{d}\right]^2 \approx 1$.

For the flame trap matrix

$$160 \times 10^{-6} = 0.5A\sqrt{2 \times 823 \times 3.2 \times 10^{-2}}$$

Therefore $A = 44 \text{ mm}^2$

For the tubular matrix

$$160 \times 10^{-6} = 0.5A\sqrt{2 \times 823 \times 4.0 \times 10^{-2}}$$

Therefore $A = 25 \text{ mm}^2$

Since the rubbing seals are 31.5 mm in length, the effective gap along the seals for the flame trap matrix = 0.7 mm and the tubular matrix = 0.4 mm.

Table (C.1)

Tubular matrix 0 revs/min

Inlet flowrate (cm^3/s)	Outlet flowrate (cm^3/s)	Pressure difference (cm H_2O)	Leakage (cm^3/s)	% Leakage	Bypass (cm^3/s)	% Bypass
800	714	1.95	86	10.8	68	8.5
700	624	2.25	76	10.8	74	10.6
600	526	1.20	74	12.4	54	9.0
500	436	1.50	64	12.8	60	12.0
400	341	1.30	59	14.8	56	14.0
300	255	0.50	45	15.0	36	12.0
200	161	0.55	39	19.6	37	18.5
100	76	0.65	24	24.0	40	20.0

Table (C.2)

Flame trap matrix 0 revs/min

Inlet flowrate (cm^3/s)	Outlet flowrate (cm^3/s)	Pressure difference (cm H_2O)	Leakage (cm^3/s)	% Leakage	Bypass (cm^3/s)	% Bypass
800	698	3.30	102	12.7	163	20.4
700	607	2.65	93	13.3	147	21.0
600	515	2.65	85	14.2	147	24.5
500	421	1.85	79	15.8	123	14.6
400	335	1.25	65	16.2	100	25.0
300	243	0.95	57	19.0	86	28.7
200	158	0.50	42	21.0	62	31.0
100	73	0.25	27	27.0	44	44.0

Table (C.3)

Tubular matrix 4.0 revs/min

Inlet flowrate (cm^3/s)	Outlet flowrate (cm^3/s)	Pressure difference (cm H_2O)	Leakage (cm^3/s)	% Leakage	Bypass (cm^3/s)	% Bypass
800	720	1.90	80	10.0	68	18.5
700	613	2.90	83	11.8	84	12.0
600	532	1.50	68	11.4	60	10.0
500	438	0.95	62	12.4	47	9.4
400	344	0.95	56	140	47	11.7
300	24.9	0.80	51	17.0	44	14.7
200	162	0.45	38	19.0	34	17.0
100	75	0.20	25	25.0	22	22.0

Table (C.4)

Flame trap matrix 4.0 revs/min

Inlet flowrate (cm^3/s)	Outlet flowrate (cm^3/s)	Pressure difference (cm H_2O)	Leakage (cm^3/s)	% Leakage	Bypass (cm^3/s)	% Bypass
800	693	3.00	107	13.4	156	19.5
700	598	3.05	102	14.5	157	22.4
600	518	2.45	82	13.7	141	23.5
500	426	1.70	74	14.8	118	23.6
400	328	1.50	72	18.0	110	27.5
300	247	0.90	53	17.7	84	28.0
200	159	0.65	41	20.5	70	35.0
100	72	0.20	28	28.0	40	40.0

APPENDIX D

Calculation of

(a) Reynold's numbers within the combustion chamber

(b) Heat losses from the rotary regenerative burner

(c) Dean and Nusselt numbers for convective transfer from product gases to the combustion chamber walls

Calculation of Reynold's numbers within the combustion chamber

The Reynold's number, Re, for the flame in the hemispherical chamber is given by

$$Re = \frac{\rho_g \, u \, de}{\mu_g}$$

$$= \frac{8\rho_g V_{gcc}}{d(2 + \pi)\mu_g} \qquad \text{(D-1)}$$

where ρ_g: gas density (Kg/m^3)

μ_g: gas viscosity (Kg/m s)

V_{gcc}: combustion chamber volumetric flowrate (cm^3/s)

d: combustion chamber diameter (m)

For $d = 90 \times 10^{-3}$ m, gas at $20^{o}C$, $\rho_g = 1.2$ Kg/m^3 and $\mu_g = 1.8 \times 10^{-5}$ Kg/m s (since mixtures are lean they are assumed 100% air) and $V_{gcc} = 400$ cm^3/s

i.e. $Re = 458$

For gas flow with gas at 1400^{o} K (i.e. $\rho_g = 0.251$ Kg/m^3 and $\mu_g = 2.28 \times 10^{-5}$ Kg/m s) and with a Reynold's number of 458

for the 60 mm chamber $V_{gcc} = 1605$ cm^3/s

and for the 90 mm chamber $V_{gcc} = 2408$ cm^3/s.

Since V_{gcc} is given in terms of the inlet flowrate, $V_{g\ in}$, by

$$V_{gcc} = (1 - \%loss)\ \frac{1400}{293}\ V_{g\ in} \qquad (D\text{-}2)$$

for the 60 mm chamber $V_{g\ in} = 420$ cm^3/s

and for the 90 mm chamber $V_{g\ in} = 630$ cm^3/s.

For gas flow with gas at 1400 K and a Reynold's number of 2000 as before

for the 60 mm chamber $V_{g\ in} = 1833$ cm^3/s

and for the 90 mm chamber $V_{g\ in} = 2749$ cm^3/s.

Calculation of heat losses from the rotary regenerative burner

The heat transfered by convection to the combustion chamber inside wall is assumed equal to the total heat loss from the system, Q_L, and is given by (see figure (D.1) for dimensions)

$$Q_L = h_{cc}\left[2\pi r_{cc}^2 + 0.09 \times 0.015\pi + \frac{\pi}{4}[(0.09)^2 - 4r_{cc}^2]\right](1400 - T_{s\ in})$$

i.e.

$$Q_L = h_{cc}\left[3.141 r_{cc}^2 + 11.0 \times 10^{-3}\right](1400 - T_{s\ in}) \qquad (D\text{-}3)$$

where h_{cc}: convective heat transfer coefficient (J/m^2 s K)

r_{cc}: combustion chamber radius (m)

$T_{s\ in}$: chamber wall surface temperature (K)

To obtain the heat loss by conduction through the cylindrical insulating layer (0.076 m thick) the temperature of the outside burner wall is assumed to be equal to $T_{s\ in}$ and a simplified burner geometry is assumend as shown in figure (D.2). "Triton" kaowool ceramic fibre blanket was used for reducing heat losses from the system.

The rate of heat loss, Q_L, is given by

$$Q_L = \left[\frac{2\pi k\ 0.308}{\ln\frac{0.330}{0.178}} + \frac{\pi(0.075)^2 k}{0.076}\right](T_{s\ in} - T_{s\ out}) \qquad (D\text{-}4)$$

The thermal conductivity, k, of the fibre increases with increasing temperature of the solid. A high temperature of 450°C is assumed for the insulating layer (k = 0.16 W/m K). This would result in predicted values for Q_L which are high and, therefore, conservative estimates for the leaness of the mixtures that can be stably burned in the system.

From eqn. (D-4) for k = 0.16 W/m K,

$$Q_L = 0.54(T_{si} - T_{so}) \qquad (D\text{-}5)$$

The heat lost by natural convection is given by

$$Q_L = \left[(0.33\pi\ 0.308)h_a + \frac{\pi(0.33)^2}{4} h_b\right](T_{so} - T_a) \qquad (D\text{-}6)$$

where h_a: heat transfer coefficient for natural convection from the cylindrical surface (J/s m^2K)

h_b: heat transfer coefficient for natural convection from the circular flat surface (J/s m^2K)

Both h_a and h_b depend on the ambient temperature and the temperature of the solid surface. The physical properties of air required for estimation of h_a and h_b are evalulated at the mean film temperature $\frac{T_{s\ out} + T_a}{2}$. $T_{s\ out}$ varies, depending on the operating conditions within the burner. A value of 60^oC is assumed for $T_{s\ out}$, and 20^oC for T_a.

The following correlation can be used for calculating the heat transfer coefficients for natural convection from isothermal surfaces.

$$h = C\frac{k_g}{L}(Gr\ Pr)^a \qquad (D\text{-}7)$$

where L: a characteristic length depending on the geometrical configuration.

For a cylindrical surface, $\frac{1}{L} = \frac{1}{0.308} + \frac{1}{0.330}$

i.e. L = 0.159 m.

For the circular surface, L = 0.9 x 0.33 = 0.297 m

Gr: Grashof number

C,a: a constant and a power that depend on the geometrical configuration and the flow regime

For the cylindrical surface, the Grashof number is given by

$$Gr = \frac{9.81 \times \frac{1}{313} \times 40 \times (0.159)^3}{(1.7 \times 10^{-5})^2} = 1.74 \times 10^7$$

For the circular surface

$$Gr = \frac{9.81 \times \frac{1}{313} \times 40 \times (0.297)^3}{(1.7 \times 10^{-5})^2} = 1.14 \times 10^8$$

1.7×10^{-5} m^2/s is the kinematic viscocity of air at 40^oC.

Since for the cylindrical surface Gr Pr = 1.23×10^7 and for the circular surface Gr Pr = 8.04×10^7, from eqn. (D-7) and reference (D.1):

for the cylindrical surface

$$h_a = 0.6\frac{0.027}{0.159}(1.23 \times 10^7)^{0.25} = 6.03$$

and for the circular surface

$$h_b = 0.14\ \frac{0.027}{0.297}(8.04 \times 10^7)^{0.33} = 5.49$$

Substituting for h_a and h_b in eqn (D-6) gives

$$Q_L = 2.4(T_{s\ out} - T_a) \qquad (D\text{-}8)$$

From eqns. (D-3), (D-5) and (D-8)

$$Q_L = \frac{1}{\frac{1}{(3.141r_{cc}^2 + 11.0 \times 10^3)h_{cc}} + 2.269}\ (1400 - T_a) \qquad (D\text{-}9)$$

Calculation of the Dean number, the Nusselt number and the convective heat tranfer coefficient from the gas to the chamber wall

The Dean number, De, in this case is given by

$$De = Re = \frac{4\ M_{gcc}}{r_{cc}(2 + \pi)\mu_g} \qquad (D\text{-}10)$$

where M_{gcc}: mass flowrate of products through the combustion chamber (Kg/s)

r_{cc}: combustion chamber radius (m)

μ_g: viscosity of products (mainly air at 1400 K, i.e. = 5.057×10^{-5} Kg/m s)

Substituting for μ in eqn. (D-10) gives

$$De = \frac{1.538 \times 10^4\ M_{gc\ out}}{r_{cc}} \qquad (D\text{-}11)$$

M_{gcc} is equal to the mass flowrate of reactants actually entering the matrix after taking into account bypass leakages and leakages to the atmosphere. The leakage across the upper circumferential seal has been assumed to be negligible.

For air at 1400 K, Pr = 0.726 and from eqn. (4.3-8)

$$\zeta = 1.248$$

Substituting for ζ in eqn. (4.3-7) gives

$$Nu = \frac{0.692\ De^{\frac{1}{2}}}{1 - 1.948\ De^{\frac{1}{2}}} \qquad (D\text{-}12)$$

For heat transfer the equivalent diameter of the passage is taken as $\frac{4\frac{\pi}{2}r^2}{\pi r}$, i.e. only the perimeter of the surface involved in heat transfer is considered. For air at 1400 K, k_g = 0.0844 W/m k and h_{cc} is, therefore, given by

$$h_{cc} = \frac{0.0422\ Nu}{r_{cc}} \qquad (D\text{-}13)$$

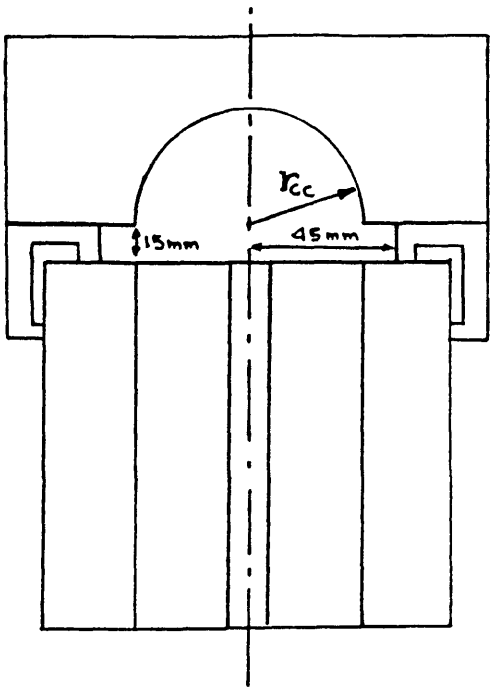


Figure (D.1): Combustion chamber dimensions

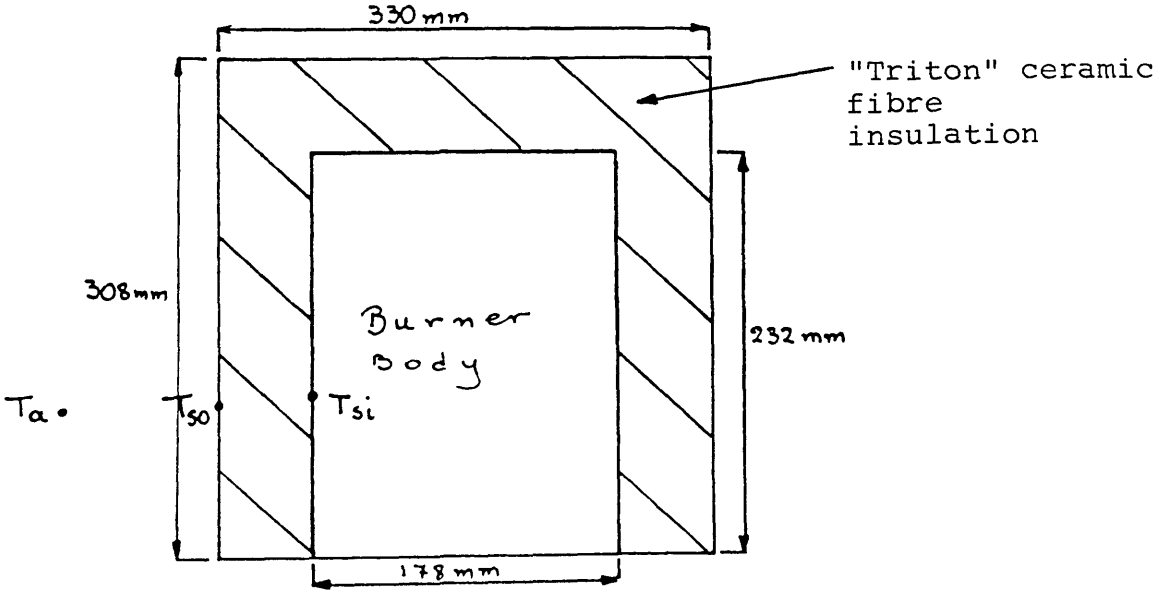


Figure (D.2): Simplified burner geometry for calculation of heat losses from the system .

APPENDIX E

The computer program

Nomenclature used in the program

TGC:	Gas temperature on the "cooling-down" matrix side
TGH:	Gas temperature on the "heating-up" matrix side
TSC:	Solid temperature on the "heating-up" matrix side
TSH:	Solid temperature on the "cooling-down" matrix side
TSCTSH:	Difference between solid temperatures on the right and left edges
GC(T):	Function for gas specific heat
GK(T):	Function for gas thermal conductivity
GV:	Gas volumetric flowrate
GM:	Gas mass flowrate
RCIN:	Combustion chamber radius
REVS:	Matrix rotational speed
SC:	Solid specific heat
Dean:	Dean number
RNUS:	Nusselt number
HTCIN:	Convective heat transfer coefficient from gas to combustion chamber wall
QLOST:	Heat lost by the hot product gases
TGHC:	Temperature of hot product gases at the entry to the matrix

H: Heat transfer coefficient for convective tranfer from gas to matrix passage wall

Y_A, Y_B: (Heat received by cold reactants/Heat given up by hot products) on successive iterations

G: Gas specific heat

RK: Gas thermal conductivity

STGC: Sum of temperatures at each mixture stream entering the combustion chamber

STGH: Sum of temperatures of each product stream entering the exhaust side of the burner

TGCC: Average mixture preheat temperature

TGHCO: Average products temperature entering the exhaust side of the system

PRBVOL: Percentage of methane by volume

The Fortran Programme

```
00100 PROGRAM PROG(INPUT,RES,TAPE5=INPUT,TAPE6=RES)
00110 PARAMETER(NR=5,NC=5)
00120 DIMENSION TGC(NR+1,NC),TGH(NR+1,NC)
00130 DIMENSION TSC(NR,NC+1),TSH(NR,NC+1)
00140 DIMENSION TSCTSH(NR)
00150 GC(T)=1004.770864+(0.1398*T)-(4.2055E-4*T*T)
00160 GK(T)=2.4019E-2+(7.5474E-5*T)-(2.0694E-8*T*T)
00170C DATA
00180 GV=95.0
00190 45 IF (GV.LT.199.9)THEN
00200          IF(GV.LT.119.9)THEN
00210          GV=GV+5.0
00220          ELSE
00230          GV=GV+20.0
00240          ENDIF
00250     ELSE
00260     GV=GV+100.0
00270     ENDIF
00280 IF(GV.GT.800.0)STOP
00290 RCIN=0.0307
00300 REVS=1.2/60.0
00310 Z=1.0
00320 SC=800.0
00330C CALCULATION OF HOT COMBUSTION PRODUCT TEMP TGHC
00340 GM=1.2E-6*0.95*GV
00350 DEAN=(1.538E4*GM)/RCIN
00360 RNUS=(0.692*SQRT(DEAN))/(1.0-(1.948/SQRT(DEAN)))
00370 HTCIN=(RNUS*0.0597)/RCIN
00380 QLOST=1107.0/((1.0/(((3.141*RCIN*RCIN)+11.10E-3)*HTCIN))+2.269)
00390 TGHC=1127.0-(8.64E-4*(QLOST/GM))
00400 IF(TGHC.LT.20.0)THEN
00410 WRITE(6,110)RCIN,REVS,GV
00420 GOTO 45
00430 110 FORMAT(5X,'CHAMBER RADIUS=',F6.4,'M',/,5X,'REVS=',F4.3,/,
00440+ 5X,'GV=',F5.1,/,5X,'U N S T A B L E  C O M B U S T I O N',/,50('-'))
00450 ENDIF
00460 DO 10 IC=1,NC
00470 TGH(1,IC)=TGHC
00480 TGC(1,IC)=20.0
00490 10 CONTINUE
00500 TSH(1,1)=21.0
00510 DO 5 IR=2,NR
00520 TSH(IR,1)=TSH(IR-1,1)+(((TGHC-1.0)-(TSH(1,1)))/REAL(NR-1))
00530 5 CONTINUE
00540C CALCULATION OF REACTANTS TEMP TGCC
00550 ICOUNT=0
00560 YA=1.0
00570 20 ICOUNT=ICOUNT+1
00580 IF(ICOUNT.GT.50)GOTO 45
00590 PRINT*,'ICOUNT=',ICOUNT
00600 CONST3=(7.3096*REAL(NR))/(REVS*SC)
00610 DO 30 IC=1,NC
00620 DO 30 IR=1,NR
00630 TA=(TSH(IR,IC)+TGC(IR,IC))/2.0
00640 G=GC(TA)
00650 RK=GK(TA)
00660 H=3000.0*RK
00670 CONST2=(2.0*REAL(NC))/(GM*G)
00680 CONST4=TSH(IR,IC)-TGC(IR,IC)
00690 CONST1=1.0/(((41.5*REAL(NC)*REAL(NR))/H)+(CONST2/2.0)+(CONST3/2.0))
00700 TGC(IR+1,IC)=TGC(IR,IC)+(CONST2*CONST1*CONST4)
00710 TSH(IR,IC+1)=TSH(IR,IC)-(CONST3*CONST1*CONST4)
00720 30 CONTINUE
00730 DO 40 IR=1,NR
00740 TSC(IR,1)=TSH(NR+1-IR,NC+1)
00750 40 CONTINUE
00760 DO 50 IC=1,NC
00770 DO 50 IR=1,NR
00780 TA=(TGH(IR,IC)+TSC(IR,IC))/2.0
00790 G=GC(TA)
00800 RK=GK(TA)
00810 H=3000.0*RK
00820 CONST6=(2.0*REAL(NC))/(GM*G)
00830 CONST7=TGH(IR,IC)-TSC(IR,IC)
00840 CONST5=1.0/(((41.5*REAL(NC)*REAL(NR))/H)+(CONST2/2.0)+(CONST3/2.0))
00850 TGH(IR+1,IC)=TGH(IR,IC)-(CONST6*CONST5*CONST7)
00860 TSC(IR,IC+1)=TSC(IR,IC)+(CONST3*CONST5*CONST7)
00870 50 CONTINUE
00880C COMPARISON OF ESTIMATED AND CALCULATED VALUES
00890 STGC=0.0
00900 STGH=0.0
00910 DO 90 IC=1,NC
00920 STGC=STGC+TGC(NR+1,NC)
00930 STGH=STGH+TGH(NR+1,IC)
```

The Fortran Programme (continued)

```
00940 90 CONTINUE
00950 TGCC=STGC/REAL(NC)
00960 TGHCO=STGH/REAL(NC)
00970 TB=(TGHC+TGHCO)/2.0
00980 TC=(TGCC+20.0)/2.0
00990 YB=(GC(TC)*(TGCC-20.0))/(GC(TB)*(TGHC-TGHCO))
01000 IF(YB.GT.1.0)YB=1.0/YB
01010 DO 65 IR=1,NR
01020 X=TSH(IR,1)-TSC(NR+1-IR,NC+1)
01030 TSCTSH(IR)=ABS(X)
01040 65 CONTINUE
01050 VMAX=TSCTSH(1)
01060 DO 70 IR=2,NR
01070 IF(TSCTSH(IR).GT.VMAX)VMAX=TSCTSH(IR)
01080 70 CONTINUE
01090 IF(VMAX.LT.0.1) GOTO 35
01100 PRINT*,'YB=',YB,'  ','YA=',YA
01110 Y=YB-YA
01120 IF(Y.LT.0.001)THEN
01130 DO 60 IR=1,NR
01140 TSH(IR,1)=TSC(NR+1-IR,NC+1)+(Z*(TSC(NR+1-IR,NC+1)-TSH(IR,1)))
01150 60 CONTINUE
01160 YA=YB
01170 GOTO 20
01180 ELSE
01190 DO 15 IR=1,NR
01200 TSH(IR,1)=TSC(NR+1-IR,NC+1)
01210 15 CONTINUE
01220 YA=YB
01230 GOTO 20
01240 ENDIF
01250C CALCULATION  OF FUEL PERCENTAGE BY VOLUME
01260 35 TA=(1127.0+TGCC)/2.0
01270 PRBVOL=4.0333E-3*GC(TA)*(1127.0-TGCC)
01280 WRITE(6,600)RCIN
01290 600 FORMAT(2(1X,70('-')),7X,'CHAMBER RADIUS=',F6.4,'M',//)
01300 WRITE(6,700)REVS
01310 700 FORMAT(7X,'ROTATIONAL SPEED=',F5.3,//)
01320 WRITE(6,100) GV,PRBVOL
01330 100 FORMAT(5X,'GV=',F6.1,10X,'PERCENT  CH4=',F6.4,///)
01340 WRITE(6,200)YB
01350 200 FORMAT(14X,'HEAT   BALANCE=',F4.3,///)
01360 WRITE(6,300)TGHC,TGCC
01370 300 FORMAT(5X,'TGHC=',F7.2,15X,'TGCC=',F7.2,//)
01380 WRITE(6,400)TGHCO,TGC(1,1)
01390 400 FORMAT(5X,'TGHCO=',F7.2,15X,'TGCI=',F7.2,/////)
01400 WRITE(6,500)
01410 500 FORMAT(11X,'TEMPERATURE',5X,'DISTRIBUTION')
01420 WRITE(6,1000)((TSH(J,K),K=1,NC+1),J=1,NR)
01430 1000 FORMAT(//,23X,'T S H',//,60('-'),//,6(1X,F8.3),/)
01440 WRITE(6,1100)((TSC(J,K),K=1,NC+1),J=1,NR)
01450 1100 FORMAT(//,23X,'T S C',//,60('-'),//,6(1X,F8.3),/)
01460 GOTO 45
01470 END
```

Appendix F - Experimental Results

Table (F.1)

Stability characteristics of burner with: Metallic matrix, 60 mm diameter combustion chamber, 0 revs/min

Inlet flowrate cm^3/s	% CH_4 by vol.	Inlet Gas temp. ^oC	Exhaust Gas temp. ^oC	Surface temp. ^oC	Position Thermocouple	Combustion chamber gas temperatures ^oC 1	2	3	4	5	6	7	8	9	
					A	324	504	685	582	438	438	434	389	294	237
143	5.85	26	86	234	B	539	652	612	547	390	319				
					C	323	406	653	625	430	420	405	354	279	235
103	5.85	. . . . . NO COMBUSTION													
					A	395	635	777	733	629	576	559	504	381	280
219	5.45	23	152	358	B	557	672	691	615	450	373				
					C	400	653	777	758	635	590	548	473	338	284
129	5.45	. . . . . NO COMBUSTION													
					A	400	671	824	814	718	657	626	544	405	288
250	5.05	24	104	268	B	581	720	720	618	476	387				
					C	386	593	801	804	720	667	612	522	367	295
248	4.80	. . . . . NO COMBUSTION													
					A	380	484	599	860	835	751	717	614	424	307
318	4.83	26	164	341	B	560	698	754	709	525	417				
					C	400	605	837	853	823	788	655	461	351	305
315	4.58	. . . . . NO COMBUSTION													

Stability characteristics of burner with: Metallic matrix, 60 mm diameter combustion chamber, 0 revs/min

					A	398	587	911	918	909	878	809	645	456	356
505	4.66	26	166	323	B	547	628	703	735	705	565				
					C	421	547	642	878	882	870	798	640	458	376
503	4.44	. . . . .			NO	COMBUSTION									
					A	478	650	759	984	964	945	921	811	588	433
673	4.56	26	185	339	B	733	842	825	775	760	650				
					C	466	625	683	931	932	930	906	737	547	445
668	4.15	. . . . .			NO	COMBUSTION									
					A	445	585	699	961	946	937	895	762	558	440
670	4.33	24	200	370	B	657	880	844	742	613	559				
					C	450	563	642	909	916	911	884	766	574	477
668	4.15	. . . . .			NO	COMBUSTION									
					A	503	690	763	1054	1010	1008	969	898	680	501
920	4.33	22	237	398	B	683	776	758	829	700	689				
					C	503	677	742	808	964	979	949	852	571	506
918	4.15	. . . . .			NO	COMBUSTION									

Stability characteristics of burner with: Metallic matrix, 60 mm diameter combustion chamber 0.6 revs/min

Inlet flowrate cm^3/s	% CH_4 by vol.	Inlet Gas temp. ^oC	Exhaust Gas temp. ^oC	Surface temp. ^oC	Position Thermocouple	Combustion chamber gas temperatures, ^oC 1	2	3	4	5	6	7	8	9	
					A	349	574	740	702	547	505	497	477	360	273	
220	5.26	19	101	256	B		560	689	677	585	437	378				
					C		394	572	712	678	528	497	475	450	347	275
168	5.26	. . . . .			NO	COMBUSTION	. . . . .									
					A		510	743	846	787	736	707	685	645	452	377
306	4.90	19	134	355	B		601	723	729	644	525	465				
					C		528	722	819	777	720	689	667	632	440	371
194	4.90	. . . . .			NO	COMBUSTION	. . . . .									
					A		384	680	830	823	728	690	652	653	616	425
330	4.78	24	93	247	B		580	730	698	710	516	427				
					C		410	689	830	818	760	691	638	525	371	279
329	4.40	. . . . .			NOCOMBUSTION		. . . . .									
					A		470	703	894	881	875	846	738	650	475	365
470	4.13	22	109	297	B		613	770	785	760	600	516				
					C		446	574	760	888	867	797	734	620	430	351
438	3.95	. . . . .			NO	COMBUSTION	. . . . .									
					A		550	916	967	977	933	890	863	724	565	440
663	3.88	25	115	385	B		678	840	869	789	660	660				
					C		540	660	702	840	917	918	894	762	549	448
661	3.68	. . . . .			NO	COMBUSTION	. . . . .									

Stability characteristics of burner with: Metallic matrix, 60 mm diameter combustion chamber, 0.6 revs/min

Inlet flowrate cm^3/s	% CH_4 by vol.	Inlet Gas temp. °C	Exhaust Gas temp. °C	Surface temp. °C	Position Thermocouple	Combustion chamber gas temperatures °C 1	2	3	4	5	6	7	8	9	
					A	880	1038	1059	1013	990	975	940	898	630	519
999	4.29	20	125	448	B	781	950	980	920	865	770				
					C	870	920	965	972	1035	1040	1030	865	616	522
994	3.88	. . . . . NO COMBUSTION													

Stability characteristics of burner with: Metallic matrix, 60 mm diameter combustion chamber, 1.2 revs/min

Inlet flowrate cm^3/s	% CH_4 by vol.	Inlet Gas temp. °C	Exhaust Gas temp. °C	Surface temp. °C	Position Thermocouple	Combustion chamber gas temperatures °C 1	2	3	4	5	6	7	8	9	
					A	370	570	715	624	536	508	500	489	434	326
180	5.85	28	112	253	B	542	679	666	649	495	343				
					C	387	579	715	646	478	454	438	405	306	256
108	5.85	. . . . . NO COMBUSTION													
					A	387	464	635	615	464	422	421	380	273	212
155	5.56	28	90	215	B	556	690	654	582	498	316				
					C	361	500	655	653	435	415	377	351	262	212
130	5.56	. . . . . NO COMBUSTION													
					A	348	558	765	818	757	676	612	530	396	283
259	4.90	28	104	256	B	592	726	732	676	558	378				
					C	364	555	730	823	770	678	605	501	377	271
219	4.90	. . . . . NO COMBUSTION													

Stability characteristics of burner with: Metallic matrix, 60 mm diameter combustion chamber, 1.2 revs/min

					A	409	646	830	866	834	772	709	633	461	326
333	4.52	28	115	276	B	605	751	774	717	523	430				
					C	400	536	715	845	816	757	660	514	358	294
331	4.39				NO COMBUSTION										
					A	433	630	825	935	884	855	800	715	506	387
528	3.95	25	133	341	B	634	805	832	800	740	559				
					C	423	552	602	715	880	867	805	642	464	376
525	3.74				NO COMBUSTION										
					A	552	820	970	1001	968	925	900	825	628	498
673	3.68	29	150	415	B	725	860	890	900	830	688				
					C	536	665	667	745	933	930	877	755	568	463
669	3.40				NO COMBUSTION										
					A	615	925	1050	1080	1040	1015	950	905	725	550
912	3.40	28	155	459	B	788	1005	960	970	925	770				
					C	600	750	780	940	995	990	950	865	649	538
909	3.13				NO COMBUSTION										
					A	610	875	1035	1060	1050	1021	984	949	785	610
1054	3.36	23	160	479	B	806	980	1026	1000	990	821				
					C	595	730	750	850	1000	1010	969	874	709	602
1052	3.19				NO COMBUSTION										

Stability characteristics of burner with: Metallic matrix, 60 mm diameter combustion chamber, 2.4 revs/min

Inlet flowrate cm^3/s	% CH_4 by vol.	Inlet Gas temp. ^oC	Exhaust Gas temp. ^oC	Surface temp. ^oC	Position Thermocouple	Combustion chamber gas temperatures ^oC 1	2	3	4	5	6	7	8	9	
					A	380	471	615	605	478	446	432	415	332	255
163	5.85	28	103	250	B	569	687	633	613	547	472				
					C	387	535	630	616	443	429	398	380	301	245
113	5.85	. . . . . NO COMBUSTION													
					A	388	555	720	668	564	525	514	501	400	268
215	5.05	25	100	2.59	B	559	710	679	605	482	333				
					C	400	584	692	677	543	495	465	430	337	273
175	5.05	. . . . . NO COMBUSTION													
					A	385	585	734	783	640	596	566	528	425	286
249	4.80	26	99	246	B	572	716	721	659	549	377				
					C	373	582	712	755	636	562	511	456	329	250
248	4.69	. . . . . NO COMBUSTION													
					A	438	631	810	821	773	718	674	629	462	330
315	4.44	24	112	282	B	577	670	759	720	604	443				
					C	424	620	806	754	692	730	608	530	367	282
313	4.22	. . . . . NO COMBUSTION													
					A	460	597	825	885	830	828	770	650	489	362
401	4.08	25	125	319	B	607	755	798	663	549					
					C	447	565	750	849	828	793	718	607	431	335
399	3.90	. . . . . NO COMBUSTION													

Stability characteristics of burner with: Metallic matrix, 60 mm diameter combustion chamber, 2.4 revs/min

Inlet flowrate cm^3/s	% CH_4 by vol.	Inlet Gas temp. ^oC	Exhaust Gas temp. ^oC	Surface temp. ^oC	Position Thermocouple	Combustion chamber gas temperatures ^oC 1	2	3	4	5	6	7	8	9
					A	555	712	933	951	900	876	820	720	568	411
496	3.92	25	128	334	B	666	810	850	837	789	680				
					C	563	668	765	893	870	848	786	683	503	368
493	3.63	. . . . . NO COMBUSTION													
					A	595	910	1043	1035	1013	989	952	909	685	519
828	3.40	24	143	431	B	764	910	945	963	920	760				
					C	565	725	910	963	957	958	905	812	635	486
824	3.14	. . . . . NO COMBUSTION													
					A	590	790	1025	1068	1026	995	956	934	770	593
1008	3.23	22	141	447	B	784	940	965	978	935	760				
					C	541	685	700	740	955	970	948	860	708	638
1006	3.13	. . . . . NO COMBUSTION													

Stability characteristics of burner with: Metallic matrix, 60 mm diameter combustion chamber, 4.0 revs/min

Inlet flowrate cm^3/s	% CH_4 by vol.	Inlet Gas temp. ^oC	Exhaust Gas temp. ^oC	Surface temp. ^oC	Position Thermocouple	Combustion chamber gas temperatures ^oC 1	2	3	4	5	6	7	8	9
					A	385	561	759	738	601	550	540	522	366	291
203	5.85	22	117	273	B	572	705	690	632	535	399				
					C	405	604	709	689	558	513	487	430	340	275
133	5.85	. . . . . NO COMBUSTION													

Stability characteristics of burner with: Metallic matrix, 60 mm diameter combustion chamber, 4.0 revs/min

				A	410	642	829	785	713	661	639	590	440	295	
285	5.05	21	104	264	B	591	732	745	709	600	377				
					C	416	667	782	805	721	642	571	523	395	297
195	5.05	. . . . .			NO	COMBUSTION	. . . . .								
					A	502	623	857	845	784	744	699	620	495	322
335	4.65	24	107	269	B	596	735	780	737	625	397				
					C	481	670	780	833	781	732	643	536	403	301
333	4.44	. . . . .			NO	COMBUSTION	. . . . .								
					A	390	510	658	894	841	820	760	662	525	318
410	4.21	22	105	267	B	599	725	790	760	686	455				
					C	388	533	590	685	822	799	729	580	418	324
409	4.13	. . . . .			NO	COMBUSTION	. . . . .								
					A	434	610	703	930	933	896	863	781	615	450
565	3.82	20	123	348	B	701	868	870	850	759	740				
					C	433	580	606	670	860	850	807	699	545	447
564	3.71	. . . . .			NO	COMBUSTION	. . . . .								
					A	506	676	863	1010	993	957	941	905	720	500
735	3.58	21	169	5.09	B	746	870	915	902	780	688				
					C	487	660	670	773	918	914	880	770	630	499
733	3.40	. . . . .			NO	COMBUSTION	. . . . .								
					A	602	840	1088	1114	1066	1080	1028	1010	970	720
1021	3.28	20	146	499	B	835	980	1016	1020	1010	950				
					C	630	760	740	850	982	990	960	910	790	689
1018	3.04	. . . . .			NO	COMBUSTION	. . . . .								

Stability characteristics of burner with: Ceramic matrix, 60 mm diameter combustion chamber, 0 revs/min

Inlet flowrate cm^3/s	% CH_4 by vol.	Inlet Gas temp. ^oC	Exhaust Gas temp. ^oC	Surface temp. ^oC	Position Thermocouple	Combustion chamber gas temperatures ^oC 1	2	3	4	5	6	7	8	9	
					A	370	540	679	683	531	494	495	470	393	250
109	5.06	21	89	257	B	559	664	655	567	415	346				
					C	345	502	658	643	440	432	401	382	295	243
74	5.06	. . . . .			NO	COMBUSTION									
					A	358	463	578	822	780	745	753	628	510	360
198	4.48	20	153	267	B	348	653	577	507	402	360				
					C	362	425	520	645	751	810	720	605	502	343
197	4.23	. . . . .			NO	COMBUSTION									
					A	394	470	504	585	808	894	864	806	667	433
341	4.46	22	218	302	B	565	725	831	743	527	441				
					C	382	465	613	752	810	865	832	708	608	428
339	4.27	. . . . .			NO	COMBUSTION									
					A	401	460	480	725	880	910	830	623	400	390
595	4.58	21	278	315	B	395	420	467	480	393	388				
					C	382	425	492	698	813	882	880	602	501	372
593	4.39	. . . . .			NO	COMBUSTION									
					A	513	550	536	685	828	930	956	920	620	663
810	4.78	22	385	400	B	514	559	945	840	539	515				
					C	501	508	518	618	792	815	930	870	602	618
807	4.58	. . . . .			NO	COMBUSTION									

Stability characteristics of burner with: Ceramic matrix, 60 mm diameter combustion chamber, 0.6 revs/min

Inlet flowrate cm^3/s	% CH_4 by vol.	Inlet Gas temp. ^oC	Exhaust Gas temp. ^oC	Surface temp. ^oC	Position Thermocouple	Combustion chamber gas temperatures ^oC 1	2	3	4	5	6	7	8	9	
					A	430	690	690	734	690	598	594	528	449	346
119	5.06	19	155	278	B	548	656	660	588	446	392				
					C	416	618	662	702	652	595	582	526	415	328
64	5.06	. . . . .			NO	COMBUSTION									
					A	385	530	550	605	506	480	491	470	370	383
81	5.87	19	130	266	B	541	641	622	533	398	342				
					C	388	512	598	592	552	471	462	443	361	375
66	5.87	. . . . .			NO	COMBUSTION									
					A	493	642	800	867	840	807	767	670	559	393
197	4.23	18	165	316	B	634	739	760	663	500	438				
					C	485	631	796	843	789	762	685	553	541	352
195	3.94	. . . . .			NO	COMBUSTION									
					A	560	700	964	956	906	885	830	800	695	505
331	3.41	21	208	404	B	760	903	871	820	629	539				
					C	518	662	713	805	920	935	932	884	702	502
327	319	. . . . .			NO	COMBUSTION									
					A	640	785	995	1026	960	860	870	830	860	680
579	3.19	21	228	460	B	880	950	1015	916	790	660				
					C	618	792	882	902	990	1018	1005	952	818	635
577	3.01	. . . . .			NO	COMBUSTION									

Stability characteristics of burner with: Ceramic matrix, 60 mm diameter combustion chamber, 0.6 revs/min

Inlet flowrate cm^3/s	% CH_4 by vol.	Inlet Gas temp. ^oC	Exhaust Gas temp. ^oC	Surface temp. ^oC	Position Thermocouple	Combustion chamber gas temperatures ^oC 1	2	3	4	5	6	7	8	9	
					A	710	863	1015	1058	1010	910	905	899	860	720
802	3.10	21	243	520	B	885	992	1041	923	830	690				
					C	703	821	885	992	1022	1048	1032	961	875	698
800	2.90	. . . . . NO COMBUSTION													

Stability characteristics of burner with: Ceramic matrix, 60 mm diameter combustion chamber, 1.2 revs/min

Inlet flowrate cm^3/s	% CH_4 by vol.	Inlet Gas temp. ^oC	Exhaust Gas temp. ^oC	Surface temp. ^oC	Position Thermocouple	Combustion chamber gas temperatures ^oC 1	2	3	4	5	6	7	8	9	
					A	420	650	710	712	711	705	700	686	528	321
83	83	5.05	19	127	288		B	574	695	697	665	560	412		
					C	418	628	700	701	692	646	692	503	492	313
35	5.05	. . . . . NO COMBUSTION													
					A	436	500	582	642	480	476	464	450	401	360
55	5.85	20	115	290	B	554	590	625	545	428	397				
					C	422	492	571	612	402	458	445	408	401	362
43	5.85	. . . . . NO COMBUSTION													
					A	435	631	790	800	765	735	717	590	494	363
177	4.23	18	105	268	B	597	717	725	646	468	385				
					C	402	560	662	690	750	748	682	502	465	343
175	3.94	. . . . . NO COMBUSTION													

Stability characteristics of burner with: Ceramic matrix, 60 mm diameter combustion chamber, 1.2 revs/min

Inlet flowrate cm^3/s	% CH_4 by vol.	Inlet Gas temp. ^oC	Exhaust Gas temp. ^oC	Surface temp. ^oC	Position Thermocouple	Combustion chamber gas temperatures ^oC 1	2	3	4	5	6	7	8	9	
					A	536	762	949	966	930	898	870	856	696	469
330	3.50	19	198	401	B	759	844	880	801	780	615				
					C	512	693	822	866	895	944	902	870	682	475
318	3.25	. . . . . NO COMBUSTION													
					A	635	820	990	1012	980	950	880	827	871	580
578	2.97	21	228	458	B	868	980	969	938	828	663				
					C	618	762	782	864	980	995	1002	918	818	572
574	2.74	. . . . . NO COMBUSTION													
					A	714	872	1080	1045	1029	999	940	955	874	680
802	2.82	20	245	517	B	969	1068	1036	1003	876	716				
					C	703	743	882	885	960	1001	1053	1013	848	672
800	2.62	. . . . . NO COMBUSTION													

Stability characteristics of burner with: Ceramic matrix, 60 mm diameter combustion chamber, 2.4 revs/min

Inlet flowrate cm^3/s	% CH_4 by vol.	Inlet Gas temp. ^oC	Exhaust Gas temp. ^oC	Surface temp. ^oC	Position Thermocouple	Combustion chamber gas temperatures ^oC 1	2	3	4	5	6	7	8	9	
					A	461	553	699	705	605	562	521	506	384	299
98	4.80	21	161	281	B	571	666	660	590	450	366				
					C	452	543	680	692	613	543	516	482	324	284
48	4.80	. . . . . NO COMBUSTION													

Stability characteristics of burner with: Ceramic matrix, 60 mm diameter combustion chamber, 2.4 revs/min

					A	464	595	730	795	706	654	622	596	515	398
108	5.85	22	200	356	B	593	661	702	687	548	459				
					C	479	577	745	782	743	625	613	586	503	352
95	5.85	. . . . .			NO	COMBUSTION									
					A	492	596	750	885	867	864	837	795	750	567
215	3.60	21	207	341	B	657	765	780	745	705	510				
					C	472	573	728	813	861	872	858	780	672	558
212	3.33	. . . . .			NO	COMBUSTION									
					A	607	708	793	930	924	909	899	901	788	545
420	3.22	25	210	417	B	806	916	905	878	736	583				
					C	595	706	785	910	918	903	873	818	705	503
418	3.06	. . . . .			NO	COMBUSTION									
					A	666	812	1015	1020	980	942	906	920	878	650
593	3.06	26	231	479	B	880	980	970	952	822	694				
					C	642	746	774	819	973	982	1003	992	843	641
589	2.83	. . . . .			NO	COMBUSTION									
					A	662	790	949	1025	985	931	915	954	814	625
771	2.60	25	245	514	B	924	1020	1013	992	869	727				
					C	672	753	817	952	1003	1013	995	981	802	654
761	2.47	. . . . .			NO	COMBUSTION									

Stability characteristics of burner with: Ceramic matrix, 90 mm diameter combustion chamber, 1.2 revs/min

Inlet flowrate cm^3/s	% CH_4 by vol.	Inlet Gas temp. ^oC	Exhaust Gas temp. ^oC	Surface temp. ^oC	Position Thermocouple	Combustion chamber gas temperatures ^oC 1	2	3	4	5	6	7	8	9	
					A	420	605	728	735	510	495	470	446	400	355
128	5.41	22	191	361	B	575	680	650	603	581	533	520	417		
					C	412	598	685	722	682	596	486	452	440	385
81	5.41	. . . . . NO COMBUSTION													
					A	420	625	840	840	775	706	640	570	418	385
241	4.49	20	178	382	B	644	780	836	841	790	749	648	472		
					C	415	589	795	782	718	626	514	495	492	372
239	4.29	. . . . . NO COMBUSTION													
					A	545	701	888	790	730	725	727	715	603	470
389	3.61	20	214	453	B	700	790	849	894	885	857	690	510		
					C	532	612	694	792	842	862	852	653	545	485
387	3.40	. . . . . NO COMBUSTION													
					A	620	734	900	850	847	838	769	768	780	535
599	2.89	20	231	519	B	730	824	945	899	827	760	780	628		
					C	631	717	732	741	843	852	895	797	732	502
599	2.73	. . . . . NO COMBUSTION													
					A	623	744	778	898	800	815	791	748	704	575
799	2.60	21	230	514	B	770	818	843	856	840	806	750	650		
					C	612	726	748	792	813	845	805	804	702	602
797	2.44	. . . . . NO COMBUSTION													

Stability characteristics of burner with: Ceramic matrix, cylindrical combustion chamber, 1.2 revs/min

					A	435	674	727	737	694	667	627	549	465	354
133	6.07	25	147	424	B										
					C										
80	6.07	. . . . . NO COMBUSTION													
					A	460	629	710	735	690	676	634	540	384	304
128	5.41	22	145	371	B										
					C										
81	5.41	. . . . . NO COMBUSTION													
					A	475	613	780	845	830	810	770	690	509	354
242	4.58	23	153	429	B										
					C										
240	4.39	. . . . . NO COMBUSTION													
				A	580	780	860	973	961	951	936	860	600	480	
389	3.61	20	208	607	B										
					C										
384	3.40	. . . . . NO COMBUSTION													
					A	580	715	830	1031	1006	950	930	735	570	500
606	3.28	25	211	562	B										
					C										
604	3.12	. . . . . NO COMBUSTION													
					A	620	810	920	1085	1010	1001	980	850	640	580
791	2.96	27	244	704	B										
					C										
789	2.79	. . . . . NO COMBUSTION													

Experimental data and calculation of leakage rates from the metallic matrix burner to the atmosphere

Immediately after completion of each experimental run, the methane supply was interrupted and with the motor running and only air flowing through the system the burner exhaust port was connected via a length of PVC tubing to a rotameter.

The temperature and the flowrate of the exhaust stream were measured by means of a Chromel-Alumel thermocouple and a 7x metric rotameter respectively. The rotameter had been calibrated for air at 25°C and 1 atm absolute. Since the air passing through the rotameter had emerged from the hot burner, its temperature was higher than 25°C (its pressure was only slightly above atmospheric) and the rotameter readings had, therefore, to be corrected.

If the volumetric flowrate, V_{g_1}, of a gas of temperature T_1, pressure P_1, and molecular weight MW, is measured by a rotameter then (F.1)

$$V_{g_1} = C_D A_2 \sqrt{\frac{2RT_{g_1}(-\Delta P)}{P_1 MW(1 - \frac{A_2}{A_1})}} \qquad (F\text{-}1)$$

where A_1 is the cross sectional area of the tube, A_2 is the area of the annular space between the float and the tube, ΔP is the pressure difference over the float and C_D is a discharge coefficient, which can be assumed to be constant. The pressure

difference over the float, $-\Delta P$, is given by:

$$-\Delta P = V_f(\rho_f - \rho_g)/A_f \qquad \text{(F-2)}$$

where V_f is the volume of the float, ρ_f the density of the material of the float, ρ_g the gas density and A_f the maximum cross sectional area of the float on a horizontal plane. Since $\rho_f >> \rho_g$, $-\Delta P$ can be assumed constant even for changing gas densities.

If the gas temperature is increased to T_2 and its pressure is held constant at P_1, for the same float position, the volumetric flowrate V_{g_2} is given by:

$$V_{g_1} = C_D A_2 \sqrt{\frac{2RT_{g_2}(-\Delta P)}{P_1 MW(1 - \frac{A_2}{A_1})}} \qquad \text{(F-3)}$$

From equations (F-1) and (F-3) the following is obtained

$$V_{g_2} = V_{g_1}\sqrt{\frac{T_{g_2}}{T_{g_1}}} \qquad \text{(F-4)}$$

In our case V_{g_1} is the value of the volumetric flowrate obtained from the calibration chart for the given position of the float, and V_{g_2} is the actual volumetric flowrate of the exhaust air.

In order to calculate the percentage of the inlet air that escaped to the atmosphere, the exhaust volumetric flowrates for air at temperatures equal to those of the inlet air must be

Table (F.2)

Inlet air flowrate cm^3/s	Inlet Air temp. ^oC	Flowrate corresponding to rotameter reading cm^3/s	Exhaust air temp. ^oC	Actual exhaust flowrate cm^3/s	Exhaust flowrate at inlet air temp cm^3/s	% leakage
4.0 revs/min						
735	21	665.6	56.0	699.4	625	15.0
545	20	463.6	36.9	472.8	447	18.0
400	22	335.6	31.0	339.0	329	17.8
285	21	233.9	29.6	235.7	229	19.6
125	20	93.0	28.0	93.5	91	27.2
2.4 revs/min						
980	22	910.9	60.0	962.9	853	12.9
810	24	727.9	56.4	765.3	690	14.8
490	25	421.8	39.4	431.9	412	15.9
390	25	329.0	34.4	334.2	324	16.9
305	24	244.9	30.1	247.0	246	19.3
240	26	191.8	29.5	193.2	191	20.4
101	25	74.4	28.1	74.8	74	26.7
0 revs/min						
630	22	572.8	61.7	607.0	535	15.1
495	24	426.2	53.3	446.0	406	18.0
300	26	246.9	34.4	250.8	244	18.7
230	26	182.8	32.9	185.2	181	21.3
120	24	90.0	29.6	90.7	89	25.8
70	26	51.1	28.3	51.4	51	27.1

calculated. Asssuming that the gases are ideal, if $T_{g\ inlet}$ is the air inlet-temperature, and $V_{g\ inlet}$ is the air inlet flowrate, the percentage of the inlet gas escaping to the atmosphere is given by:

$$\% \text{ leakage} = \frac{V_{g\ inlet} - \frac{T_{g\ inlet}}{T_{g_2}} V_{g_2}}{V_{g\ inlet}} \qquad \text{(F-5)}$$

Leakage data were obtained for 0 revs/min, 2.4 revs/min and 4.0 revs/min of the matrix. The experimental data and the leakage flowrates as percentages of the inlet flowrate are given in Table (F.2).

Correction of the ceramic matrix burner predicted flame stability characteristics for the actual higher overall leakages

In calculating the ceramic matrix burner stability characteristics the model described in Chapter 4 was used. In the calculation, the overall leakage rates (i.e. both leakages to the surrounds and bypass leakages) were assumed to be a constant 15% of the inlet flowrates. Furthermore, gas leakages to the atmosphere were assumed to occur only across the lower circumferential seal, i.e. before the mixture entered the matrix passages. In practice, leakages occur across both the upper and lower seals but the individual rates can not be estimated. In addition the overall leakage rates were found to vary with the

inlet flowrate as shown in figures (3.27) and (3.28).

The experimental data contained therein were for cold operation of the burner; it has, however, been shown that the leakage rates from the metallic matrix burner to the surroundings during hot operation only differed slightly from those during cold operation (see figure (6.7)) and it can, therefore, be safely assumed that for both systems (since the geometric configuration of the seals is similar) the leakages to the environment and the bypass leakages during hot operation are similar to those during cold operation.

If for the ceramic matrix system gas leakages to the environment are assumed to occur across the lower seal only, the overall leakages, and consequently the actual flowrates through the matrix passages, can be estimated from figures (3.27) and (3.28). The results in terms of the mixture flowrates are given in Table F.3.

Table (F.3)

Inlet Flowrate cm^3/s	% leakage to surroundings	% bypass	% overall leakage	Actual flow through matrix cm^3/s
800	10.50	9.25	19.75	642
700	11.10	10.00	21.10	552
600	12.00	10.50	22.50	465
500	13.00	11.25	24.25	379
400	14.30	12.25	26.55	294
300	16.20	14.00	30.20	209
200	19.00	17.00	36.00	128
155	20.80	19.20	40.00	93

Since in calculating the composition of the limiting mixture for a given inlet mixture flowrate, the overall leakages from and within the ceramic matrix system were assumed to be 15% of the inlet flowrate, and since the leakage rates were found not to vary with the matrix rotational speed, the actual flowrates through the matrix and the calculated mixture compositions can be obtained from figure (4.4) and they are presented here in Table (F.4).

Table (F.4)

Inlet flowrate cm^3/s	Actual flowrate through matrix cm^3/s	composition of limiting mixtures % CH_4 by volume 4.8 revs/min	2.4 revs/min	1.2 revs/min	0.6 revs/min
800	680	2.04	2.12	2.30	2.56
700	595	2.05	2.12	2.26	2.50
600	510	2.10	2.18	2.29	2.46
500	425	2.20	2.27	2.36	2.50
400	340	2.38	2.45	2.52	2.65
300	255	2.71	2.79	2.87	2.95
200	170	3.40	3.46	3.56	3.56
110	93.5	4.75	4.75	4.75	4.75

From the data of Table (F.4) the curves of actual matrix inlet flowrate against composition, presented in figure (F.1) can be plotted. From these and the data of Table (F.3) the corrected stability curves presented in figure (6.13) can be obtained.

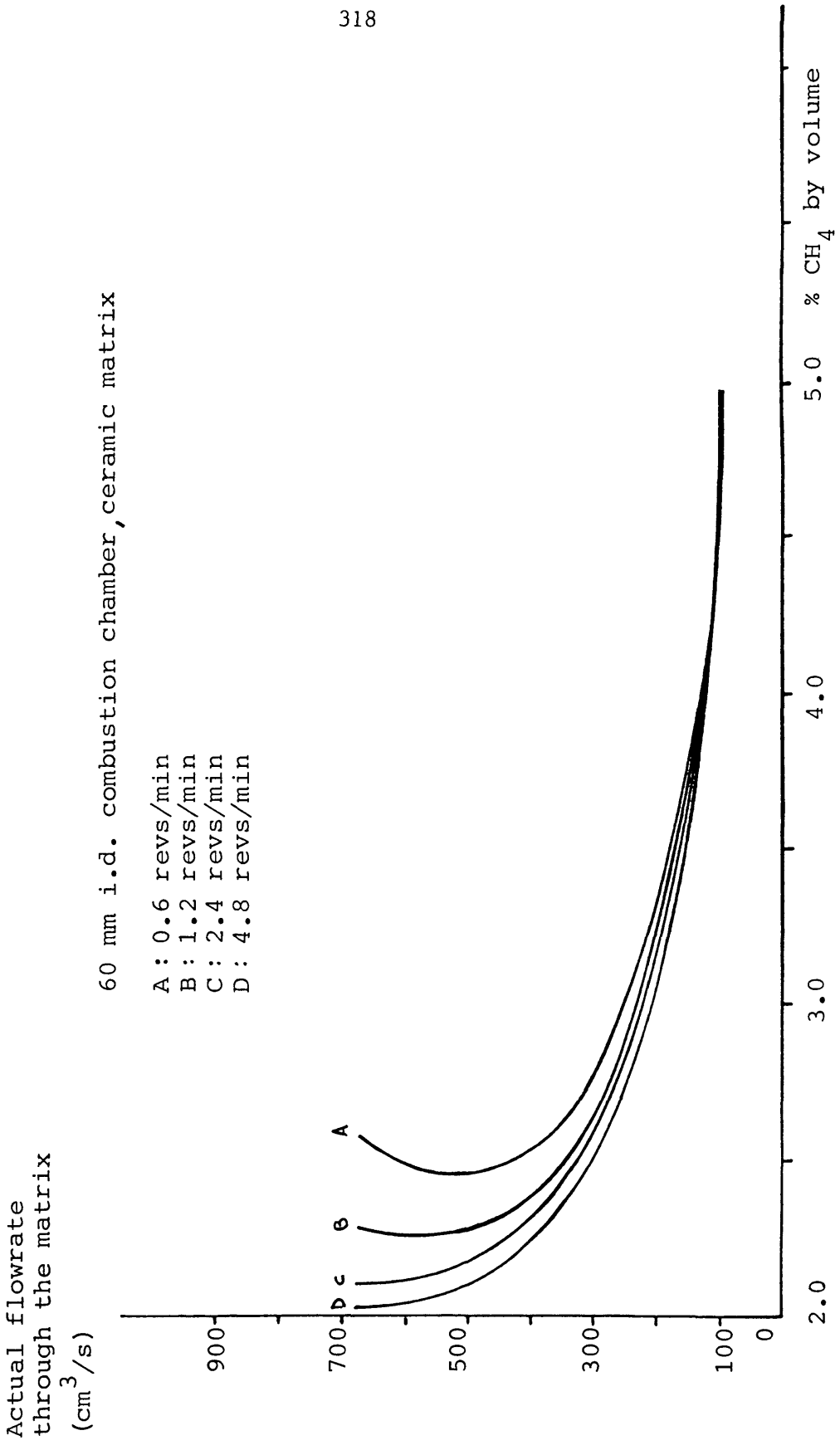


Figure (F.1): Predicted stability characteristics corrected for leakages (i.e. in terms of actual flowrates through the matrix).

References

I.1 Zabetakis, M.G., Lambiris, S. and Scott, G.S., 7th Symp. (Int.) on Combustion, The Combustion Institute, Pittsburgh, 484-487, (1959).

I.2 Smith, I.E., Ph.D. Thesis, London University, (Imperial College), 1955.

I.3 Burdon, M.G., Burgoyne, J.H. and Weinberg, F.S., 5th Symp. (Int.) on Combustion, The Combustion Institute, New York, 647-651, (1955).

I.4 Roxbee-Cox, H., Proc. Instr. Mech. Eng., **164**, 407, (1951).

I.5 I.C.I. "Calalyst Handbook with Special Reference to Unit Process in Ammonia and Hydrogen Manufacture", Wolfe Scientific Books, London, (1970).

I.6 Weinberg, F.J., Private communication.

1.1. Weinberg, F.J., Nature, **233**, 240, (1971).

1.2. Ibid., p.239.

1.3. Syred, N., Dahmen, K.R., Styles, A.C.and Nejim, S.A., Journal of Institute of Fuel, 195-204, (1977).

1.4. Mizutani, Y. and Satomura, M., 19th Symp. (Int.) on Combustion, The Combustion Institute, 529-536, (1982).

1.5. Harderty , D.R. and Weinberg, F.J., Combustion Science and Technology, **8**, 203, (1974).

1.6. Harderty, D.R. and Weinberg, F.J., Combustion Science and Technology, **12**, 153, (1976).

1.7 Malik, T.I., Ph.D. Thesis University of London, (Imperial College), 1982.

1.8. Jones, A.R., Lloyd, S.A. and Weinberg, F.J., Proc. Roy. Soc., A360, 97, 1978.

1.9. Lloyd, S.A. and Weinberg, F.J., Nature, Lond., 251, 47, 1974.

1.10. Lloyd, S.A. and Weinberg, F.J., Nature, Lond., 257, 367, 1975.

1.11. Arbib, H.A., Sawyer, R.F. and Weinberg, F.J., 18th Symp. (Int.) on Combustion, The Combustion Institute, Pittsburgh, 233, (1981).

1.12. Weinberg, F.J., Private communication.

1.13. Takeno, T. and Sato, K., Combustion Science and Technology, 20, 73-84, 1979.

1.14. Takeno, T., Sato, K. and Hase, K., 18th Symp. (Int.) on Combustion, The Combustion Institute, 465-472, (1981).

1.15. Buckmaster, J. and Takeno, T., Combustion Science and Technology, 25, 153-158, 1981.

1.16. Kotani, Y. and Takeno, T., 19th Symp. (Int.) on Combustion, The Combustion Institute, 1503-1509, 1982.

1.17. Kawamura, T., Asako, K. and Hayashi, T., ASME-JSM Thermal Eng. Joint Conference (Honolulu, 1983), 93-98, 4.

1.18. Echigo, R., Kurusu, M., Ichimiya, K. and Yoshizowa, Y., ASME-JSM Thermal Eng. Joint Conference (Honolulu, 1983), 99-103, 4.

1.19. Weinberg, F.J., The Institute of Physics, 124-158, 1982.

2.1. Jakob, M., Heat transfer, Vol. II, New York, Wiley, 1957.

2.2. Sogin, H.H. and Hussan, K.E., A disign manual for regenerative heat exchangers of the rotary type, WADC Technical Report 55-13, 1956.

2.3. Dunkle, R.V. and Maclaine-Cross, B.E., Trans. of ASME. **102**, 4, 1980.

2.4. London, A.L. and Keys, W.M., Trans. of ASME, **72**, 611-621, 1950.

2.5. Karlsson, H. and Holm, S., Trans. of ASME. **65**, 61-72, 1943.

2.6. Hansrani, S.P., Ph.D. Thesis, University of Aston, 1984.

2.7. Coppage, J.E., London, A.L., Trans. ASME, **75**, 781, 1953.

2.8. Hausen, H., 1932.

2.9. Hausen, H., R.A.E. Translation No. 126.

2.10. Saunders, O.A. and Smoleniec, S., Proceedings of the 7th Int. Congress for Applied Mechanics, **3**, 91-105, 1948.

2.11. Hausen, H., MAP Reports and Translations, No. 312, 1946.

2.12. Iliffe, C.E., Proc. at the Inst. of Mechanical Engineers, **159**, 363, 1948.

2.13. Saunders, O.A. and Smoleniec, S., IME-ASME General discussion on heat transfer, London, Section 5, Sixth Paper, 443, 1951.

2.14. Nusselt, W., Zeitschrift des Vareines Deutscher Ingenieur, **72**, 1052, 1928.

2.15. Boested, G., Feuerungstechnik, Stockholm, **26**, 282-286, 1938.

2.16. Lambertson, T.J., Trans. ASME, **80**, 586-592, 1958.

2.17. Bahnke, G.D. and Howard, G.P., Journal of Eng. for Power, 105-120, 1964.

2.18. Maclaine-Cross, I.L., Trans. of ASME, **102**, 572-574, 1980.

2.19. Romie, F.E., Trans. of ASME, **101**, pp. 726-731, 1979.

2.20. Mondt, J.R., Journal of Eng. for Power, pp. 121-126, 1964.

2.21. Kays, W.M. and London, A.L., Compact Heat Exchangers, 2nd Edition, McGraw Hill, New York, pp.44-49, 1964.

3.1. Perrry, R.H. and Green, D., Perry's Chemical Engineer's Handbook, 6th Edition, McGraw Hill.

3.2. Pitts, D.R. and Sissom, L.E., Heat Transfer, McGraw Hill.

3.3. Handbook of Chemistry and Physics, 62nd Edition, CRC Press.

3.4. Hughes, E., Electrical Technology, 5th Edition, Longman.

3.5. Moss, J.B., Properties of Engineering Materials, London, Butterworths.

4.1 Mori, Y., Nakayama, W., Int. J. Heat and Mass Transfer, **8**, 67-82, 1965.

4.2 Knudsen, J.G., Katz, D.L., Fluid Dynamics and Heat Transfer, McGraw-Hill, 1958.

5.1. Adams, L.F., Engineering Measurements and Instrumentation, The English Universities Press Ltd., 1975.

5.2. Mullikin, H.F., Gas-temperature measurement and the high velocity thermocouple, Paper presented at Symposium held in New York City, November 1939, American Institute of Physics.

6.1. Burgoyne, J.H. and Hirsch, W., Proc. R. Soc. Lon., A227, 73, 1954.

D.1 McAdams, W.H., Heat Transmission, 3rd edition, McGraw-Hill.

F.1. Coulson, J.M. and Richardson, J.F., Chemical Engineering, Vol. 1, Pergammon Press.